2019

HOST RESTRICTION FACTORS IN THE REPLICATION OF TOMBUSVIRUSES: FROM RNA HELICASES TO NUCLEOCYTOPLASMIC SHUTTLING

Cheng-Yu Wu
University of Kentucky, cwu228@uky.edu
Digital Object Identifier: https://doi.org/10.13023/etd.2019.260

STUDENT AGREEMENT:

I represent that my thesis or dissertation and abstract are my original work. Proper attribution has been given to all outside sources. I understand that I am solely responsible for obtaining any needed copyright permissions. I have obtained needed written permission statement(s) from the owner(s) of each third-party copyrighted matter to be included in my work, allowing electronic distribution (if such use is not permitted by the fair use doctrine) which will be submitted to UKnowledge as Additional File.

I hereby grant to The University of Kentucky and its agents the irrevocable, non-exclusive, and royalty-free license to archive and make accessible my work in whole or in part in all forms of media, now or hereafter known. I agree that the document mentioned above may be made available immediately for worldwide access unless an embargo applies.

I retain all other ownership rights to the copyright of my work. I also retain the right to use in future works (such as articles or books) all or part of my work. I understand that I am free to register the copyright to my work.

REVIEW, APPROVAL AND ACCEPTANCE

The document mentioned above has been reviewed and accepted by the student's advisor, on behalf of the advisory committee, and by the Director of Graduate Studies (DGS), on behalf of the program; we verify that this is the final, approved version of the student's thesis including all changes required by the advisory committee. The undersigned agree to abide by the statements above.

Cheng-Yu Wu, Student

Dr. Peter D. Nagy, Major Professor

Dr. Rick Bennett, Director of Graduate Studies

HOST RESTRICTION FACTORS IN THE REPLICATION OF TOMBUSVIRUSES: FROM RNA HELICASES TO NUCLEOCYTOPLASMIC SHUTTLING

DISSERTATION

A dissertation submitted in partial fulfillment of the
requirements for the degree of Doctor of Philosophy in the
College of Agriculture, Food and Environment
at the University of Kentucky

By
Cheng-Yu Wu
Lexington, Kentucky
Director: Dr. Peter D. Nagy, Professor of Plant Pathology
Lexington, Kentucky
2019

ABSTRACT OF DISSERTATION

HOST RESTRICTION FACTORS IN THE REPLICATION OF TOMBUSVIRUSES: FROM RNA HELICASES TO NUCLEOCYTOPLASMIC SHUTTLING

Positive-stranded (+)RNA viruses replicate inside cells and depend on many cellular factors to complete their infection cycle. In the meanwhile, (+)RNA viruses face the host innate immunity, such as cell-intrinsic restriction factors that could block virus replication.

Firstly, I have established that the plant DDX17-like RH30 DEAD-box helicase conducts strong inhibitory function on tombusvirus replication when expressed in plants and yeast surrogate host. This study demonstrates that RH30 blocks the assembly of viral replicase complex, the activation of RNA-dependent RNA polymerase function of $p92^{pol}$ and viral RNA template recruitment.

In addition, the features rendering the abundant plant DEAD-box helicases either antiviral or pro-viral functions in tombusvirus replication are intriguing. I found the reversion of the antiviral function of DDX17-like RH30 DEAD-box helicase and the co-opted pro-viral DDX3-like RH20 helicase due to deletion of unique N-terminal domains. The discovery of the sequence plasticity of DEAD-box helicases that can alter recognition of different cis-acting elements in the viral genome illustrates the evolutionary potential of RNA helicases in the arms race between viruses and their hosts.

Moreover, I discovered that Xpo1 possesses an anti-viral function and exports previously characterized cell-intrinsic restriction factors (CIRFs) from the nucleus to the replication compartment of tombusviruses. Altogether, in my PhD studies, I found plant RH30 DEAD-box helicase is a potent host restriction factor inhibiting multiple steps of the tombusvirus replication. In addition, I provided the evidence supporting that the N-terminal domain determines the functions of antiviral DDX17-like RH30 DEAD-box helicase and pro-viral DDX3-like RH20 DEAD-box helicase in tombusvirus replication. Moreover, I discovered the emerging significance of the Xpo1-dependent nuclear export pathway in tombusvirus replication.

KEYWORDS: Positive strand RNA virus; DEAD-box RNA helicase; protein domain function; Nucleocytoplasmic shuttling; Xpo1

Cheng-Yu Wu

06/26/2019

HOST RESTRICTION FACTORS IN THE REPLICATION OF TOMBUSVIRUSES: FROM RNA HELICASES TO NUCLEOCYTOPLASMIC SHUTTLING

By
Cheng-Yu Wu

Peter D Nagy
Director of Dissertation

Rick Bennett
Director of Graduate Studies

06/26/2019

ACKNOWLEDGEMENTS

I would like to express my sincere gratitude to my advisor Dr. Peter Nagy for having me and supporting me as his tenth PhD student in his lab at University of Kentucky. I really enjoyed discussing and having brainstorm with him in our weekly personal discussion. He not only always provided me useful suggestion but also has an open mind to listen to my idea and gave me feedback from different points of view. I would not have accomplished this dissertation without his guidance. All the memory and experience I gained are precious to me and will lead me to accomplish more in the future.

I also want to thank my PhD committee members, Dr. Michael Goodin, Dr. Mark Farman and Dr. Rebecca Dutch for their efforts and priceless suggestion to make my research better.

Additionally, I would like to thank Nagy's lab members for all their support. I would like to express warmest gratitude to both Judit Pogany and Nikolay Kovalev. Judy is always willing to help me to do the trouble shooting for my research and to explain me about the mystery of previous publications. Nick is the best bench mate who makes the research more enjoyable.

Also, I want to thank Department Chair Dr. Christopher Schardl, Director of Graduate Studies Dr. Rick Bennett and Former Director of Graduate studies Dr. Lisa Vaillancourt for supporting me and choosing me as part of Academic Program Committee.

Moreover, the most important aspect of my PhD journey is the unconditional support of my parents, my sister and my lovely wife.

TABLE OF CONTENTS

LIST OF TABLES

LIST OF FIGURES

Chapter 1

Introduction

1.1 Tombusviruses

Tombusviruses belong to the family tombusviridae. The type species in the group is tomato bushy stunt virus (TBSV). TBSV encapsidates a single copy of a ~4,800 nucleotide long, single-stranded, positive-sense RNA genome with a 5' non-capped and 3' non-polyadenylated end structure [1]. There are many *cis*-acting elements within its viral genome which have critical functions in many fundamental virus processes, including virus disassembly, translation, replication, subgenomic mRNA transcription, and packaging [2].

TBSV encodes five viral proteins including replication proteins p33 and $p92^{pol}$, a capsid protein p42, a movement protein p22, and a gene silencing suppressor p19 [3, 4]. The replication proteins are translated from 5'-proximal of TBSV ORFs, where the sequence of p33 overlaps with the N-terminus of $p92^{pol}$. However, p33 and $p92^{pol}$ represent noncomplementary functions during tombusvirus replication [5]. The role of p33 is an auxiliary replication cofactor [6, 7]. It possesses several functional domains, including a RNA binding domain (named RPR)[8], two trans-membrane domains [9] and a p33:p33/p92 interaction domain (composed of S1 and S2 subdomains)[10].

Briefly, RPR, which allows p33 to bind the viral RNA, is essential for p33 function, while the p33:p33/p92 interaction domain is responsible for the multimerization of p33 proteins and the interaction between p33 and $p92^{pol}$. Moreover, the RPR and p33:p33/p92 domains together allow p33 to specifically recognize and bind to the TBSV RNA p33RE region, which forms a stem loop structure containing a C-C mis-match named RII(+)-SL, for TBSV RNA template recruitment [11, 12].

Another replication protein, $p92^{pol}$, is a translational read-through of the p33 UAG stop codon, which results in a 20-30 times more of p33 amount than $p92^{pol}$ during replication [5, 13]. Besides having the same corresponding domains to p33 [10, 14], $p92^{pol}$ has a RNA-dependent RNA polymerase (RdRp) domain that is responsible for synthesizing the viral RNA progeny [15].

Like many other plus-stranded RNA viruses, such as hepatitis C virus, dengue virus, and Zika virus, TBSV remodels host intracellular membranes to build multi-vesicle body- like viral replication compartments [16, 17]. The VRCs of TBSV are about 70 nm on the cytosolic side of peroxisome membranes [18, 19], while other viruses replicate on the membranes of endoplasmic reticulum, vacuole, or chloroplast [20, 21]. The function of VRCs is vital for viral replication, concentrating viral and host proteins to facilitate virus replication and also to protect viral RNA from cellular RNases and antiviral responses [16, 22].

1.2 Yeast as a surrogate host to study virus-host interaction

In order to gain insight into host-virus interactions, genome-wide screens can be comprehensive strategies to identify host factors that influence virus replication[23]. In comparison with other eukaryotic organisms, yeast *Saccharomyces cerevisiae* has a relatively small genome (~6000 genes), and 75% of the genes has been addressed for functions and subcellular localizations (http://www.yeastgenome.org/). Moreover, yeast possesses many fundamental and functionally conserved genes and pathways compared to other eukaryotes, for example, vesicle trafficking, actin network, microtubules, protein chaperones, nucleic acid and protein modifying factors, as well as glycolysis pathway, protein translation and lipid synthesis [24]. Therefore, yeast has been developed as a surrogate host for TBSV to study virus replication and recombination at a single cell level [5, 7, 24]. In this TBSV-based yeast system, the replication proteins p33 and $p92^{pol}$ as well as TBSV replicon RNA, named defective interfering RNA (DI RNA), are expressed from plasmids. With the help of p33 and $p92^{pol}$, the TBSV repRNA can be replicated in an asymmetric manner [25]. Furthermore, many yeast strain collections, including a YKO gene deletion library,

the essential gene knockdown library (yTHC, yeast tet promoter Hughes Collection), the protein over-expression library and the temperature-sensitive library of essential genes, have been firmly established, which therefore facilitate genome-wide screening to identify host factors that are involved in TBSV replication [26-30].

1.3 *In vitro* yeast cell-free based system for the mechanistic studies

In order to gain more insight into host-tombusvirus interaction, an *in vitro* yeast cell-free extract (CFE) based assay has been developed to allow mechanistic studies [31, 32]. In the yeast CFE based assay, CFE preparation provides membranes and host factors for the *in vitro* assembly of membrane-bound tombusviral replicase. The added recombinant p33 and $p92^{pol}$ replication proteins are able to utilize the added (+)repRNA template for one complete cycle of replication, including viral RNA template recruitment, replicase assembly, RdRp activation, (-)RNA and (+)RNA synthesis [31-33]. The yeast CFE prepared from various yeast strain collections, such as YKO gene deletion library and temperature-sensitive library of essential genes, can be employed to dissect the mechanisms of host factors or subcellular pathways involved in tombusvirus replication [34-42].

1.4 Cell intrinsic restriction factors against TBSV identified by our lab

After centuries of being co-evolved with viruses, hosts have developed distinct strategies against virus invasion. Among all the anti-viral strategies, even though plants have different immune systems from animals [43], cell-intrinsic restriction factors (CIRF) are host cellular proteins that stand on the first line of defense suppressing viral replication and propagation in plants and humans [24, 44-51]. During virus infection, CIRF with anti-viral functions can affect various stage of the (+)RNA virus life cycle, including translation, assembly of the viral replicase complex, replication and release.

Protein cochaperones have also been found inhibiting virus replication. Yeast Cns1p, a cochaperone for heat shock protein 70 (Hsp70) and Hsp90 chaperones, interacted with TBSV replication proteins and blocked the assembly of virus replicase complex as well as RNA synthesis [52]. This CIRF contains a tetratricopeptide repeat (TPR) domain, which is also carried by another documented yeast CIRF cyclophilin Cpr7p [53], suggesting several TPR-containing cellular proteins might perform as CIRF.

On the other hand, host ribonuclease also can act as CIRF against virus infections. Cellular Xrn1 cytoplasmic 5′–3′exoribonuclease (plant ortholog Xrn4) has been shown to degrade tombusvirus RNA and to decrease the emergence of truncated viral RNA products [54].

Another intriguing CIRF is cellular cofilin, an actin depolymerization factor. Cofilin dissembles actin filaments and modulates the dynamics of the actin network. TBSV p33 replication protein has shown to bind cofilin and therefore blocked the severing of actin filaments and the formation of new actin filaments [39]. This process facilitates TBSV to co-opt cellular factors and lipids. On the contrary, overexpression of cofilin suppressed TBSV replication likely through keeping the TBSV from recruiting essential host factors.

A few of the host RNA-binding proteins have been found as CIRFs involved in limiting virus infection [51]. For example, nucleolin (yeast ortholog Nsr1p), and RNA binding protein, has been shown to interfere the recruitment of TBSV RNA for viral replication [55]. In addition, Cyclophilin A (Cpr1p in yeast; Roc1 in plant) bound to the TBSV RNA, led to the inhibition of the VRC assembly and RNA synthesis[56].

1.5 DEAD-box RNA helicases: potent players in RNA virus infections

Nearly all known RNA metabolism in eukaryotes is associated with RNA helicases

[57, 58]. DEAD-box helicases are the largest group of RNA helicase superfamily II (SF2) [59]. This group of RNA helicases is named by the feature of carrying a conserved amino acid sequence of D-E-A-D in motif II [59]. The ATPase domain of DEAD-box RNA helicases contributes to the binding and hydrolysis of ATP, while the helicase domain is responsible for unwinding activity. Most DEAD-box RNA helicases reported to date require only ATP binding to separate RNA duplexes [60-62], while they need hydrolysis of ATP to be dissociated from RNA and therefore be recycled for the next unwinding [61]. Moreover, it has been reported that ATP changes the affinity of helicases to bind to RNA. Unlike DNA helicases and other RNA helicases translocating on the substrate, DEAD-box RNA helicases directly load onto the RNA duplex and locally separate strands in an ATP-dependent manner [57, 63-67]. Beside the helicase core domain, all SF1 and SF2 helicases possess N- and C-terminal domains [57], which normally retain specific functionalities including protein binding domains (such as the CARD domain in RIG-I) [68, 69], DNA- or RNA-binding domains [70] and oligomerization modules [71]. N- and C-terminal domains has been shown to be critical for the specificity of cellular functions by facilitating the recruitment of nucleic acid or proteins to particular complexes [72-74].

Recently, host cellular DEAD-box RNA helicases has been reported to be involved in various steps in the life cycle of many (+)RNA viruses, such as hepatitis C virus,

influenza A virus, potyviruses and tombusviruses [75-79]. Moreover, through systematic genome-wide screens and proteomic approaches, 11 yeast cellular RNA helicases have been identified to be involved in TBSV infections, indicating the importance of cellular RNA helicases in TBSV infections [80, 81].

According to the intriguing roles of cellular RNA helicases in RNA virus infections, I hypothesized that there are DEAD-box RNA helicases as restriction factors against tombusvirus replication. Screens to identify novel functions of plant DEAD-box helicases in tombusvirus infections will be discussed in Chapter 2. A mechanistic study for the anti-viral activity of a newly identified DEAD-box helicase will be characterized in Chapter 3. On the other hand, we have found that two cellular DEAD-box helicases containing similar amino acid sequence have completely opposite roles in tombusvirus replication. The role of N- or C- terminal domains in determining the specificity of helicase activities in tombusvirus replication will be discussed in Chapter 4. Moreover, there are many nuclear RNA-binding proteins identified as restriction factors against RNA virus replication. I hypothesized that Xpo1-mediated nucleocytoplasmic shuttling pathway contributes the export of nuclear restriction factors to the viral replication compartments. How Xpo1-mediated export of nuclear-localized restriction factors will be discussed for its involvement in tombusvirus replication in Chapter 5.

Chapter 2

Screening plant DEAD-box RNA helicases reveals an inhibitory role of AtRH30 DEAD-box helicase in tombusvirus replication

2.1 Introduction

Plus-stranded RNA [(+)RNA] viruses replicate and produce RNA progeny in membrane-bound viral replication compartments of infected cells [5, 82-85]. During infection, many host factors are co-opted by (+)RNA viruses to aid the replication, while others possess restriction functions by blocking distinct steps of viral replication [24, 85-90]. Recently, an emerging picture of the role of host cellular proteins in (+)RNA viruses was revealed by genome-wide screens performed with several RNA viruses such as tomato bushy stunt virus (TBSV), brome mosaic virus (BMV), West Nile virus, hepatitis C virus (HCV) and dengue virus [23, 29, 46, 91-93].

Since yeast *Saccharomyces cerevisiae* has been developed as a surrogate host, TBSV has emerged as a model virus for identification of host cellular factors affecting virus replication [5, 24, 29, 88]. TBSV is a nonsegmented small (+)RNA virus that requires two viral replication protein p33 and $p92^{pol}$ for the viral replication. Although

sequence of p33 overlaps the N-terminus of $p92^{pol}$, these two viral proteins play distinct roles from each other in TBSV replication. p33, which possesses RNA chaperone activity, is responsible for recruiting the TBSV (+)RNA to the site of replication, the cytosolic surface of the peroxisomal membrane [10-12, 94, 95]. On the other hand, $p92^{pol}$ plays the role of RNA-dependent RNA polymerase (RdRp) and is recruited by p33 to form a functional viral replicase complex on intracellular membranes [10, 15, 32, 96, 97].

Based on high-through put screens and proteomic approaches with a TBSV-based yeast system, approximately 500 different yeast proteins affecting TBSV replication have been identified [5, 26, 27, 29, 80, 98]. Among these, at least seven proteins, such as TBSV p33, TBSV $p92^{pol}$, heat shock protein 70 chaperones (Hsp70), glyceraldehyde-3-phosphate dehydrogenase (GAPDH), pyruvate decarboxylase (Pdc1), Cdc34p ubiquitin conjugating enzyme and eukaryotic translation elongation factor 1A (eEF1A) have been documented as essential components of a functional viral replicase complex during TBSV replication [15, 80, 98-102]. Moreover, 11 yeast cellular RNA helicases, including Ded1p, Dbp2p, Sen1p, Fal1p, Prp22, Has1p, Prp5p, Dbp7p, Dbp3, Irc5p and Tif1p, have been identified, suggesting many cellular RNA helicases might be involved in TBSV infections [80, 81].

Host cellular DEAD-box RNA helicases has been reported to participate in the

replication of many (+)RNA viruses such as hepatitis C virus, influenza A virus, potyvirus and tombusvirus [75-79]. The mechanistic functions of cellular DEAD-box helicases in viral replication have been especially well documented in the case of TBSV. It has been reported that yeast DDX3-like Ded1 DEAD-box helicase (RH20 in plants) binds to the 5' region of the TBSV (+)RNA and releases p92 RdRp from the (+)RNA as long as the (-)RNA synthesis is finished [103]. Yet, TBSV likely utilizes this feature of Ded1 to suppress viral RNA recombination, which depends on the association of the viral RdRp to the RNA template during the template-switching step and facilitates RNA replication [103]. In addition, it was found that a group of cellular DEAD-box helicases including yeast Ded1p, Dbp2p and plant AtRH20 can separate the 5' region of the double-stranded TBSV RNA intermediates, where the promoter of (+)RNA synthesis initiation and a 3'-proximal replication enhancer locate, during the (+)RNA synthesis [78, 104]. This process locally opens the dsRNA structure and allows $p92^{pol}$ to access the (-)RNA template efficiently for (+)RNA synthesis. Moreover, a second group of cellular DEAD-box helicases, eIF4AIII-like yeast Fal1p (plant ortholog AtRH2) and the DDX5-like yeast Dbp3p (plant ortholog AtRH5) have been shown to stimulate TBSV replication in yeast and plants [79]. Different from Ded1p, Dbp2p and plant AtRH20 described earlier, the second group of DEAD-box helicases binds to a 5′ proximal *cis*-acting sequence of the TBSV (−)RNA, which has

been reported as a RNA replication enhancer [5' (-)REN] element [105, 106]. The dsRNA replication intermediate within the 5′ (-)REN can be separated by eIF4AIII-like AtRH2 and DDX5-like AtRH5. These features lead to a proposed model that local unwinding of the dsRNA structure within the 5′ (-)REN allows a long-range 6-bp RNA-RNA interaction between the bridge sequence of 5′ (-)REN and 3' proximal of (-)RNA, which is opened by Ded1p, Dbp2p and DDX3-like AtRH20 [79, 107]. This long-range RNA-RNA interaction likely circularizes the (-)RNA template and therefore facilitates multiple rounds of $p92^{pol}$-mediated (+)RNA synthesis, resulting in an asymmetric nature of RNA synthesis [83, 108, 109].

To gain further knowledge of the roles of cellular helicases in tombusvirus replication, I have tested twelve Arabidopsis cellular DEAD-box helicases that highly express in plant root and leaf tissues, where tombusviruses highly accumulate. While the transient expression of most cellular DEAD-box helicases selected affected tombusvirus accumulation, AtRH30 strongly inhibited the accumulation of tomato bushy stunt virus (TBSV), cucumber necrotic virus (CNV) and carnation Italian ringspot virus (CIRV) in *Nicotiana benthamiana* plants. In the wild-type yeast and two Ded1p temperature-sensitive yeast mutants, AtRH30 reduced the TBSV repRNA replication more than other inhibitory plant helicases. We also observed that AtRH30 interacted with TBSV p33 but not p92 replication protein. Overall, I have identified a

new plant DEAD-box helicase playing a role as a restriction factor in tombusvirus replication.

2.2 Materials and methods

Yeast strain and expression plasmids. Parental yeast strain BY4741 (*MATa his3Δ1 leu2Δ0 met15Δ0 ura3Δ0*) was purchased from Open Biosystems.

The RT-PCR products of *Arabidopsis* DEAD-box helicases were obtained from *Arabidopsis* cDNA as follows: The sequence of RH3 was PCR-amplified with primers #5974 and #5975, followed by the digestion with *Xho*I and *Spe*I. The digested product was ligated to *Xho*I/*Xba*I-digested pGD vector and pYC2/NT vector, respectively, resulting in pGD-RH3 and pYC-RH3. RH4 was RT-PCR-amplified with primers #4813 and #4871, followed by the digestion with *Bam*HI and *Sal*I. The *Bam*HI/*Sal*I-digested product was ligated to *Bam*HI/*Sal*I-digested pGD vector and *Bam*HI/*Xho*I-digested pYC2/NT vector, resulting in pGD-RH4 and pYC-RH4. In addition, the PCR product of RH6 was amplified with primers #5980 and #5981, followed by the digestion with *Xho*I and *Xba*I. The *Xho*I/*Xba*I-digested product was ligated to *Xho*I/*Xba*I-digested pGD vector and pYC2/NT vector, resulting in pGD-RH6 and pYC-RH6. Besides, the PCR product of RH8 was amplified with primers

#5745 and #5744, followed by the digestion with *Bam*HI and *Xba*I. The *Bam*HI/*Xba*I-digested product was ligated to *Bam*HI/*Xba*I-digested pGD vector and *Bam*HI/*Xba*I-digested pYC2/NT vector, resulting in pGD-RH8 and pYC-RH8. On the other hand, the PCR product of RH12 was amplified with primers #5748 and #5747, followed by the digestion with *Bam*HI and *Sac*I or *Not*I. The *Bam*HI/*Sac*I or *Bam*HI/*Not*I-digested products were ligated to *Bam*HI/*Sac*I-digested pGD vector or *Bam*HI/*Not*I-digested pYC2/NT vector, resulting in pGD-RH12 and pYC-RH12. The PCR product of RH14 was amplified with primers #5182 and #3050, followed by the digestion with *Bam*HI and *Xho*I. The *Bam*HI/*Xho*I-digested products were ligated to *Bam*HI/*Xho*I-digested pGD or pYC2/NT vector, resulting in pGD-RH14 and pYC-RH14. Furthermore, the PCR product of RH19 was amplified with primers #5751 and #5750, followed by the digestion with *Xho*I and *Xba*I. The digested product was ligated to *Xho*I/*Xba*I-digested pGD vector and pYC2/NT vector, resulting in pGD-RH19 and pYC-RH19. Moreover, the PCR product of RH30 was amplified with primers #5754 and #5753, followed by the digestion with *Xho*I and *Xba*I. The digested product was ligated to *Xho*I/*Xba*I-digested pGD vector and pYC2/NT vector, resulting in pGD-RH30 and pYC-RH30. The PCR product of RH37 was amplified with primers #5982 and #5983, followed by the digestion with *Bam*HI and *Xba*I. The *Bam*HI/*Xba*I-digested product was ligated to *Bam*HI/*Xba*I-digested pGD vector and *Bam*HI/*Xba*I-digested pYC2/NT vector,

resulting in pGD-RH37 and pYC-RH37. Also, the sequence of RH40 was PCR-amplified with primers #5978 and #5979, followed by the digestion with *Bam*HI and *Xba*I. The *Bam*HI/*Xba*I-digested product was ligated to *Bam*HI/*Xba*I-digested pGD vector and pYC2/NT vector, resulting in pGD-RH40 and pYC-RH40. Likewise, the PCR product of RH41 was amplified with primers #5972 and #5973, followed by the digestion with *Bam*HI and *Xba*I. The *Bam*HI/*Xba*I-digested product was ligated to *Bam*HI/*Xba*I-digested pGD vector and pYC2/NT vector, resulting in pGD-RH41 and pYC-RH41. Yet, the PCR product of RH46 was amplified with primers #5976 and #5977, followed by the digestion with *Xho*I and *Xba*I. The *Xho*I/*Xba*I-digested product was ligated to *Xho*I/*Xba*I-digested pGD vector and pYC2/NT vector, resulting in pGD-RH46 and pYC-RH46.

In order to detect the interaction between Arabidopsis DEAD-box helicases and TBSV p33 or p92 replication proteins, the sequences of helicases were fused to NubG prey constructs at either 5' or 3'-proximal ends (pPR3N-RE or pPR3C-RE). The PCR-product of RH3 was amplified with primers #6374 and #6375 from plasmid pGD-RH3, followed by the digestion with *Apa*I and *Nhe*I. The *Apa*I/*Nhe*I-digested product was ligated to *Apa*I/*Nhe*I-digested pPR3N-RE or pPR3C-RE vector, generating pPR3N-RH3 and pPR3C-RH3. The sequence of RH8 was PCR-amplified with primers #5745 and #6370 from plasmid pGD-RH8, followed by the digestion with

*Bam*HI and *Nco*I. The *Bam*HI/*Nco*I-digested product was ligated to *Bam*HI/*Nco*I-digested pPR3N-RE or pPR3C-RE vector, generating pPR3N-RH8 and pPR3C-RH8. The PCR-product of RH14 was amplified with primers #5182 and #6373 from plasmid pGD-RH14, followed by the digestion with *Bam*HI and *Nco*I. The *Bam*HI/*Nco*I-digested product was ligated to *Bam*HI/*Nco*I-digested pPR3N-RE or pPR3C-RE vector, generating pPR3N-RH14 and pPR3C-RH14. The sequence of RH30 was PCR-amplified with primers #6371 and #6372 from plasmid pGD-RH30, followed by the digestion with *Eco*RI and *Nco*I. The *Eco*RI/*Nco*I-digested product was ligated to *Eco*RI/*Nco*I -digested pPR3N-RE or pPR3C-RE vector, generating pPR3N-RH30 and pPR3C-RH30.

TBSV replication assay in yeast. To test the effect of plant helicases on TBSV replication in yeast, *Saccharomyces cerevisiae* strain BY4741, cells were transformed with both LpGAD-CUP1::HisFlag-p92 and HpGBK-CUP1::HisFlag-p33/GAL1::DI-72 along with one of the following plasmids: pYC-empty (as a control), pYC-RH8, pYC-RH12, pYC-RH14, pYC-RH19, pYC-RH30, pYC-RH3, pYC-RH6, pYC-RH37, pYC-RH40, pYC-RH41 or pYC-RH46 as described [103]. The transformed yeast cells were cultured in SC-ULH$^-$ media containing 2 % galactose and 0.1 mM bathocuproine disulfonate (BCS) at 29 °C for 18 h, followed by the incubation in SC-

ULH$^-$ media containing 2 % galactose and 50 μM $CuSO_4$ at 23 °C for 24 h. On the other hand, two yeast strains, ts-ded1-95 and ts-ded1-199, carrying temperature-sensitive (ts) mutants of Ded1p were also used for the depletion of the endogenous Ded1 pool. The transformation for the two ts-yeast cells was performed as previously described [103]. The resulting yeast cells were then grown in SC-ULH$^-$ media containing 2 % galactose and 0.1 mM BCS at 29 °C for 18 h, followed by the incubation in SC-ULH$^-$ media containing 2 % galactose and 50 μM $CuSO_4$ at 29 °C for 24 h [103]. The obtained yeast cells were used for further Northern blotting and Western blotting assays [10].

Tombusvirus accumulation in *N. benthamiana* plants expressing *Arabidopsis* DEAD-box helicases. In order to test the function of Arabidopsis DEAD-box helicases in tombusvirus infection, *N. benthamiana* plants were co-infiltrated with *Agrobacterium* carrying pGD-P19 (OD_{600} 0.2) as well as pGD-empty (as a control), pGD-RH4, pGD-RH6, pGD-RH8, pGD-RH12, pGD-RH14, pGD-RH19, pGD-RH30, pGD-RH37, pGD-RH40, pGD-RH41 or pGD-RH46 (OD_{600} 0.6 for each). For the test of CNV accumulation, the plants were also simultaneously co-infiltrated with *Agrobacterium* carrying pGD-CNV^{20Kstop} (OD_{600} 0.2). For TBSV or CIRV infection, the agro-infiltrated leaves of *N. benthamiana* plants were inoculated with TBSV or

CIRV crude sap inoculum. The leaves were collected at 2.5 days post inoculation (dpi) for CNV tests; 2 dpi for TBSV and CIRV tests for further RNA extraction and Northern blotting analysis as described [79].

Split-ubiquitin-based yeast two hybrid assay. To test if DEAD-box helicases interact with TBSV p33 and p92 replication proteins, we performed a split-ubiquitin based, yeast two hybrid assay as previously described [98, 110, 111]. The yeast strain NMY51was transformed with the bait expression vector pGAD-BT2-N-His92 or pGAD-BT2-N-His33 [98] along with prey expression vector pPR3N-RE (as a control), pPR3N-RH3, pPR3N-RH8, pPR3N-RH14, pPR3N-RH30, or pPR3N-SSA1 (as a positive control). The transformed yeast cells were plated on synthetic minimal medium plates lacking Trp and Leu (TL^-). The obtained yeast colonies were then re-suspended in water and transferred to plates lacking Trp, Leu, His and Ade ($TLHA^-$) for another 3 to 5 days at 29°C to detect the interaction between prey and bait.

2.3 Results

Expression of *Arabidopsis* DEAD-box RNA helicases to identify new cell-intrinsic restriction factors in *N. benthamiana* plants. The mechanistic functions of several

yeast DEAD-box RNA helicases and their *Arabidopsis* orthologs involved in tombusvirus replication as pro-viral factors have been addressed in detail [78, 79, 104]. Compared to the yeast genome, *Arabidopsis* encodes two times as many cellular DEAD-box RNA helicases (58 versus 26) [112, 113]. Most of them are not well-characterized and their functions in virus replication remain unknown. Therefore, I wanted to know if other Arabidopsis DEAD-box RNA helicases play a role in tombusvirus replication. A screening composed of two small groups of Arabidopsis DEAD-box RNA helicases, which are well characterized with functions in their yeast or human orthologs (Table 1), was performed to test if the transient expression of Arabidopsis DEAD-box helicases affects tombusvirus infection in *N. benthamiana* plants.

Firstly, *N. benthamiana* plants were infiltrated with *Agrobacterium* to express RH4, RH8, RH12, RH14, RH19, and RH30, respectively, and challenged by the infection of peroxisome-replicating *cucumber necrosis virus* (CNV), peroxisome-replicating *tomato bushy stunt virus* (TBSV), and mitochondria-replicating *carnation Italian ringspot virus* (CIRV), respectively (Fig. 2.1 A, B, and C). We found that RH4 and RH8 did not influence the accumulation of CNV and CIRV but inhibited TBSV accumulation by ~60 % in the inoculated leaves. Besides, both RH12 and RH30 showed inhibitory activities against CNV and TBSV, while RH30 possessed broader

restriction effect against a mitochondria-replicating CIRV. Notably, the accumulation of all three tombusviruses tested were blocked by 70 - 90% when RH30 was transiently expressed. In addition, RH14 stimulated the accumulation of CIRV by 3-fold but inhibited TBSV accumulation by 60 %. The transient expression of RH19 enhanced CIRV accumulation by 2-fold but had no effect on CNV and TBSV accumulation.

On the other hand, the transient expression of RH3, RH6, RH37, RH40, RH41, and RH46 via *Agrobacterium* infiltration in *N. benthamiana* plants was performed with the infection of CNV, TBSV and CIRV, respectively (Fig. 2.2 A, B, and C). The results show that RH3 decreased the accumulation of CNV and TBSV by ~35 % but not CIRV. The transient expression of RH6 only had inhibitory activity against CIRV by decreasing 40 % of virus accumulation. Interestingly, the accumulation of CIRV and TBSV but not a closely related CNV was stimulated by 2-fold when RH37 was transiently expressed. In addition, the expression of RH40 generally reduced the accumulation of CNV, TBSV and CIRV by ~15 %. The transient expression of RH41 reduced CNV accumulation by ~70 % but not the closely-related tombusviruses TBSV and CIRV. Furthermore, the transient expression of RH46 did not influence accumulation of any of the viruses tested. Altogether, 11 out of 12 Arabidopsis DEAD-box helicases affected tombusvirus accumulations one way or the other, while

RH30 showed strong and consistent restriction activities blocking CNV, TBSV and CIRV accumulation in plants.

Screening of *Arabidopsis* DEAD-box helicases affecting TBSV RNA accumulation in yeast. To test if Arabidopsis DEAD-box helicases could affect TBSV repRNA replication, we took the advantage of an efficient tombusvirus replication system established previously in yeast. Five *Arabidopsis* DEAD-box helicases including RH8, RH12, RH14, RH19 and RH30 that have shown intriguing activities in previous plant screening were expressed in yeast cells based on a low-copy expression vector pYC. The TBSV repRNA replication was also launched in the same yeast cells. In this study, I used not only wild-type (wt) strain BY4741 yeast but also two strains carrying temperature-sensitive (ts) mutants of Ded1p, named ts-ded1-95 and ts-ded1-199, to deplete the pro-viral Ded1p DEAD-box helicase [28, 114]. Interestingly, the expression of most helicases enhanced TBSV replication in wt yeast, except for RH30 which did not influence TBSV replication (Fig. 2.3 A). On the other hand, yeast cells of ts-ded1-95 or ts-ded1-199 grown at semi-permissive temperature (29 °C) to test if *Arabidopsis* DEAD-box helicases could affect TBSV repRNA replication. The semi-permissive temperature for yeast growth was settled about 4 °C below the non-permissive temperature, resulting in partial inactivation of the ts-ded1 essential

function [28]. Note that the ts-ded1 mutant was expressed as the only copy of a given gene in this haploid yeast system. In the ts-ded1-95 yeast cells, the expression of all selected RNA helicases had no significant function to TBSV replication (Fig. 2.3 B). On the contrary, in the yeast cells of ts-ded1-199, the TBSV repRNA replication was inhibited by 40-60 % by the expression of RH14 and RH30 (Fig. 2.3 C). For the expression of selected RNA helicases, I used a low-copy expression vector pYC-NT. However, I found that the expression of RH30 reduced TBSV replication by 80 % in wt yeast cells when a high-copy expression vector was employed (will be discussed in Chapter 3). Altogether, these results suggest that RH30 plays an inhibitory role in TBSV repRNA replication in yeast.

Screening *Arabidopsis* DEAD-box helicases interacting with tombusvirus replication proteins in membrane yeast two-hybrid split-ubiquitin assay. To test if *Arabidopsis* DEAD-box helicases could interact with the tombusvirus p33 and p92 replication proteins in the intracellular membranes, we performed membrane yeast two-hybrid (MYTH) split ubiquitin screens. The cDNA of *Arabidopsis* DEAD-box helicases including RH3, RH8, RH14 and RH30 were fused to the NubG prey construct either at the 5’ or 3’- proximal positions (NubG-x or x-NubG) [115, 116]. In comparison with NubG-x prey vector control, the counts of yeast colonies expressing

fusion of RH3, RH8, RH14 and RH30 are 3, 6, 5 or 3-fold (Fig. 2.4A, lane 2), respectively. In addition, the counts of yeast colonies expressing fusion of RH3, RH8, RH14 and RH30 are 20, 15, 2.5 and 2.5-fold, respectively, (Fig. 2.4B, lane 1) as many as x-NubG control. The results of MYTH assay revealed that RH3, RH8, RH14 and RH30 interacted with TBSV p33 replication protein. Moreover, when the p92 bait was co-expressed in yeast cells, the counts of yeast colonies expressing the fusion of NubG prey to RH8 and RH14 shows the interaction between p92 replication protein and RH3 (Fig. 2.5B, lane 3), RH8 (Fig. 2.5A, lane 4) and RH14 (Fig. 2.5A, lane 4; 2.5B, lane 3), respectively. On the contrary, RH30 did not interact with p92 replication protein when fused to NubG at 5'- or 3'-proximal positions (Fig. 2.5 A and B).

2.4 Discussion

Many host DEAD-box helicases are involved in plus-stranded RNA virus replication [76, 77, 117, 118]. Previous reports have addressed mechanistic studies on how co-opted host DEAD-box RNA helicases are critical for the replication of *Tomato bushy stunt virus* (TBSV) in yeast and plants. These pro-viral helicases are the eIF4AIII-like AtRH2/AtRH5 and the DDX3-like Ded1/AtRH20, which promote plus-

strand synthesis through locally unwinding the viral dsRNA replication intermediate [78, 79]. However, the possible roles of many cellular helicases are not well characterized in virus replication. According to previous yeast genome-wide screens and global proteomic approaches with TBSV, 11 yeast cellular RNA helicases were identified that could be involved in TBSV replication [80, 81], while plant RNA helicases remain largely unknown. As a result, we performed several screens to identify novel roles of Arabidopsis DEAD-box helicases during tombusvirus infection. First of all, the transient expression of twelve Arabidopsis DEAD-box helicases in *N. benthamiana* plants showed 11 out of 12 helicases are functional in peroxisome-replicating TBSV or a closely-related CNV or mitochondria-replicating CIRV infection. Notably, AtRH14 showed inhibitory activity against TBSV accumulation but pro-viral functions to an unrelated CIRV. The previous studies of AtRH14 yeast ortholog (Dbp2p) (Table 2.2) with TBSV and human ortholog (DDX5) (Table 2.2) with Japanese encephalitis virus (JEV) have shown to bind viral RNA and stimulate viral replication [104, 119]. This suggests that AtRH14 can be a potent candidate to study features of TBSV RNA, by comparing the sequences of TBSV and CIRV and JEV, determine the function of co-opted helicases in terms of viral replication. On the other hand, AtRH30 retained a broad range of restriction against TBSV, CNV and CIRV. In addition, the AtRH30 human ortholog DDX17 (Table 2.2)

has been shown to bind stem-loops of host pri-miRNA, which therefore facilitates miRNA processing, as well as to bind an essential stem loop in rift valley fever virus (RVFV) RNA to restrict infection [120]. This suggests that AtRH30 might possess a novel restriction activity through RNA binding in tombusvirus infections.

Yeast has been developed as a surrogate host for TBSV to study replication at a single cell level [5, 7, 24]. Expression of five Arabidopsis DEAD-box helicases in yeast wild-type (wt) strain BY4741 revealed that RH8, RH12 and RH14 enhanced TBSV replication in yeast, which is opposite to the inhibitory activities shown in the plant screening. Interestingly, the partial inactivation of yeast Ded1 DEAD-box helicase by growing yeast temperature-sensitive (ts) mutants (ts-ded1-199) at semi-permissive temperature led to the inhibition of TBSV replication by the expression of AtRH14. This suggest that yeast Ded1 (plant ortholog AtRH20) might influence the function of AtRH14 in TBSV replication since it has been reported that many co-opted factors work tightly in TBSV replication [40, 79, 80]. Similar to plant results, AtR30 showed restriction activities against TBSV replication in ts-ded1 yeast mutants, suggesting the possibility of AtRH30 is involved in TBSV infection by blocking viral replication.

I have also characterized that AtRH3, AtRH8, AtRH14 and AtRH30 interacted with TBSV replication proteins. Although the role of protein-protein interaction needs

further investigation, it seems likely that TBSV replication proteins interact with a number of host RNA helicases.

In this paper, we have identified AtRH30 DEAD-box helicase as a cellular restriction factor by plant and yeast screens. Further mechanistic studies are required to gain insight of TBSV replication.

N.O. of primers	Sequences
3050	CGGCTCGAGGTCGACTCATCTGTGTTTCATCATCATC
4813	CCAGGGATCCATGGCAGGATCTGCACCAGAAG
4871	CCAGGTCGACTCACAGCAGATCGGCCACGTTC
5182	GCCGGATCCATGGCTGCTACCGCTGCTG
5744	CGCGTCTAGATTATTGGCAATAAATTGCC
5745	CGCGGGATCCATGAACAATCGAGGAAGGT
5747	CGCGGAGCTCGCGGCCGCTTACTGACAGTAGATTGCTTGATC
5748	CGCGGGATCCATGAATACTAACAGAGGAAG
5750	CGCGTCTAGATCACAGCAAATCAGCCACGT
5751	CGCTCGAGATGGCAGGATCCGCACCGGAA
5753	CGCGTCTAGATTACCAAGTCCTCTTTCCAC
5754	CGCGCTCGAGATGAGCTCGTATGATCGTAG
5972	CGCGGGATCCATGAACGAAGAAGGCTGCGT
5973	CGCGTCTAGATCAGTACCCAACCCTTCTC
5974	CGCGCTCGAGATGGCGTCGACGGTAGGAGT
5975	CGCGACTAGTCTAAAATCCTCTCTTATCAGGAC
5976	CGCGCTCGAGATGGCTGCTACTGCTTCTGC
5977	CGCGTCTAGATTATCTATTTTTCATCATCATCGCCTC
5978	CGCGGGATCCATGGCCACAACAGAAGATAC
5979	CGCGTCTAGATTAGGGTTCTTCATCAACCAC
5980	CGCGCTCGAGATGAATAATAATAATAATAATAGAGGAAGATT TCCACCGG
5981	CGCGTCTAGATTACTGACAGTAGATTGCCTTG
5982	CGCGGGATCCATGAGTGCATCATGGGCTGA
5983	CGCGTCTAGATTAGTCCCAAGCACTTGGAGG
6370	CATGCCATGGTTGGCAATAAATTGCCTGATCG
6371	CGGAATTCATGAGCTCGTATGATCGTAGATTTGC
6372	CATGCCATGGCCAAGTCCTCTTTCCACCGTGAGGTAC
6373	CATGCCATGGTCTGTGTTTCATCATCATCGTCTCGTG
6374	CGGGCCCATGGCGTCGACGGTAGGAGTTCCATC
6375	CTAGCTAGCAAATCCTCTCTTATCAGGACAATC

Table 2.1

Table 2.1 The sequence of the primers used in this study.

Arabidobsis (Gene IDs)	Yeast	Human	References
AtRH3 (At5g26742)	Dbp1	DDX21	[112]
AtRH4 (At3g13920)	Tif1	eIF4A-1	[112]
AtRH6 (At2g45810)	Dhh1p	DDX6	Swiss-Prot (www.expasy.ch/sprot)
AtRH8 (At4g00660)	Dhh1p	DDX6	[112]
AtRH12 (At3g61240)	Dhh1p	DDX6	Swiss-Prot (www.expasy.ch/sprot)
AtRH14 (At3g01540)	Dbp2p	DDX5	[112]
AtRH19 (At1g54270)	Dhh1p	eIF4A-2	Swiss-Prot (www.expasy.ch/sprot)
AtRH30 (At5g63120)	Dbp2	DDX5/DDX17	[112, 121]
AtRH37 (At2g42520)	Dbp1	DDX3Y	[112]
AtRH40 (At3g06480)	Dbp2	DDX5	Swiss-Prot (www.expasy.ch/sprot)
AtRH41 (At3g02065)	Ded1/Sgs1	Werner	[112]
AtRH46 (At5g14610)	Dbp2	DDX5	Swiss-Prot (www.expasy.ch/sprot)

Table 2.2

Table 2.2 The Arabidopsis DEAD-box helicases and their orthologs in yeast and human.

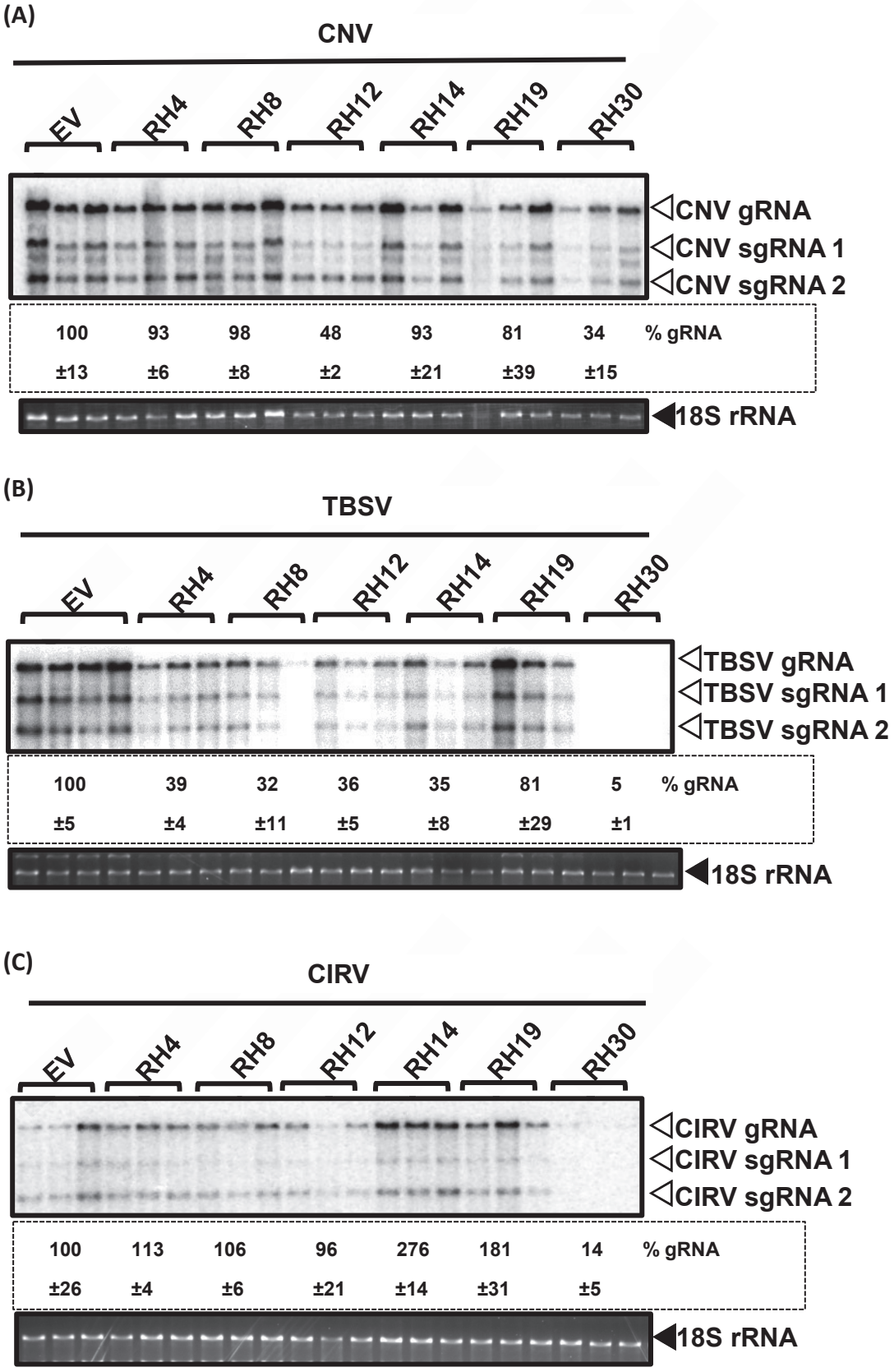
(A)
CNV
EV
RH4
RH8
RH12
RH14
RH19
RH30
CNV gRNA
CNV sgRNA 1
CNV sgRNA 2
100 93 98 48 93 81 34 % gRNA
±13 ±6 ±8 ±2 ±21 ±39 ±15
18S rRNA
(B)
TBSV
EV
RH4
RH8
RH12
RH14
RH19
RH30
TBSV gRNA
TBSV sgRNA 1
TBSV sgRNA 2
100 39 32 36 35 81 5 % gRNA
±5 ±4 ±11 ±5 ±8 ±29 ±1
18S rRNA
(C)
CIRV
EV
RH4
RH8
RH12
RH14
RH19
RH30
CIRV gRNA
CIRV sgRNA 1
CIRV sgRNA 2
100 113 106 96 276 181 14 % gRNA
±26 ±4 ±6 ±21 ±14 ±31 ±5
18S rRNA

Fig. 2.1

Fig. 2.1 Screening for DEAD-box RNA helicases affecting tombusvirus genomic (g)RNA replication by the expression of AtRH4, AtRH8, AtRH12, AtRH14, AtRH19, and AtRH30 in N. benthamiana plants. N. benthamiana plants were infiltrated with Agrobacterium to express AtRH4, AtRH8, AtRH12, AtRH14, AtRH19, and AtRH30, respectively. (A) the plants were inoculated with Cucumber necrosis virus (CNV) via Agrobacterium co-infiltration to simultaneously express $CNV^{20Kstop}$ gRNA and RNA helicases. The infiltrated leaves of N. benthamiana plants were collected 2.5 days after infiltration. (B) and (C) The Agrobacterium-infiltrated leaves were inoculated with Tomato bushy stunt virus (TBSV) or carnation Italian ringspot virus (CIRV) crude sap inoculum, respectively, 16 hours after infiltration. The leaves were then collected at 1.5 days post inoculation (dpi) for TBSV or 2.5 dpi for CIRV detection. The N. benthamiana plants agro-infiltrated with pGD-empty vector were used as controls. The collected leaves were used for RNA extraction and Northern blot analysis. Northern blot analysis of tombusvirus gRNA was performed with CNV, TBSV, or CIRV 3' end specific ^{32}P-labled probes, respectively. The 18S ribosomal RNA was detected by Ethedium bromide (EtBr) staining and was used as a loading control. Each experiment was repeated at least three times.

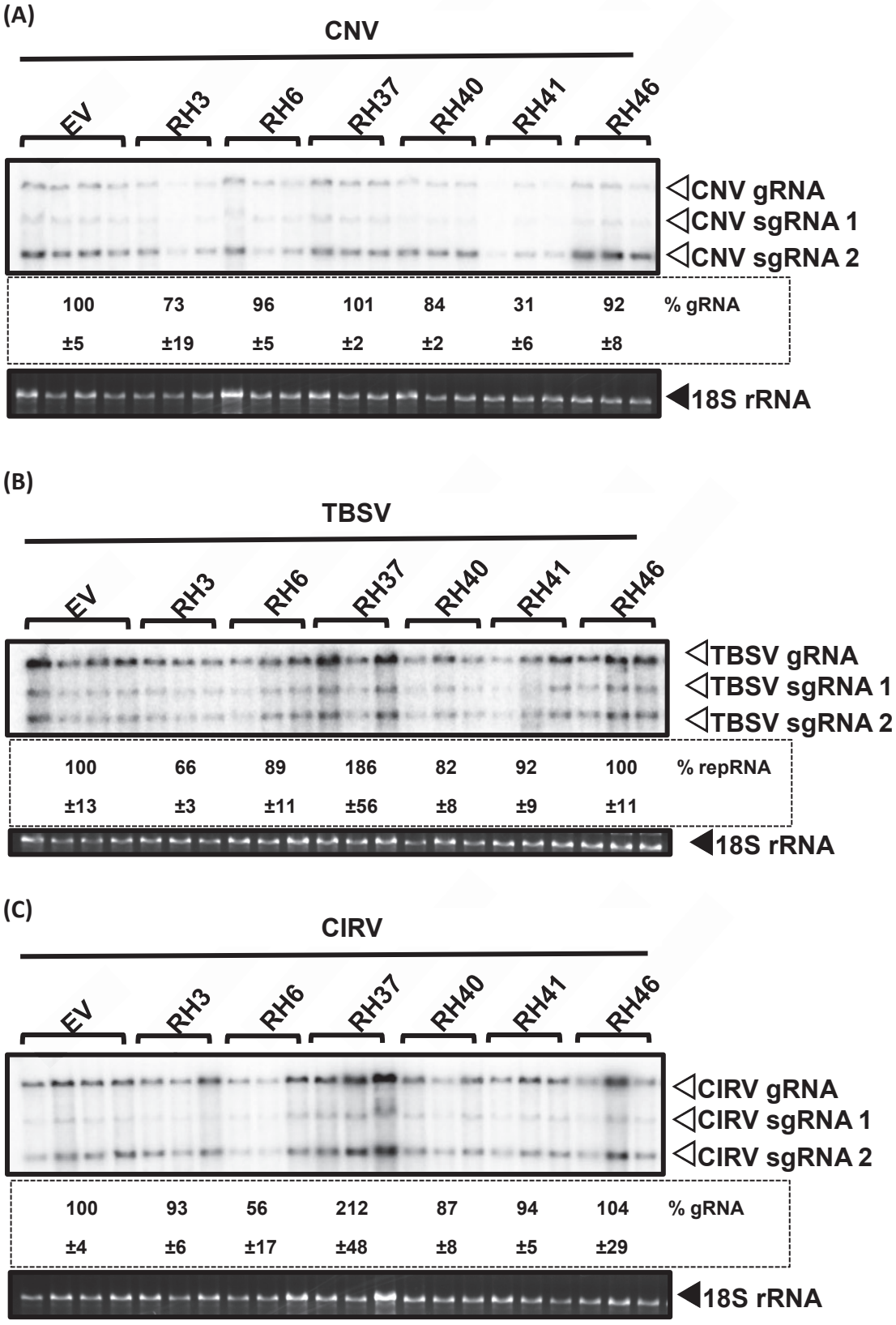
(A)
CNV
EV
RH3
RH6
RH37
RH40
RH41
RH46
CNV gRNA
CNV sgRNA 1
CNV sgRNA 2
100 73 96 101 84 31 92 % gRNA
±5 ±19 ±5 ±2 ±2 ±6 ±8
18S rRNA
(B)
TBSV
EV
RH3
RH6
RH37
RH40
RH41
RH46
TBSV gRNA
TBSV sgRNA 1
TBSV sgRNA 2
100 66 89 186 82 92 100 % repRNA
±13 ±3 ±11 ±56 ±8 ±9 ±11
18S rRNA
(C)
CIRV
EV
RH3
RH6
RH37
RH40
RH41
RH46
CIRV gRNA
CIRV sgRNA 1
CIRV sgRNA 2
100 93 56 212 87 94 104 % gRNA
±4 ±6 ±17 ±48 ±8 ±5 ±29
18S rRNA

Fig. 2.2

Fig. 2.2 Screening for DEAD-box RNA helicases affecting tombusvirus genomic (g)RNA replication by the transient expression of AtRH3, AtRH6, AtRH37, AtRH40, AtRH41, and AtRH46 in N. benthamiana plants. N. benthamiana plants were infiltrated with Agrobacterium to express AtRH3, AtRH6, AtRH37, AtRH40, AtRH41, and AtRH46, respectively. (A) the plants were inoculated with Cucumber necrotic virus (CNV) via Agrobacterium co-infiltration to simultaneously express $CNV^{20Kstop}$ gRNA and RNA helicases. The infiltrated leaves of N. benthamiana plants were collected 2.5 days after infiltration. (B) and (C) The Agrobacterium-infiltrated leaves were inoculated with Tomato bushy stunt virus (TBSV) or carnation Italian ringspot virus (CIRV) crude sap inoculum, respectively, 16 hours after infiltration. The leaves were then collected at 1.5 days post inoculation (dpi) for TBSV or 2.5 dpi for CIRV detection. The N. benthamiana plants expressing pGD-empty vector were used as controls. The collected leaves were used for RNA extraction and Northern blot analysis. Northern blot analysis of tombusvirus gRNA was performed with CNV, TBSV, or CIRV 3' end specific ^{32}P-labled probe, respectively. The 18S ribosomal RNA was detected by Ethedium bromide (EtBr) staining and was used as a loading control. Each experiment was repeated at least three times.

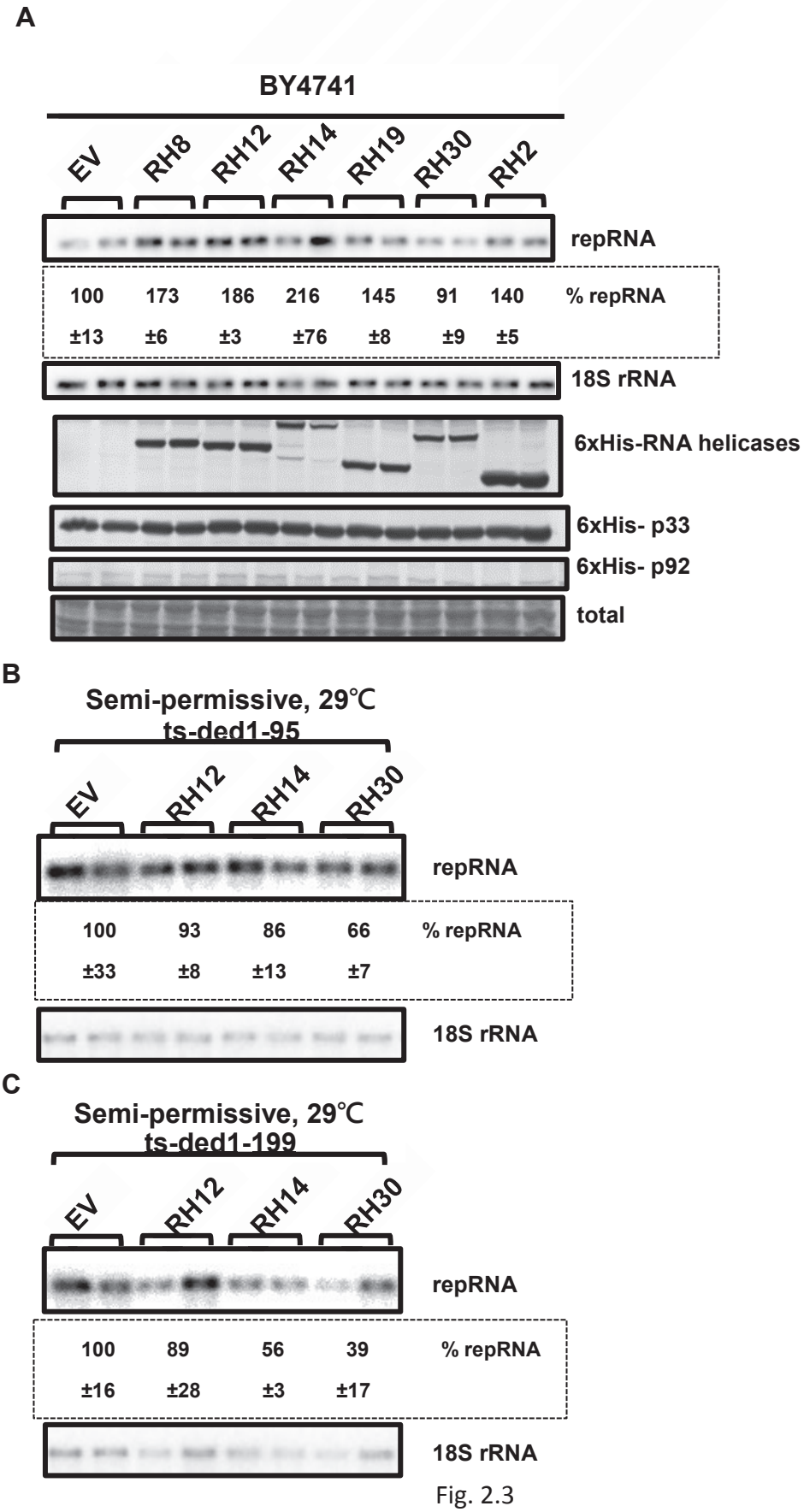
A
BY4741
EV
RH8
RH12
RH14
RH19
RH30
RH2
repRNA
100 173 186 216 145 91 140 % repRNA
±13 ±6 ±3 ±76 ±8 ±9 ±5
18S rRNA
6xHis-RNA helicases
6xHis- p33
6xHis- p92
total
B
Semi-permissive, 29℃
ts-ded1-95
EV
RH12
RH14
RH30
repRNA
100 93 86 66 % repRNA
±33 ±8 ±13 ±7
18S rRNA
C
Semi-permissive, 29℃
ts-ded1-199
EV
RH12
RH14
RH30
repRNA
100 89 56 39 % repRNA
±16 ±28 ±3 ±17
18S rRNA

Fig. 2.3

Fig. 2.3 Screening for DEAD-box RNA helicases affecting tombusvirus genomic (g)RNA replication by the expression of AtRH8, AtRH12, AtRH14, AtRH19, AtRH30, and AtRH2 in surrogate host yeast Saccharomyces cerevisiae. The accumulation of TBSV repRNA was detected in the (A) wt yeast strain grown at permissive temperature (23°C) and (B) ts-ded1-95 yeast mutant grown at semipermissive temperature (29°C) and (C)ts-ded1-199 yeast mutant grown at semipermissive temperature (29°C). TBSV repRNA replication was launched by expressing 6xHis-p33 and 6xHis-p92 from the CUP1 promoter (copper inducible) and DI-72 (+)repRNA from the GAL1 promoter (galactose-inducible) in the wt yeast strain BY4741 and ts-ded1 yeast mutants. Top panels: the detection of DI-72 (+)repRNA accumulation by a specific ^{32}P-labeled probe in Northern blot analysis. Middle panels: 18S rRNAs were used loading controls. Bottom panels: Western blot analysis of Arabidopsis DEAD-box RNA helicases, p33 and p92 accumulation by anti-His antibody. Coomassie blue-stained SDS-PAGE gels shows total protein levels in the samples.

TBSV p33 interaction:

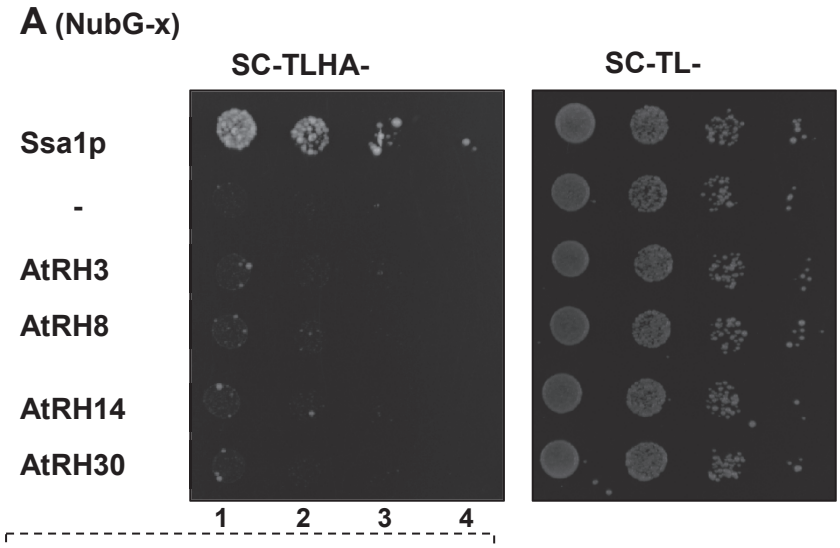

	>100 (counts)
Ssa1p	
-	1
AtRH3	3
AtRH8	6
AtRH14	5
AtRH30	3

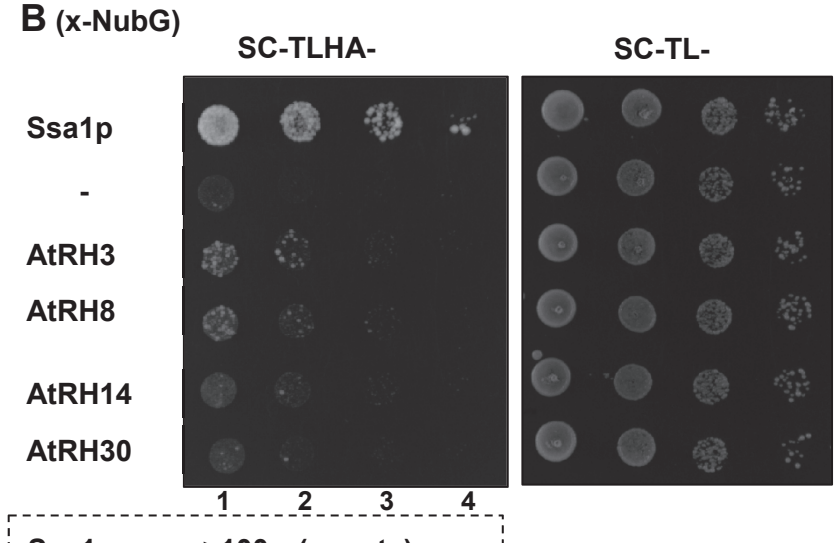

	>100 (counts)
Ssa1p	
-	2
AtRH3	~40
AtRH8	~30
AtRH14	5
AtRH30	5

Fig. 2.4

Fig. 2.4 Interaction between TBSV p33 replication protein and Arabidopsis DEAD-box helicases in a MYTH assay. Split-ubiquitin based yeast two-hybrid assays were performed to test binding between p33 replication protein and full-length Arabidopsis DEAD-box helicases. The bait p33 protein was expressed together with the prey helicases in yeast. SSA1 (Hsp70 chaperone) and the empty prey vector (NubG) were used as controls, respectively. Yeast cells were grown on a SC-TLHA$^-$ plate to test protein interactions. A nonselective SC-TL$^-$plate was used to show the growth of yeast transformants. SC, synthetic complete medium.

TBSV p92 interaction:

A (NubG-x)

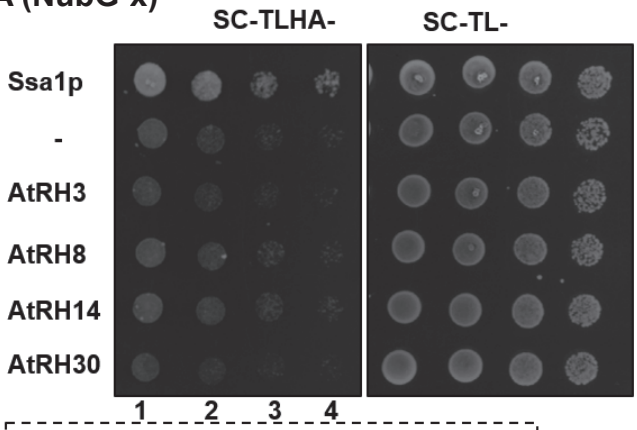

Ssa1p	>100 (counts)
-	~23
AtRH3	~22
AtRH8	~35
AtRH14	~48
AtRH30	~20

B (x-NubG)

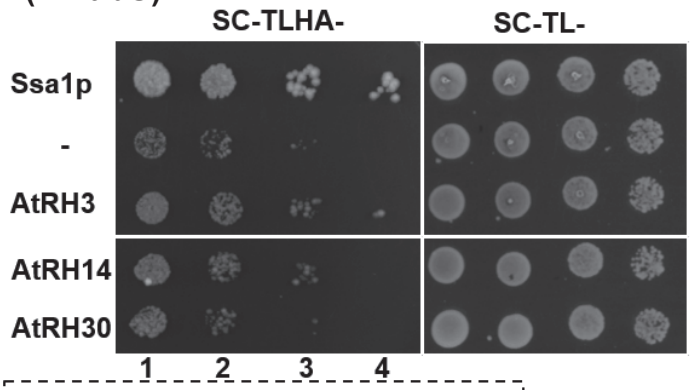

Ssa1p	~21 (counts)
-	3
AtRH3	~14
AtRH14	~10
AtRH30	2

Fig. 2.5

Fig. 2.5 Interaction between TBSV p92 replication protein and Arabidopsis DEAD-box helicases in a MYTH assay. Split-ubiquitin based yeast two-hybrid assays were performed to test binding between p92 replication protein and full-length Arabidopsis DEAD-box helicases. The bait p92 protein was expressed together with the prey helicases in yeast. SSA1 (Hsp70 chaperone) and the empty prey vector (NubG) were used as controls, respectively. Yeast cells were grown on a SC-TLHA$^-$ plate to test protein interactions. A nonselective SC-TL$^-$plate was used to show the growth of yeast transformants. SC, synthetic complete medium.

Chapter 3

Blocking tombusvirus replication through the antiviral functions of DDX17-like RH30 DEAD-box helicase

(This chapter was published as follows: Wu C-Y, Nagy PD (2019) Blocking tombusvirus replication through the antiviral functions of DDX17-like RH30 DEAD-box helicase. PLoS Pathog 15(5): e1007771.)

3.1 Introduction

Positive-stranded (+)RNA viruses replicate inside cells and depend on many co-opted cellular factors to complete their infection cycle. These viruses build elaborate membranous viral replication compartments, consisting of viral replication proteins, viral RNAs and recruited host factors, in the cytosol of the infected cells. The hijacked host factors participate in all steps of RNA virus replication, including the assembly of membrane-bound viral replicase complexes (VRCs), viral RNA-dependent RNA polymerase (RdRp) activation and viral RNA synthesis. The growing list of co-opted host factors facilitating VRC assembly includes translation initiation and elongation factors, protein chaperones, RNA-modifying enzymes, SNARE and ESCRT proteins, actin network, and lipids [21, 23, 26, 29, 46, 122-125]. Many (+)RNA viruses extensively rewire metabolic pathways, remodel subcellular membranes and take advantage of intracellular trafficking.

The host utilizes cellular proteins to sense viral pathogenicity factors and block

virus replication with the help of cell-intrinsic restriction factors (CIRFs) as an early line of defense [47, 51, 93, 122]. These CIRFs can be part of the innate immune responses and used for antiviral defense as sensors or effectors [126-129]. The identification and characterization of the many CIRFs against different viruses is still in the early stages.

Viral RNA replication is intensively studied with *Tomato bushy stunt virus* (TBSV), a tombusvirus infecting plants, based on yeast (*Saccharomyces cerevisiae*) surrogate host [81, 130, 131]. Expression of the two TBSV replication proteins, termed p33 and $p92^{pol}$, and a replicon (rep)RNA leads to efficient viral replication. $p92^{pol}$ is the RdRp [132, 133], whereas the more abundant p33 is an RNA chaperone. P33 functions in RNA template selection and recruitment and in the assembly of VRCs within the replication compartment [11, 12, 31, 95, 133, 134].

TBSV, which does not code for its own helicase, usurps several yeast and plant ATP-dependent DEAD-box RNA helicases as host factors promoting TBSV RNA replication. The yeast DDX3-like Ded1p and the p68-like Dbp2p, and the plant DDX3-like RH20, DDX5-like RH5 and the eIF4AIII-like RH2 DEAD-box proteins were shown as pro-viral factors, which affect plus- and minus-strand synthesis, maintenance of viral genome integrity and RNA recombination in TBSV [78, 79, 103].

DEAD-box helicases are the largest family of RNA helicases and are known to be involved in cellular metabolism [58, 135, 136], and affect responses to abiotic stress and

pathogen infections [112, 137, 138]. They function in unwinding of RNA duplexes, RNA folding, remodeling of RNA-protein complexes, and RNA clamping [57]. They have no unwinding polarity and can open up completely double-stranded RNA regions, however, unlike many other helicases, DEAD-box helicases do not unwind RNA duplexes based on translocation on the RNA strand. Instead, DEAD-box helicases directly load on duplexes and open up a limited number of base pairs. Strand separation within the duplexes is not coordinated with ATP hydrolysis, which is used for enzyme dissociation from the template. This unwinding mode is termed local strand separation [57, 113]. DEAD-box helicases also affect RNA virus replication [77, 139-141], and viral translation [142, 143]. In case of plant viruses, turnip mosaic virus and brome mosaic virus have been described to co-opt cellular DEAD-box helicases for proviral function in translation or replication [77, 144]. Altogether, cellular helicases are important co-opted host factors for several viruses, playing critical roles in virus-host interactions.

However, cellular RNA helicases also act as antiviral restriction factors, including functioning as viral RNA sensors (e.g., Dicer or RIG-I) or directly inhibiting RNA virus replication as effectors [145-147]. For example, DDX17 restricts Rift Valley fever virus [120], while DDX21 helicase inhibits influenza A virus and DDX3 blocks Dengue virus infections [118, 148-150]. Thus, the emerging picture is that host helicases are important for the host to restrict RNA virus replication, but the mechanism of their activities or

substrates are not well characterized.

In this work, we find that the plant DDX17-like RH30 DEAD-box helicase plays a strong restriction factor function against tombusviruses and related plant viruses. RH30 DEAD-box helicase is expressed in all plant organs, but its cellular function is not known yet [151]. We find that RH30 is re-localized from the nucleus to the sites of tombusvirus replication via interacting with the TBSV p33 and $p92^{pol}$ replication proteins. Several in vitro assays provide evidence that RH30 inhibits tombusvirus replication through blocking several steps in the replication process, including VRC assembly, viral RdRp activation and the specific interaction between p33 replication protein and the viral (+)RNA. RH30 knockout lines of *Arabidopsis* supported increased accumulation level for the related turnip crinkle virus, confirming the restriction factor function of RH30 against a group of plant viruses. This is the first identification and characterization of a plant helicase with an effector type restriction factor function against plant viruses. Since plant genomes codes for over 100 RNA helicases, it is likely that additional helicases have CIRF function against plant viruses.

3.2 Materials and methods

Biotinylated RNA-protein interaction assay. Biotinylated RII RNA of DI-72(+) was synthesized by *in vitro* T7 transcription in the presence of 7.5 µl of 10 mM ATP, CTP, GTP and 5 mM UTP as well as 0.35 µl of 10 mM biotin16-UTP (Roche) in a total of 50 µl reaction volume. The interaction assay was performed with 3.8 µM of recombinant MBP-RH30 and 1.9 µM of MBP-p33C along with 0.1 µg of biotinylated RNA, 0.1 µl of tRNA (1 mg/ml), 2 U RNase inhibitor, and 1 mM ATP in the presence of biotin-RNA binding buffer (100 mM Tris [pH 7.9], 10% glycerol, 100 mM KCl, 5 mM $MgCl_2$, 0.1% NP-40) in a 10 µl reaction mixture. Non-biotinylated RII of DI-72(+) RNA or absence of ATP was used as controls.

Assay #1: Recombinant MBP-RH30 was incubated first with biontinylated RII(+) RNA at 25°C for 15 min. Then, the recombinant MBP-p33C was added to the reaction and incubated for another 15 min. Assay #2: Recombinant MBP-RH30 and MBP-p33C were co-incubated simultaneously with biontinylated RII(+) RNA at 25°C for 30 min. The reaction mixtures were incubated with 20 µl of Promega Streptavidin MagneSphere Paramagnetic Particles (VWR) at room temperature for 20 min. The particles were collected in a magnetic stand and washed with binding buffer for five times. The protein-RNA complexes were then eluted with 20 µl of SDS loading dye containing β-mercaptoethanol by boiling for 15 min. The eluted samples were analyzed by Western blot with anti-p33 antibody.

Assay #3: For the detection of p33 released from protein-biotinylated RNA complex, 1.9 μM of recombinant MBP-p33C was incubated with 0.1 μg of biontinylated RII of DI-72(+) RNA at 25°C for 15 min, followed by the addition of 20 μl of Promega Streptavidin MagneSphere Paramagnetic Particles for another 30 min incubation at room temperature. After collection of the beads and washing with biotin-RNA binding buffer for five times, the particles were incubated with either 0.95 or 3.8 μM of MBP-RH30 or MBP (used as control) in the presence of biotin-RNA binding buffer containing 1 mM ATP at 25°C for 15 min. The supernatant of the mixture was collected after collecting the particles in a magnetic stand and was analyzed by Western blot with anti-p33 antibody.

Gel mobility shift assay (EMSA) and dsRNA strand-separation assay. The conditions for the EMSA experiments were described previously [12]. Briefly, the EMSA assay was performed with 0.1 pmol of ^{32}P-labeled RNA probes along with different concentrations (0.4, 1.9, and 5.7 μM) of purified recombinant MBP-fusion proteins or MBP in the presence of RNA binding buffer (10 mM HEPES [pH7.4], 50 mM NaCl, 1 mM DTT, 1 mM EDTA, 5% Glycerol, 2.5 mM $MgCl_2$), 2 U of RNase inhibitor, as well as 0.1 μg of tRNA in a total of 10 μl reaction volume. Two different

amounts (2 and 4 pmol) of unlabeled RNAs together with 5.7 μM of either MBP-RH30 or MBP were used for template competition.

To study if purified proteins could unwind partial dsRNA duplex, the dsRNA strand-separation assay was performed as described [79]. Firstly, the unlabeled single-stranded DI-72 (-) or DI-72 (+) RNAs were synthesized via T7 polymerase- based in vitro transcription. The ^{32}P-labeled single-stranded RI(-) or RII(+) RNAs were synthesized by T7-based in vitro transcription using ^{32}P-labeled UTP. To prepare partial dsRNA duplexes, consisting of either RI(-)/DI-72 (+) or RII(+)/DI-72 (-) (see Fig. 7E-F), 2 pmol of ^{32}P -labeled RI(-) or RII(+) were annealed to 6 pmol of unlabeled DI-72(+) or DI-72 (-) in STE buffer (10 mM TRIS [pH 8.0], 1 mM EDTA, and 100mM NaCl) by slowly cooling down the samples (in a total volume of 20 μl) from 94°C to 25°C in 30 min. To test if the purified recombinant proteins could separate the partial dsRNA duplex, 1.9 and 5.7 μM purified MBP fusion proteins or MBP as a negative control were added separately to the partial dsRNA duplex in the RNA binding buffer (10 mM HEPES [pH7.4], 50 mM NaCl, 1 mM DTT, 1 mM EDTA, 5% Glycerol, 2.5 mM $MgCl_2$) along with 1mM ATP, followed by incubation at 25°C for 25 min. The reaction mixtures were then treated with Proteinase K (2 μg/per reaction) at 37°C for 20 min, followed by loading onto 5% nondenaturing polyacrylamide gel with 200V for 1 h.

Yeast strains and expression plasmids. The yeast (*Saccharomyces cerevisiae*) strains BY4741 (MATa his3Δ1 leu2Δ0 met15Δ0 ura3Δ0), and TET::DED1 (yTHC library) were obtained from Open Biosystems. RT-PCR products of *Arabidopsis RH30* gene and its mutant $RH30^{F416L}$ were obtained as follows: Total RNA from *Arabidopsis* was isolated and used for RT-PCR with primers #5753 and #5754 to obtain the sequence of *RH30*. Meanwhile, two PCR-generated fragments that partly overlap with each other and introduce the point mutation in RH30 were amplified with RT-PCR using primers #6706 and #5753 or #5754 and #6707. These two PCR-generated fragments were then used as templates to obtain the whole sequence of $RH30^{F416L}$ by PCR. To generate plasmids for expression of *Arabidopsis RH30* and $RH30^{F416L}$ in yeast and plants, the obtained PCR products were digested with XhoI and XbaI and then inserted into XhoI/XbaI digested pYES-NT and pGD-35S, resulting in pYES-RH30, pGD-RH30, and pGD-$RH30^{F416L}$.

To prepare expression plasmids for recombinant protein purification from E.*coli*, Arabidopsis RH30 and $RH30^{F416L}$ sequences were PCR-amplified with primers #6061 and #6062 using pGD-RH30 and pGD-$RH30^{F416L}$ plasmids, respectively. The obtained PCR products were digested with XbaI and XhoI, followed by the ligation into XbaI/SalI digested pMAL-c2x, generating pMAL-RH30 and pMAL-$RH30^{F416L}$.

To obtain plasmids for expression of N-terminal Green Fluorescent Protein (GFP) or Red Fluorescent Protein (RFP)-tagged proteins, Arabidopsis RH30 sequence was RT-PCR-amplified with primers #5754 and #6839 and digested with XhoI and ApaI, followed by ligation into XhoI/ApaI digested pGDG and pGDR [152], respectively, resulting in pGD-GFP-RH30 and pGD-RFP-RH30.

The sequence of bacteriophage MS2 coat protein gene was PCR-amplified from pGBK-MS2CP-EYFP [10] with primers #1567 and #1568, followed by digestion with XhoI and BamHI. The PCR product of mRFP was obtained by PCR-based amplification with primers #2691 and # 5051, and the obtained PCR product was digested with BglII and XbaI. These two digested PCR products were co-inserted into XhoI/XbaI digested pGD-35S to generate pGD-MS2CP-RFP. The sequence of the full-length DI-72 carrying of six repeats of MS2 hairpin [10], which binds specifically to the MS2 phage coat protein, [153] and a 3' ribozyme were PCR-amplified from pYC-DI-72(+)-MS2 or pYC-DI-72(-)-MS2 [10] with primers #471 and #1069. The obtained PCR products were digested with XhoI and SacI, followed by ligation into XhoI/SacI digested pGD-35S, creating pGD-DI-72(+)-MS2hp and pGD-DI-72(-)-MS2hp.

To make *Arabidopsis* RH30 restricted in localization to the nucleus, a nuclear retention signal (NRS) was fused to RH30. The NRS fragment was PCR-amplified from pCiNeo-3XFlag-NRS-NCL [154] (a generous gift from Dr. Glaunsinger) using primers

#6877 and #6876, followed by digestion with XhoI and HindIII. RH30 sequence was PCR-amplified from pGD-RH30 using primers #6880 and #5753, followed by digestion with HindIII and XbaI. These two digested fragments were then inserted to XhoI/XbaI digested pGD-35S, generating pGD-His6-NRS-RH30. GFP sequence was PCR-amplified from pGDG using primers #6512 and #6513. This PCR product was then digested with XhoI and SacI, followed by the ligation into SalI/SacI digested pGD-His6-NRS-RH30. This created a plasmid pGD-His6-NRS-RH30-GFP, which expresses C-terminal GFP-tagged NRS-RH30.

To generate the expression plasmids for the BiFC assays in plants, the sequence of *Arabidopsis* RH30 was PCR-amplified from pGD-RH30 with primers #5754 and #5753, followed by the digestion with XbaI and XhoI. Also, the N-terminal half of yellow fluorescence protein (nYFP) sequence was PCR-amplified using pGD-nYFP-MBP plasmid as template [42] and primers #5905 and #6069, followed by the digestion with BglII and BamHI. BglII/BamHI digested nYFP fragment was ligated into BamHI digested pGD-35S, resulting in pGD-nYFP. The pGD-nYFP plasmid was then digested with XbaI and XhoI and was used for the ligation with XbaI/XhoI digested RH30, generating pGD-nYFP-RH30.

Tombusvirus replication assay in yeast. To test tombusvirus replication in yeast, BY4741 strain of *Saccharomyces cerevisiae* was transformed with LpGAD-CUP1::HisFlag-p92 and HpGBK-CUP1::HisFlag-p33/GAL1::DI-72 together with pYES-empty (as control), pYES-RH30 or pYES-RH30^{F416L}. The obtained yeast transformants were grown in SC-ULH$^-$ media containing 2 % galactose and 0.1 mM BCS at 29 °C. After 18h, the yeast culture was transferred to SC-ULH$^-$ media supplemented with 2% galactose and 50 μM $CuSO_4$ and incubated at 23°C for 7h. The obtained yeast cells were used for further Northern blot analysis and Western blot analysis [10].

To test FHV replication in yeast, BY4741 strain was transformed with HpESC-Gal 1::FHV RNA1-frameshift and LpGAD-CUP1::cHaFlag-FHV protein A [155] along with pYES-empty (as control), pYES-RH30 or pYES-RH30^{F416L}. The transformed yeast cells were grown in SC-ULH$^-$ media supplemented with 2 % galactose and 0.1 mM BCS at 23 °C for 18 h. After that, the yeast cultures were transferred to SC-ULH$^-$ media supplemented with 2% galactose and 50 μM $CuSO_4$ and incubated at 23°C for 48 h. The yeast cells were collected for further Northern blot analysis and Western blot analysis.

To test NoV replication in yeast, BY4741 strain was transformed with HpESC-CUP1::NOV RNA1-frameshift and LpESC-CUP1:: cHaFlag-NOV protein A [155] along with pYES-empty (as control), pYES-RH30 or pYES-RH30^{F416L}. The obtained

yeast transformants were grown in SC-ULH$^-$ media supplemented with 2 % galactose and 0.1 mM BCS at 29 °C for 18 h. The yeast culture was then transferred to SC-ULH$^-$ media containing 2 % galactose and 50 μM $CuSO_4$ and incubated at 29 °C for 48 h.

Recombinant protein purification from *E. coli.* Recombinant proteins MBP-RH30, MBP-RH30^{F416L}, MBP-p33, MBP-p92 and MBP were expressed in E. *coli* and affinity-purified as described [78]. Briefly, E. *coli* strain BL21 (DE3) CodonPlus (Stratagene) cells were transformed with the above plasmids to express the recombinant proteins. Then, the E. *coli* cells were cultured at 37°C for 16h, followed by dilution of the culture to OD_{600} 0.2 with fresh media. The E. *coli* cultures were incubated at 37°C until reaching 1.0 OD_{600}. Subsequently, the E. *coli* cultures were incubated at 16°C in the presence of isopropyl-β-D-thiogalactopyranoside (IPTG) for 8 h. The E. *coli* cells were then collected by centrifugation at 5000 rpm for 5 min at 4°C, followed by the resuspension in ice-cold column buffer (20mM HEPES [pH7.4], 25 mM NaCl, 1mM EDTA [pH 8.0]) containing 10 mM β-mercaptoethanol and 1 μl of RNase A (1 mg/ml) per 4 ml of E. *coli* cell-suspension. The cells were then sonicated on ice and the lysates were centrifuged at 15,000 rpm for 15 min at 4°C. The obtained supernatants were incubated with amylose resin (NEB) at 4°C for 2 h. After the resin was washed with column buffer, the

recombinant proteins were eluted with column buffer containing 0.36% [W/V] maltose and 1mM DTT.

Co-purification of RH30 with the Tombusvirus replication complex. Yeast BY4741 strain was transformed with plasmids pYES-RH30, HpGBK-CUP1::FLAGp33/GAL1::DI-72, and LpGAD-CUP1::FLAGp92, while yeasts transformed with pYES-RH30, HpGBK-CUP1::Hisp33/GAL1::DI-72 and LpGAD-CUP1::Hisp92 were used as control. The assay was performed as described [25, 156] with minor modification. Briefly, the obtained yeast transformants were grown in SC-ULH$^-$ media containing 2% glucose at 23°C for 16 h. The culture was then transfer to SC-ULH$^-$ media supplemented with 2% galactose for another 24 h at 23°C, followed by the addition of 50 μM $CuSO_4$ and incubation for 6 h at 23°C. The obtained yeast cells were resuspended in high salt TG buffer (50 mM Tris-HCl [pH 7.5], 10% glycerol, 0.5 M NaCl, 10 mM KCl, 15 mM $MgCl_2$, 1% [V/V] yeast protease inhibitor cocktail [Ypic]) and broken in a FastPrep Homogenizer (MP Biomedicals) with glass beads, followed by centrifugation at 500 g for 5 min at 4°C. The membrane fraction containing viral replicase complex was collected by centrifugation at 35,000 g for 20 min at 4°C, followed by solubilization in high salt TG buffer containing 2 % Triton X-100, 1% [V/V] Ypic for 3 h at 4°C. The supernatant of detergent-solubilized membranes was collected

by centrifugation at 35,000 g for 20 min at 4°C and then was incubated with anti-FLAG M2-agarose affinity resin (Sigma) in columns for 16 h at 4°C. After that, the columns were washed with high salt buffer for three times. To elute the protein samples from the column, the preparations were incubated with SDS-PAGE loading dye at 85°C for 6 min, followed by centrifugation at 500xg for 3 min. β-mercaptoethanol was added to the samples, then they were boiled for 20 min. Affinity-purified p33 was analyzed by Western blot with anti-FLAG antibody, and co-purified 6xHis-tagged RH30 was analyzed by Western blot with anti-His antibody.

Pull-down assay. E. *coli* strain BL21 (DE3) CodonPlus (Stratagene) cells were transformed with expression plasmids for expression and purification of recombinant proteins, including MBP-RH30, MBP-RH30^{F416L}, GST-TBSV p33C and MBP. The methods to obtain E. *coli* cell lysate as described previously [8, 157]. E. *coli* lysates containing MBP, MBP-AtRH30, or MBP-RH30^{F416L} were separately incubated with amylose resin (NEB) for 2 h at 4°C, followed by washing with cold column buffer three times. The amylose resin was then incubated with E. *coli* lysates containing GST-TBSV p33C for 4 h at 4 °C in the presence of 0.5 % NP-40 and 0.1 % [V/V] Ypic, followed by washing with cold column buffer containing 0.5 % NP-40 three times. The protein

complexes bound to resin were eluted with cold column buffer containing 0.36% [W/V] maltose and 1mM DTT, followed by the analysis with Western blot assay.

Yeast cell-free extract (CFE)-based *in vitro* TBSV replication assay and *in vitro* RdRp activation assay. The yeast CFE that supports TBSV RNA replication in vitro was prepared using BY4741 yeast strain as described [31, 32]. The *in vitro* CFE assay #1 (Fig. 6) was performed with the mixture of 2 µl of CFE, 0.5 µg DI-72 (+)repRNA, 0.2 µg affinity-purified maltose-binding protein (MBP)-p33 as well as MBP-p92^{pol} (both recombinant proteins were purified from E. *coli*) [8], 5 µl of buffer A (30 mM HEPES-KOH [pH 7.4], 150 mM potassium acetate, 5 mM magnesium acetate, 0.13 M sorbitol), 2 µl of 150 mM creatine phosphate, 0.2 µl of 10 mg/ml creatine kinase, 0.4 µl actinomycin D (5mg/ml), 0.2 µl of 1 M dithiothreitol (DTT), 0.2 µl of RNase inhibitor, 2 µl a ribonucleotide (rNTP) mixture (10 mM of ATP, CTP, and GTP as well as 0.25 mM UTP), 0.1 µl of [^{32}P]UTP and affinity-purified recombinant proteins MBP-RH30, MBP-RH30^{F416L}, or MBP in a total of 20 µl reaction volume. The reaction was performed at 25°C for 3h and then stopped by the addition of a 110 µl of 1% SDS and 50 mM EDTA, followed by phenol-chloroform extraction and RNA precipitation. In order to detect the amount of dsRNA, the obtained ^{32}P-labeled repRNA products were then divided into two halves: one was heat denatured at 85°C for 5 min in the presence

of 50% formamide, while the other one was not denatured. Then, the repRNA products were analyzed by electrophoresis in a 5% polyacrylamide gel (PAGE) containing 8 M urea and 0.5X Tris-borate-EDTA (TBE) buffer.

To dissect the mechanisms of RH30 antiviral function in tombusvirus replication, a step-wise *in vitro* CFE replication assay #2 (Fig. 6) was performed. The purified proteins (MBP or MBP-RH30) were added during either step 1 reaction (i.e., VRC assembly step) or step 2 reaction (i.e., tombusviral RNA synthesis step) [31]. In the first step, a mixture of 2 µl of yeast CFE, 0.5 µg DI-72 (+)repRNA transcripts, 0.2 µg MBP-p33 and MBP-p92^{pol}, 5 µl of buffer A, 2 µl of 150 mM creatine phosphate, 0.2 µl of 10 mg/ml creatine kinase, 0.4 µl actinomycin D (5mg/ml), 0.2 µl of 1 M DTT, 0.2 µl of RNase inhibitor, 2 µl of 10 mM ATG and GTP mixture in a 20 µl reaction volume, followed by incubation at 25°C for 1 h. The reaction mixture was centrifuged at 15,000 rpm for 10 min at 4°C. The collected membrane-fraction of CFE, which contains the membrane-bound VRCs, was washed with 100 µl of buffer A for once, followed by centrifugation at 15,000 rpm for 10 min at 4°C. The obtained membrane preparations were dissolved in 8 µl buffer A. In second step, the 8 µl of collected samples was added to 12 µl reaction mixture composed of 3 µl of buffer A, 2 µl of 150 mM creatine phosphate, 0.2 µl of 10 mg/ml creatine kinase, 0.4 µl actinomycin D (5mg/ml), 0.2 µl of 1 M DTT, 0.2 µl of RNase inhibitor, 2 µl of rNTP mixture (10 mM of ATP, CTP, and

GTP as well as 0.25 mM UTP) and 0.1 µl of [^{32}P]UTP [31]. Then, the assays were performed at 25°C for 3 h, and stopped by the addition of a 1/10 volume of 1% SDS and 50 mM EDTA, followed by phenol-chloroform extraction and RNA precipitation [31].

For the *in vitro* RdRp activation assay, the CFE soluble fraction and recombinant affinity purified MBP-p92-Δ167N was used as described [15]. The CFE soluble fraction (supernatant) was collected by centrifugation of the original CFE at 42,000 g for 20 min at 4°C [31, 32]. Then 2 µl of the obtained CFE soluble fraction and approximately 0.2 µg of MBP-p92-Δ167N along with different concentration (1.9, and 3.8 µM) of MBP-RH30 or MBP were incubated with 5 µl of buffer A (30mM HEPES-KOH [pH 7.4], 150 mM potassium acetate, 5 mM magnesium acetate, 0.13 M sorbitol), 2 µl of 150 mM creatine phosphate, 0.2 µl of 10 mg/ml creatine kinase, 0.4 µl actinomycin D (5 mg/ml), 0.2 µl of 1 M dithiothreitol (DTT), 0.2 µl of RNase inhibitor, 2 µl a ribonucleotide (rNTP) mixture (10 mM of ATP, CTP, and GTP as well as 0.25 mM UTP) and 0.1 µl of [^{32}P]UTP in a total of 20 µl reaction volume. The following reaction was then performed and analyzed as described [133].

In vitro translation assay. To test if AtRH30 influences the translation of tombusvirus genomic RNA, an *in vitro* translation assay was performed as described [158]. Briefly, approximately 0.5 µg of CIRV genomic RNA and TDH2 mRNA were incubated with

different concentrations (1.9 µM, and 3.8 µM) of recombinant MBP-RH30 along with 2.5 µl of wheat germ extract, 0.4 µl amino acid mix (minus Methionine), 0.47 µl of 1M KOAC, 6 U of RNase inhibitor, 0.1 µl of [^{35}S]Methionine in a total of 10 µl reaction volume. After 1.5 h incubation at room temperature, the samples were boiled with SDS-PAGE loading dye for 5 min, followed by analysis with 10 % acrylamide gel.

Confocal microscopy. The subcellular localization of *Arabidopsis* RH30 in plant epidermal cells or protoplasts was observed with the help of N-terminal fusion of RH30 to GFP. Protoplasts were isolated from *N. benthamiana* leaves as described [159, 160]. The wild-type or transgenic *N. benthamiana* (constitutively expressing H2B fused to RFP) leaves were infiltrated with *Agrobacterium* carrying expression plasmids pGD-GFP-RH30 (OD_{600} 0.3), pGD-p33-BFP (OD_{600} 0.3), pGD-P19 (OD_{600} 0.2), pGD-$CNV^{20KSTOP}$ (OD_{600} 0.2). The wild-type *N. benthamiana* leaves were co-infiltrated with *Agrobacterium* carrying pGD-RFP-SKL (OD_{600} 0.3) to visualize peroxisomes. The absence of pGD-$CNV^{20KSTOP}$ or pGD-p33-BFP was used as control. Approximately 72 h post-agroinfiltration, imaging of infiltrated leaves or protoplasts was performed on an Olympus FV1200 confocal microscopy using 40X or 60X water-immersion objective equipped lasers. BFP was excited with 405 nm laser, GFP was excited with 488 nm laser,

and RFP was excited with 543 nm laser. Images were obtained and merged using Olympus FLUOVIEW 1.5.

The subcellular localization of repRNA(+)-MS2hp and repRNA(-)-MS2hp RNAs was observed in plant epidermal cells with C-terminal fusion of MS2 coat protein to RFP, which recognizes MS2 six hairpins inserted into repRNA(+) and repRNA(-) [10]. The *N. benthamiana* leaves were infiltrated with agrobaterium carrying pGD-CNV^{20KSTOP}, pGD-P19, pGD-p33-BFP, pGD-GFP-RH30, and pGD-DI-72(+)-MS2hp or pGD-DI-72(-)-MS2hp (OD_{600} 0.2 of each). The absence of pGD-GFP-RH30, pGD-DI-72(+)/(-)-MS2hp or pGD-CNV^{20KSTOP} was used as control. Approximately 84 h post-infiltration, imaging of infiltrated leaves was obtained as described above.

To visualize the subcellular localization of tombusvirus dsRNA, *N. benthamiana* leaves were co-infiltrated with pGD-CNV^{20KSTOP} (OD_{600} 0.2), pGD-P19 (OD_{600} 0.2), pGD-p33-BFP (OD_{600} 0.2), pGD-RFP-RH30 (OD_{600} 0.2), pGD-VP35-YC (OD_{600} 0.1), and pGD-B2-YN (OD_{600} 0.1) (a generous gift from Dr. Aiming Wang) [161]. The absence of pGD-RFP-RH30, pGD-CNV^{20KSTOP}, or pGD-p33-BFP was used as control. Approximately 84 h post-infiltration, imaging of infiltrated leaves was obtained as described above except YFP was excited with 488 nm laser.

Bimolecular fluorescence complementation assay. The interaction between TBSV p33 replication protein and AtRH30 helicase was detected in *N. benthamiana* leaves by bimolecular fluorescence complementation (BiFC). The *N. benthamiana* leaves were infiltrated with *Agrobacterium* carrying pGD-p19 (OD_{600} 0.2), pGD-RFP-SKL (OD_{600} 0.4), pGD-T33-cYFP (OD_{600} 0.4) [5] and pGD-nYFP-RH30 (OD_{600} 0.4) or pGD-nYFP-MBP (as a control, OD_{600} 0.4), followed by inoculation with TBSV crude sap inoculum 16 h after agro-infiltration. Two days post-virus inoculation, confocal microscopy imaging of infiltrated leaves was performed as described above.

Virus accumulation in *N. benthamiana* expressing AtRH30 and in RH30 knockout *Arabidopsis* plants. *N. benthamiana* leaves were co-infiltrated with *Agrobacterium* carrying pGD-RH30 and pGD-P19. In the experiment of $CNV^{20KSTOP}$ or TMV infection, plants were also co-infiltrated with *Agrobacterium* carrying pGD-$CNV^{20KSTOP}$ or pJL-36 for TMV [162]. In the experiment for TBSV, CIRV, TCV, and RCNMV infections, plants were inoculated with crude sap inocula 16 h after agro-infiltration. About 36 h (for TBSV infection); 48 h (for CNV, CIRV and TMV infections); 72 h (for RCNMV); 144 h (for TCV) post-virus inoculation, the virus-inoculated leaves were collected for total RNA extraction and Northern blot as described [79] to analyze the accumulation levels of these viruses.

To detect the accumulation level of TCV in RH30 knockout *Arabidopsis* plants, transgenic *Arabidopsis* line (#CS372806) containing T-DNA insertion within endogenous RH30 ORF was obtained from the Arabidopsis Biological Resource Center. After self-fertilization and confirmation by genotyping, the homozygous lines were collected and the leaves were inoculated with TCV crude sap inoculum. After 48h post-inoculation, total RNA from inoculated leaves was extracted and analyzed by Northern blot as described above.

VIGS-based knockdown of RH30 in *N. benthamiana* plants. To knockdown the expression levels of endogenous NbRH30 in *N. benthamiana* plants, virus-induced gene silencing (VIGS) assay was performed as described [163, 164]. The predicted cDNA sequence of NbRH30 (Accession number: Nbv5.1tr6207343) was obtained by a blast search using the sequence of AtRH30 in QUT *Nicotiana benthamiana* database. To generate the VIGS vectors (pTRV2-Nb30-5, targeting 5' region in NbRH30 mRNA; pTRV2-Nb30-3, targeting 3' region in NbRH30 mRNA), an NbRH30 gene fragment was PCR-amplified from *N. benthamiana* cDNA using primers #7304 and #7307. This fragment was used as a template to obtain two 300-bp cDNA fragments encoding 5' or 3' region of NbRH30 gene via PCR using primers #7304 and #7305 or #7306 and #7307, respectively. The obtained fragments were digested with BglII and SalI, respectively,

followed by the ligation into BamHI/XhoI digested pTRV2-empty, resulting in pTRV2-Nb30-5 or pTRV2-Nb30-3.

The leaves of *N. benthamiana* plants were infiltrated with *Agrobacterium* carrying pTRV1 together with pTRV2-Nb30-5 (targeting 5' region in NbRH30 mRNA) or pTRV2-Nb30-3 (targeting 3' region in NbRH30 mRNA) or pTRV2-cGFP (as a control). 12 days post-infiltration, the RH30 mRNA level in upper systemic leaves were investigated by semi-quantitative RT-PCR with primers #7306 and #7307 (in case of TRV1/TRV2-Nb30-5 silenced plants); primers #7304 and #7305 (in case of TRV1/TRV2-Nb30-3 silenced plants). The levels of 18S rRNA or tubulin mRNA were used as internal control in Northern blotting or RT-PCR using primers #2859 and #2860. After the silencing effects were confirmed, the silenced upper leaves were inoculated with TBSV crude sap. Approximately 36 h post-inoculation, the total RNA of inoculated leaves were extracted and analyzed by Northern blot as described above.

The expression level of NbRH30 mRNA in upper systemic leaves was investigated by Northern blotting assay. The ^{32}P-labeled probes targeting either 5' or 3'-regions of NbRH30 mRNA for the detection in Northern blotting were prepared as follows: The 5' or 3'-regions of NbRH30 sequence were PCR-amplified with primers #7304 and #7990 or #7306 and #7991, respectively. The obtained PCR-products were utilized as templates for *in vitro* T7-trancription along with [^{32}P]UTP to produce ^{32}P-

labeled probes. The probe targeting 5'-region of NbRH30 mRNA was used for plants silenced by TRV1/TRV2-Nb30-3, while the probe targeting 3'-region of NbRH30 mRNA was used for plants silenced by TRV1/TRV2-Nb30-5.

For the detection of TMV genomic RNA in plants, we utilized a ^{32}P-labeled probe targeting 3'-region of TMV gRNA. The probe was prepared by PCR-amplification of the 3' proximal of TMV genome with primers #6192 and #6193 from plasmid pJL-36. The obtained PCR products were then used as templates for *in vitro* T7-trancription along with [^{32}P]UTP to generate the ^{32}P-labeled probe for Northern blotting assay.

3.3 Results

The host RH30 RNA helicase is a potent restriction factor of tombusvirus replication in yeast and plants. To test if the host RH30 RNA helicase could affect tombusvirus replication, we expressed the *Arabidopsis* RH30 using agroinfiltration in *Nicotiana benthamiana* plants. Interestingly, expression of AtRH30 blocked TBSV replication by ~90% in the inoculated leaves (Fig. 3.1A). The closely-related cucumber necrosis virus (CNV), which also targets the peroxisomal membranes for VRC formation, was also inhibited by ~4-fold through the expression of AtRH30 (Fig. 3.1B). Replication of another tombusvirus, carnation Italian ringspot virus (CIRV), which

builds the replication compartment using the outer membranes of mitochondria, was inhibited by ~9-fold by the transient expression of AtRH30 in *N. benthamiana* (Fig. 3.1C).

To test if RH30 was also effective against TBSV when expressed in yeast cells, we launched the TBSV repRNA replication assay in wt yeast by co-expressing the viral components with RH30. After 24 h of incubation, TBSV repRNA analysis revealed strong inhibition of viral replication by RH30 expression (Fig. 3.1F), suggesting that RH30 is a highly active inhibitor against TBSV replication even in a surrogate host.

To learn if the putative helicase function of RH30 is required for its cell intrinsic restriction factor (CIRF) function, we expressed a motif IV helicase core mutant of RH30($F_{416}L$) in *N. bentamiana* via agroinfiltration. Mutation of the highly conserved F residue within the helicase core domain (see Fig. 3.13) has been shown to greatly decrease both ATP binding/hydrolysis and strand displacement activities in Ded1 and other DEAD-box helicases [165]. Northern blot analysis revealed the lack of inhibition of TBSV replication, and only partial inhibition of CIRV replication by RH30($F_{416}L$) (Fig. 3.1D-E, lanes 9-12). Thus, we suggest that the full helicase/ATPase function of RH30 is required for its CIRF function against tombusviruses.

VIGS-based silencing of the endogenous RH30 in *N. benthamiana* led to ~5-fold, ~3-fold and ~11-fold increased accumulation of TBSV, CNV and CIRV, respectively, in

the inoculated leaves (Fig. 3.2). The leaves of virus-infected and VIGS-treated plants showed severe necrotic symptoms earlier and died earlier than the control plants (i.e., TRV-cGFP treatment) in case of all three tombusvirus infections (Fig. 3.2). On the other hand, the mock-inoculated and VIGS-treated plants became only slightly smaller than the TRV-cGFP treated control plants (Fig. 3.2). Based on these and the RH30 over-expression data, RH30 DEAD-box helicase seems to act as a major restriction factor against tombusviruses in plants and yeast.

RH30 DEAD-box helicase is re-localized into the tombusvirus replication compartment in plants. To identify the cellular compartment where RH30 DEAD-box helicase performs its CIRF function, first we used co-localization studies in *N benthamiana* protoplasts co-expressing GFP-RH30, p33-BFP (to mark the site of viral replication) and RFP-tagged H2B, which is a nuclear marker protein. We detected the re-localization of GFP-RH30 into the large p33 containing replication compartment from the nucleus during CNV replication (Fig. 3.3A, top panel versus second panel). Both the p33-BFP and RFP-SKL (a peroxisomal matrix marker) showed the re-localization of GFP-RH30 into the large TBSV replication compartment, which consists of aggregated peroxisomes. Part of the ER is also recruited to the p33 and RH30 containing replication compartment (Fig. 3.3A bottom panel), as shown previously [166,

167].

A similar re-localization pattern of RH30 was observed in epidermal cells of whole plants infected with CNV (Fig. 3.3B, top panel versus second panel). The expression of only p33-BFP was satisfactory to recruit the RH30 into the replication compartment (Fig. 3.3B). RH30 was also re-targeted in CIRV-infected *N. benthamiana* cells into the p36 and p95 containing replication compartment (Fig. 3B, bottom panel), which consists of aggregated mitochondria [168, 169]. Based on these experiments, we propose that the mostly nuclear localized RH30 helicase is capable of entering the tombusvirus replication compartment via interaction with the replication proteins. However, the formation of large tombusvirus-induced replication compartments seemed to be normal in the presence of RH30, indicating the lack of interference with the biogenesis of the replication compartment by RH30.

Nuclear retention of RH30 DEAD-box helicase blocks its antiviral function in plants. To test if the cytosolic localization of RH30 is required for its CIRF function, we fused RH30 with a nuclear retention signal (NRS) [154] to enrich RH30 in the nucleus at the expense of the cytosolic pool of RH30. Interestingly, unlike WT RH30, expression of NRS-RH30 did not result in inhibition of CNV replication in *N. benthamiana* (Fig. 3.4A). Confocal microscopy experiments confirmed that NRS-

RH30-GFP is localized exclusively in the nucleus (Fig. 3.4B). Infection of the *N. benthamiana* protoplasts with CNV did not result in the re-targeting of NRS-RH30-GFP from the nucleus to the replication compartment visualized via p33-BFP. The nuclear retention of NRS-RH30-GFP was also confirmed in *N. benthamiana* epidermal cells infected with CNV or mock inoculated (Fig. 3.4C). Altogether, these experiments demonstrated that re-localization of RH30 helicase from the nucleus to the replication compartment is critical for its CIRF function in plants.

RH30 helicase interacts with the viral replication proteins in yeast and plants. To learn about the tombusviral target of RH30 DEAD-box helicase, we co-expressed the His_6-tagged RH30 with Flag-tagged p33 and Flag-p92 replication proteins and the TBSV repRNA in yeast, followed by Flag-affinity purification of p33/p92 from the detergent-solubilized membrane fraction of yeast, which is known to harbor the tombusvirus replicase [25, 132]. Western blot analysis of the affinity-purified replicase revealed the effective co-purification of His_6-RH30 (Fig. 3.5A, lane 3), suggesting that RH30 targets the VRCs for its CIRF function. Interestingly, His_6-RH30 was co-purified from yeast co-expressing either Flag-p33 or Flag-p92 replication proteins (Fig. 3.5A, lanes 1-2), suggesting that RH30 likely directly interacts with the tombusvirus replication proteins in a membranous compartment.

To show direct interaction between RH30 DEAD-box helicase and the TBSV p33 replication protein, we performed a pull-down assay with MBP-tagged RH30 and GST-tagged p33 proteins from *E. coli*. We found that MBP-RH30 captured GST-p33 protein on the maltose-column (Fig. 3.5B, lane 2), indicating direct interaction between the host RH30 and the viral p33 protein. In the pull-down assay, we used truncated TBSV p33 replication protein missing its N-terminal region including the membrane-binding region to aid its solubility in *E. coli* [8]. Interestingly, the helicase core mutant RH30($F_{416}L$) also bound to p33 replication protein as efficiently as the wt RH30 (Fig. 3.5B, lane 3 versus 2). Altogether, these data suggest that the direct interaction between RH30 host protein and the replication protein of TBSV occurs within the viral protein C-terminal domain facing the cytosolic compartment.

To provide additional evidence that RH30 helicase interacts with the tombusvirus replication proteins, we have conducted bimolecular fluorescence complementation (BiFC) experiments in *N. benthamiana* leaves. The BiFC experiments revealed interaction between RH30 and the TBSV p33 replication protein within the viral replication compartment, marked by the peroxisomal matrix marker RFP-SKL (Fig. 3.5C). Altogether, these experiments revealed direct interaction between the cellular RH30 DEAD-box helicase and the TBSV p33 replication protein, which results in re-targeting of RH30 into the viral replication compartment.

RH30 DEAD-box helicase interferes with the assembly of tombusvirus VRCs and activation of p92 RdRp. To gain insight into the mechanism of CIRF function of RH30 helicase, we affinity-purified the recombinant RH30 and tested its activity in vitro in a TBSV replicase reconstitution assay, which is based on yeast cell-free extract [31, 32]. Addition of RH30 to the replicase reconstitution assay led to inhibition of TBSV repRNA replication by ~10-fold (Fig. 3.6A, lanes 9-10). The in vitro production of double-stranded repRNA replication intermediate was also inhibited by ~10-fold by RH30, indicating that RH30 likely inhibits an early step, such as the VRC assembly during TBSV replication.

We then used a step-wise TBSV replicase reconstitution assay [31, 78], in which RH30 was added at different stages of VRC assembly (schematically shown in Fig. 3.6B). RH30 showed significant inhibitory activity when added at the beginning of the TBSV replicase reconstitution assay (Fig. 3.6B, lanes 3-4 versus 1-2). On the contrary, RH30 was ineffective, when added to TBSV replicase reconstitution assay after the VRC assembly step and prior to RNA synthesis (Fig. 3.6B, lanes 7-8). These in vitro data support the model that the inhibitory role of RH30 is performed during or prior to the VRC assembly step, but RH30 is ineffective at the latter stages of TBSV replication.

We also utilized an in vitro RdRp activation assay based on the purified recombinant TBSV p92 RdRp, which is inactive and requires Hsp70 chaperone and the viral (+)RNA template to become an active polymerase [133]. Addition of the recombinant RH30 helicase strongly inhibited the polymerase activity of the p92 RdRp (Fig. 3.6C), suggesting that RH30 blocks the critical RdRp activation step during tombusvirus replication.

Several RNA helicases are involved in regulation of cellular translation [170]. Therefore, we tested if RH30 affected the translation of tombusvirus genomic RNA, which is uncapped and lacks poly(A) tail [3]. CIRV genomic RNA was used in this in vitro assay based on wheat germ extract [158]. Addition of recombinant RH30 to the in vitro translation assay inhibited slightly the production of p36 replication protein from the gRNA when RH30 was used in high amount (Fig. 3.6D). The highest amount of RH30 also had minor inhibition on translation of the control Tdh2 mRNA (Fig. 3.6D). Thus, RH30 is unlikely to specifically affect the translation of tombusvirus RNAs during infection.

RH30 helicase binds to critical cis-acting elements in the viral RNA. Since the canonical function of RNA helicases to bind RNA substrates and unwind base-paired structures [57], we tested if RH30 DEAD-box helicase could perform these functions

with the TBSV RNA in vitro. First, we used a gel-mobility shift assay with purified recombinant RH30, which showed that RH30 bound to both the (+) and (-)repRNA (Fig. 3.7A-B). Since each of the four regions in the TBSV repRNA contains well-defined cis-acting elements, we performed template competition assays with the four regions separately in the presence of recombinant RH30 helicase. This assay defined that the best competitors for binding to RH30 was RII(+) and RII(-), whereas RI(+), RIV(+) and RI(-), RIV(-) also become competitive when added in high amounts (Fig. 3.7C). Because RII(+) contains a critical cis-acting stem-loop element, termed RII(+)SL, which is involved in p33-mediated recruitment of the TBSV (+)RNA template [12], and the activation of the p92 RdRp [133], we tested if the purified RH30 could bind to this stem-loop element in vitro. Interestingly, RH30 bound to RII(+)SL in the absence of added ATP (Fig. 3.7D). However, the presence of extra ATP enhanced the binding of RH30 to RII(+)SL, suggesting that RH30 binds to RNAs in an ATP-dependent fashion, similar to other DEAD-box helicases [57, 165, 171]. The control p33 (an N-terminally-truncated, soluble version) bound to RII(+)SL more efficiently and in an ATP-independent manner (Fig. 3.7D), as also shown previously [12]. This highlight the possibility that RH30 and p33 replication protein compete with each other in binding to this critical cis-acting element.

To test the RNA helicase function of RH30, we performed strand separation assays, where parts of the TBSV repRNA was double-stranded as shown schematically in Fig. 3.7E-F. The RNA helicase activity of RH30 in the presence of ATP was found to efficiently separate the partial dsRNA templates, involving RI and RII sequences (Fig. 3.7E-F). RH30 was much less efficient to separate the partial dsRNA templates in the absence of ATP or when we added its helicase core mutant RH30($F_{416}L$) (Fig. 3.7E, lanes 6-9; 3.7F, lanes 5-8). It is possible that the residual strand-separation activity of RH30($F_{416}L$) might come from its RNA binding and RNA chaperone activity with the TBSV RNA substrates. Additional biochemical assays will be needed to test if the partial activity of RH30 in the absence of added ATP is due to the possibly copurified residual ATP bound to RH30.

To test if RH30($F_{416}L$) helicase core mutant still has antiviral activity, we performed a TBSV replicase reconstitution assay with yeast cell-free extract [31, 32]. Addition of RH30($F_{416}L$) to the replicase reconstitution assay led to minor inhibition of TBSV repRNA replication (Fig. 3.7G, lanes 1-2). Thus, mutation within the helicase core region of RH30 affected its antiviral activity on TBSV replication in vitro.

RH30 helicase inhibits the binding of the viral replication proteins to the template recruitment element in the viral (+)RNA. To further characterize the restriction

function of RH30 during tombusvirus replication, we tested if RH30 helicase could inhibit the selective binding of p33 replication protein to the viral RNA template in vitro. To this end, we biotin-labeled the RII(+) sequence of TBSV RNA, which represents the RII(+)-SL RNA recognition element required for template recruitment into replication by p33 replication protein [12]. Moreover, RII(+)-SL RNA is also an essential part of an assembly platform for the replicase complex [96]. The biotin-labeled RII(+) RNA was then pre-incubated with purified RH30 (Fig. 3.8A). Then, purified p33C (the soluble C-terminal region, including the RNA-binding and p33:p33/p92 interaction region of p33 replication protein) was added, which can bind specifically to RII(+)-SL if the hairpin structure with the C•C mismatch in the internal loop was formed [12]. After a short incubation, the biotin-labeled RII(+) RNA was captured on streptavidin-coated magnetic beads. After thorough washing of the streptavidin beads, the proteins bound to the RNA were eluted. Western blot analysis with anti-p33 antibody revealed that RH30 in the presence of ATP inhibited the binding of p33C to RII(+)-SL by 50 % (Fig. 3.8A, lane 2 versus lane 3) when compared with the control containing the MBP protein that does not bind to RII(+)-SL [12]. RH30 was less inhibitory of the p33C - RII(+)-SL interaction in the absence of ATP (Fig. 3.8A, lane 4). We also performed the experiments when RH30 and p33C were incubated with biotin-labeled RII(+) RNA simultaneously. Western-blot analysis showed that RH30 was still inhibitory of p33C binding to RII(+)-SL (Fig. 3.8B),

but less effectively than above when RH30 was pre-incubated with the RII(+) RNA. These in vitro results suggest that one of the mechanisms by which RH30 helicase inhibits tombusvirus replication is to inhibit the binding of p33 to the critical RII(+)-SL RNA recognition element required for template recruitment into replication. This inhibition is likely due to local unwinding RII(+)-SL, because the presence of ATP enhanced the inhibitory effect of RH30.

In another set of experiments, we first incubated biotin-labeled RII(+) RNA with p33C, followed by capturing the RNA-p33 complex with streptavidin-coated magnetic beads and then, the addition of RH30 helicase to the beads (Fig. 3.8C). Here we tested the released p33C from the beads in the eluted fraction by Western blotting. Interestingly, increasing the amounts of RH30 added in the presence of ATP led to the release of p33C from the RII(+) RNA (Fig. 3.8C, lane 3-4), whereas RH30 was less efficient in replacing p33C in the absence of ATP (lanes 1-2). Based on these *in vitro* data, we suggest that RH30 helicase could replace the RNA-bound p33C by likely remodeling the RNA-p33 complex in an ATP-dependent manner.

RH30 helicase is co-localized with the viral dsRNA replication intermediate within the tombusvirus replication compartment in plants. We also tested the localization of RH30 helicase in comparison with the viral repRNA in *N. benthamiana*. The TBSV

repRNA carried six copies of the RFP-tagged coat protein recognition sequence from bacteriophage MS2 in either plus or minus polarity [10]. CNV served as a helper virus in these experiments. Interestingly, RH30 was co-localized with both (-)repRNA and (+)repRNA, which were present in the replication compartment decorated by the TBSV p33-BFP (Fig. 3.9A-B). The RFP signal within the replication compartment was usually weaker when RH30 helicase was expressed, likely due to the inhibitory effect of RH30 on tombusvirus replication. A similar outcome was observed when the viral dsRNA replication intermediate, detected via dsRNA probes [161], was co-localized with RH30 helicase within the replication compartment (Fig. 3.10). These data demonstrate that RH30 helicase relocates to the replication sites where tombusvirus RNA synthesis takes place.

RH30 DEAD-box helicase inhibits the accumulation of related and unrelated plant and insect viruses in yeast or plants. To learn if RH30 has restriction function against additional plant viruses, we tested the effect of RH30 expression on TCV carmovirus and red clover necrosis mosaic virus (RCNMV) dianthovirus, both of which belong to the *Tombusviridae* family. Expression of AtRH30 in *N. benthamiana* plants led to complete block of TCV gRNA accumulation and ~4-fold reduction in RCNMV RNA1 accumulation (Fig. 3.11A-B). On the contrary, two separate transgenic RH30 knock-out

lines of *Arabidopsis thaliana* supported increased levels of TCV gRNA accumulation by up to 2-fold (Fig. 3.11C).

The *Arabidopsis*-TCV system was also used to estimate if TCV infection could induce RH30 gene transcription. RT-PCR analysis revealed induction of RH30 mRNA transcription in TCV-infected versus mock-inoculated plants (Fig. 3.11D). All these data are in agreement that RH30 is a strong restriction factor against tombusviruses and related viruses in plants.

To learn if RH30 also has restriction function against an unrelated plant virus, we over-expressed AtRH30 in *N. benthamiana* and measured the accumulation of the unrelated tobacco mosaic tobamovirus (TMV). We observed a ~3-fold reduction in TMV RNA accumulation in *N. benthamiana* leaves expressing the WT RH30, but not in those leaves expressing the helicase core mutant of RH30($F_{416}L$) (Fig. 3.11E). Expression of WT RH30, but not that of the RH30($F_{416}L$) helicase core mutant, also inhibited the accumulation of the insect-infecting Nodamura virus (NoV) by ~3-fold in yeast (Fig. 3.14A). Interestingly, the accumulation of Flock House virus (FHV), an alphanodavirus, which is related to NoV, was only slightly inhibited by the expression of WT RH30 in yeast (Fig. 3.14B). Based on these observations, we suggest that the plant RH30 DEAD-box helicase has a broad-range CIRF activity against several RNA viruses.

3.4 Discussion

DEAD-box RNA helicases are the most numerous among RNA helicases [112, 113]. They are involved in all facets of RNA processes in cells. RNA viruses and retroviruses also usurp several DEAD-box helicases to facilitate their replication and other viral processes during infection [172, 173]. However, the host also deploys DEAD-box helicases to inhibit RNA virus replication [172, 174]. Accordingly, in this work we present several pieces of evidence that the DDX17-like RH30 DEAD-box helicase restricts tombusvirus replication, including the peroxisomal replicating TBSV and CNV and the mitochondrial-replicating CIRV in yeast and plants, and the more distantly related TCV and RCNMV and the unrelated TMV in plants. On the contrary, knock-down of RH30 enhances the replication of these three tombusviruses in *N. benthamiana* or the related TCV in RH30 knock-out lines of *Arabidopsis*. On the other hand, the helicase core mutant RH30 can only partially inhibit tombusvirus replication in plants or in vitro, suggesting that the helicase function of RH30 is needed for its full antiviral activity.

How can RH30 restrict TBSV replication? We show that the antiviral RH30 helicase binds to p33 and p92 replication proteins based on co-purification experiments of the

viral replicase complex, a pull down assay, and BiFC in *N. benthamiana*. We propose that the interaction of RH30 helicase with the viral replication proteins might be important for the targeting of RH30 into the viral replication compartment (Fig. 12). Accordingly, RH30 is recruited into the viral replication compartment from the cytosol and the nucleus based on live imaging in plant cells (Fig. 3). The targeting of RH30 into the replication compartment is critical for its antiviral function, because fusion of a nuclear retention signal with RH30, which leads to its enrichment in the nucleus at the expense of the cytosolic pool of RH30, in turn, cancelled out the antiviral effect of RH30. Yeast CFE-based replicase reconstitution assays showed that RH30 acts in the early steps of replication, since both (-) and (+)RNA synthesis was inhibited by RH30 (Fig. 6). Moreover, the in vitro RdRp activation assay demonstrated that RH30 inhibited the TBSV RdRp activation step during the replication process as well (Fig. 6C). In contrast, the CFE-based TBSV replication was not inhibited by RH30 after replicase assembly was completed (see step 2, Fig. 6B). These data suggest that RH30 DEAD-box helicase must act at the earliest steps in the replication process to inhibit TBSV replication.

RH30 also binds to the viral RNA, including the 5' UTR (i.e., RI) and RII internal sequence present within the p92 coding region (Fig. 7). Using in vitro interaction and replication assays between RNA-p33 replication protein, we show that RH30 inhibits several steps in tombusvirus replication. These include the RH30-based inhibition of (i)

the specific recognition of the critical RII(+)-SL cis-acting element in the viral (+)RNA by p33 replication protein, which is absolutely required for template recruitment into VRCs, (ii) the activation of the viral p92 RdRp, and (iii) the assembly of the VRCs [31, 133, 175]. Moreover, RH30 helicase could disassemble viral RNA-p33 complexes by likely remodeling the RNA structure in an ATP-dependent manner (Fig. 8). However, RH30-mediated disassembly of viral RNA-p33 complexes is unlikely to occur after VRC assembly is completed, because RH30 helicase was not an effective restriction factor when added at a late step of TBSV replication (step 2, Fig. 6B). We propose that the membrane-bound TBSV VRCs are protecting the viral RNA-p33 complexes by restricting accessibility of the VRC complex to RH30 DEAD-box helicase. Accordingly, we have shown before that the fully-assembled TBSV VRCs are resistant to cellular ribonucleases [38]. Therefore, RH30 helicase might only be able to disassemble viral RNA-p33 complexes before the vesicle-like spherule formation, which is the characteristic structure of the TBSV VRCs in yeast and plants [176]. Altogther, the in vitro assays provide plentiful data on the direct inhibitory effect of RH30 helicase on TBSV replication, indicating that RH30 functions as an effector-type, not signaling-type, DEAD-box helicase, which detect viral RNA and send signals to downstream components of the innate immunity network [174]. Future experiments will address if RH30 might have additional mechanisms to restrict tombusvirus replication.

A recently emerging concept in innate immunity is the significant roles of DEAD-box helicases expressed by host cells that greatly reduce virus replication and facilitate combating viruses and making the induced and passive innate immune responses more potent. Many of the identified yeast DEAD-box helicases with restriction functions are conserved in plants and mammals. Altogether, the genome-wide screens performed with animal viruses have shown that helicases are the largest group of host proteins affecting RNA virus replication. For example, in case of HIV, the involvement of several cellular helicases has been demonstrated, including DDX17 and DDX3 [173, 177, 178]. Yet, the functions of the cellular helicases during virus replication are currently understudied.

The emerging picture in plant-virus interactions, similar to animal-virus interactions, is the diverse roles of various host RNA helicases. Different plant viruses have been shown to co-opt plant RNA helicases for pro-viral functions. These include RH8 and RH9 for potyvirus replication and RH20, RH2 and RH5 for TBSV replication [77-79, 103, 104, 144]. However, this paper shows evidence that a plant DEAD-box helicase, RH30, can also be utilized by host plants for antiviral functions. Thus, in addition to the previously identified Dicer-like RNA helicases [129, 179-181], additional plant RNA helicases might function as CIRFs by recognizing plant virus RNAs. The DDX17-like RH30 DEAD-box helicase characterized here opens up the possibility that

among the more than 100 DEAD-box helicases of plants, there are additional ones with antiviral functions, serving as effector-type or sensor-like RNA helicases. The discovery of the antiviral role of RH30 helicase illustrates the likely ancient roles of RNA helicases in plant innate immunity.

Primers (# NO.)	Sequences
471	CCCGCTCGAGGGAAATTCTCCAGGATTTCTC
1069	CCGGTCGAGCTCTACCAGGTAATATACCACAACGTGTGT
1567	GCAGCTCGAGACCATGCCAAAAAAGAAAAGAAAAAGTGGCT
1568	CGACGGATCCGTAGATGCCGGAGTTT
2691	CGGAGATCTATGGCCTCCTCCGAGGAC
2859	TAATACGACTCACTATAGGAACCAAATCATTCATGTTGCTCTC
2860	TAGTGTATGTGATATCCCACCAA
5051	GGATCTAGATTAGGCGCCGGTGGAGTGG
5753	CGCGTCTAGATTACCAAGTCCTCTTTCCAC
5754	CGCGCTCGAGATGAGCTCGTATGATCGTAG
5905	GGAAGATCTATGGTGAGCAAGGGCGAG
6061	CGCGTCTAGAATGAGCTCGTATGATCGTAG
6062	CGCGCTCGAGTTACCAAGTCCTCTTTCCAC
6069	GCGCGGATCCGTCCTCGATGTTGTGGC
6512	CCGCTCGAGCTGAGTCCGGACTTGTATAG
6192	CGCAACAAGCTAGGACAACAGTCC
6193	TAATACGACTCACTATAGGGCCGCTACCGGCGGTTAGGGGAGG
6513	CGCGGAGCTCTTACTGAGTCCGGACTTGTATAG
6706	ATGGGAGTAAAATCCTAATTTTGGTGGAGACAAAGAGAGGGTGTG
6707	CACACCCTCTCTTTGTCTCCACCAAAATTAGGATTTTACTCCCAT
6839	CCGGGCCCTTACCAAGTCCTCTTTCCAC
6876	CCCAAGCTTGCCAACTTTTTTGTACAAAC
6877	CCGCTCGAGATGCATCATCACCATCACCATATGCCAAAAGTGAACCGAGGAA
6880	ATGAGCTCGTATGATCGTAG
7304	GAAGATCTATGAGCTACTCTAATTACGACTCC
7305	ACGCGTCGACAAAGCCACTGTCCCGGCCCATAC
7306	GAAGATCTTATGATTTCCCTTCAAATCTTGAGG
7307	ACGCGTCGACCTACCAAGGCCTTCTACCAAGC
7990	GGAGTTAATACGACTCACTATAGGGAGAGAGAGGAAAACCCACCTTCAAAAGGTG
7991	GGAGTTAATACGACTCACTATAGGGAGAGAGAGACCAAGCGGAATTACGTTGG

Table 3.1 Sequences of primers used in this study.

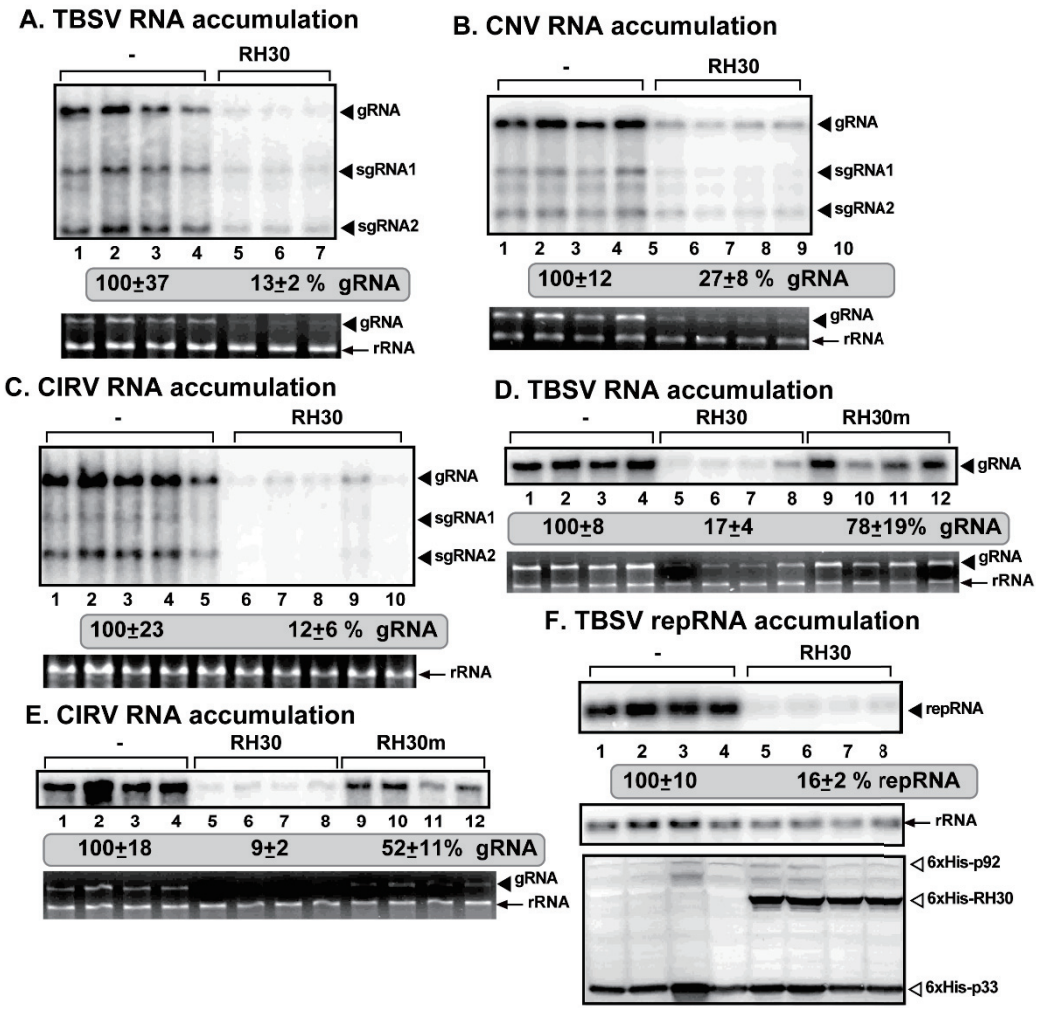
A. TBSV RNA accumulation
-
RH30
gRNA
sgRNA1
sgRNA2
1 2 3 4 5 6 7
100±37
13±2 % gRNA
gRNA
rRNA
B. CNV RNA accumulation
-
RH30
gRNA
sgRNA1
sgRNA2
1 2 3 4 5 6 7 8 9 10
100±12
27±8 % gRNA
gRNA
rRNA
C. CIRV RNA accumulation
-
RH30
gRNA
sgRNA1
sgRNA2
1 2 3 4 5 6 7 8 9 10
100±23
12±6 % gRNA
rRNA
D. TBSV RNA accumulation
-
RH30
RH30m
gRNA
1 2 3 4 5 6 7 8 9 10 11 12
100±8
17±4
78±19% gRNA
gRNA
rRNA
E. CIRV RNA accumulation
-
RH30
RH30m
1 2 3 4 5 6 7 8 9 10 11 12
100±18
9±2
52±11% gRNA
gRNA
rRNA
F. TBSV repRNA accumulation
-
RH30
repRNA
1 2 3 4 5 6 7 8
100±10
16±2 % repRNA
rRNA
6xHis-p92
6xHis-RH30
6xHis-p33

Fig. 3.1

Figure 3.1 Expression of AtRH30 DEAD-box helicase inhibits tombusvirus genomic (g)RNA replication in N. benthamiana plant and in yeast surrogate host. *N. benthamiana plants expressing AtRH30 were inoculated with (A) TBSV, (B) CNV, (C) CIRV, respectively. Top panel: Northern blot analyses of tombusvirus gRNA using a 3' end specific probe shows reduced accumulation of gRNA and subgenomic RNAs in plants expressing RH30 than in control plants. Bottom panel: Ethidium-bromide stained gel shows 18S ribosomal RNA as a loading control. (D-E) Expression of the helicase core mutant of RH30 (RH30m, $F_{416}L$) inhibited TBSV or CIRV replication, respectively, to a lesser extent, demonstrating the requirement of the helicase/ATPase function of RH30 for its full virus restriction function. See further details in panel A. Each experiment was repeated at least three times. (F) Expression of RH30 inhibits TBSV replication in yeast. Top panel: Northern blot analysis of TBSV repRNA using a 3' end specific probe shows reduced accumulation of repRNA in WT yeast strain expressing RH30. Viral proteins His_6-p33 and His_6-$p92^{pol}$ were expressed from plasmids from the CUP1 promoter, while DI-72(+) repRNA was expressed from the GAL1 promoter. His_6-RH30 was expressed from a plasmid. Middle panel: Northern blot with 18S ribosomal RNA specific probe was used as a loading control. Bottom images: Western blot analysis of the level of His_6-p33, His_6-$p92^{pol}$ and His_6-RH30 with anti-His antibody.*

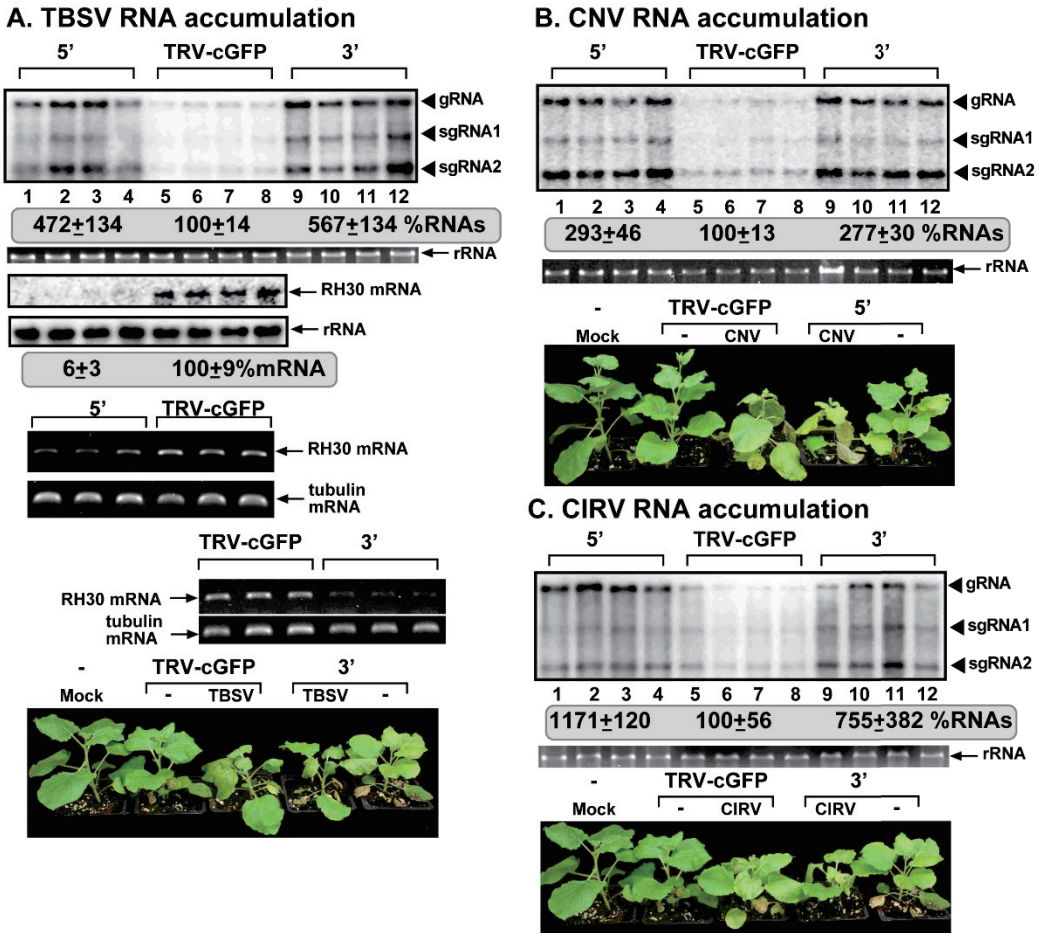
A. TBSV RNA accumulation
5'
TRV-cGFP
3'
gRNA
sgRNA1
sgRNA2
1 2 3 4 5 6 7 8 9 10 11 12
472±134 100±14 567±134 %RNAs
rRNA
RH30 mRNA
rRNA
6±3 100±9%mRNA
5'
TRV-cGFP
RH30 mRNA
tubulin mRNA
TRV-cGFP
3'
RH30 mRNA
tubulin mRNA
-
TRV-cGFP
3'
Mock
-
TBSV
TBSV
-
B. CNV RNA accumulation
5'
TRV-cGFP
3'
gRNA
sgRNA1
sgRNA2
1 2 3 4 5 6 7 8 9 10 11 12
293±46 100±13 277±30 %RNAs
rRNA
-
TRV-cGFP
5'
Mock
-
CNV
CNV
-
C. CIRV RNA accumulation
5'
TRV-cGFP
3'
gRNA
sgRNA1
sgRNA2
1 2 3 4 5 6 7 8 9 10 11 12
1171±120 100±56 755±382 %RNAs
rRNA
-
TRV-cGFP
3'
Mock
-
CIRV
CIRV
-

Fig. 3.2

Figure 3.2 Knockdown of NbRH30 gene expression leads to enhanced tombusvirus replication in N. benthamiana plants. *(A) Top panel: Accumulation of the TBSV genomic (g)RNA and sgRNAs in RH30-silenced N. benthamiana plants 1.5 days post-inoculation (dpi) was measured by Northern blot analysis. Inoculation of TBSV gRNA was done 12 d after silencing of RH30 expression. VIGS was performed via agroinfiltration of tobacco rattle virus (TRV) vector carrying 5' or 3'-terminal NbRH30 sequences, whereas as a control, 3'-terminal GFP sequences. Second panel: Ribosomal RNA is shown as a loading control in an ethidium-bromide stained agarose gel. Third panel: Northern blot analysis shows the knock-down level of NbRH30 mRNA in the silenced and control plants. Fourth panel: Northern blot analysis shows 18S ribosomal RNA as a loading control. Fifth and seventh panels: RT-PCR analysis of NbRH30 mRNA level in the silenced and control plants. Sixth and eighth panels: RT-PCR analysis of TUBULIN mRNA level in the silenced and control plants. Each experiment was repeated three times. Bottom panel: Accelerated and more severe TBSV-induced symptom development is observed in RH30-silenced N. benthamiana plants as compared with the control plants. Note the mild growth defect phenotype in RH30-silenced N. benthamiana plants. The picture was taken 5 dpi. (B-C) Top panel: Accumulation of the CNV or CIRV gRNA in RH30-silenced N. benthamiana plants 2 days post-inoculation (dpi) was measured by Northern blot analysis. See further details in panel A.*

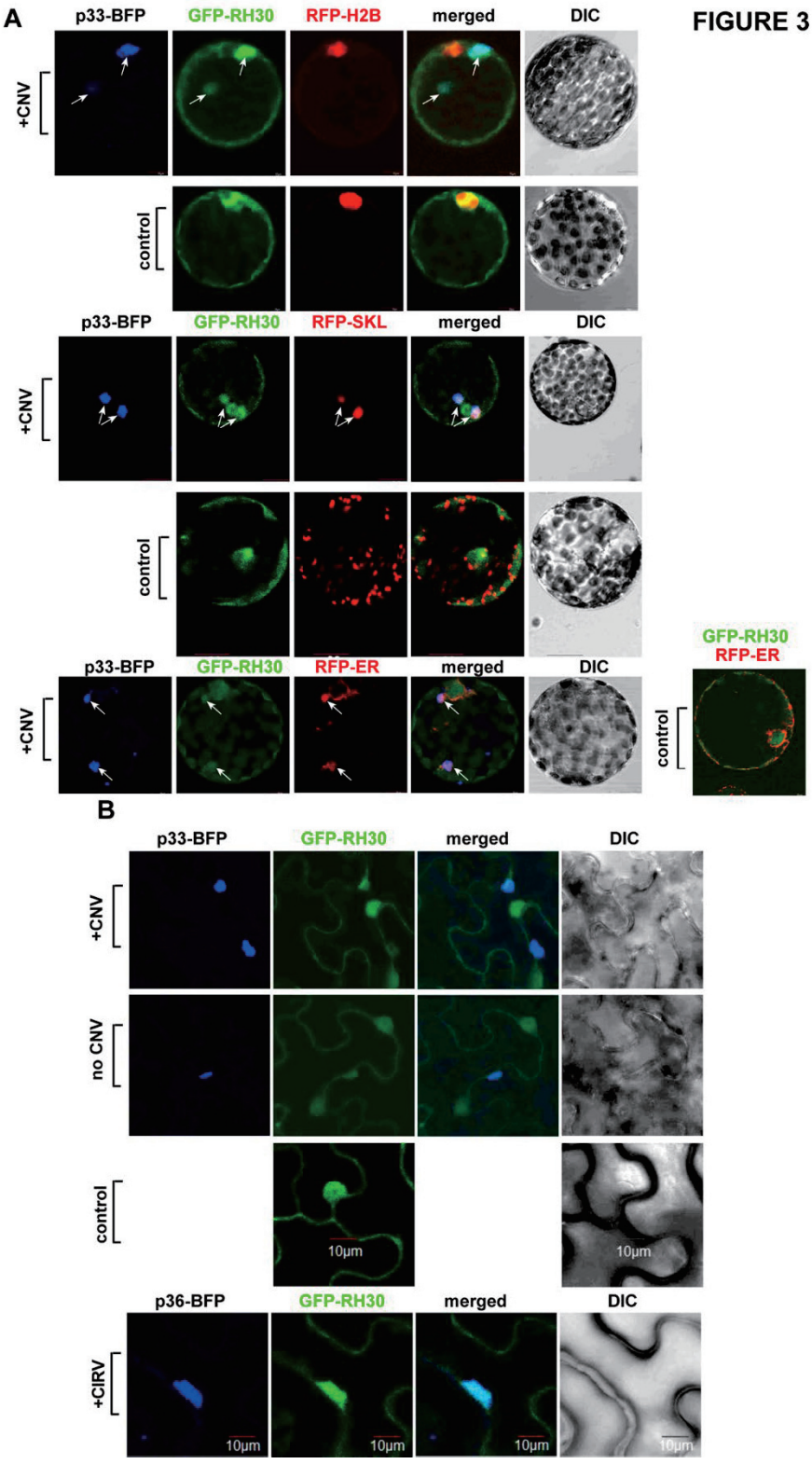

FIGURE 3

Fig. 3.3

Figure 3.3 Confocal microscopy shows the retargeting of the mostly nuclear RH30 into the large replication compartment in plant protoplasts and whole plants infected with CNV. *(A) Most of RH30 is re-targeted into the replication compartment marked by the BFP-tagged p33 replication protein (pointed by arrows) in N. benthamiana protoplasts. Second panel: in the absence of viral components, GFP-tagged RH30 is mostly present in the nucleus, as marked by the histone protein (RFP-H2B). Third panel: The re-targeted GFP-RH30 is present in the viral replication compartment, marked by p33-BFP replication protein and RFP-SKL peroxisomal matrix marker. Arrows point at the viral replication compartment. Fourth panel: RH30 is not co-localized to the peroxisomes in the absence of tombusvirus replication. Fifth panel: The re-targeted GFP-RH30 is partially co-localized with the ER marker within the viral replication compartment, marked by p33-BFP replication protein. The leaves of N. benthamiana plants (transgenic plants expressing nucleus marker RFP-H2B or ER marker RFP-ER) were agro-infiltrated to express p33-BFP, GFP-RH30, and $CNV^{20KSTOP}$ gRNA as described [42]. Leaves without the expression of p33-BFP and $CNV^{20KSTOP}$ gRNA were used as controls. The agro-infiltrated leaves were collected to isolate protoplasts for confocal imaging 2.5 days post agro-infiltration. Scale bars represent 10 μm. (B) Confocal microscopy images show co-localization of TBSV p33-BFP or CIRV p36-BFP replication proteins and the GFP-RH30 in planta. The large replication compartment*

was visualized via expression of TBSV p33-BFP or CIRV p36-BFP. Expression of the above proteins from the 35S promoter was done after co-agroinfiltration into N. benthamiana leaves. The leaves of N. benthamiana plants were agro-infiltrated to express TBSV p33-BFP or the CIRV p36-BFP, GFP-RH30, and CNV^{20KSTOP} or CIRV gRNAs as described [42]. Leaves without the expression of p33-BFP or p36-BFP and the viral RNAs were used as controls. The agro-infiltrated leaves were collected for confocal imaging 2.5 days post agro-infiltration. Scale bars represent 10 μm. Each experiment was repeated.

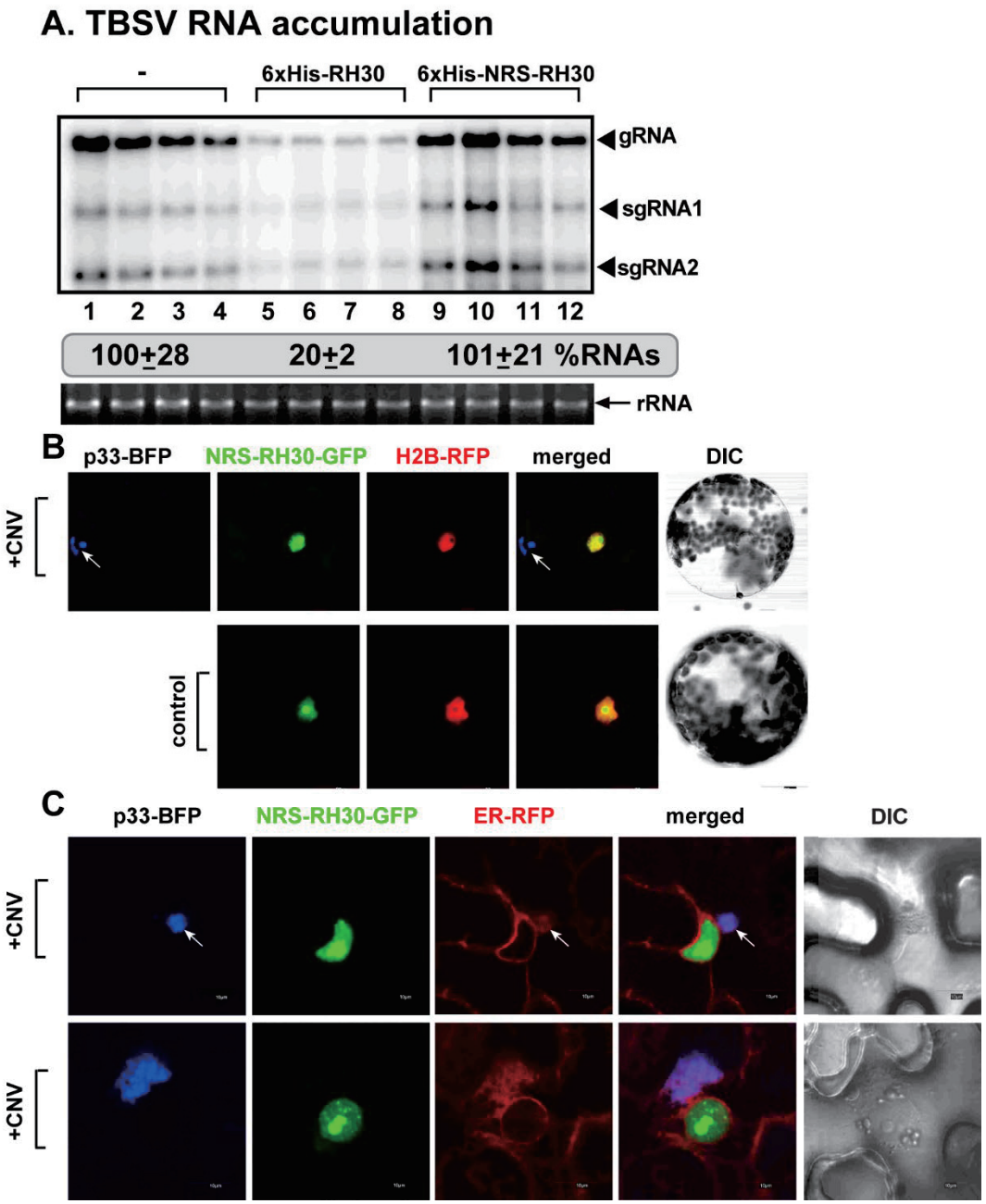
A. TBSV RNA accumulation
-
6xHis-RH30
6xHis-NRS-RH30
gRNA
sgRNA1
sgRNA2
1 2 3 4 5 6 7 8 9 10 11 12
100±28
20±2
101±21 %RNAs
rRNA
B
p33-BFP
NRS-RH30-GFP
H2B-RFP
merged
DIC
+CNV
control
C
p33-BFP
NRS-RH30-GFP
ER-RFP
merged
DIC
+CNV
+CNV

Fig. 3.4

Figure 3.4 Enrichment of AtRH30 in the nucleus nullifies its antiviral effect against TBSV. *(A) Northern blot analysis of TBSV gRNA using a 3' end specific probe shows lack of inhibition of gRNA accumulation in plants expressing RH30 fused to an NRS. Bottom panel: Ethidium-bromide stained gel to show 18S ribosomal RNA as a loading control. (B) NRS-RH30-GFP is not re-targeted into the replication compartment marked by the TBSV BFP-tagged p33 replication protein (pointed by an arrow) in N. benthamiana protoplasts. Second panel: in the absence of viral components, NRS-RH30-GFP is present in the nucleus, as marked by the histone protein (H2B-RFP). The leaves of N. benthamiana plants (transgenic plants expressing nucleus marker RFP-H2B) were agro-infiltrated to express p33-BFP, GFP-RH30, and $CNV^{20KSTOP}$ gRNA as described [42]. Leaves without the expression of p33-BFP and $CNV^{20KSTOP}$ gRNA were used as controls. The agro-infiltrated leaves were collected to isolate protoplasts for confocal imaging 2.5 days post agro-infiltration. (C) Confocal microscopy images show different localization of TBSV p33-BFP replication protein and NRS-RH30-GFP in N. benthamiana cells infected with CNV. The large replication compartment was visualized via expression of TBSV p33-BFP. Expression of the above proteins from the 35S promoter was done after co-agroinfiltration into N. benthamiana leaves. See further details in Fig. 3B. Scale bars represent 10 μm. Each experiment was repeated.*

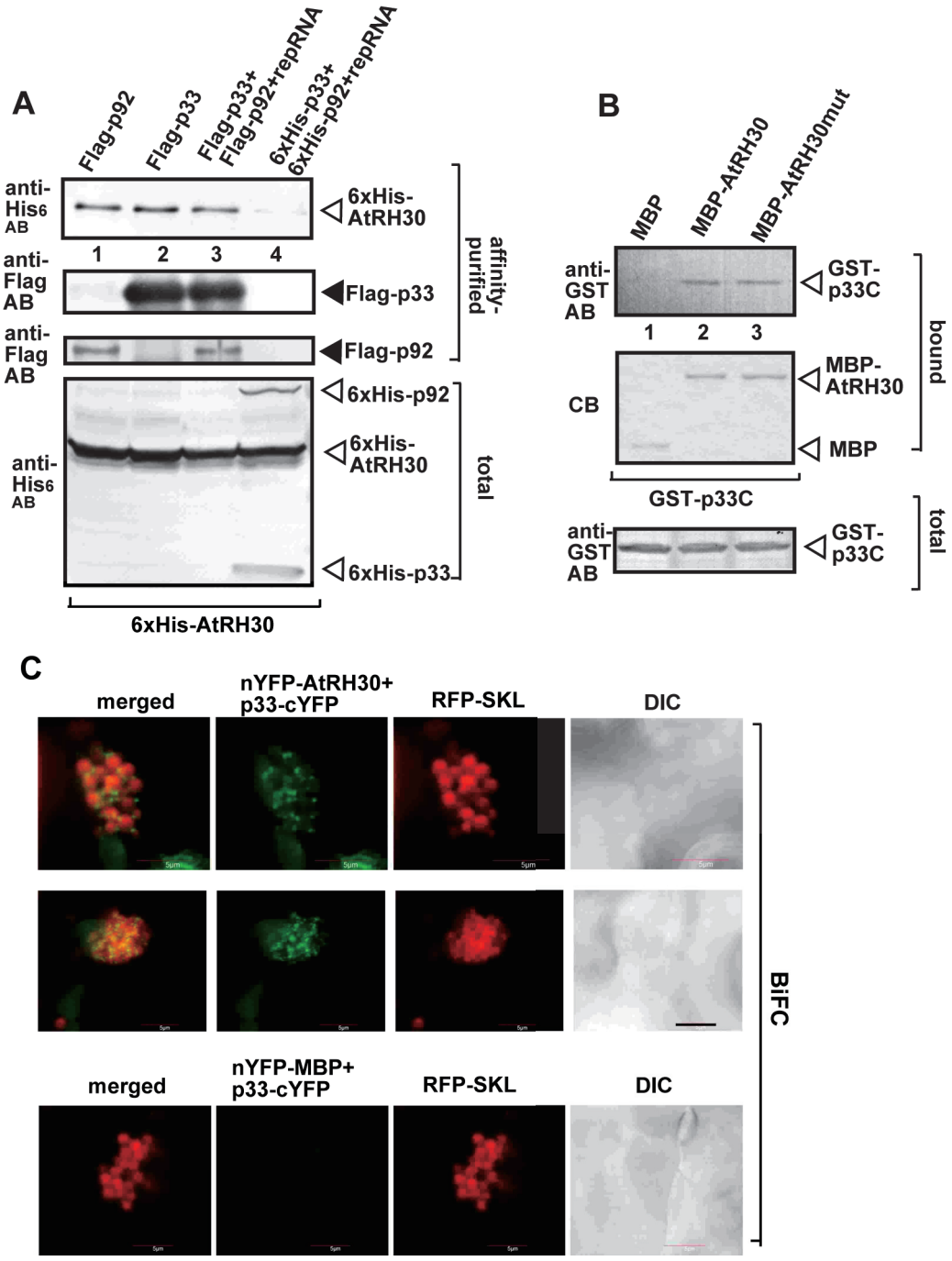
A
Flag-p92
Flag-p33
Flag-p33+ Flag-p92+repRNA
6xHis-p33+ 6xHis-p92+repRNA
anti-His6 AB
6xHis-AtRH30
1 2 3 4
anti-Flag AB
Flag-p33
anti-Flag AB
Flag-p92
affinity-purified
6xHis-p92
anti-His6 AB
6xHis-AtRH30
6xHis-p33
total
6xHis-AtRH30
B
MBP
MBP-AtRH30
MBP-AtRH30mut
anti-GST AB
GST-p33C
1 2 3
CB
MBP-AtRH30
MBP
bound
GST-p33C
anti-GST AB
GST-p33C
total
C
merged
nYFP-AtRH30+ p33-cYFP
RFP-SKL
DIC
BiFC
merged
nYFP-MBP+ p33-cYFP
RFP-SKL
DIC

Fig. 3.5

Figure 3.5 Co-purification of RH30 helicase with the viral replicase from membranous fraction of yeast. *(A) Co-purification of His_6-tagged RH30 with Flag-p33 and Flag-$p92^{pol}$ replication proteins from subcellular membranes. Top panels: Western blot analysis of co-purified His_6-RH30 (lanes 1, 2, and 3) with Flag-affinity purified replicase, Flag-p33 and Flag-$p92^{pol}$ replication proteins, respectively as shown. His_6-p33, His_6-$p92^{pol}$ and His_6-RH30 were detected with anti-His antibody, while Flag-p33 and Flag-$p92^{pol}$ replication proteins were detected with anti-FLAG antibody. The negative control was from yeast expressing His_6-RH30, His_6-p33 and His_6-$p92^{pol}$ purified in a FLAG-affinity column (lane 4). Bottom panel: blot of total His_6-p33 and His_6-$p92^{pol}$ and His_6-RH30 in the total yeast extracts detected with anti-His antibody. (B) Pull-down assay including TBSV GST-p33 replication protein and the MBP-tagged RH30. Note that we used the soluble C-terminal region of TBSV p33 replication protein, which lacked the N-terminal sequence, including the trans-membrane TM domain. Top panel: Western blot analysis of the captured GST-p33C with the MBP-affinity purified MBP-RH30 or the helicase core mutant of RH30 (RH30mut, $F_{416}L$) was performed with anti-His antibody. The negative control was MBP (lane 1). Middle panel: Coomassie-blue stained SDS-PAGE of the captured MBP-RH30 and MBP. Bottom panel: Western blot analysis of GST-p33C in total E. coli lysates. Each experiment was repeated three times. (C) Interactions between TBSV p33 replication protein and the RH30 helicase*

was detected by BiFC. The TBSV p33-cYFP replication protein and the nYFP-RH30 and the RFP-SKL peroxisomal marker protein were expressed via agro-infiltration. The merged image shows the efficient co-localization of the peroxisomal RFP-SKL with the BiFC signals, indicating that the interaction between the tombusvirus replication protein and the recruited RH30 helicase occurs in the large viral replication compartments, which consist of aggregated peroxisomes. Scale bars represent 5 μm.

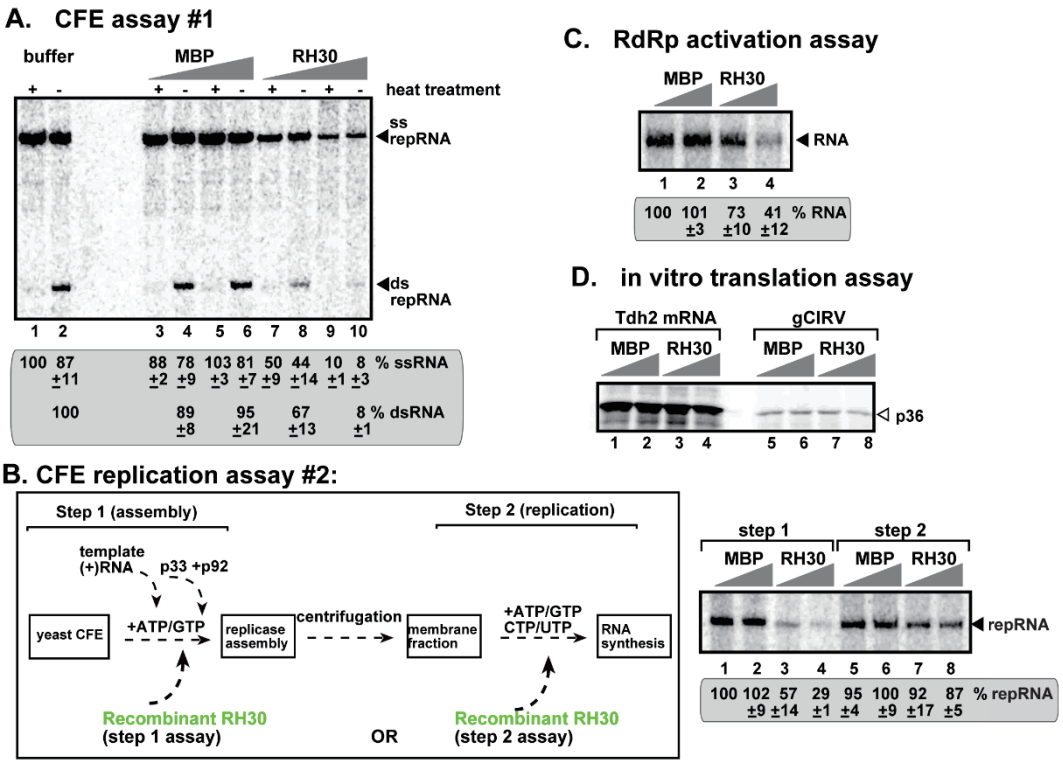
A. CFE assay #1
buffer
MBP
RH30
heat treatment
ss repRNA
ds repRNA
1 2 3 4 5 6 7 8 9 10
100 87 ±11
88 ±2 78 ±9 103 ±3 81 ±7 50 ±9 44 ±14 10 ±1 8 ±3 % ssRNA
100
89 ±8 95 ±21 67 ±13 8 ±1 % dsRNA
C. RdRp activation assay
MBP RH30
RNA
1 2 3 4
100 101 ±3 73 ±10 41 ±12 % RNA
D. in vitro translation assay
Tdh2 mRNA
gCIRV
MBP RH30
MBP RH30
p36
1 2 3 4 5 6 7 8
B. CFE replication assay #2:
Step 1 (assembly)
Step 2 (replication)
template (+)RNA
p33 +p92
yeast CFE
+ATP/GTP
replicase assembly
centrifugation
membrane fraction
+ATP/GTP CTP/UTP
RNA synthesis
Recombinant RH30 (step 1 assay)
OR
Recombinant RH30 (step 2 assay)
step 1
step 2
MBP RH30 MBP RH30
repRNA
1 2 3 4 5 6 7 8
100 102 ±9 57 ±14 29 ±1 95 ±4 100 ±9 92 ±17 87 ±5 % repRNA

Fig. 3.6

Figure 3.6 Inhibition of TBSV repRNA accumulation by RH30 in in vitro replication assay based on cell-free extract (CFE) obtained from WT yeast. *(A) The purified recombinant tombusvirus p33 and p92 replication proteins from E. coli were added in combination with the template (+)repRNA to program the in vitro tombusvirus replication assay. Increasing amounts (1.9 and 5.7 μM) of purified recombinant MBP-RH30 or MBP, as a control, were added to the reactions. Non-denaturing PAGE shows the accumulation of ^{32}P-labeled (+)repRNAs and the dsRNA replication intermediate products made by the reconstituted replicases. Heat treatment, as shown, was applied to demonstrate the dsRNA nature of the replication intermediate. (B) Scheme of the two-step CFE-based in vitro replication assay. Step #1 promotes the assembly of the functional tombusvirus replicase, whereas step #2 supports viral RNA synthesis in the presence of all four ribonucleotides. Note that MBP-RH30 or MBP (1.9 and 5.7 μM), as a control, were added to the reactions either at step #1 or step #2, as shown. The ^{32}P-labeled TBSV repRNA products of the reconstituted replicases were detected by denaturing PAGE. (C) The in vitro RdRp activation assay is based on (+)repRNA and p92-Δ167N RdRp protein in the presence of the soluble fraction of yeast CFE. Purified MBP-RH30 and MBP were added in increasing amounts. Denaturing PAGE analysis of the ^{32}P-labeled RNA products obtained in an in vitro assay with recombinant p92-Δ167N RdRp. (D) In vitro translation assay with wheat germ extract programmed with CIRV*

gRNA. Purified MBP-RH30 and MBP were added in increasing amounts (1.9 μM and 3.8 μM). The ^{35}S-methionine-labeled p36 replication protein translation product is detected by SDS-PAGE. Tdh2 mRNA was used as a control. Each experiment was repeated three times.

FIGURE 7

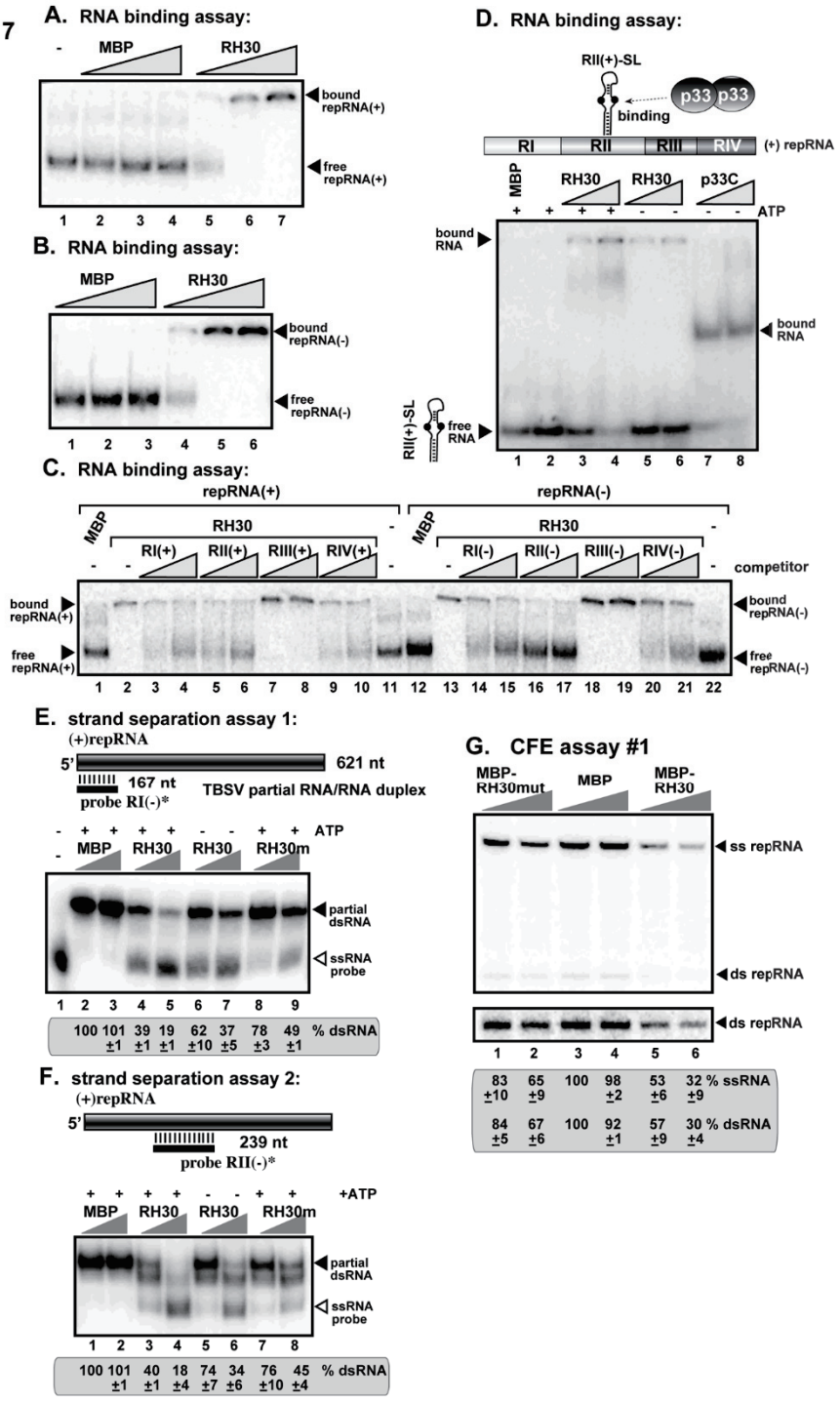

Fig. 3.7

Figure 3.7 RH30 binds to the RII(+)-SL cis-acting element involved in RNA template selection. *(A-B) RNA gel mobility shift analysis shows that MBP-RH30 binds to ^{32}P-labeled (+)repRNA and (-)repRNA, respectively, in vitro. Purified MBP-RH30 or MBP were added in increasing amounts (0.4, 1.9 μM and 5.7 μM) to the assays. The MBP-RH30 - ^{32}P-labeled ssRNA complex was visualized on nondenaturing 5% polyacrylamide gels. Each experiment was repeated at least three times. (C) In vitro RNA binding assay with purified RH30. The assay contained 5.7 μM of purified MBP-RH30 or MBP in combination with the ^{32}P-labeled (+)repRNA template (~0.1 pmol) or (-)repRNA template (~0.1 pmol) and unlabeled competitor RNAs (2 and 4 pmol) representing one of the four regions of TBSV DI-72 RNA from both RNA strands (see panel D) were used in the competition assay. The MBP-RH30 - ^{32}P-labeled ssRNA complex was visualized on nondenaturing 5% acrylamide gels. Each experiment was repeated at least three times. (D) Schematic representation of the four regions carrying cis-acting sequences in the DI-72 (+)repRNA. In vitro RNA binding assay with purified MBP-RH30 (1.9 and 5.7 μM) and the ^{32}P-labeled RII(+)-SL was performed in the presence or absence of 1 mM ATP. MBP-p33C (1.9 and 5.7 μM) representing the C-terminal soluble portion of TBSV p33 replication protein was used as a positive control, whereas MBP was the negative control. See further details in panel A. (E-F) Top: Schematic representation of the partial RNA/RNA duplexes used in the strand separation*

assay. The unlabeled template consists of DI-72 (+)repRNA and a short ^{32}P-labeled complementary (-)RNA (representing either RI or RII in DI-72), which anneals to the 621 nt DI-72 (+)repRNA. Increasing amounts of purified recombinant MBP-RH30, an helicase core mutant of MBP-RH30m or MBP, as a control, were added to the reactions in the presence or absence of ATP. Bottom: Representative native gel of ^{32}P-labeled RNA products after the in vitro strand separation assay. Quantification of the partial dsRNA probe was done with a Phosphorimager. This experiment was repeated two times. (G) Increasing amounts (1.9 and 3.8 μM) of purified MBP-fusion protein or MBP (as a control) were added to the in vitro CFE assay #1. The ^{32}P-labeled RNA productswere detected by nondenaturing PAGE. The bottom image shows the contrasted image of the dsRNA bands of the top image.

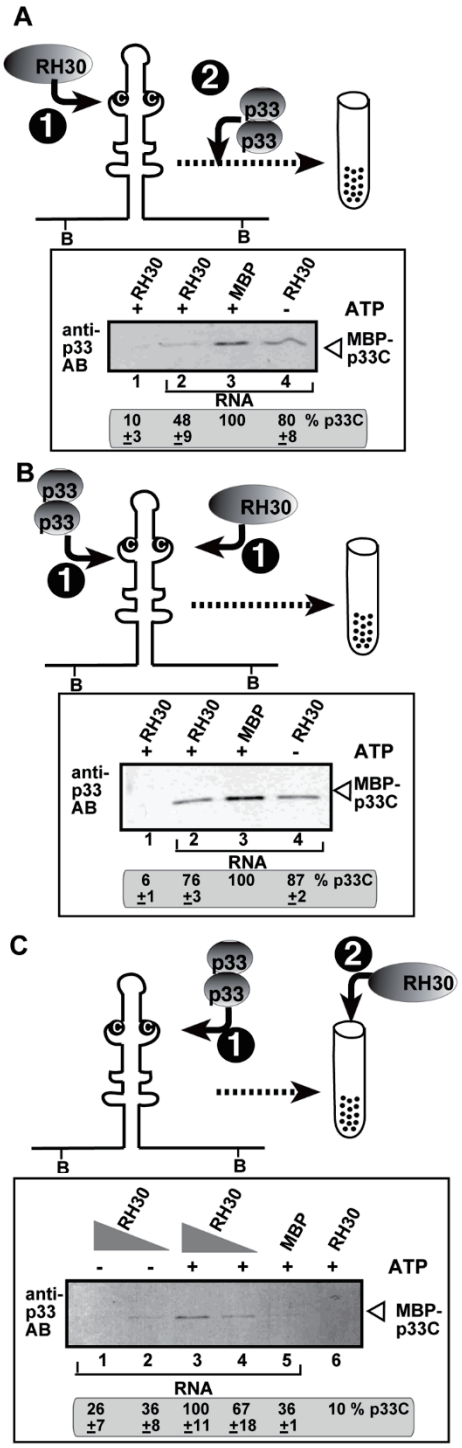
A
RH30
1
2
p33
p33
B
B
+ RH30
+ RH30
+ MBP
- RH30
ATP
anti-
p33
AB
MBP-
p33C
1
2
3
4
RNA
10
±3
48
±9
100
80
±8
% p33C
B
p33
p33
1
RH30
1
B
B
+ RH30
+ RH30
+ MBP
- RH30
ATP
anti-
p33
AB
MBP-
p33C
1
2
3
4
RNA
6
±1
76
±3
100
87
±2
% p33C
C
p33
p33
1
2
RH30
B
B
RH30
RH30
MBP
RH30
- - + + + +
ATP
anti-
p33
AB
MBP-
p33C
1
2
3
4
5
6
RNA
26
±7
36
±8
100
±11
67
±18
36
±1
10 % p33C

Fig. 3.8

Figure 3.8 RH30 DEAD-box helicase inhibits the template recruitment by p33 and promotes the release of the viral (+)RNA from p33 replication protein in vitro. *(A) Top: Scheme of the in vitro assay with biotinylated RII(+) RNA from TBSV bound to streptavidin-coated magnetic beads. The scheme shows the order of addition of biotin-labeled RII(+) RNA, MBP-RH30 and MBP-p33C to the in vitro assay. The RNA probe and MBP-RH30 was allowed to form an RNP complex for 15 min, followed by addition of MBP-p33C protein, and incubation for 15 min. Then, the biotin-labeled RII(+) RNA – protein complex was captured on streptavidin-coated magnetic beads and washed the beads with a buffer. We eluted the proteins from the beads and measured the amounts of MBP-p33C in the eluates by Western blotting using anti-p33 antibody. Reduced amounts of MBP-p33C in the eluates mean that RH30 prevented the binding of p33C to the viral RNA, likely due to remodelling the RNA structure that could not be recognized by p33 any longer. Nonbiotinylated RNA (lane 1) was used as a control. (B) The scheme shows that the biotin-labeled RII(+) RNA, MBP-RH30 and MBP-p33C were added simultaneously to the in vitro assay. See additional details in panel A. (C) Top: The scheme shows that the biotin-labeled RII(+) RNA probe and MBP-p33C was allowed to form an RNP complex for 30 min, followed by capturing the biotin-labeled RII(+) RNA – protein complex on streptavidin-coated agarose beads. Then, we added MBP-RH30 protein with or without ATP, followed by incubation for 15 min and washing the beads*

with a small amount of buffer. Then, we measured the amount of MBP-p33C in the eluates by Western blotting using anti-p33 antibody. Increased amounts of MBP-p33C in the eluates mean that RH30 replaced of p33C to the viral RNA, likely due to remodelling the RNA structure that could not be recognized by p33 any longer. Nonbiotinylated RNA (lane 6) was used as a control. Each experiment was repeated four times.

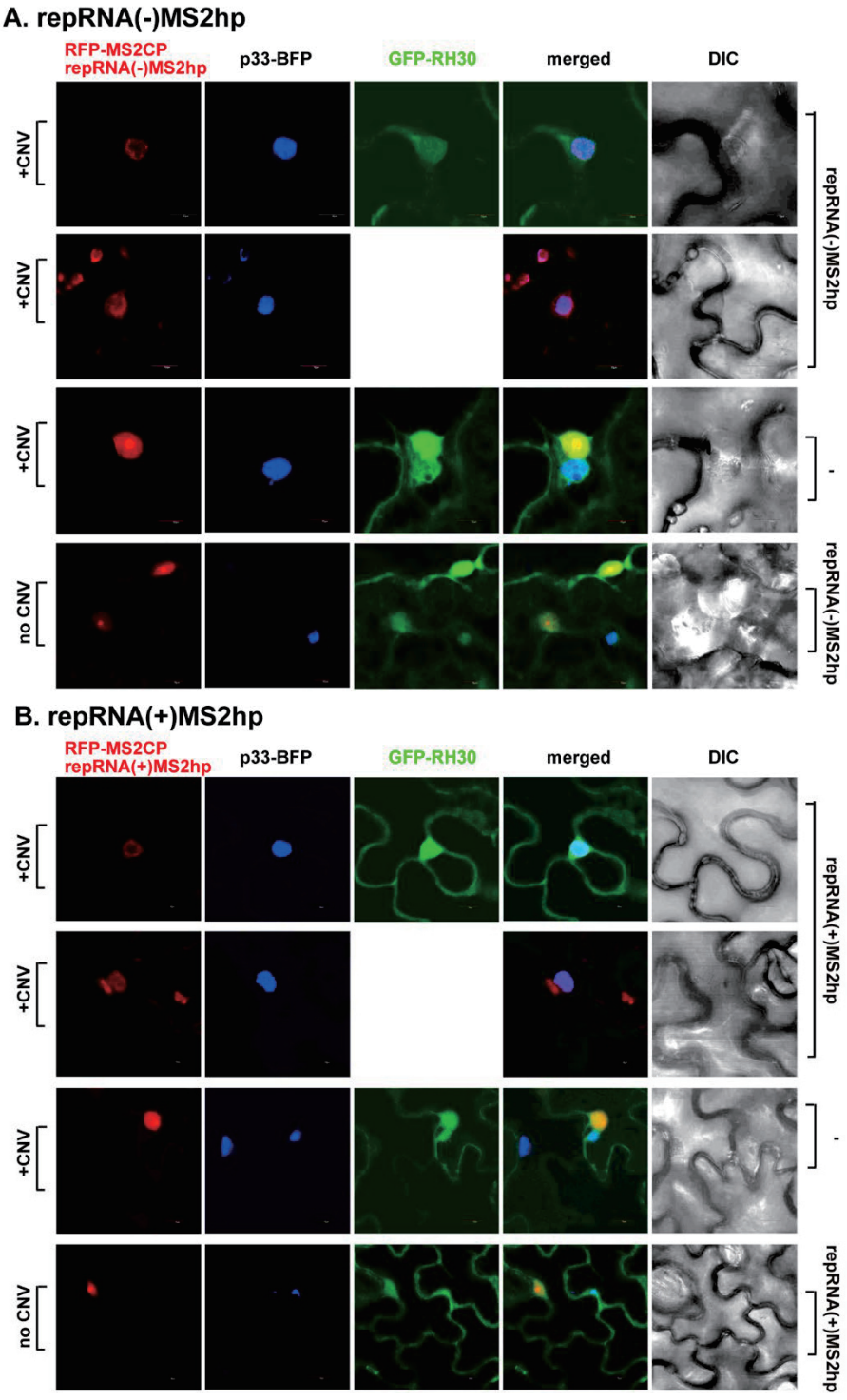
A. repRNA(-)MS2hp
RFP-MS2CP
repRNA(-)MS2hp
p33-BFP
GFP-RH30
merged
DIC
+CNV
+CNV
+CNV
no CNV
repRNA(-)MS2hp
-
repRNA(-)MS2hp
B. repRNA(+)MS2hp
RFP-MS2CP
repRNA(+)MS2hp
p33-BFP
GFP-RH30
merged
DIC
+CNV
+CNV
+CNV
no CNV
repRNA(+)MS2hp
-
repRNA(+)MS2hp

Fig 3.9

Figure 3.9 Confocal microscopy shows co-localization of RH30 with the viral repRNAs in whole plants infected with CNV. *(A-B) Most of RH30 is re-targeted into the replication compartment where RNA synthesis takes place. The viral (-)repRNA and (+)repRNA carried six copies of the MS2 phage RNA hairpin (MS2hp) recognized by MS2 CP fused with RFP. The replication compartment was also marked by the BFP-tagged p33 replication protein in N. benthamiana. Note that RFP-MS2CP contains a weak nuclear localization, therefore this protein ends up in the nucleus in the absence of target RNAs in the cytosol. Expression of the above proteins from the 35S promoter was done after co-agroinfiltration into N. benthamiana leaves. The leaves of N. benthamiana plants were agro-infiltrated to express TBSV p33-BFP, GFP-RH30, RFP-MS2CP, repRNA(-)MS2hp or repRNA(+)MS2hp and the helper virus $CNV^{20KSTOP}$ gRNA. The repRNA(+)MS2hp consists of the repRNA(+) carrying six copies of cis-MS2 hairpin, which can be bound by RFP-MS2CP to show the subcellular localization of repRNA(+). The repRNA(-)MS2hp consists of repRNA(+) carrying six copies of trans-MS2 hairpin, which can only be recognized by RFP-MS2CP when viral RNA replication produces the complimentary strand repRNA(-) by the helper virus $CNV^{20KSTOP}$. The absence of transient expression of GFP-RH30, repRNA(+)/(-)MS2hp or $CNV^{20KSTOP}$ were used as controls. The agro-infiltrated leaves were collected for confocal microscopy imaging 3.5 days post infiltration. Scale bars represent 10 μm. Each experiment was repeated.*

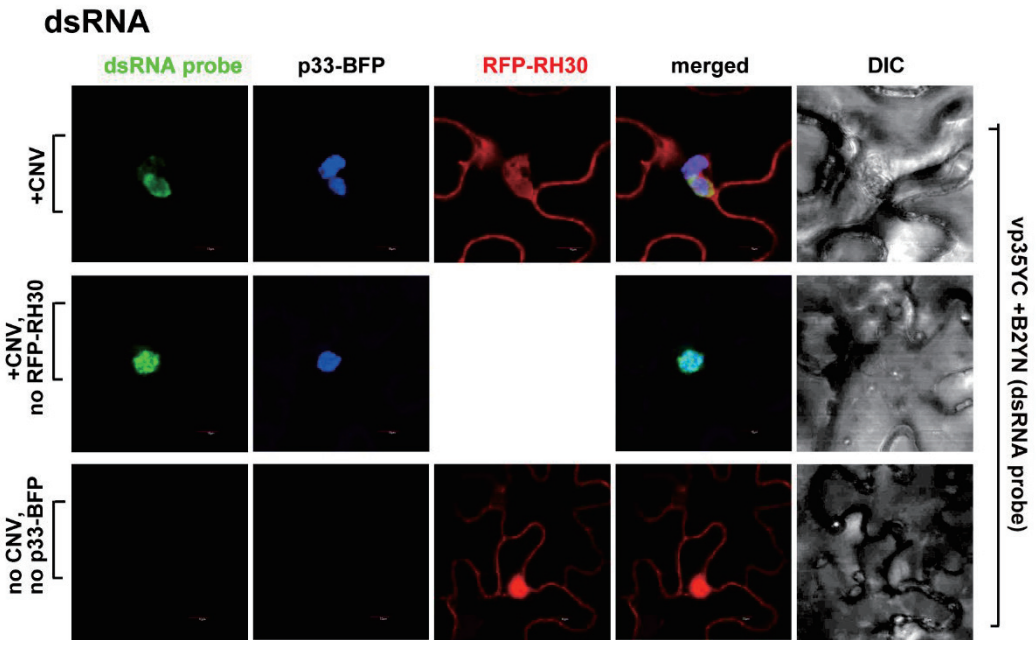
dsRNA
dsRNA probe
p33-BFP
RFP-RH30
merged
DIC
+CNV
+CNV, no RFP-RH30
no CNV, no p33-BFP
vp35YC +B2YN (dsRNA probe)

Fig .3.10

Figure 3.10 Co-localization of the viral double-stranded gRNA with RH30 in whole plants infected with CNV. *The CNV genomic dsRNA replication intermediate was detected via a dsRNA detector assay based on dsRNA binding-dependent fluorescence complementation assay [161]. The assay was performed with two dsRNA binding proteins (i.e., vp35 and B2), which are fused to N- and C-terminal halves of the yellow fluorescence protein (YFP), respectively. Simultaneous binding of the two fusion proteins to the same CNV dsRNA replication intermediate leads to the restoration of YFP fluorescence, allowing the visualization of the viral dsRNA replication intermediate location via confocal microscopy. The dsRNA sensor B2YN and VP35YC plasmids were agro-infiltrated into N. benthamiana leaves at OD_{600} of 0.15, respectively, together with RFP-RH30 and p33-BFP at OD_{600} of 0.5. CNV infection was initiated via agro-infiltration (OD_{600} of 0.15). Leaves were harvested and then immediately subjected to confocal microscopic analysis 2 days after agro-infiltration. The fluorescence complementation was detected via the GFP channel (excitation/emission: 488nm/500-530nm). Top panel: viral dsRNA replication intermediate is co-localized with RFP-RH30 within the replication compartment, which is marked by TBSV p33-BFP. Middle panel: no expression of RFP-RH30 was used as control. Bottom panel: N. benthamiana leaves with no viral components expressed were used as control. Expression of the above*

proteins from 35S promoter was done after co-agroinfiltration into N. benthamiana leaves. Scale bars represent 10 µm. Each experiment was repeated.

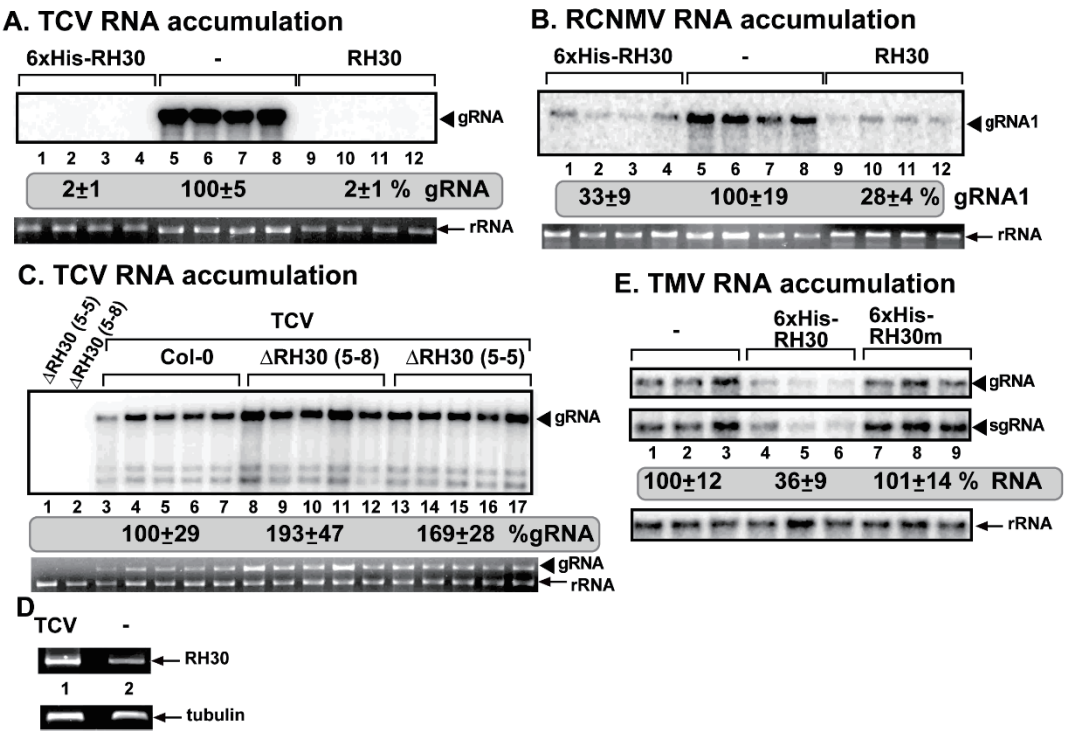
A. TCV RNA accumulation
6xHis-RH30
-
RH30
gRNA
1 2 3 4 5 6 7 8 9 10 11 12
2±1
100±5
2±1 % gRNA
rRNA
B. RCNMV RNA accumulation
6xHis-RH30
-
RH30
gRNA1
1 2 3 4 5 6 7 8 9 10 11 12
33±9
100±19
28±4 %
gRNA1
rRNA
C. TCV RNA accumulation
ΔRH30 (5-5)
ΔRH30 (5-8)
TCV
Col-0
ΔRH30 (5-8)
ΔRH30 (5-5)
gRNA
1 2 3 4 5 6 7 8 9 10 11 12 13 14 15 16 17
100±29
193±47
169±28 %gRNA
gRNA
rRNA
E. TMV RNA accumulation
-
6xHis-RH30
6xHis-RH30m
gRNA
sgRNA
1 2 3 4 5 6 7 8 9
100±12
36±9
101±14 % RNA
rRNA
D
TCV
-
RH30
1 2
tubulin

Fig 3.11

Figure 3.11 Expression of AtRH30 DEAD-box helicase inhibits TCV and RCNMV genomic (g)RNA replication in N. benthamiana plants. *N. benthamiana plants expressing AtRH30 were inoculated with (A) TCV, and (B) RCNMV, respectively. Expression of the above proteins from the 35S promoter was done via co-agroinfiltration into N. benthamiana leaves. Top panel: Northern blot analyses of TCV gRNA and RCNMV RNA1 using 3' end specific probes show reduced accumulation of TCV gRNA and RCNMV RNA1, respectively, in plants expressing RH30 than in control plants. Bottom panel: Ethidium-bromide stained gel to show 18S ribosomal RNA as a loading control. (C) Increased accumulation level of TCV in Arabidopsis RH30 knockout mutants based on Northern blot analysis. Samples in lanes 1 and 2 are from mock inoculated Arabidopsis RH30 knockout mutants. See further details in panel A. (D) Semi-quantitative RT-PCR shows the induction of RH30 mRNA expression in Arabidopsis plants infected with TCV when compared the mock-inoculated plants. Each experiment was repeated. (E) Expression of RH30 and its mutant protein together with the cDNA of full-length TMV from the 35S promoter was done via co-agroinfiltration into N. benthamiana leaves [162]. Top panel: Northern blot analysis of TMV gRNA and subgenomic RNA using a 3' end specific probe shows reduced accumulation of TMV RNAs in leaves expressing RH30, but not RH30m in comparison with the control plants.*

Bottom panel: Northern blot analysis shows the 18S ribosomal RNA as a loading control.

Each experiment was repeated.

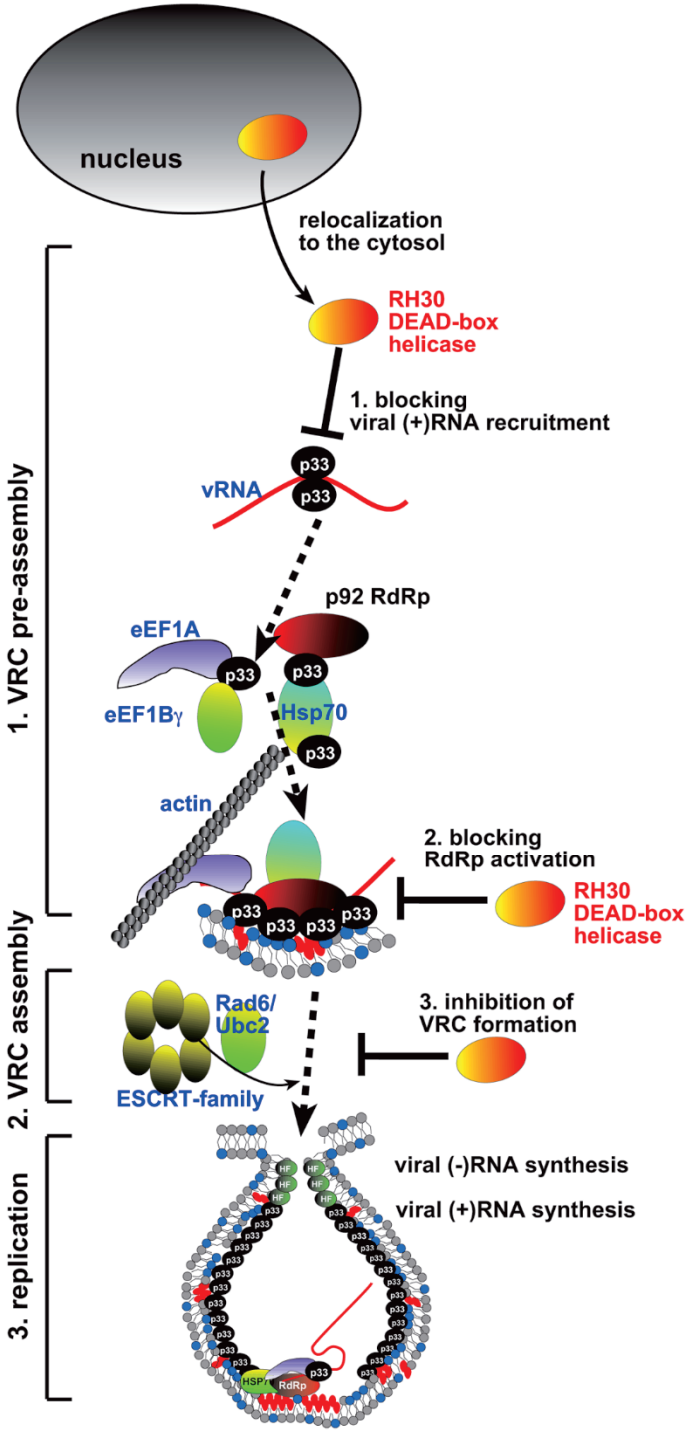
nucleus
relocalization
to the cytosol
RH30
DEAD-box
helicase
1. blocking
viral (+)RNA recruitment
p33
vRNA
p33
p92 RdRp
eEF1A
p33
p33
eEF1Bγ
Hsp70
p33
actin
2. blocking
RdRp activation
RH30
DEAD-box
helicase
p33
p33
p33
p33
Rad6/
Ubc2
3. inhibition of
VRC formation
ESCRT-family
viral (-)RNA synthesis
viral (+)RNA synthesis
HSP70
RdRp
p33
1. VRC pre-assembly
2. VRC assembly
3. replication

Fig. 3.12

Figure 3.12 *Models showing the antiviral functions of the plant RH30 DEAD-box helicase during TBSV replication. Based on our current and previous data, we propose that the DDX17-like RH30 helicase interferes with several major steps during TBSV replication. First, RH30 interferes with the recruitment of the viral (+)RNA through unwinding RII(+)-SL cis-acting RNA element, which specifically binds to p33 replication protein only when the stem-loop structure is formed. Also, RH30 can potentially remodel the p33-(+)RNA complex, thus displacing p33 from the complex. Second: Inhibition of p33-(+)RNA complex formation by RH30 also leads to blocking the activation of the p92 RdRp, which requires the (+)RNA with the stem-loop structure in RII(+)-SL formed. Third, displacing p33 from the p33-(+)RNA complex by RH30 inhibits VRC assembly as well. This is because the stem-loop structure in RII(+)-SL is essential part of the VRC assembly platform. The cytosolic pool of RH30 is essential for the antiviral activity.*

```
CLUSTAL O(1.2.4) multiple sequence alignment

RH30      MSSYDRRFADPNSYRQRSGAPVGSSQPMDPSAAPYNPRYTGGGGGYGPSPVMAGDNSGYN    60
DED1      MAELSEQVQN------------------------LSINDNNENGYVPPHLRGKPRSARN    35
          *:. ..:. :                              .. .** *  : .  .*. *

RH30      RYPSFQPPSGGFSVGRGGG-------RGGYG---QYGDRNGGGNWGGGGGRGGSSKRELD    110
DED1      NSSNYNNNNGGYNGGRGGGSFFSNNRRGGYGNGGFFGGNNGGSRS-----NGRSGGRWID    90
          .  .::  .**:. *****       *****    :*..***..      .* *. * :*

RH30      SV--SLPKQNFGNLVHFEKNFYVESPTVQAMTEQDVAMYRTERDISVEGRDVPKPMKMFQ    168
DED1      GKHVPAPRNEKAEIAIFGV---PEDPNFQSS-GINFDN-YDDIPVDASGKDVPEPITEFT    145
          .     *::: .::. *      *.*..*:    :.     :  :...*:***:*:. *

RH30      DANFPDNILEAIAKLGFTEPTPIQAQGWPMALKGRDLIGIAETGSGKTLAYLLPALVHVS    228
DED1      SPPLDGLLLENIKLARFTKPTPVQKYSVPIVANGRDLMACAQTGSGKTGGFLFPVLSESF    205
          .  : . :** *    **:***:*  . *:. :****:. *:****** .:*:*.* .

RH30      AQP----------RLGQDDGPIVLILAPTRELAVQIQEESRKFGLRSGVRSTCIYGGAPK    278
DED1      KTGPSPQPESQGSFYQRKAYPTAVIMAPTRELATQIFDEAKKFTYRSWVKACVVYGGSPI    265
                       :.  * .:*:*******.** :*::**  ** *::  :***:*

RH30      GPQIRDLRRGVEIVIATPGRLIDMLECQHTNLKRVTYLVLDEADRMLDMGFEPQIRKIVS    338
DED1      GNQLREIERGCDLLVATPGRLNDLLERGKISLANVKYLVLDEADRMLDMGFEPQIRHIVE    325
          * *:*::.** ::::****** *:**  : .* .*.********************:**.

RH30      QIR----PDRQTLLWSATWPREVETLARQFLRDPYKAIIGSTDLKANQSINQVIEIVPTP    394
DED1      DCDMTPVGERQTLMFSATFPADIQHLARDFLSDYIFLSVGRVGSTS-ENITQKVLYVENQ    384
          :       :****::***:* ::: ***:** *     :* .. .: :.*.* :  * .

RH30      EKYNRLLTLLKQLMDGSKILIFVETKRGCDQVTRQLRMDGWPALAIHGDKTQSERDRVLA    454
DED1      DKKSALLDLLSASTDG-LTLIFVETKRMADQLTDFLIMQNFRATAIHGDRTQSERERALA    443
          :* . ** **.   **   ******** .**:*  * *:.: * *****:*****:*.**

RH30      EFKSGRSPIMTATDVAARGLDVKDIKCVVNYDFPNTLEDYIHRIGRTGRAGAKGMAFTFF    514
DED1      AFRSGAATLLVATAVAARGLDIPNVTHVINYDLPSDVDDYVHRIGRTGRAGNTGLATAFF    503
           *:** : ::.** *******: ::. *:***:*. ::**:********** .*:* :**

RH30      THDNAKFARELVKILQEAGQVVPPTLSALVRSS-G------SGYGGSGGGRNFRPRGGGR    567
DED1      NSENSNIVKGLHEILTEANQEVPSFLKDAMMSAPGSRSNSRRGGFGRNNNRDYRKAGGAS    563
          . :*:::.: * :** **.* **  *.  : *: *       *  * ...*::*  **.

RH30      GGGFGDKRSRSTSNFV-----PHGGKRTW------------ 591
DED1      AGGWGSSRSRDNSFRGGSGWGSDSKSSGWGNSGGSNNSSWW 604
          .**:*..***..*         .. .  *
```

Figure 3.13

Figure 3.13 Comparison of the conserved F position in the helicase core domain in the yeast Ded1 and the Arabidosis RH30 DEAD-box helicases.

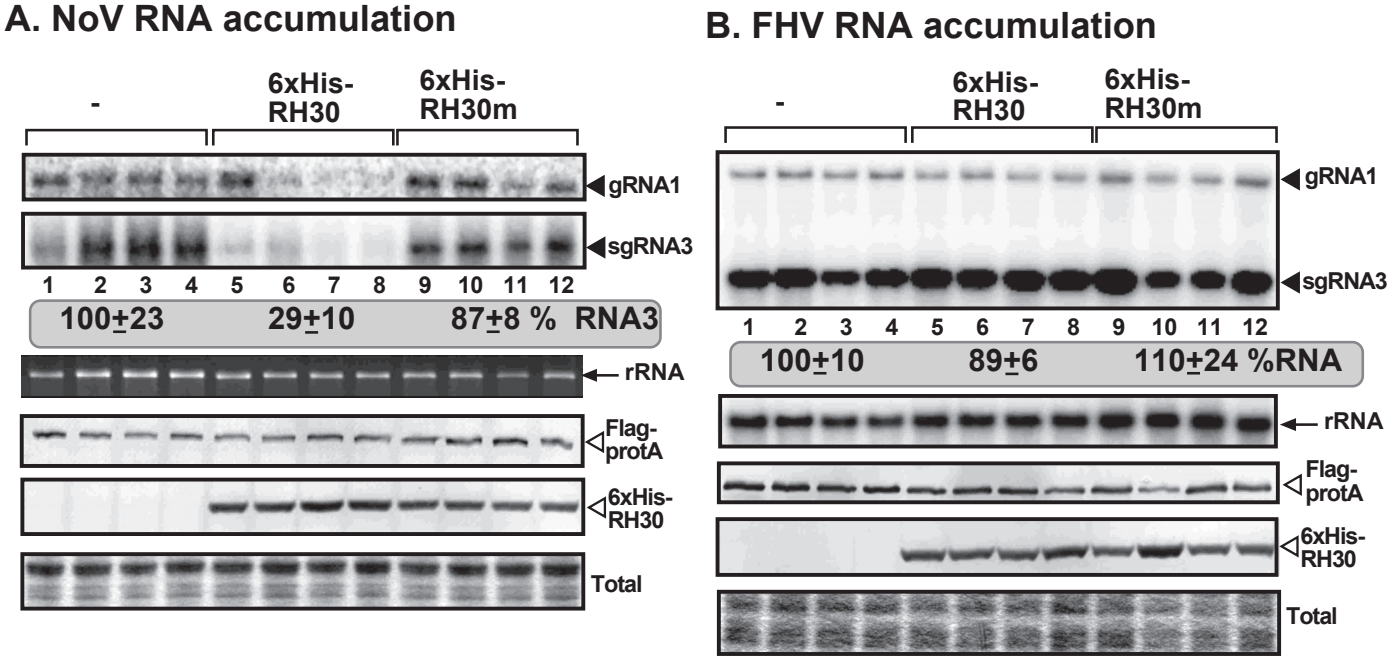
A. NoV RNA accumulation
-
6xHis-RH30
6xHis-RH30m
gRNA1
sgRNA3
1 2 3 4 5 6 7 8 9 10 11 12
100±23
29±10
87±8 % RNA3
rRNA
Flag-protA
6xHis-RH30
Total
B. FHV RNA accumulation
-
6xHis-RH30
6xHis-RH30m
gRNA1
sgRNA3
1 2 3 4 5 6 7 8 9 10 11 12
100±10
89±6
110±24 %RNA
rRNA
Flag-protA
6xHis-RH30
Total

Figure 3.14

Figure 3.14 Expression of AtRH30 DEAD-box helicase inhibits NoV RNA accumulation in yeast. *(A-B) Top panel: Northern blot analysis of NoV (panel A) or FHV (panel B) RNA1 and the subgenomic RNA3 using a 3' end specific probe shows the reduced accumulation of NoV but not FHV RNAs in WT yeast strain expressing His_6-RH30. Viral replication proteins, termed protA, were expressed with a Flag-tag from plasmids from the GAL1 promoter, while the viral RNA templates were also expressed from the GAL1 promoter. His_6-RH30 was expressed from a plasmid. Middle panel: Northern blot with 18S ribosomal RNA specific probe was used as a loading control. Bottom images: Western blot analyses of the level of Flag-protA with anti-Flag antibody and His_6-RH30 with anti-His antibody are shown in the bottom panels with total protein extracts from yeast stained with Coomassie Blue.*

Chapter 4

Changing functional identity: dissecting features affecting pro-viral versus antiviral functions of cellular DEAD-box helicases in tombusvirus replication

4.1 Introduction

Positive-stranded (+)RNA viruses exploit host cells by co-opting many cellular factors to facilitate viral replication. In addition, many (+)RNA viruses take advantage of metabolic pathways, subcellular membranes and intracellular trafficking to build elaborate membranous viral replication compartments (also called viral replication organelles, VROs), which are the sites of viral replication, in the cytosol of the infected cells [21, 23, 26, 29, 46, 122-125]. The emerging picture is that the co-opted host factors affect many steps of RNA virus replication. For example, the assembly of membrane-bound viral replicase complexes (VRCs) is assisted by host translation initiation and elongation factors, protein chaperones, RNA-modifying enzymes, SNARE and ESCRT proteins, the actin network, and lipids [21, 23, 26, 29, 46, 122-125].

The mechanistic roles of host factors in viral RNA replication is intensively studied with *Tomato bushy stunt virus* (TBSV) and other tombusviruses infecting plants. [81, 130, 131]. Expression of the two TBSV replication proteins, termed p33 and $p92^{pol}$,

and a replicon (rep)RNA leads to efficient viral replication in yeast (*Saccharomyces cerevisiae*) surrogate host [24, 132, 133]. The abundant p33 is an RNA chaperone and a master regulator of replication, whereas $p92^{pol}$ is the RdRp [88]. Several cis-acting replication elements have been defined in the TBSV (+) and (-) RNAs which have critical functions in RNA template selection, recruitment, in the assembly of VRCs and in viral RNA synthesis [11, 12, 31, 95, 133, 134, 182].

Among the largest family of cellular proteins affecting TBSV replication is the ATP-dependent DEAD-box RNA helicases. Multiple global screens in yeast with TBSV have identified 11 yeast helicases (10 DEAD-box and 1 DEAH-box helicases) which are involved in viral replication or recombination [90]. Moreover, TBSV, which lacks its own helicase, usurps several plant ATP-dependent DEAD-box RNA helicases to promote TBSV RNA replication. For example, the plant DDX3-like RH20, DDX5-like RH5 and the eIF4AIII-like RH2 DEAD-box proteins affect plus-strand synthesis, viral genome integrity and RNA recombination [78, 79, 103]. On the other hand, the DDX17-like RH30 DEAD-box protein is re-localized from the nucleus to the site of tombusvirus replication via interacting with the TBSV p33 and $p92^{pol}$ replication proteins and inhibits tombusvirus replication through blocking several steps in the replication process. The action of RH30 DEAD-box helicase interferes with VRC assembly, viral RdRp activation and the specific interaction between p33 replication protein and the viral (+)RNA

(Chapter 3).

DEAD-box helicases are a large family of RNA helicases and they are involved in cellular metabolism [58, 135, 136], and in responses to abiotic stress and pathogen infections [112, 137, 138]. DEAD-box helicases unwind RNA duplexes, affect RNA folding and RNA-protein complexes [57]. Interestingly, DEAD-box helicases can open up completely double-stranded RNA regions by directly loading on duplexes and opening up a limited number of base pairs. This unwinding mode is termed local strand separation [57, 113]. Ever increasing data suggest that cellular DEAD-box helicases affect translation and replication of many RNA viruses [77, 139-141]. For example, turnip mosaic virus and brome mosaic virus co-opt cellular DEAD-box helicases for proviral functions in translation or replication [77, 142, 144]. HIV infections are affected by several helicases providing either pro-viral or antiviral functions [173, 183]. Thus, the emerging idea is that cellular DEAD-box helicases are important co-opted host factors for several viruses, whereas other cellular DEAD-box helicases play active roles in restricting RNA virus replication. Overall, cellular DEAD-box helicases perform critical roles in virus-host interactions.

In this work, we characterized domains that specify the viral restriction function of the cellular RH30 DEAD-box RNA helicase and the pro-viral function of the RH20 helicase in tombusvirus replication. Expression of deletion mutants of RH30 and RH20

in *Nicotiana benthamiana* plants revealed that the N-terminal domain is important in determining the function of these helicases. We found that the antiviral helicases target a cis-acting element (RII(+)-SL) in the viral RNA, which is critical during the early steps of replication. Therefore, we suggest that the antiviral DEAD-box helicase must act at the earliest steps in the replication process to inhibit TBSV replication. On the contrary, the pro-viral helicases in this work targeted a different cis-acting element (RI, 5' noncoding region) in the viral RNA, which is needed for (+)RNA synthesis, a latter step in the replication process. This surprising outcome suggests that the antiviral or proviral DEAD-box helicases could be reversed when inhibitory domains are removed from the helicase protein.

4.2 Materials and methods

Yeast strain and expression plasmids. *Saccharomyces cerevisiae* strain BY4741 was obtained from Open Biosystems.

To make deletion mutants of N-terminal domain, helicase core or C-terminal domain of AtRH30, the sequence of AtRH30$^{\Delta 2\text{-}162}$ (also named RH30$^{\Delta N}$ for abbreviation), AtRH30Δ163-591 (named RH30$^{\Delta Hel/\Delta C}$), AtRH30Δ2-162/Δ547-591 (named RH30$^{\Delta N/\Delta C}$) (Fig 4.12) were PCR-amplified from plasmid pGD-AtRH30 [Wu

and Nagy, in press] as follows: the sequence of $RH30^{\Delta N}$ was PCR-amplified with primers #6709 and #5753, followed by the digestion with XhoI and XbaI. The digested product was ligated with XhoI/XbaI-digested pYES-NT vector, resulting in pYES-$AtRH30^{\Delta N}$. In addition, the sequence of $RH30^{\Delta Hel/\Delta C}$ was PCR-amplified with primers #5754 and #6708, followed by the digestion with XhoI and XbaI. The digested product was ligated with XhoI/XbaI-digested pYES-NT vector, resulting in pYES-$AtRH30^{\Delta Hel/\Delta C}$. Moreover, the sequence of $RH30^{\Delta N/\Delta C}$ was amplified by PCR with primers #6709 and #6710, followed by the digestion with XhoI and XbaI. The digested product was ligated with XhoI/XbaI-digested pGD vector, resulting in pGD-$AtRH30^{\Delta N/\Delta C}$.

To generate plasmids for expression of N-terminal Green Fluorescent Protein (GFP)-tagged $AtRH30^{\Delta N/\Delta C}$, the sequence of $AtRH30^{\Delta N/\Delta C}$ was PCR-amplified from plasmid pGD-AtRH30 with primers #6709 and #7838, followed by the digestion with XhoI. The digested product was then ligated with XhoI-digested pGDG vector [152], resulting pGD-GFP-$AtRH30^{\Delta N/\Delta C}$, which was confirmed by PCR with primers #7198 and #7838 for the correct orientation of the ORF.

To clone deletion mutants of N-terminal domain of AtRH20 (Fig 4.1), firstly, a pGD expression vector fused with 3 repeats of HA tag at upstream of multiple cloning sites was created. The sequence of 3xHA was PCR-amplified from pESC-Ura-Vps34-

3xHA [184] with primer #7391 and #7392, followed by the digestion with BglII and XhoI. The digested product was ligated to BamHI/XhoI-digested pGD vector, resulting in pGD-3HA-CY. The sequences of AtRH20 was PCR-amplified from plasmid pGD-AtRH20 [78] with #6509 and #6972, followed by the digestion with BamHI and XbaI. The digested product was then used for the ligation to BamHI/XbaI-digested pGD-3HA-CY vector, resulting in pGD-3HA-AtRH20. The sequences of AtRH20$^{\Delta N2-36}$, AtRH20$^{\Delta N2-58}$ or AtRH20$^{\Delta N2-96}$ were PCR-amplified from plasmid pGD-AtRH20 with #7051 and #6972, #7102 and #6972 or #7393 and #6972, respectively, followed by the digestion with XhoI and XbaI. These digested PCR products were used for ligation with XhoI/XbaI-digested pGD-3HA-CY vector, resulting in pGD-3HA-AtRH20$^{\Delta N2-36}$, pGD-3HA-AtRH20$^{\Delta N2-58}$ and pGD-3HA-AtRH20$^{\Delta N2-96}$.

To obtain the expression vectors for BiFC assay, an N-terminal nYFP expression vector carrying multiple restriction enzyme sites was generated. The sequence of nYFP was PCR-amplified from plasmid pGD-nYFP-MBP [42] with primers #5905 and #6069, followed by the digestion with BglII and BamHI. The digested fragment was ligated with BamHI-digested pGD vector, creating pGD-nYFP-CY. On the other hand, the previous XhoI/XbaI-digested AtRH30$^{\Delta N/\Delta C}$ was used for the ligation with XhoI/XbaI-digested pGD-nYFP-CY, resulting pGD-nYFP-AtRH30$^{\Delta N/\Delta C}$. Besides, the

sequences of AtRH20 or AtRH20$^{\Delta N2\text{-}96}$ were PCR-amplified from plasmid pGD-AtRH20 with primers #6509 and #6972 or #7638 and #6972, respectively, followed by the digestion with BamHI and XbaI. These digested products were used for the ligation with BamHI/XbaI-digested pGD-nYFP-CY, respectively, resulting pGD-nYFP-AtRH20 and pGD-nYFP-AtRH20$^{\Delta N2\text{-}96}$.

To obtain the expression plasmids for MBP or GST fusion proteins, the sequence of RH30$^{\Delta N/\Delta C}$ was PCR-amplified from plasmid pGD-AtRH30 with primers #7638 and #7639, followed by the digestion with XbaI and XhoI. The digested product was ligated to XbaI/SalI-digested pMAL-c2x vector, generating pMAL-AtRH30$^{\Delta N/\Delta C}$. In addition, the previously BamHI/XhoI-digested products of AtRH20 or AtRH20$^{\Delta N2\text{-}96}$ were used for the ligation to pGEX-his-RE vector, producing pGEX-AtRH20 or pGEX-AtRH20$^{\Delta N2\text{-}96}$.

To make chimeric constructs with AtRH20 and AtRH30, the N-terminal domains were swapped between AtRH20 and AtRH30 (Fig 4.1). The sequence of AtRH20$^{\Delta Hel/\Delta C}$ was PCR-amplified from plasmid pGD-AtRH20 with primers #1818 and #6849. The sequence of AtRH30$^{\Delta N}$ was PCR amplified from pGD-AtRH30 with primer #6850 and #5753. These two fragments were used as templates for PCR with primers #1818 and #5753, followed by the digestion with XhoI and XbaI. The digested product was ligated to XhoI/XbaI-digested pGD-3HA-CY vector, resulting

in pGD-3HA-RH233. On the other hand, the sequence of AtRH30$^{\Delta Hel/\Delta C}$ was PCR-amplified from plasmid pGD-AtRH30 with primers #5754 and #6844. The sequence of AtRH20$^{\Delta N}$ was PCR amplified from pGD-AtRH20 with primer #6845 and #6972. These two fragments were used as templates together for PCR with primers #5754 and #6972, followed by the digestion with XhoI and XbaI. The digested product was ligated to XhoI/XbaI-digested pGD-3HA-CY vector, resulting in pGD-3HA-RH322.

The accumulation of viral RNA in yeast and plants. To launch TBSV repRNA replication in yeast *Saccharomyces cerevisiae* wild-type (wt) strain BY4741, yeast cells were transformed with LpGAD-CUP1::HisFlag-p92 and HpGBK-CUP1::HisFlag-p33/GAL1::DI-72. The plasmids for expression of RH30 and its mutants, including pYEX-vector (as a control), pYES-AtRH30, pYES-AtRH30^{F416L}, pYES-AtRH30$^{\Delta N}$ or pYES-AtRH30$^{\Delta Hel/\Delta C}$, were also introduced into yeast cells, respectively. The obtained yeast transformants were grown in SC-ULH^{-} media containing 2% galactose and 0.1mM BCS at 23°C. After 18h, the yeast culture was transferred to SC-ULH^{-} media containing 2% galactose and 50 μM $CuSO_4$ and incubated at 29°C. After 7 h, the obtained yeast cells were used for further Northern blot analysis and Western blot analysis.

To detect the accumulation of tombusviruses in N. *benthamiana* plants

expressing *Arabidopsis* RH20, RH30 and their mutants, the leaves of N. *benthamiana* were infiltrated with *Agrobacterium* carrying pGD-P19 (OD_{600} 0.2) and pGD vector (OD_{600} 0.2, as a control for RH30 and its mutant), pGD-AtRH30 (OD_{600} 0.6), pGD-AtRH30$^{\Delta N/\Delta C}$ (OD_{600} 0.6), pGD-3HA-CY (OD_{600} 0.2, as a control for 3HA-RH20 and it mutants), pGD-AtRH20$^{\Delta N2\text{-}36}$ (OD_{600} 0.6), pGD-AtRH20$^{\Delta N2\text{-}58}$ (OD_{600} 0.6) or AtRH20$^{\Delta N2\text{-}96}$ (OD_{600} 0.6). In the experiment of CNV infection, plants were also co-infiltrated with *Agrobacterium* carrying pGD-CNV^{20Kstop} (OD_{600} 0.2). In the experiment for TBSV or CIRV infections, plants were inoculated with TBSV or CIRV crude sap incoculum, 16 h after agro-infiltration, respectively. Total RNA extraction and Northern blot were performed as described [79] to analyze the accumulation levels of tombusviruses in inoculated leaves at 2.5 d post virus inoculation (dpi) for CNV or CIRV infections and at 1.5 dpi for TBSV infection. Western blot analysis was performed with anti-HA antibody.

Confocal laser microscopy. The subcellular localization of AtRH30$^{\Delta N/\Delta C}$ was observed in plant epidermal cells with the expression of an N-terminal fusion of AtRH30$^{\Delta N/\Delta C}$ to GFP. In the experiments with TBSV and CNV, the transgenic N. *Benthamiana* (expressing H2B fused to RFP, as a nuclear marker) leaves were infiltrated with *Agrobacterium* carrying expression plasmids pGD-p33-BFP (OD_{600}

0.4), pGD-GFP-AtRH30$^{\Delta N/\Delta C}$ (OD_{600} 0.4) and pGD-P19 (OD_{600} 0.2). The leaves were also co-infiltrated with *Agrobacterium* to express CNV^{20Kstop} gRNA for CNV inoculation. For TBSV infection, the infiltrated leaves were inoculated with TBSV sap inoculum 16 h post agro-infiltration. To observe the subcellular localization of GFP-AtRH30$^{\Delta N/\Delta C}$ with cellular markers, the wild-type N. *Benthamiana* leaves were agro-infiltrated to express p36-BFP and CoxIV-RFP (a mitochondria marker) in the case of CIRV infection or p33-BFP and RFP-SKL (peroxisome luminar marker) in the case of TBSV infection together with GFP-AtRH30$^{\Delta N/\Delta C}$ and P19 (as a gene silencing supressor). Approximately 2 days post-virus inoculation, imaging of infiltrated leaves was performed on an Olympus FV1200 confocal microscopy using 60X water-immersion objective equipped lasers. BFP was excited by 405 nm laser. GFP was excited by 488 nm laser and RFP was excited by 543 nm laser. Images were obtained and merged using Olympus FLUOVIEW 1.5.

To detect the interaction between proteins in N. *Benthamiana* plants, bimolecular fluorescence complementation (BiFC) assay was performed with *Agrobacterium* infiltration. The leaves of wild-type N. *benthamiana* were infiltrated with *Agrobacterium* carrying pGD-P19 (OD_{600} 0.2), pGD-RFP-SKL (OD_{600} 0.4) along with different combination of constructs as follows: pGD-nYFP-AtRH30 (OD_{600} 0.4) and pGD-T33-cYFP (OD_{600} 0.4) [42]; pGD-nYFP-AtRH30$^{\Delta N/\Delta C}$ (OD_{600} 0.4) and

pGD-T33-cYFP (OD_{600} 0.4); pGD-nYFP-MBP (OD_{600} 0.4, as a control) and pGD-T33-cYFP (OD_{600} 0.4); pGD-nYFP-AtRH20 (OD_{600} 0.4) and pGD-T33-cYFP (OD_{600} 0.4); pGD-nYFP-AtRH20$^{\Delta N2\text{-}96}$ (OD_{600} 0.4) and pGD-T33-cYFP (OD_{600} 0.4). After 16 h, infiltrated leaves of N. *benthamiana* plants was inoculated with TBSV crude sap inoculum. Approximately 2 days post-virus inoculation, imaging of infiltrated leaves was performed as described above except YFP was excited by 514nm laser.

Purification of recombinant proteins from E. *coli*. Recombinant proteins GST-AtRH20, GST-AtRH20$^{\Delta N2\text{-}96}$, GST, MBP-AtRH30, MBP-AtRH30$^{\Delta N/\Delta C}$, MBP, MBP-p33, MBP-p92 were expressed in E. *coli* and affinity-purified as described [78]. Briefly, E. *coli* strain BL21 (DE3) CodonPlus (Stratagene) cells were transformed with expression plasmids to express the recombinant proteins. The obtained E. *coli* cells were cultured at 37°C for 16h, followed by dilution of the culture to OD_{600} 0.2 with fresh media. The E. *coli* culture was then incubated at 37°C until its OD600 reach 1.0. The culture was added with isopropyl-β-D-thiogalactopyranoside (IPTG) and incubated at 16°C for 8 h. The E. *coli* cells were then collected by centrifugation at 5,000 rpm at 4°C for 5 min, followed by the resuspension with ice- cold column buffer (20mM HEPES [pH7.4], 25 mM NaCl, 1mM EDTA [pH 8.0]) containing 10 mM β-mercaptoethanol and 1 μg of RNase A in each 4 ml of E. *coli* cells suspension.

Sonication was performed on ice to get the cell lysates, followed by centrifugation at 15,000 rpm at 4°C for 15 min. The obtained supernatant was incubated with GST bind resin (EMD Millipore) for GST fusion proteins or amylose resin (NEB) for MBP fusion proteins at 4°C for 2 h, respectively. The resin was then washed with ice- cold column buffer fourtimes. The recombinant protein was eluted with column buffer containing 10mM glutathione and 1mM DTT in pH 7.5 for GST fusion proteins or 0.36% [W/V] maltose and 1mM DTT for MBP fusion proteins.

Analysis of TBSV replication with *in vitro* reconstituted TBSV replicase in yeast cell-free extract (CFE). The yeast cell-free extract (CFE) that supports *in vitro* TBSV reconstituted replicase was prepared with yeast strain BY4741 as described [31, 32]. The *in vitro* reconstituted TBSV replicase assay was performed with the mixture of 2 µl of CFE, 0.5 µg DI-72 (+)repRNA, 0.2 µg affinity-purified maltose-binding protein (MBP)-p33 as well as MBP-$p92^{pol}$ (both recombinant proteins were purified from E. *coli*), 5 µl of buffer A (30mM HEPES-KOH [pH 7.4], 150 mM potassium acetate, 5 mM magnesium acetate, 0.13 M sorbitol), 2 µl of 150 mM creatine phosphate, 0.2 µl of 10 mg/ml creatine kinase, 0.4 µl actinomycin D (5mg/ml), 0.2 µl of 1 M dithiothreitol (DTT), 0.2 µl of RNase inhibitor, 2 µl a ribonucleotide (rNTP) mixture (10 mM of ATP, CTP, and GTP as well as 0.25 mM

UTP) and 0.1 µl of [^{32}P]UTP in a total of 20 µl reaction volume. In addition, about 3.8 µM of purified recombinant proteins was also added in the reaction. The reaction was performed at 25°C for 3h and then stopped by the addition of 5 volumes of 1% SDS and 5 mM EDTA, followed by phenol-chloroform extraction and RNA precipitation. Then the repRNA products and dsRNA intermediates were analyzed by electrophoresis in 0.5X Tris-borate-EDTA (TBE) buffer in a 5% polyacrylamide gel (PAGE) containing 8 M urea.

Double stranded (ds) RNA separation assay. To study if purified recombinant proteins separate dsRNA duplex, the dsRNA separation assay was performed as described [79]. Firstly, the unlabeled single stranded (ss) TBSV (-)repRNA or TBSV (+)repRNA were synthesized by T7 polymerase-based *in vitro* transcription. On the other hand, ^{32}P-labeled ss RI(-), RII(+),RIII(-) or RIV(+) RNAs was synthesized by T7-based *in vitro* transcription along with ^{32}P-labeled UTP, respectively. To prepared partial dsRNA duplexs [RI(-)/ (+)repRNA, RII(+)/ (-)repRNA, RIII(-)/ (+)repRNA and RIV(+)/ (-)repRNA], 2 pmol of ^{32}P-labeled ssRNA were annealed to 6 pmol of unlabeled repRNA in STE buffer (10 mM TRIS, [pH 8.0], 1 mM EDTA, and 100mM NaCl) by slowly cooling down the samples (in a total volume of 20 µl) from 94 °C to 25 °C in 30 min. An increasing amounts (0.95 µM, 1.9 µM, 3.8 µM and 7.6 µM or

with an additional 11.4 μM) of purified MBP fusion proteins or GST fusion proteins were added to the partial dsRNA duplex in RNA binding buffer (10 mM HEPES [pH7.4], 50 mM NaCl, 1 mM DTT, 1 mM EDTA, 5% Glycerol, 2.5 mM $MgCl_2$) supplemented with 1mM ATP, followed by incubation at 25 °C for 25 min. The reaction mixture was then treated with Proteinase K (2 μg/ per reaction) at 37°C for 20 min, followed by analysis with nondenaturing PAGE containing 5% polyacrylamide.

4.3 Results

Dissecting domains specifying the viral restriction function of the cellular RH30 DEAD-box RNA helicase in tombusvirus replication. Sequence comparison of the DDX17-like RH30 DEAD-box RNA helicase from *Arabidopsis*, which shows restriction function against tombusviruses, with the pro-viral DDX3-like RH20 DEAD-box RNA helicase suggests the existence of three domains. The highly conserved core DEAD-box helicase domain is present in the center of these two helicases, whereas the N-terminal and short C-terminal domains are divergent from one another. To identify what domains are responsible for the antiviral function of RH30 DEAD-box RNA helicase, we expressed deletion mutants of RH30 in *Nicotiana benthamiana* plants via agro-

infiltration. Interestingly, expression of the N-domain deletion mutant of RH30 lost its antiviral effect against TBSV replication in the inoculated leaves ($RH30^{\Delta N2\text{-}162}$, Table 4.1). Similarly, expression of the N-terminal domain deletion mutant of $RH30^{\Delta N2\text{-}162}$ did not show antiviral activity in yeast surrogate host (Fig. 4.1A, lanes 17-20 versus 5-8). This conclusion was based on TBSV replicon RNA analysis, which showed no inhibition of viral replication by $RH30^{\Delta N2\text{-}162}$ expression after 24 h of incubation (Fig. 4.1A), suggesting that RH30 requires the N-terminal domain to be an active restriction factor against TBSV replication. Replication of another tombusvirus, carnation Italian ringspot virus (CIRV), which utilizes the outer membranes of mitochondria to build the viral replication compartment, was also not inhibited in *N. benthamiana* by the transient expression of the $RH30^{\Delta N2\text{-}162}$ missing the N-terminal domain (Table 4.1).

As expected, deletion of the core DEAD-box helicase domain in RH30 nullified its antiviral activity against both TBSV and CIRV in *N. benthamiana* ($RH30^{\Delta Hel}$, Table 4.1). In contrast, deletion of the short C-terminal domain in RH30 did not interfere with the restriction function in *N. benthamiana* ($RH30^{\Delta C}$, Table 4.1). Combined deletion of the core DEAD-box helicase and C-terminal domains in RH30 nullified the antiviral activity of RH30 in *N. benthamiana* ($RH30^{\Delta Hel/\Delta C}$, Table 4.1) and in yeast (Fig. 4.1A, lanes 13-16). However, combined deletion of both N- and C-terminal domains, which left only the core DEAD-box helicase domain in RH30, converted this helicase into a

pro-viral factor by increasing TBSV replication by ~2-to-3-fold in *N. benthamiana* (RH30$^{\Delta N/\Delta C}$, Table 4.1 and Fig. 4.1C, lanes 1-4). Expression of RH30$^{\Delta N/\Delta C}$, also enhanced the accumulation of the accumulation of closely-related CNV and CIRV by 2-to-3-fold in *N. benthamiana* (Fig. 4.1E-F, lanes 1-4). This surprising outcome suggests that an antiviral DEAD-box helicase could become a pro-viral factor by modifying domains in the protein.

The pro-viral RH30$^{\Delta N/\Delta C}$ DEAD-box helicase is re-localized into the tombusvirus replication compartment in plants. The antiviral RH30 DEAD-box helicase has to re-localize from the nucleus into the large p33-containing replication compartment in order to restrict tombusvirus replication (Chapter 3). To test if the pro-viral RH30$^{\Delta N/\Delta C}$ helicase is also present in the replication compartment, we co-expressed GFP-tagged RH30$^{\Delta N/\Delta C}$ with p33-BFP replication protein and either H2B-RFP (nuclear marker) or RFP-SKL (a peroxisomal matrix marker) in *N. bentamiana* (Fig. 4.2A-B). Confocal microscopy analysis of in *N. bentamiana* leaves showed the partial re-localization of GFP-RH30$^{\Delta N/\Delta C}$ into the large TBSV replication compartment, which consists of aggregated peroxisomes. GFP-RH30$^{\Delta N/\Delta C}$ helicase was also partially re-targeted in CIRV-infected *N. benthamiana* cells into the CIRV p36 and p95^{pol}-containing replication compartment (Fig. 4.2B, top panel), which consists of aggregated mitochondria [168, 169]. Based on these

experiments, we propose that the nuclear and cytosolic-localized RH30$^{\Delta N/\Delta C}$ helicase is re-targeted into the tombusvirus replication compartment, similar to the full-length RH30 helicase with antiviral function.

To test if the RH30$^{\Delta N/\Delta C}$ helicase interacts with the tombusvirus replication protein, we have conducted bimolecular fluorescence complementation (BiFC) experiments in *N. benthamiana* leaves. Comparison with the antiviral full-length RH30 helicase, RH30$^{\Delta N/\Delta C}$ helicase also showed interaction with the TBSV p33 replication protein within the viral replication compartment, marked by the peroxisomal matrix marker RFP-SKL (Fig. 4.3A-B).

The pro-viral RH30$^{\Delta N/\Delta C}$ DEAD-box helicase promotes tombusvirus RNA synthesis *in vitro*. To gain deeper insight into the pro-viral function of RH30$^{\Delta N/\Delta C}$ helicase, we affinity-purified the recombinant RH30$^{\Delta N/\Delta C}$ helicase from *E. coli*, followed by testing its activity *in vitro* in a TBSV replicase reconstitution assay [31, 32]. Addition of the purified RH30$^{\Delta N/\Delta C}$ helicase to the replicase reconstitution assay, which is based on yeast cell-free extract, led to increased TBSV repRNA replication by ~50% (Fig. 4.4, lanes 1-2). The double-stranded repRNA replication intermediate was also produced by ~40% more efficiently in the presence of RH30$^{\Delta N/\Delta C}$ helicase. These *in vitro* data suggest that RH30$^{\Delta N/\Delta C}$ helicase likely promotes RNA synthesis or the VRC assembly during TBSV

replication. This idea is also supported by the increased level of both (-)RNAs and (+)RNAs observed when RH30$^{\Delta N/\Delta C}$ helicase was expressed in *N. benthamiana* (Fig. 4.1D, lanes 1-3).

The pro-viral RH30$^{\Delta N/\Delta C}$ DEAD-box helicase unwinds critical cis-acting elements in the viral RNA differently than the antiviral RH30 helicase. The antiviral activity of the full-length RH30 DEAD-box helicase is attributed to the efficient unwinding of the secondary structure of the RII(+) region in the TBSV RNA (Chapter 3). RII(+) contains a critical cis-acting stem-loop element, termed RII(+)SL, which is required for the p33-mediated recruitment of the TBSV (+)RNA template into replication [12], and for the activation of the p92 RdRp [133]. Therefore, we tested if the purified RH30$^{\Delta N/\Delta C}$ helicase could unwind partial dsRNA substrates in a dsRNA-strand separation assay, where parts of the TBSV repRNA were double-stranded as shown schematically in Fig. 4.5. Interestingly, unlike the full-length RH30 helicase, the RH30$^{\Delta N/\Delta C}$ helicase was found to inefficiently separate the partial dsRNA template, involving the RII sequence, in the presence of ATP (Fig. 4.5B, lanes 1-4 versus 9-12). These findings suggest that, in contrast with the full-length RH30 helicase, the RH30$^{\Delta N/\Delta C}$ helicase cannot change the RII(+)SL hairpin structure, thus it might not block the binding of TBSV p33 replication protein to the critical RII(+)-SL RNA recognition element required for template

recruitment into replication. In contrast, RH30$^{\Delta N/\Delta C}$ helicase was able to unwind the RI-containing partial dsRNA in vitro (Fig. 4.5A, lanes 1-4 versus 5-8). Helicase-driven unwinding of the dsRNA structure within RI sequence of the dsRNA replication intermediate is critical during initiation of (+)-strand RNA synthesis [78, 104]. The RI(-) region contains the promoter for (+)RNA synthesis, including loading of the p92^{pol} on the (-)RNA template [14].

The pro-viral role of the N-terminal domain of the cellular RH20 DEAD-box RNA helicase in tombusvirus replication. To learn if the above findings of reversing the viral restriction function of the RH30 DEAD-box RNA helicase from *Arabidopsis* could be generalized, we also tested the pro-viral DDX3-like RH20 DEAD-box RNA helicase [78, 104]. To identify what domains are responsible for the pro-viral function of RH20 DEAD-box RNA helicase, we expressed deletion mutants of RH20 in *N. benthamiana* plants via agro-infiltration. Expression of a short N-domain truncation mutant of RH20 led to elimination of the pro-viral activity of the RH20 helicase in TBSV replication in the inoculated leaves (RH20$^{\Delta N2-36}$, Table 4.1). More importantly, expression of the N-terminal domain deletion mutant of RH20 helicase showed antiviral activity in *N. benthamiana* plants (RH20$^{\Delta N2-96}$, Table 4.2 and Fig. 4.6A, lanes 13-15 versus 1-3). This suggests that RH20 requires the N-terminal domain to be an active pro-viral host factor

in TBSV replication. Replication of other tombusviruses, such as CNV (Fig. 4.6C) and CIRV (Table 2) was also inhibited by 2-to-3-fold in *N. benthamiana* by the transient expression of the RH20$^{\Delta N2\text{-}96}$ missing the N-terminal domain. In contrast, deletion of the short C-terminal domain in RH20 did not interfere with the pro-viral function in *N. benthamiana* (RH20$^{\Delta C}$, Table 4.2). Thus, similar to the case with RH30 helicase, the functional identity of RH20 pro-viral helicase could be reversed by removing a functional domain.

The antiviral RH20$^{\Delta N}$ DEAD-box helicase inhibits tombusvirus RNA synthesis *in vitro*. To learn what features of RH20$^{\Delta N2\text{-}96}$ helicase caused it to become antiviral, we affinity-purified the recombinant RH20$^{\Delta N2\text{-}96}$ helicase from *E. coli*, and tested its activity *in vitro* in a TBSV replicase reconstitution assay [31, 32]. Addition of the purified RH20$^{\Delta N2\text{-}96}$ helicase to the replicase reconstitution assay resulted in decreased TBSV repRNA replication by ~40% (Fig. 4.6D, lanes 1-2). The double-stranded repRNA replication intermediate was also reduced by ~15% in the presence of RH20$^{\Delta N2\text{-}96}$ helicase. Based on these data, we suggest that RH20$^{\Delta N2\text{-}96}$ helicase likely inhibits both (-) and (+)-strand RNA synthesis during TBSV replication. This is in agreement with *in planta* data on TBSV accumulation, which also showed decreased levels of both

(-)RNAs and (+)RNAs when RH20$^{\Delta N2\text{-}96}$ helicase was expressed in *N. benthamiana* (Fig. 4.6A, lanes 13-15 and Fig. 4.6B, lanes 4-6).

The antiviral RH20$^{\Delta N}$ DEAD-box helicase is re-targeted into the tombusvirus replication compartment in plants. To test if the antiviral RH20$^{\Delta N2\text{-}96}$ helicase is present in the replication compartment, we conducted BiFC experiments in *N. benthamiana* leaves. The antiviral RH20$^{\Delta N2\text{-}96}$ helicase, similar to the pro-viral full-length RH20 helicase, also showed interaction with the TBSV p33 replication protein within the viral replication compartment, marked by the peroxisomal matrix marker RFP-SKL (Fig. 4.7A-B). Thus, both the pro-viral and antiviral cellular helicases are re-targeted to the viral replication compartment during TBSV replication.

The antiviral RH20$^{\Delta N}$ DEAD-box helicase efficiently unwinds critical cis-acting elements in the TBSV RNA. Here, we again used the *in vitro* strand-separation assay to test the antiviral activity of the RH20$^{\Delta N2\text{-}96}$ helicase. Surprisingly, we observed a largely enhanced unwinding activity of RH20$^{\Delta N2\text{-}96}$ helicase in comparison with the pro-viral full-length RH20 helicase. For, example, the purified RH20$^{\Delta N2\text{-}96}$ helicase, unlike the full-length RH20 helicase, could efficiently unwind the partial dsRNA template, involving the RII sequence, in the presence of ATP (Fig. 4.7B, lanes 1-5 versus 11-15).

These findings suggest that, in contrast with the full-length RH20 helicase, the RH20$^{\Delta N2-96}$ helicase can 'destroy" the RII(+)SL hairpin structure, thus it might be able to block the binding of TBSV p33 replication protein to the critical RII(+)-SL RNA recognition element, which event is required for template recruitment into replication. Actually, RH20$^{\Delta N2-96}$ helicase was able to efficiently unwind all the TBSV dsRNA templates provided (Fig. 4.7). This efficient unwinding of viral RNA structures by RH20$^{\Delta N2-96}$ helicase likely is the reason for its antiviral function. The pro-viral full-length RH20 is more selectively targets RI sequence of the dsRNA replication intermediate, which is critical during initiation of (+)-strand RNA synthesis [78, 104]. Therefore, we suggest that the RH20$^{\Delta N2-96}$ helicase becomes antiviral based on its lost template selectivity in comparison with the more selective pro-viral full-length RH20 helicase.

The N-terminal-domain in the DEAD-box helicases is needed for the co-opted Rpn11 deubiqitinase to regulate TBSV replication. The recruitment of the DDX3-like yeast Ded1 and the homologous plant RH20 DEAD-box helicases into the viral replication compartment is affected by the cellular Rpn11 deubiqitinase [30]. To study if Rpn11 is also critical for the functions of the above helicases, we knocked down Rpn11 levels via VIGS in *N. benthamiana*, followed by the expression of the full-length and truncated cellular helicases. These experiments revealed that the antiviral activity of

RH30 and the pro-viral function of RH20 are dependent on Rpn11 (Fig. 4.9). In contrast, $RH20^{\Delta N2\text{-}96}$ helicase still showed antiviral activity, whereas $RH30^{\Delta N/\Delta C}$ helicase was pro-viral in plants with knock down of Rpn11 (Fig. 4.9). Therefore, these results suggest that Rpn11 requires the N-terminal domain of these helicases to regulate TBSV replication. Dissection of the actual function of Rpn11 will require further experiments.

Chimeric DEAD-box helicases confirm the critical roles of the N-terminal domains in DEAD-box helicases in TBSV replication. To obtain further evidence on the critical roles of the N-terminal domains of DEAD-box helicases in TBSV replication, we constructed two chimeric DEAD-box helicases by switching the N-terminal domains between RH20 and RH30 (Fig. 4.10). The chimeric helicase containing the N-terminal domain from RH20 and the remaining sequences from RH30 (i.e., RH322) showed antiviral activity against TBSV when expressed in *N. benthamiana* (Fig. 4.10). On the contrary, the other chimeric helicase containing the N-terminal domain from RH30 and the remaining sequences from RH20 (i.e., RH33) showed pro-viral activity on TBSV replication when expressed in *N. benthamiana* (Fig. 4.10). These results support the notion that the N-terminal domain in the DEAD-box helicases might determine the specific role of DEAD-box helicases in TBSV replication.

4.4 Discussion

Unlike many other pathogens, (+)RNA viruses code for only a rather limited number of genes, making them highly dependent on numerous co-opted host factors for supporting viral replication and other viral processes during their infections. This overm dependence on subverted host factors, however, renders (+)RNA viruses vulnerable to host restriction factors that could block virus replication. Accordingly, tombusviruses are dependent on the cellular DDX3-like and DDX5-like DEAD-box helicases during their replication in yeast or plants [78, 79, 103, 104]. However, there are a large number of similar DEAD-box helicases in plants (58 in Arabidopsis), which might not assist tombusvirus replication, but instead, block the viral replication process. Indeed, we have previously shown that the DDX17-like RH30 helicase, which is rather similar to the pro-viral DDX3-like RH20 helicase, has strong anti-tombusvirus activity in plants (Chapter 3). However, it is currently unknown what features make particular DEAD-box helicases either pro-viral or antiviral.

In this work, we have shown that the functional identity of the co-opted DEAD-box helicases could be altered by changing the pro-viral RH20 helicase into antiviral and the antiviral RH30 helicase into a pro-viral helicase via altering the sequences of these cellular helicases. Notably, the unique N-terminal domain of the DEAD-box helicases

seems to be important to specify the activity of the given cellular helicase. In the absence of the N-terminal domain, the core helicase domain becomes unhinged, showing altered specificity in RNA duplex unwinding activities.

The tombusvirus genome is loaded with cis-acting RNA replication and translation elements to facilitate well-orchestrated and efficient viral replication [182]. The emerging picture from recent studies with TBSV is that cellular helicases could target various cis-acting elements. Accordingly, in vitro studies revealed that one of the most important features of the cellular helicases is their abilities to unwind the RNA structures within particular regions of the TBSV RNA. The critical feature for the pro-viral DEAD-box helicases, such as RH30$^{\Delta N/\Delta C}$ helicase (this work) and the full-length RH20, is to selectively target and unwind the RI sequence (5'UTR) of the dsRNA replication intermediate, which is critical during initiation of (+)-strand RNA synthesis [78, 79, 103, 104]. On the contrary, the critical feature of the antiviral DEAD-box helicases, such as RH20$^{\Delta N2-96}$ helicase (this work) and the full-length RH30, is to efficiently target and "destroy" the RII(+)SL hairpin structure, and thus block the binding of TBSV p33 replication protein to the critical RII(+)-SL RNA recognition element, which is absolutely required for template recruitment into replication, VRC assembly and viral RdRp activation (Fig. 11) [11, 12, 15, 133].

Although RH30$^{\Delta N/\Delta C}$ helicase facilitates the unwinding of RI-containing sequences, which are important for initiation of (+)RNA synthesis by the TBSV RdRp [78, 104], this "pro-viral" feature of RH30$^{\Delta N/\Delta C}$ helicase might not be important in vivo. This is because the antiviral activity of RH30$^{\Delta N/\Delta C}$ helicase, involving unwinding of RII(+), which inhibits RII(+)-SL and the recruitment of the viral RNA into replication, is an earlier step during TBSV replication (Fig. 11). Thus, blocking this early step by RH30$^{\Delta N/\Delta C}$ helicase is a dominant feature, which likely prevents the seemingly pro-viral potential of RH30$^{\Delta N/\Delta C}$ helicase during the initiation of (+)RNA synthesis by unwinding the RI portion of the dsRNA replication intermediate.

Unlike with the full-length RH20 and RH30 helicases, the Rpn11-dependence is not observed with the truncated RH30$^{\Delta N/\Delta C}$ or RH20$^{\Delta N2-96}$ helicases. It is possible that RH30$^{\Delta N/\Delta C}$ or RH20$^{\Delta N2-96}$ helicases might be directly recruited by the viral replication proteins into the tombusvirus replication compartment without the help of the cytosolic Rpn11 host factor.

Interestingly, the altered functional identity of the cellular helicases was not affected by several features. For example, BiFC experiments in *N. benthamiana* showed the antiviral and pro-viral helicases interacted with the viral replication proteins and they were re-targeted into the viral replication compartment from either the cytosol or the nucleus. Also, the antiviral and pro-viral helicases were able to unwind viral dsRNA

structures. What was different, however, is that the antiviral and pro-viral helicases targeted different regions within the viral RNA as discussed above. The RNA helicase activity, however, seems to be important for both pro-viral and antiviral activities, because deletion of the core helicase domain eliminated these activities (Table 1-2). We also observed that the changed functional identity of the cellular helicases manifested with both the peroxisomal-replicating TBSV and the mitochondrial-replicating CIRV in plants.

Overall, the evolving features of the unique N-terminal domains of cellular DEAD-box helicases seem to be key components of the arms race between tombusviruses and their hosts. We propose that deletions/mutations in critical positions within the N-terminal domains of cellular DEAD-box helicases might render them either antiviral or pro-viral. These findings open up the possibility to turn the pro-viral host factors into antiviral factors, for the benefit of agriculture and health science.

It will be interesting to learn if the function of helicases could be reversed in case of other RNA viruses and retroviruses. Those viruses also usurp several cellular DEAD-box helicases to facilitate their replication and other viral processes during infection [172, 173]. Moreover, the host also deploys DEAD-box helicases to inhibit the replication of the above viruses [172, 174]. Many of the identified DEAD-box helicases with restriction functions are conserved in plants and mammals.

Name	TBSV	CIRV replication
Empty vector	100	100
RH30	19±13	24±6
N-terminal mutants:		
RH30$^{\Delta N2\text{-}17}$	22±3	21±15
RH30$^{\Delta N2\text{-}103}$	36±13	79±6
RH30$^{\Delta N2\text{-}124}$	88±19	138±15
RH30$^{\Delta N2\text{-}162}$	118±17	105±15
Helicase core mutants:		
RH30^{F416L}	111±31	101±8
RH30$^{\Delta Hel\ (\Delta 163\text{-}546)}$	92±11	77±30
C-terminal mutants:		
RH30$^{\Delta C547\text{-}592}$	25±7	5±4
Dual-mutants:		
RH30$^{\Delta Hel/\Delta C\ (\Delta 163\text{-}592)}$	93±1	99±25
RH30$^{\Delta N/\Delta C\ (\Delta N2\text{-}162/\Delta C547\text{-}592)}$	200±27	190±10

Table 4.1 The effect of deletions on the antiviral activity of RH30 DEAD-box helicase, compared to empty vector control.

Name	TBSV	CIRV replication
Empty vector	100	100
RH20	161±30	175±10
N-terminal mutants:		
$RH20^{\Delta N2\text{-}17}$	114±42	40±7
$RH20^{\Delta N2\text{-}36}$	30±16	45±11
$RH20^{\Delta N2\text{-}96}$	39±17	36±8
C-terminal mutants:		
$RH20^{\Delta C480\text{-}501}$	166±20	ND

Table 4.2 The effect of deletions on the pro-viral activity of RH20 DEAD-box helicase, compared to empty vector control.

N. O. of primers	Sequences
1818	CAGGCTCGAGATCATGAGTCGCTACGATAGCCGGA
5753	CGCGTCTAGATTACCAAGTCCTCTTTCCAC
5754	CGCGCTCGAGATGAGCTCGTATGATCGTAG
5905	GGAAGATCTATGGTGAGCAAGGGCGAG
6069	GCGCGGATCCGTCCTCGATGTTGTGGC
6509	CGCGGATCCATGAGTCGCTACGATAGCCG
6708	GCTCTAGATTACTTAGGAACATCACGACCTTCAAC
6709	CCGCTCGAGATGCCGATGAAGATGTTCCAAGATGC
6710	GCTCTAGATTATGATCGGACTAGTGCGGAGAGAG
6844	ATCAGGAAAGCCAACATCACGAAAACTCTTCATCGGCTTAGGAACATCACGACCT
6845	GTTGAAGGTCGTGATGTTCCTAAGCCGATGAAGAGTTTTCGTGATGTTGGCTTTC
6849	ATCTGGAAAGTTAGCATCTTGGAACATCTTGACAGGTTTTGGAATATCTTTGCCT
6850	GTTGAAGGCAAAGATATTCCAAAACCTGTCAAGATGTTCCAAGATGCTAACTTTC
6972	TGCTCTAGATCAGCTCCACCCTCTTCTGCTC
7051	CCGCTCGAGATGTCTAGCAAAAAGGATAACGAT
7102	CCGCTCGAGATGTTTGAGAAGAATTTTTATGTCGAGTCTCCCGC
7198	CATTTCTTTTAAAGCAAAAGC
7391	GAAGATCTATGGGTTACCCATACGATGTTC
7392	CCGCTCGAGCCAGGATCCAGCAGCGTAATCTGGAACGT
7393	CCGCTCGAGATGCCTGTCAAGAGTTTTCGTGATGTTG
7638	CGGGATCCATGCCTGTCAAGAGTTTTCGTGATGTTG
7639	GCTCTAGAATGCCGATGAAGATGTTCCAAGATGC
7838	CCGCTCGAGTTATGATCGGACTAGTGCGGAGAGA

Table 4.3

Table4.3 The sequences of primers used in this study.

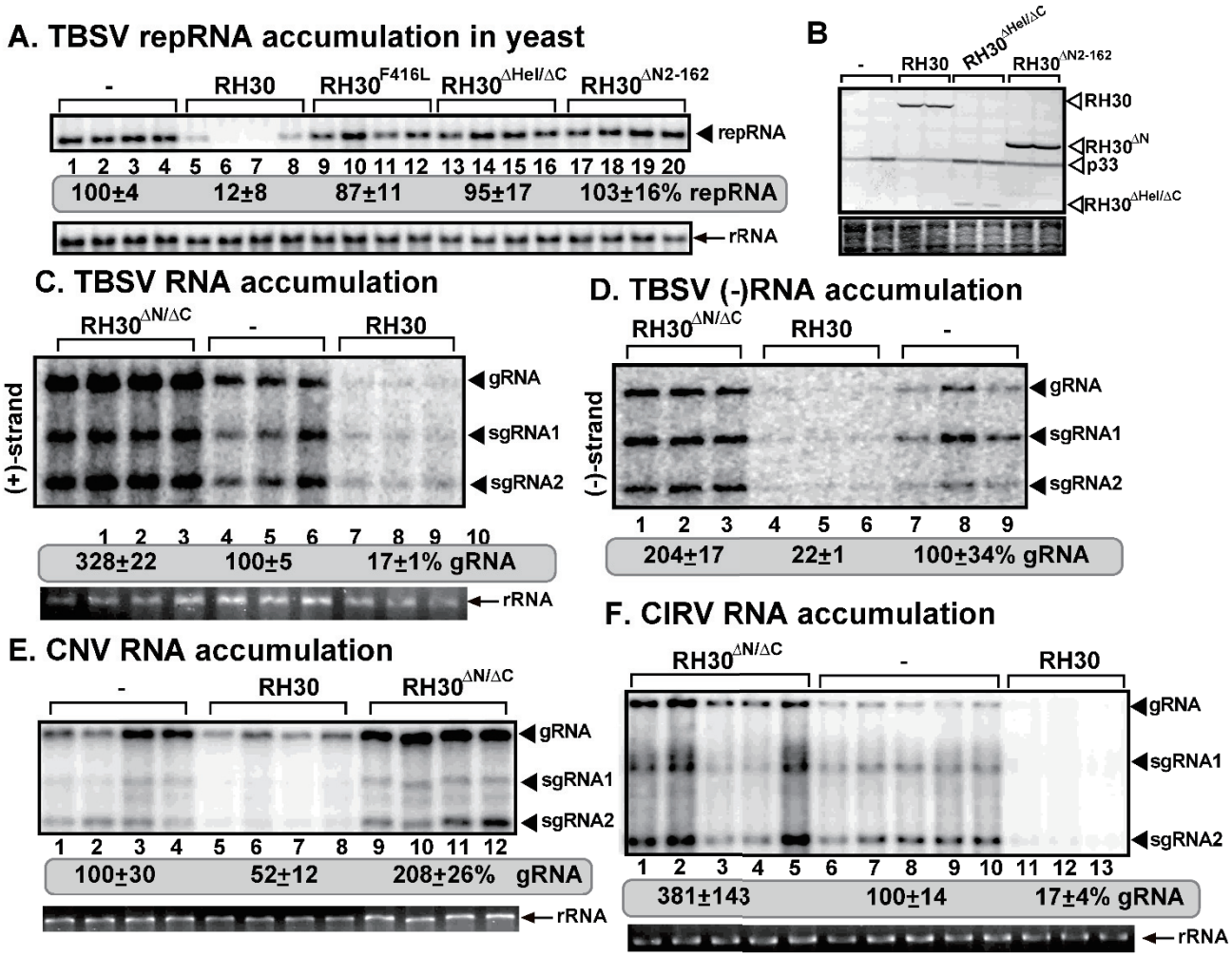
A. TBSV repRNA accumulation in yeast
-
RH30
RH30F416L
RH30ΔHel/ΔC
RH30ΔN2-162
repRNA
1 2 3 4 5 6 7 8 9 10 11 12 13 14 15 16 17 18 19 20
100±4
12±8
87±11
95±17
103±16% repRNA
rRNA
B
-
RH30
RH30ΔHel/ΔC
RH30ΔN2-162
RH30
RH30ΔN
p33
RH30ΔHel/ΔC
C. TBSV RNA accumulation
RH30ΔN/ΔC
-
RH30
(+)-strand
gRNA
sgRNA1
sgRNA2
1 2 3 4 5 6 7 8 9 10
328±22
100±5
17±1% gRNA
rRNA
D. TBSV (-)RNA accumulation
RH30ΔN/ΔC
RH30
-
(-)-strand
gRNA
sgRNA1
sgRNA2
1 2 3 4 5 6 7 8 9
204±17
22±1
100±34% gRNA
E. CNV RNA accumulation
-
RH30
RH30ΔN/ΔC
gRNA
sgRNA1
sgRNA2
1 2 3 4 5 6 7 8 9 10 11 12
100±30
52±12
208±26% gRNA
rRNA
F. CIRV RNA accumulation
RH30ΔN/ΔC
-
RH30
gRNA
sgRNA1
sgRNA2
1 2 3 4 5 6 7 8 9 10 11 12 13
381±143
100±14
17±4% gRNA
rRNA

Figure 4.1

Figure 4.1 Effects of expression of truncation mutants of the antiviral RH30 DEAD-box helicase on tombusvirus genomic (g)RNA replication in N. benthamiana plant and in yeast surrogate host. *(A) The effect of expression of truncation mutants of AtRH30 on TBSV replication in yeast. Top panel: Northern blot analysis of TBSV repRNA using a 3' end specific probe shows the level of accumulation of repRNA in WT yeast strain expressing truncation mutants of AtRH30. Viral proteins His_6-p33 and His_6-$p92^{pol}$ were expressed from plasmids from the CUP1 promoter, while DI-72(+) repRNA was expressed from the GAL1 promoter. His_6-RH30 derivatives were expressed from a plasmid. Bottom panel: Northern blot with 18S ribosomal RNA specific probe was used as a loading control. (B) Western blot analysis of the level of His_6-p33, His_6-$p92^{pol}$ and His_6-RH30 with anti-His antibody. The samples were from WT yeast strain expressing truncation mutants of AtRH30. (C) N. benthamiana plants expressing $RH30^{\Delta N/\Delta C}$ helicase were inoculated with (C-D) TBSV, (E) CNV, (F) CIRV, respectively. Top panel: Northern blot analyses of tombusvirus gRNA using a 3' end specific probe shows increased accumulation of gRNA and subgenomic RNAs in plants expressing $RH30^{\Delta N/\Delta C}$ helicase when compared with plants expressing RH30 or in control plants. Bottom panel: Ethidium-bromide stained gel shows 18S ribosomal RNA as a loading control. (D) Northern blot analyses of TBSV gRNA using a 3' end specific probe for (-)RNA detection. Each experiment was repeated at least three times.*

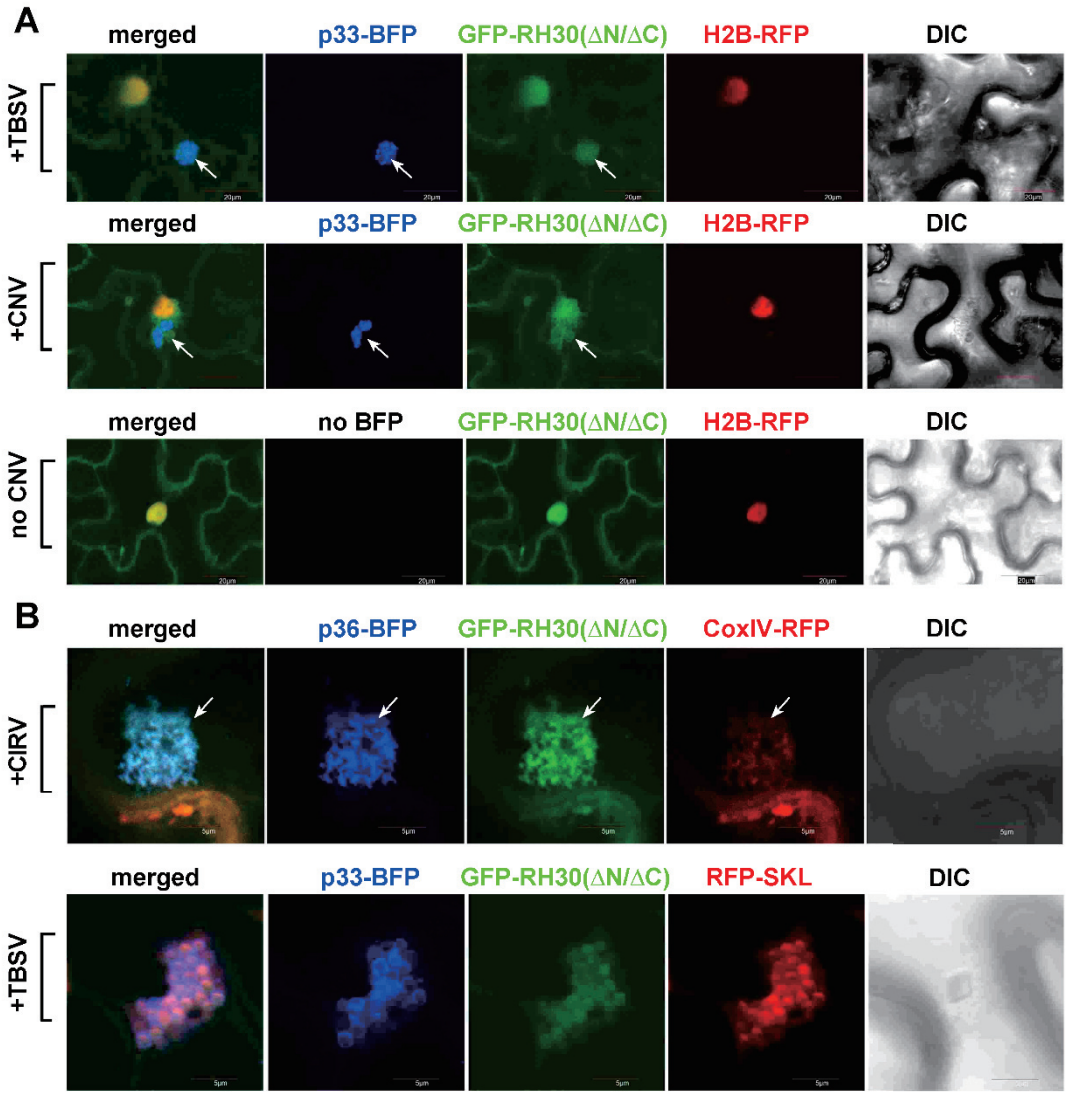
A
merged
p33-BFP
GFP-RH30(ΔN/ΔC)
H2B-RFP
DIC
+TBSV
merged
p33-BFP
GFP-RH30(ΔN/ΔC)
H2B-RFP
DIC
+CNV
merged
no BFP
GFP-RH30(ΔN/ΔC)
H2B-RFP
DIC
no CNV
B
merged
p36-BFP
GFP-RH30(ΔN/ΔC)
CoxIV-RFP
DIC
+CIRV
merged
p33-BFP
GFP-RH30(ΔN/ΔC)
RFP-SKL
DIC
+TBSV

Figure 4.2

Figure 4.2 Confocal microscopy shows the retargeting of the nuclear/cytosolic RH30$^{\Delta N/\Delta C}$ helicase into the large replication compartment in whole plants infected with a tombusvirus. *(A) Confocal microscopy images show that most of RH30$^{\Delta N/\Delta C}$ helicase is re-targeted into the replication compartment marked by the BFP-tagged p33 replication protein (pointed by arrows) in N. benthamiana plants infected with TBSV or CNV. Bottom panel: distribution of RH30$^{\Delta N/\Delta C}$ helicase in the absence of viral components. The nucleus is marked by a histone protein (transgenic plants expressing nucleus marker RFP-H2B). Scale bars represent 20 μm. (B) Confocal microscopy images show that the re-targeted GFP-RH30$^{\Delta N/\Delta C}$ helicase is present in the viral replication compartment, marked by the CIRV p36-BFP replication protein and CoxIV-RFP mitochondrial marker. Arrows point at the viral replication compartment. Expression of the above proteins from the 35S promoter was done after co-agroinfiltration into N. benthamiana leaves. The agro-infiltrated leaves were collected for confocal imaging 2.5 days post agro-infiltration. Bottom panel: The TBSV p33-BFP replication protein and RFP-SKL peroxisomal matrix marker co-localize with the GFP-RH30$^{\Delta N/\Delta C}$ helicase in the viral replication compartment. Scale bars represent 5 μm. Each experiment was repeated.*

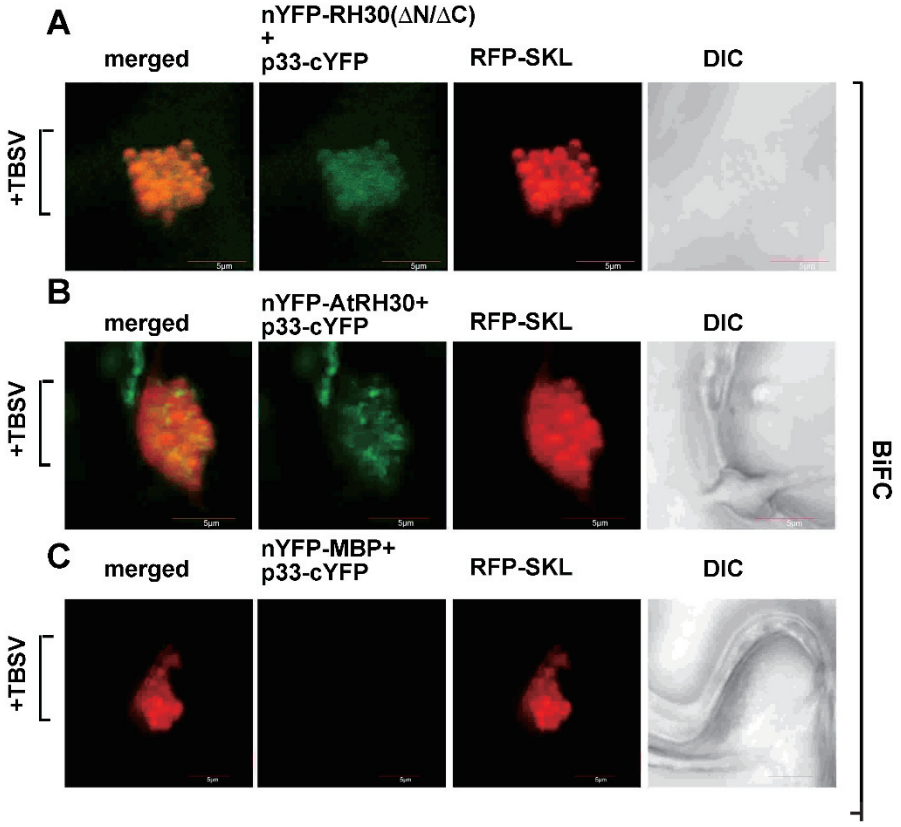
A
nYFP-RH30(ΔN/ΔC)
+
p33-cYFP
merged
RFP-SKL
DIC
+TBSV
B
nYFP-AtRH30+
p33-cYFP
merged
RFP-SKL
DIC
+TBSV
C
nYFP-MBP+
p33-cYFP
merged
RFP-SKL
DIC
+TBSV
BiFC

Figure 4.3

Figure 4.3 Interaction between RH30$^{\Delta N/\Delta C}$ helicase and the TBSV replication protein in plants. *(A) Interactions between TBSV p33 replication protein and the RH30$^{\Delta N/\Delta C}$ helicase were detected by BiFC. The TBSV p33-cYFP replication protein and the nYFP-RH30 and the RFP-SKL peroxisomal marker protein were expressed via agro-infiltration. The merged image shows the efficient co-localization of the peroxisomal RFP-SKL with the BiFC signals, indicating that the interaction between the tombusvirus replication protein and the recruited RH30$^{\Delta N/\Delta C}$ helicase takes place in the large viral replication compartments, which consist of aggregated peroxisomes. Scale bars represent 5 μm.*

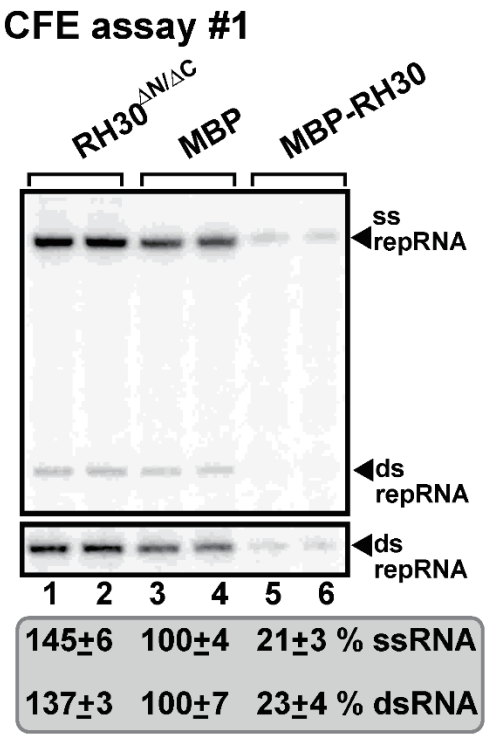
CFE assay #1
RH30ΔN/ΔC
MBP
MBP-RH30
ss repRNA
ds repRNA
ds repRNA
1 2 3 4 5 6
145±6 100±4 21±3 % ssRNA
137±3 100±7 23±4 % dsRNA

Figure 4.4

Figure 4.4 Enhanced TBSV repRNA accumulation by RH30$^{\Delta N/\Delta C}$ helicase in in vitro replicase reconstitution assay based on CFE obtained from WT yeast. *The purified recombinant tombusvirus p33 and p92 replication proteins from E. coli were added in combination with the template (+)repRNA to program the in vitro tombusvirus replication assay. The affinity-purified recombinant MBP-RH30$^{\Delta N/\Delta C}$, MBP-RH30 (1.9 μM) or MBP, as a control, were added to the reactions. Non-denaturing PAGE shows the accumulation of ^{32}P-labeled (+)repRNAs and the dsRNA replication intermediate products made by the reconstituted replicases. The bottom image shows the contrasted image of the dsRNA bands of the top image. Each experiment was repeated three times.*

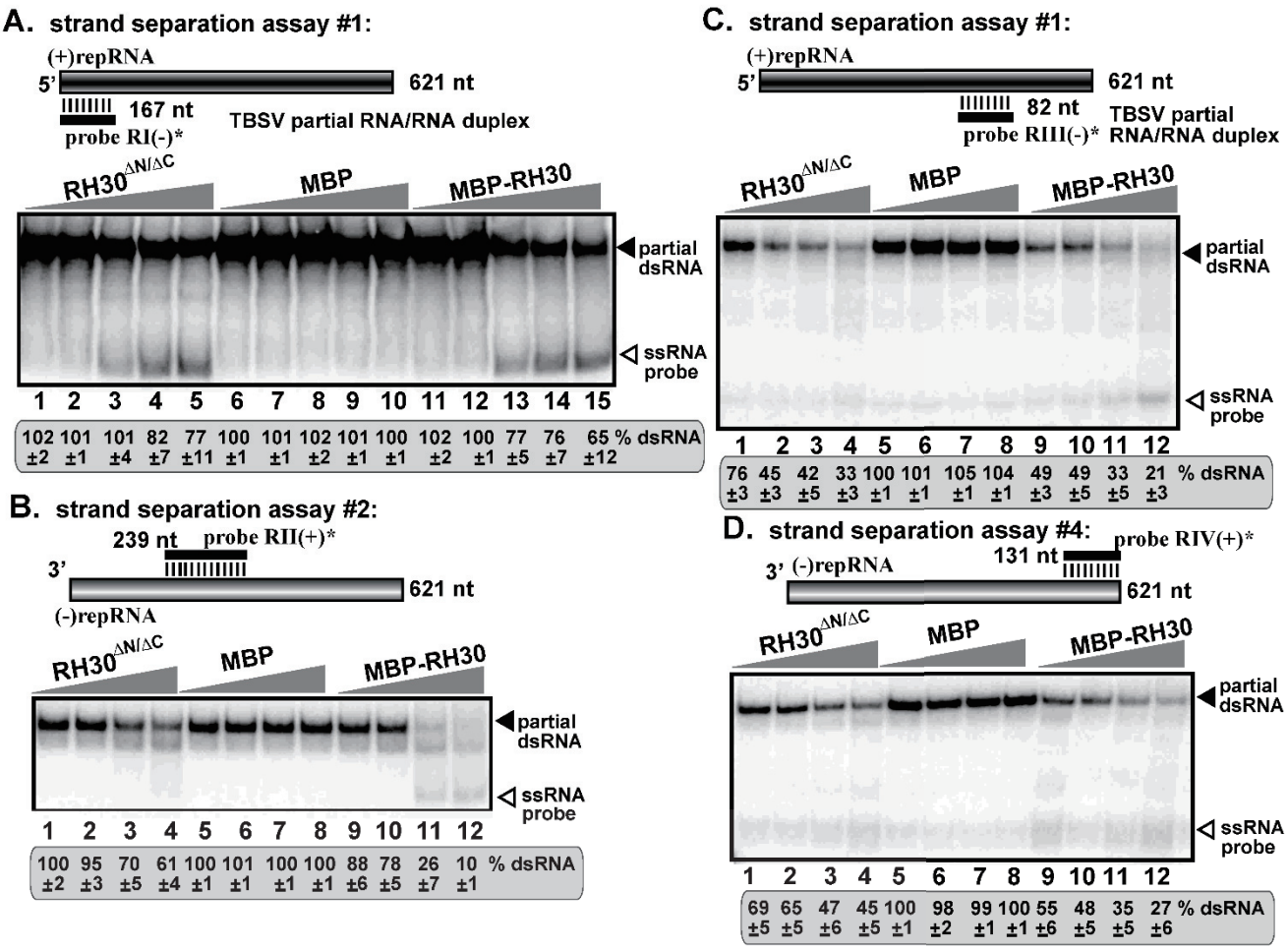
A. strand separation assay #1:
(+)repRNA
5'
621 nt
167 nt
probe RI(-)*
TBSV partial RNA/RNA duplex
RH30ΔN/ΔC
MBP
MBP-RH30
partial dsRNA
ssRNA probe
1 2 3 4 5 6 7 8 9 10 11 12 13 14 15
102 ±2 101 ±1 101 ±4 82 ±7 77 ±11 100 ±1 101 ±1 102 ±2 101 ±1 100 ±1 102 ±2 100 ±1 77 ±5 76 ±7 65 ±12 % dsRNA
B. strand separation assay #2:
239 nt
probe RII(+)*
3'
621 nt
(-)repRNA
RH30ΔN/ΔC
MBP
MBP-RH30
partial dsRNA
ssRNA probe
1 2 3 4 5 6 7 8 9 10 11 12
100 ±2 95 ±3 70 ±5 61 ±4 100 ±1 101 ±1 100 ±1 100 ±1 88 ±6 78 ±5 26 ±7 10 ±1 % dsRNA
C. strand separation assay #1:
(+)repRNA
5'
621 nt
82 nt
probe RIII(-)*
TBSV partial RNA/RNA duplex
RH30ΔN/ΔC
MBP
MBP-RH30
partial dsRNA
ssRNA probe
1 2 3 4 5 6 7 8 9 10 11 12
76 ±3 45 ±3 42 ±5 33 ±3 100 ±1 101 ±1 105 ±1 104 ±1 49 ±3 49 ±5 33 ±5 21 ±3 % dsRNA
D. strand separation assay #4:
3' (-)repRNA
131 nt
probe RIV(+)*
621 nt
RH30ΔN/ΔC
MBP
MBP-RH30
partial dsRNA
ssRNA probe
1 2 3 4 5 6 7 8 9 10 11 12
69 ±5 65 ±5 47 ±6 45 ±5 100 ±1 98 ±2 99 ±1 100 ±1 55 ±6 48 ±5 35 ±5 27 ±6 % dsRNA

Figure 4.5

Figure 4.5 Decreased level of unwinding of the dsRNA region containing the RII(+)-SL cis-acting element involved in RNA template selection by RH30$^{\Delta N/\Delta C}$ helicase in vitro. *(A) Top: Schematic representation of the partial RNA/RNA duplexes used in the strand separation assay. The unlabeled template consists of DI-72 (+)repRNA and a short ^{32}P-labeled complementary (-)RNA (representing RI of DI-72 repRNA), which anneals to the 621 nt DI-72 (+)repRNA. Increasing amounts of purified recombinant MBP-RH30$^{\Delta N/\Delta C}$, MBP-RH30, or MBP, as a control, were added to the reactions in the presence of ATP. Bottom: Representative native gel of ^{32}P-labeled RNA products after the in vitro strand separation assay. Quantification of the partial dsRNA probe was done with a Phosphorimager. This experiment was repeated two times. (B-D) Comparable strand separation assays using different regions of the repRNA as shown. See panel A for further details.*

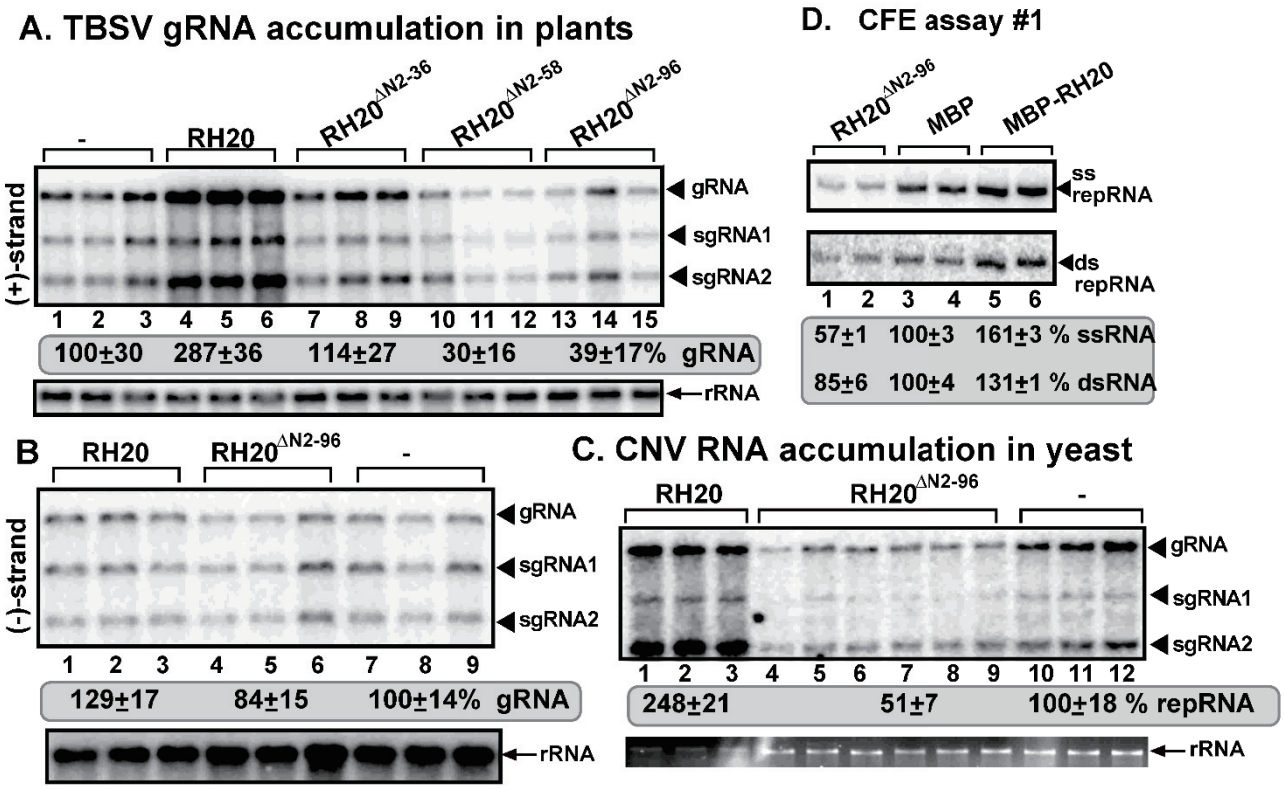
A. TBSV gRNA accumulation in plants
-
RH20
RH20ΔN2-36
RH20ΔN2-58
RH20ΔN2-96
(+)-strand
gRNA
sgRNA1
sgRNA2
1 2 3 4 5 6 7 8 9 10 11 12 13 14 15
100±30 287±36 114±27 30±16 39±17% gRNA
rRNA
D. CFE assay #1
RH20ΔN2-96
MBP
MBP-RH20
ss repRNA
ds repRNA
1 2 3 4 5 6
57±1 100±3 161±3 % ssRNA
85±6 100±4 131±1 % dsRNA
B
RH20
RH20ΔN2-96
-
(-)-strand
gRNA
sgRNA1
sgRNA2
1 2 3 4 5 6 7 8 9
129±17 84±15 100±14% gRNA
rRNA
C. CNV RNA accumulation in yeast
RH20
RH20ΔN2-96
-
gRNA
sgRNA1
sgRNA2
1 2 3 4 5 6 7 8 9 10 11 12
248±21 51±7 100±18 % repRNA
rRNA

Figure 4.6

Figure 4.6 Effects of expression of truncation mutants of the pro-viral RH20 DEAD-box helicase on tombusvirus genomic (g)RNA replication in N. benthamiana plants. *(A) N. benthamiana plants expressing the N-terminal truncation derivatives of RH20 helicase were inoculated with TBSV. Top panel: Northern blot analyses of tombusvirus gRNA using a 3' end specific probe shows the accumulation level of gRNA and subgenomic RNAs in plants expressing RH20 helicase and its derivatives when compared with control plants. Bottom panel: Northern blot shows 18S ribosomal RNA as a loading control. (B) Northern blot analyses of TBSV gRNA using a 3' end specific probe for (-)RNA detection. Each experiment was repeated at least three times. (C) N. benthamiana plants expressing RH20$^{\Delta N2\text{-}96}$ or RH20 helicases were inoculated with CNV. See further details in panel A. (D) An in vitro replicase reconstitution assay shows the inhibitory effect of RH20$^{\Delta N2\text{-}96}$ helicase on TBSV repRNA accumulation. The purified recombinant tombusvirus p33 and p92 replication proteins from E. coli were added in combination with the template (+)repRNA to program the in vitro tombusvirus replication assay. The affinity-purified recombinant RH20$^{\Delta N2\text{-}96}$, MBP-RH20 (1.9 μM) or MBP, as a control, were added to the reactions. Non-denaturing PAGE shows the accumulation of ^{32}P-labeled (+)repRNAs and the dsRNA replication intermediate products made by the reconstituted replicases. Each experiment was repeated three times.*

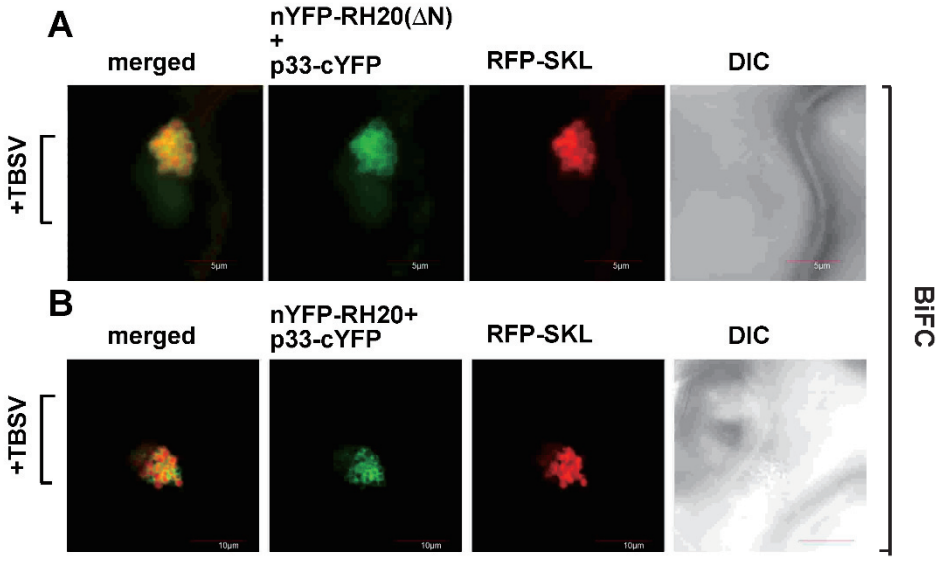
A
merged
nYFP-RH20(ΔN)
+
p33-cYFP
RFP-SKL
DIC
+TBSV
B
merged
nYFP-RH20+
p33-cYFP
RFP-SKL
DIC
+TBSV
BiFC

Figure 4.7

Figure 4.7 Interaction between RH20$^{\Delta N2\text{-}96}$ helicase and the TBSV replication protein in plants. *(A-B) Interactions between TBSV p33 replication protein and the RH20$^{\Delta N2\text{-}96}$ helicase or the full-length RH20 (panel B) were detected by BiFC. The TBSV p33-cYFP replication protein and the nYFP-RH20$^{\Delta N2\text{-}96}$, nYFP-RH20 and the RFP-SKL peroxisomal marker protein were expressed via agro-infiltration. The merged image shows the efficient co-localization of the peroxisomal RFP-SKL with the BiFC signals, indicating that the interaction between the tombusvirus replication protein and the recruited RH20$^{\Delta N2\text{-}96}$ helicase occurs in the large viral replication compartments, which consist of aggregated peroxisomes. Scale bars represent 10 μm.*

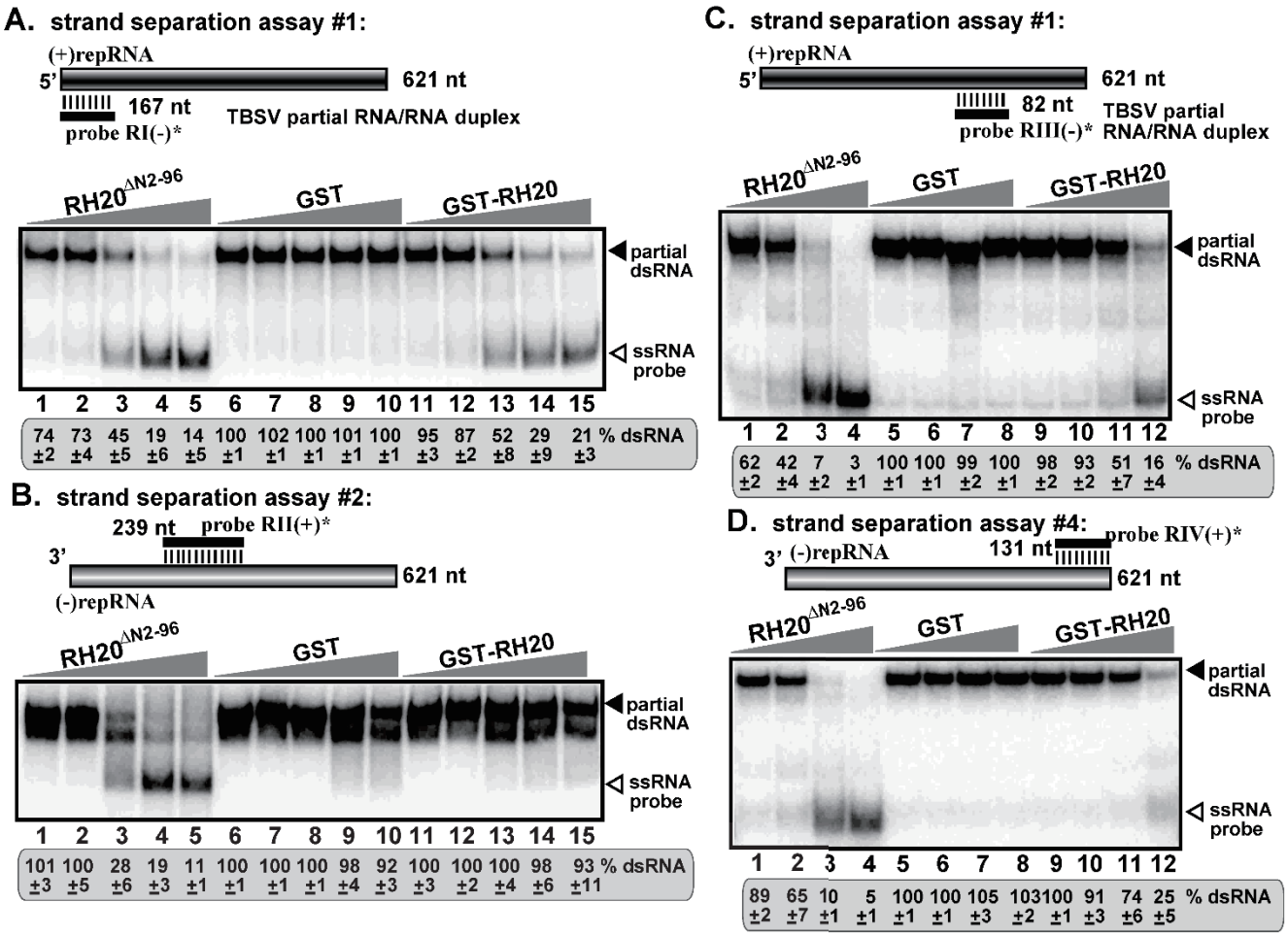
A. strand separation assay #1:
(+)repRNA
5'
621 nt
167 nt
probe RI(-)*
TBSV partial RNA/RNA duplex
RH20ΔN2-96
GST
GST-RH20
partial dsRNA
ssRNA probe
1 2 3 4 5 6 7 8 9 10 11 12 13 14 15
74 ±2 73 ±4 45 ±5 19 ±6 14 ±5 100 ±1 102 ±1 100 ±1 101 ±1 100 ±1 95 ±3 87 ±2 52 ±8 29 ±9 21 ±3 % dsRNA
B. strand separation assay #2:
239 nt
probe RII(+)*
3'
621 nt
(-)repRNA
RH20ΔN2-96
GST
GST-RH20
partial dsRNA
ssRNA probe
1 2 3 4 5 6 7 8 9 10 11 12 13 14 15
101 ±3 100 ±5 28 ±6 19 ±3 11 ±1 100 ±1 100 ±1 100 ±1 98 ±4 92 ±3 100 ±3 100 ±2 100 ±4 98 ±6 93 ±11 % dsRNA
C. strand separation assay #1:
(+)repRNA
5'
621 nt
82 nt
probe RIII(-)*
TBSV partial RNA/RNA duplex
RH20ΔN2-96
GST
GST-RH20
partial dsRNA
ssRNA probe
1 2 3 4 5 6 7 8 9 10 11 12
62 ±2 42 ±4 7 ±2 3 ±1 100 ±1 100 ±1 99 ±2 100 ±1 98 ±2 93 ±2 51 ±7 16 ±4 % dsRNA
D. strand separation assay #4:
probe RIV(+)*
3' (-)repRNA
131 nt
621 nt
RH20ΔN2-96
GST
GST-RH20
partial dsRNA
ssRNA probe
1 2 3 4 5 6 7 8 9 10 11 12
89 ±2 65 ±7 10 ±1 5 ±1 100 ±1 100 ±1 105 ±3 103 ±2 100 ±1 91 ±3 74 ±6 25 ±5 % dsRNA

Figure 4.8

Figure 4.8 Enhanced level of unwinding of the dsRNA region containing the RII(+)-SL cis-acting element involved in RNA template selection by RH20$^{\Delta N2-96}$ helicase in vitro. *(A-D) Top: Schematic representation of the partial RNA/RNA duplexes used in the strand separation assay. Increasing amounts of purified recombinant GST-RH20$^{\Delta N2-96}$ helicase, GST-RH20, or GST, as a control, were added to the reactions in the presence of ATP. See Fig. 5 for further details.*

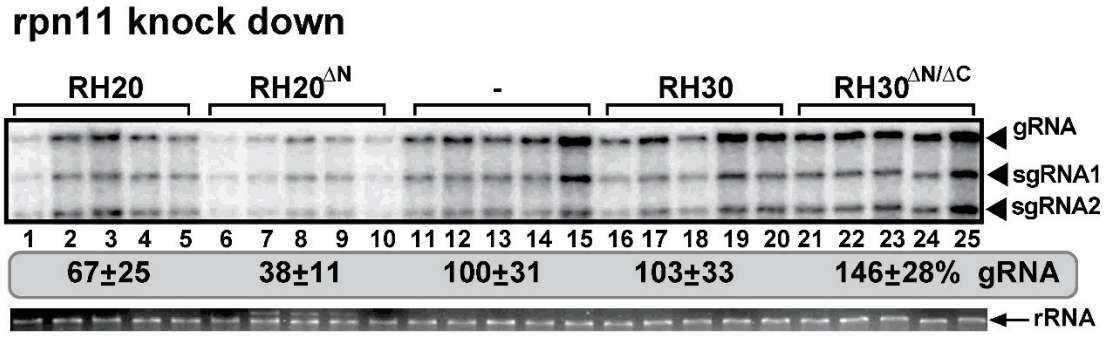
rpn11 knock down
RH20
RH20ΔN
-
RH30
RH30ΔN/ΔC
gRNA
sgRNA1
sgRNA2
1 2 3 4 5 6 7 8 9 10 11 12 13 14 15 16 17 18 19 20 21 22 23 24 25
67±25
38±11
100±31
103±33
146±28% gRNA
rRNA

Figure 4.9

Figure 4.9 The effect of expression of truncation mutants of the RH20 and RH30 DEAD-box helicases on tombusvirus genomic (g)RNA replication in N. benthamiana plants with knock- down of Rpn11. *The plant Rpn11 deubiquitinase level was knocked down via VIGS in N. benthamiana plants. The plants expressing the shown truncation derivatives of RH20 and RH30 helicases were inoculated with TBSV. Top panel: Northern blot analyses of tombusvirus gRNA using a 3' end specific probe shows the accumulation level of gRNA and subgenomic RNAs. The experiment was repeated.*

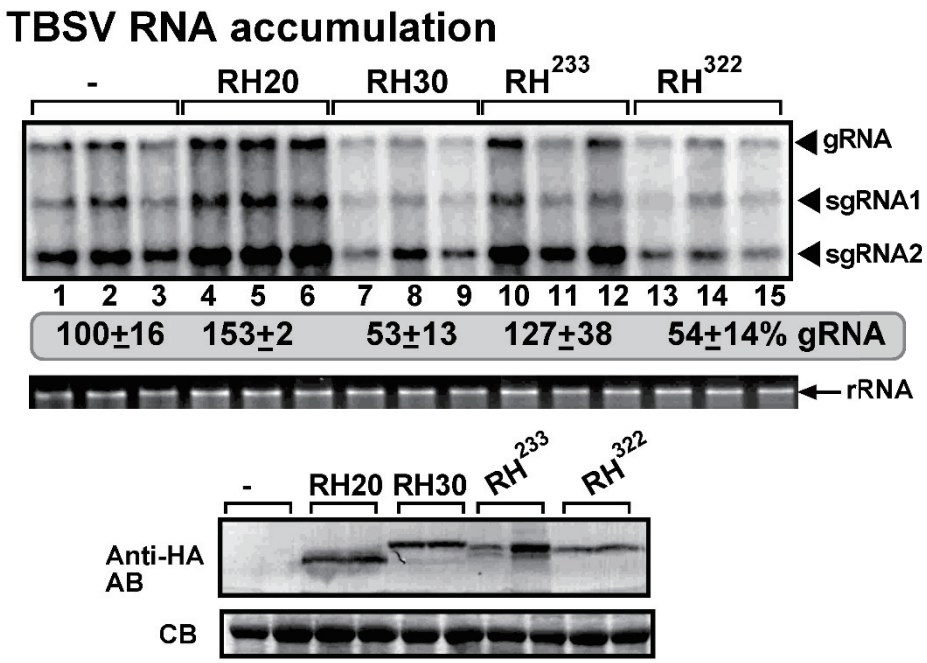
TBSV RNA accumulation
-
RH20
RH30
RH233
RH322
gRNA
sgRNA1
sgRNA2
1 2 3 4 5 6 7 8 9 10 11 12 13 14 15
100±16 153±2 53±13 127±38 54±14% gRNA
rRNA
-
RH20 RH30
RH233
RH322
Anti-HA AB
CB

Figure 4.10

Figure 4.10 The effect of expression of chimeric RH20 and RH30 DEAD-box helicases on tombusvirus genomic (g)RNA replication in N. benthamiana plants. *The chimeric helicases either contained the N-terminal domain of RH20 combined with the core helicase domain and C-terminal domain of RH30 (RH^{233}) or the N-terminal domain of RH30 combined with the core helicase domain and C-terminal domain of RH20 (RH^{322}). The plants expressing the chimeric derivatives of RH20 and RH30 helicases were inoculated with TBSV. Top panel: Northern blot analyses of tombusvirus gRNA using a 3' end specific probe shows the accumulation level of gRNA and subgenomic RNAs. (B) Western blot analysis of the level of HA-tagged chimeric derivatives of RH20 and RH30 helicases with anti-HA antibody. The experiment was repeated.*

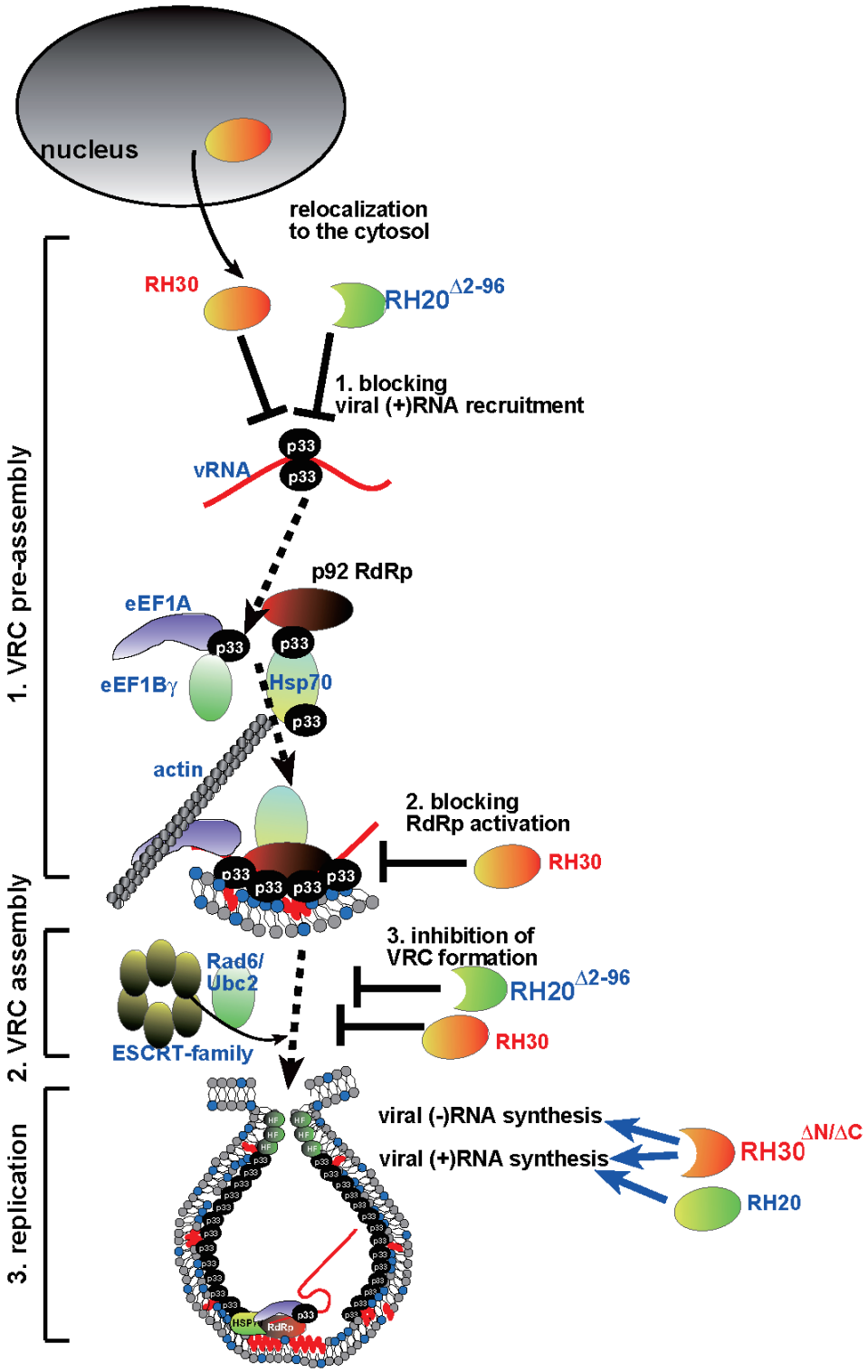
nucleus
relocalization
to the cytosol
RH30
RH20Δ2-96
1. blocking
viral (+)RNA recruitment
vRNA
p33
p33
p92 RdRp
eEF1A
eEF1Bγ
Hsp70
actin
2. blocking
RdRp activation
RH30
3. inhibition of
VRC formation
Rad6/
Ubc2
ESCRT-family
RH20Δ2-96
RH30
viral (-)RNA synthesis
viral (+)RNA synthesis
RH30ΔN/ΔC
RH20
1. VRC pre-assembly
2. VRC assembly
3. replication

Figure 4.11

Figure 4.11 Models showing either the pro-viral for antiviral functions of the derivatives of the plant RH20 and RH30 DEAD-box helicases during TBSV replication. *Based on our current and previous data, we propose that the RH20$^{\Delta N2\text{-}96}$ helicase becomes an antiviral restriction factor by inhibiting the recruitment of the viral (+)RNA and blocking VRC formation. This inhibitory effect of RH20$^{\Delta N2\text{-}96}$ helicase is likely through the unwinding RII(+)-SL cis-acting RNA element, which might block the specific recognition by p33 replication protein, which requires the RII(+)-SL stem-loop structure. RH20$^{\Delta N2\text{-}96}$ helicase inhibits VRC assembly as well, because the stem-loop structure in RII(+)-SL is essential part of the VRC assembly platform. In contrast, RH30$^{\Delta N/\Delta C}$ helicase becomes a pro-viral factor by opening up the RI-containing dsRNA structure within the dsRNA replication intermediate. This, in turn, likely facilitates the initiation of (+)-strand synthesis by the TBSV RdRp. Enhancement of (-)RNA synthesis by the RH30$^{\Delta N/\Delta C}$ helicase might be indirect and originates from the enhanced (+)RNA production.*

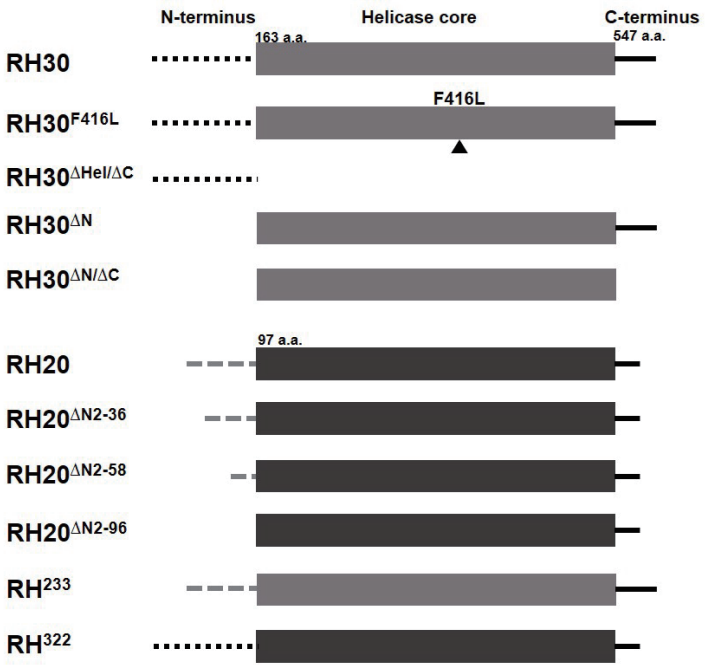
N-terminus
Helicase core
C-terminus
163 a.a.
547 a.a.
RH30
F416L
RH30F416L
RH30ΔHel/ΔC
RH30ΔN
RH30ΔN/ΔC
97 a.a.
RH20
RH20ΔN2-36
RH20ΔN2-58
RH20ΔN2-96
RH233
RH322

Figure 4.12

Fig. 4.12 The schematic representation for AtRH30, AtRH20 and their mutants as well as chimeric DEAD-box helicases. The domains include N-terminal domain, helicase core domain and C-terminal domain. Two chimeric DEAD-box helicases, named RH233 and RH322, were constructed by switching the N-terminal domains between RH20 and RH30.

Chapter 5
The XPO1-dependent nucleocytoplasmic shuttling inhibits the replication of tombusviruses

5.1 Introduction

Plus-stranded RNA [(+)RNA] viruses have small genomes encoding limited numbers of viral proteins. In order to build the intracellular replication organelles for viral replication, (+)RNA viruses co-opt a large number of host cellular proteins and lipids by rewiring host cellular pathways, remodeling subcellular membranes and retargeting the trafficking vesicles [82, 85-87, 176, 185-187]. A group of host factors retains restriction activities by inhibiting distinct replication steps of (+)RNA viruses during the infections[49, 51-54, 88]. The expanding knowledge of host factors involved in the replication of (+)RNA viruses reveals the amazing complexity of virus-host interactions.

Tomato bushy stunt virus (TBSV), one of the best characterized (+)RNA virus, induces the aggregation of peroxisomal and ER membranes through building hundreds of vesicle-like spherule structures in the boundary membrane of peroxisomes [18, 19, 156, 167]. In addition, TBSV has been shown to manipulate

cellular metabolic pathways, the actin network and endosomal trafficking to facilitate viral replication [39, 41, 42, 187]. Systematic genome-wide screens with TBSV have also identified a large number of nuclear localized proteins affecting the replication of TBSV [26-29]. Moreover, several host factors including nucleolin [55], parvulin [110], AtRH20 [104] and AtRH30 DEAD-box helicases (Chapter 3) that fully or partially localize in the nucleus [188] have been characterized to influence the replication of TBSV. However, it remains unclear yet if only the cytosolic pool of the host proteins plays a role in virus replication or if there is a mechanism involving protein translocation from the nucleus into the virus replication compartments.

In eukaryotic cells, the nuclear envelope (NE) separates the nucleus and the cytoplasm, which controls the transport of molecules through the nuclear pore complexes (NPCs) embedded within the NE [189, 190]. Large molecules (>40 KDa) (namely cargoes) generally require nuclear transport receptors, including importin-β-related exportins and importins, for the relocation [191-194]. Xpo1, also known as CRM1, is one of the major highly conserved, RanGTPase-driven exportins that exports proteins and RNAs, which are in the form of ribonucleoproteins (RNPs), from nucleus to cytoplasm [195-197]. Xpo1 recognizes cargoes through a specific leucine-rich nuclear export signal (NES) [198-200]. An active transport of cargoes requires not only the NE and NPCs, but also input of metabolic energy, typically by the

RanGTPase system. Xpo1 bundles cargoes with RanGTP as a transport complex in nucleus and releases the cargoes in the cytoplasm by GTP-hydrolysis [201-205]. In addition, free Xpo1 can re-enter the nucleus for another transport cycle.

It has been reported that Xpo1 facilitates many virus infections. For example, Xpo1 has been shown to transport HIV-1 RNA though binding the NES-containing HIV-1 Rev protein [203, 206, 207]. In addition, respiratory syncytial virus (RSV) matrix (M) protein, which contains a NES, has been shown to bind to Xpo1 for nuclear export [208]. Moreover, it has been reported that influenza A virus exports viral RNA with viral nucleoprotein (NP) as an RNP complex through Xpo1-mediated nuclear export [209]. On the other hand, Xpo1 has been shown to act as a restriction factor against a few virus infections including human T cell leukemia virus type 1 [210] and adenovirus type 2 [211]. Moreover, a previous yeast genome-wide screen with TBSV has shown that overexpression of Xpo1 (CRM1 in yeast) inhibited TBSV replication in yeast [27].

According to previous findings, Xpo1-mediated nuclear export is critical to a wide variety of viruses, most likely through facilitating the nuclear export of viral RNPs or viral proteins. Unlike those viruses replicating their viral genome in the nucleus, TBSV is known for building replication organelles in intracellular membranes facing the cytoplasm. It seems likely that Xpo1 might play distinct roles

in (+)RNA viruses. In this study, I discovered that Xpo1 possessed an anti-viral function that exports previously characterized cell-intrinsic restriction factors (CIRFs) from nucleus to the replication compartment of tombusviruses. The transient expression of Xpo1 inhibited the accumulation of tombusviruses in plants. I provide evidence that the inhibitory effects of nucleolin or Xpo1 were blocked by a small molecule inhibitor of Xpo1-cargo binding in plants. Furthermore, interactions between Xpo1 and CIRFs or TBSV p33 were relocated from the perinucleus to the viral replication compartment. Thus, Xpo1-dependent nucleocytoplasmic shuttling is essential for the active relocation of CIRFs into the replication compartment of tombusviruses. Further mechanistic studies are needed to gain insight into the role of nucleocytoplasmic shuttling in TBSV replication.

5.2 Materials and methods

Yeast strain and expression plasmids. Yeast *Saccharomyces cerevisiae* strain BY4741 was obtained from Open Biosystems (Huntsville, AL, USA). The temperature-sensitive (ts) mutant of Srm1p in S. cerevisiae is a generous gift from Charles Boone [114]. The yeast cells of ts strain were transformed and cultured as described [30].

The RT-PCR products of *Arabidopsis* Xpo1 was obtained from *Arabidopsis* cDNA with primers #7221 and #7222, followed by the digestion with BamHI and SalI. The digested product was ligated to BamHI/SalI-digested pGD-vector or BamHI/XhoI-digested pGEX-his-RE vector, respectively, generating pGD-AtXpo1 pGEX-his-AtXpo1.

To clone a BiFC expression vector for nYFP-AtXpo1, the previously published plasmid pGD-nYFP-MBP[42] was digested with BamHI and SalI to remove the sequence of MBP, followed by the ligation with BamHI/SalI-digested AtXpo1 product, resulting in pGD-nYFP-AtXpo1.

In order to perform BiFC assay in N. *benthamiana*, a pGD-cYFP was constructed to carry multiple restriction enzyme sites (5'-BamHI/XhoI/XbaI-cYFP ORF- SacI-3'). The sequence of cYFP was PCR-amplified from plasmid pGD-T33-cYFP[42] with primers #7378 and #5910, followed by the digestion with XbaI and XhoI. The digested product was then ligated with XbaI/SalI-digested pGD vector, resulting in pGD-cYFP-CY. The previous BamHI/SalI-digested AtXpo1 product was used for ligation with BamHI/XhoI-digested pGD-cYFP-CY, creating pGD-Xpo1-cYFP. In addition, the sequence of AtNuc-L1 was PCR amplified from the plasmid pGWB5 [212], a generous gift of Dr. K. Nakamura, with primers #7301 and #7302, followed by the digestion with BamHI and PstI. On the other hand, the plasmid pGD-

T33-cYFP was digested with BamHI and PstI to remove the sequence of p33 of TBSV, followed by the ligation with BamHI/PstI-digested AtNuc-L1 product, generating pGD-AtNucL1-cYFP.

To test the interaction of AtXpo1-cYFP with Arp2 and Arp3 by BiFC assay in plants, the constructs were cloned as follows: The sequences of Arp2 or Arp3 were RT-PCR amplified from *Arabidopsis* cDNA with primers #7395 and #7396 or #7397 and #7398, respectively. The RT-PCR products of Arp2 or Arp3 were digested with BglII and XhoI, followed by the ligation with previously BamHI/SalI-digested pGD-nYFP vector, resulting in pGD-nYFP-Arp2 or pGD-nYFP-Arp3, respectively.

Confocal laser microscopy. To observe if *Arabidopsis* RH30 DEAD-box helicase is relocated through Xpo1-dependent nuclear transport, the subcellular localization of Arabidopsis RH30 in plant protoplasts was observed with an N-terminal fusion of RH30 to GFP. The transgenic N. *benthamiana* (expressing H2B fused to RFP, a generous gift from Dr. Goodin) leaves were infiltrated with *Agrobacterium* carrying expression plasmids pGD-GFP-RH30 (OD_{600} 0.8) [Wu and Nagy, in press] and pGD-P19 (OD_{600} 0.2). Approximately 48 h post-infiltration, protoplasts were isolated from the infiltrated leaves as described [159], followed by a 6 h treatment with 40 nM Leptomycin B (LMB) (Cell Signaling Technology, Inc.) or equal volume of EtOH as a

control. Imaging of plant protoplast was performed on an Olympus FV1000 confocal microscopy using 60X water-immersion objective. GFP was excited by 488 nm laser and RFP was excited by 543 nm laser. Images were obtained and merged using Olympus FLUOVIEW 1.5.

To detect the interaction of proteins in N. *benthamiana* plants, bimolecular fluorescence complementation (BiFC) assay was performed with *Agrobacterium* infiltration. The leaves of wild-type or transgenic N. *benthamiana* (expressing CFP-H2B as a nuclear marker) were infiltrated with *Agrobacterium* carrying pGD-P19 (OD_{600} 0.2), pGD-RFP-SKL (OD_{600} 0.4) along with different combination of constructs as following description: nYFP-AtXpo1 (OD_{600} 0.4) and pGD-T33-cYFP (OD_{600} 0.4) [42]; pGD-nYFP-MBP (OD_{600} 0.4, as a control) and pGD-T33-cYFP (OD_{600} 0.4); pGD-nYFP-AtNucL1 (OD_{600} 0.4) and pGD-cYFP-AtXpo1 (OD_{600} 0.4); pGD-nYFP-AtArp2 (OD_{600} 0.4) and pGD-cYFP-AtXpo1 (OD_{600} 0.4); pGD-nYFP-AtArp3 (OD_{600} 0.4) and pGD-cYFP-AtXpo1 (OD_{600} 0.4); pGD-nYFP-MBP (OD_{600} 0.4, as a control) and pGD-cYFP-AtXpo1 (OD_{600} 0.4). After 16 h, infiltrated leaves of N. *benthamiana* plants were inoculated with MOCK or TBSV crude sap inoculum. Approximately 2 days post-virus inoculation, imaging of infiltrated leaves was performed as described above except YFP was excited by 514nm laser and CFP was excited by 485 nm laser.

The accumulation of viral RNA in yeast and plants. To launch TBSV repRNA replication in the wild-type (wt) yeast *Saccharomyces cerevisiae* or yeast cells expressing ts-srm1p, yeast cells were transformed with LpGAD-CUP1::HisFlag-p92 and HpGBK-CUP1::HisFlag-p33/GAL1::DI-72 [187]. The obtained yeast transformants were grown in SC-LH$^-$ media containing 2% galactose and 0.1mM BCS at 23°C. After 18h, the yeast culture was transferred to SC-LH$^-$ media containing 2% galactose and 50 μM $CuSO_4$ and incubated at permissive temperature (23°C) for wt yeast or at semi-permissive temperature (29°C) for ts-srm1p yeast. After 24 h, the obtained yeast cells were used for further Northern blot analysis and Western blot analysis.

To detect the accumulation of tombusviruses in N. *benthamiana* plants expressing Arabidopsis Xpo1, the leaves of N. *benthamiana* were infiltrated with *Agrobacterium* carrying pGD-P19 and pGD-AtXpo1 or pGD vector (as a control). In the experiment of CNV infection, plants were also co-infiltrated with *Agrobacterium* carrying pGD-CNV^{20Kstop}. In the experiment for CIRV infection, plants were inoculated with CIRV crude sap incoculum, 16 h after agro-infiltration. The agro-infiltrated leaves were also infiltrated with 40 nM LMB or equal volume of EtOH (as a control) on the first day of *Agrobacterium* infiltration and second time 1 day after

the first infiltration. Total RNA extraction and Northern blot were performed as described [79] to analyze the accumulation levels of tombusviruses in inoculated leaves 2.5 d post virus inoculation.

Purification of recombinant proteins from E. *coli*. Recombinant proteins GST-AtXpo1, GST, MBP-p33, MBP-p92 were expressed in E. *coli* and affinity-purified as described [78]. Briefly, E. *coli* strain BL21 (DE3) CodonPlus (Stratagene) cells were transformed with expression plasmids to express the recombinant proteins. The transformed E. *coli* cells were cultured at 37°C for 16h, followed by dilution of the culture to OD_{600} 0.2 with fresh media. The E. *coli* culture was then incubated at 37°C until its OD600 1.0. The culture was supplemented with isopropyl-β-D-thiogalactopyranoside (IPTG) and incubated at 16°C for 8 h. The E. *coli* cells were then collected by centrifugation at 5,000 rpm at 4°C for 5 min, followed by the resuspension with ice- cold column buffer (20mM HEPES [pH7.4], 25 mM NaCl, 1mM EDTA [pH 8.0]) containing 10 mM β-mercaptoethanol and 1 µg of RNase A in each 4 ml of E. *coli* cells suspension. After sonication on ice, the cell lysates were centrifuged at 15,000 rpm at 4°C for 15 min. The obtained supernatant was incubated with GST bind resin (EMD Millipore) for GST fusion proteins or amylose resin (NEB) for MBP fusion proteins at 4°C for 2 h, respectively. After the resin was

washed with ice- cold column buffer, elution of the recombinant protein was performed with column buffer containing 10mM glutathione and 1mM DTT in pH 7.5 for GST fusion proteins or 0.36% [W/V] maltose and 1mM DTT for MBP fusion proteins.

Analysis of TBSV replication with *in vitro* reconstituted TBSV replicase in yeast cell-free extract (CFE). The yeast cell-free extract (CFE) that supports *in vitro* TBSV repRNA replication was prepared with yeast strain BY4741 as described [31, 32]. The *in vitro* reconstituted TBSV replicase assay was performed with the mixture of 2 µl of CFE, 0.5 µg DI-72 (+)repRNA, 0.2 µg affinity-purified maltose-binding protein (MBP)-p33 as well as MBP-$p92^{pol}$ (both recombinant proteins were purified from E. *coli*), 5 µl of buffer A (30mM HEPES-KOH [pH 7.4], 150 mM potassium acetate, 5 mM magnesium acetate, 0.13 M sorbitol), 2 µl of 150 mM creatine phosphate, 0.2 µl of 10 mg/ml creatine kinase, 0.4 µl actinomycin D (5mg/ml), 0.2 µl of 1 M dithiothreitol (DTT), 0.2 µl of RNase inhibitor, 2 µl a ribonucleotide (rNTP) mixture (10 mM of ATP, CTP, and GTP as well as 0.25 mM UTP) and 0.1 µl of [^{32}P]UTP in a total of 20 µl reaction volume. The reaction was performed at 25°C for 3h and then stopped by the addition of 5 volumes of 1% SDS and 5 mM EDTA, followed by phenol-chloroform extraction and RNA precipitation. Then the repRNA products and

dsRNA intermediates were analyzed by electrophoresis in 0.5X Tris-borate-EDTA (TBE) buffer in a 5% polyacrylamide gel (PAGE) containing 8 M urea.

RNA gel shift assay (EMSA). For RNA-binding studies, EMSA was performed as described previously [12] with minor modification. Briefly, the assay was performed with 0.1 pmol of ^{32}P-labeled TBSV (+)repRNA or (-)repRNA probes with increasing amounts (1.9μM, 3.8μM and 5.7 μM) of purified GST or GST-AtXpo1 in the presence of RNA binding buffer (10 mM HEPES [pH7.4], 50 mM NaCl, 1 mM DTT, 1 mM EDTA, 5% Glycerol, 2.5 mM $MgCl_2$), 2 U of RNase inhibitor and 0.1 μg of tRNA in a total of 10 μl reaction volume. To test if LMB inhibitor influence the RNA affinity, 500 nM of LMB or EtOH (as a control) were added in the reaction mixture, followed by incubation at 25°C for 15 min. The ^{32}P-labeled probes were analyzed by non-denaturing 5% polyacrylamide gel (PAGE) in 1X Tris-acetate-EDTA (TAE) buffer.

Plant cell fractionation. To exam if CNV infection induces the relocation of RH30 DEAD-box helicase from nucleus to cytoplasm, fractionation of infected or healthy N. *benthamiana* cells was performed as described [213]. The leaves of N. *benthamiana* were infiltrated with *Agrobacterium* carrying pGD-p19 (OD_{600} 0.2) and

pGD-6xHis-RH30 [Wu and Nagy, in press] (OD_{600} 0.8). For CNV infection, the leaves were co-infiltrated with *Agrobacterium* to express $CNV^{20Kstop}$ gRNA. At 2.5 d post infiltration, about 0.5g of plant leaves were harvested and ground to a fine powder in liquid nitrogen, followed by mixing with 2 ml/g of lysis buffer (20mM Tris-HCl [pH 7.5], 20 mM KCl, 2 mM EDTA, 2.5 mM $MgCl_2$, 25% glycerol, 250 mM Sucrose and 5 m M DTT) containing protease inhibitor cocktail (Roche). The obtained homogenate was filtered through a double-layer of Cheesecloth. The flow-through was centrifuged at 1,500 g for 10 min to remove the cell debris. The obtained supernatant was centrifuged at 10,000g at 4°C for 10 min. The supernatant was collected as soluble fraction (cytoplasmic fraction), while the pellet was washed with NRBT buffer (20 mM Tris-HCl [pH 7.5], 25% glycerol, 2.5 mM $MgCl_2$ and 0.2% Triton X-100) four times, followed by resuspension with 500 µl of NRB2 buffer (20 mM Tris-HCl [pH 7.5], 250 mM Sucrose, 10 mM $MgCl_2$ 0.5% Triton X-100 and 5 mM β-mercaptoethanol) containing protease inhibitor cocktail (Roche). The mixture was loaded carefully on the top of 500 µl of NRB3 buffer (20 mM Tris-HCl [pH 7.5], 1.7 M Sucrose, 10 mM $MgCl_2$ 0.5% Triton X-100 and 5 mM β-mercaptoethanol) containing protease inhibitor cocktail (Roche), followed by centrifugation at16,000 g 4°C for 45 min. The obtained pellet was resuspended in 400µl of lysis buffer. For the quality control of the fractionation, tRNA detected by ^{32}P-labeled specific probe and

HSP70 detected by anti-HSP70 antibody were used as cytoplasmic markers. U6 snRNA detected by ^{32}P-labeled specific probe was used as a nuclear marker. The sequence of tRNA were fused with T7 promoter by PCR-amplified from *Arabidopsis* cDNA with primers #7034 and #7035 and used as a template for in vitro T7 transcription to generate ^{32}P-labeled tRNA probe. Similar approach was applied with primer #7032 and #7033 for U6 snRNA.

5.3 Results

Xpo1 exportin has anti-viral function in plants and yeast. A previous proteome-wide screen with TBSV in yeast has shown that the overexpression of Crm1p (named Xpo1 in plants) inhibited TBSV replication in yeast [27]. The plant exportin 1, namely Xpo1, controls the nuclear export of many nucleocytoplasmic shuttling proteins. Therefore, I firstly tested if expression of Xpo1 inhibits the accumulation of tombusviruses in plants. I found that the transient expression of Xpo1 by agro-infiltration inhibited the accumulation of *cucumber necrosis virus* (CNV), a close relative of *tomato bushy stunt virus* (TBSV), and *carnation Italian ringspot virus* (CIRV) by 70-80 % (Fig 5.1A and B) in *N. benthamiana* plants. CNV and TBSV utilize similar set of host factors and intracellular membrane of peroxisome for viral

replication [88]. To get insight into the role of Xpo1 in TBSV replication, bimolecular fluorescence complementation (BiFC) assay was performed by agro-infiltration to express nYFP-Xpo1, TBSV p33-cYFP and RFP-SKL (peroxisomal luminar marker) in transgenic *N. benthamiana* plants expressing CFP-H2B (nucleus marker). I found that Xpo1 interacted with TBSV p33 in the perinuclear region and TBSV replication compartment, which was marked by RFP-SKL peroxisomal luminal marker protein (Fig 5.1C). MBP was used as a control that shows no BiFC signal with TBSV p33 (Fig 5.1D). Moreover, the replication of TBSV repRNA was inhibited by 80% when recombinant Xpo1 was added into an *in vitro* CFE-based TBSV replicase reconstitution assay (Fig 5.1E, lane 4). Because both the dsRNA replication intermediate and new (+)RNA were reduced (Fig 5.1E, lane 4), it is likely that Xpo1 targets an early step in TBSV replication. Thus, I conclude that Xpo1 targets TBSV replication through direct interaction with p33 replication proteins into the viral replication compartment in plant cells.

Nucleocytoplasmic shuttling pathway is critical in TBSV replication. Leptomycin B (LMB) has been characterized as a highly efficient and selective inhibitor of nuclear export mediated by Xpo1. The covalent conjugation of LMB by the nuclear export signal (NES)-binding groove of Xpo1 inactivates the function of binding cargoes

[214, 215]. To test if the inhibitory activity of Xpo1 expression is attributed to its cargoes, I infiltrated LMB, which is dissolved in EtOH, into the leaves of *N. benthamiana* plants transiently expressing Xpo1 upon CNV and CIRV infections. I found that the LMB treatment not only reduced the inhibitory effect of Xpo1 expression against CNV by 20%, but also increased the CNV accumulation by ~10 % in the pGD vector control in comparison to EtOH-treated sets (Fig 5.1A). Moreover, the accumulation of CIRV was increased by 8-fold with the LMB treatment in the Xpo1 expressed plants (Fig 5.1B). Also, the accumulation of CIRV was increased by 2-fold in pGD vector control in comparison to EtOH-treated plants (Fig 5.1B). Based on the results of LMB treatment, I suggest that the cargoes of Xpo1 contribute to the inhibitory effect of Xpo1 expression on tombusvirus replication.

The loading and unloading of karyopherins, an collective term for exportins and importins, with cargo molecules are controlled by the ratio of Ran GTPase (Ran GTP and Ran GDP) [191, 195]. The Ran guanine nucleotide exchange factor, RCC1 (Srm1/Prp20 in yeast), maintains the high ratio of Ran GTP:Ran GDP in the nucleus, which results in a concentration gradient of Ran GTP across the nuclear envelope [193, 216-218]. This asymmetric distribution of Ran GTP has been shown as the major driving force for nuclear protein translocation in both directions. In order to gain insight into the nucleocytoplasmic shuttling pathway, I launched the highly

efficient TBSV repRNA replication in yeast expressing the temperature sensitive mutant of Srm1p, namely ts-srm1. The semi-permissive temperature for yeast culturing was used at 4 °C below the non-permissive temperature, resulting in partial inactivation of the ts-srm1p essential functions[28]. The ts-srm1p mutant was expressed as the only copy of this gene in this haploid yeast system. Interestingly, the accumulation of TBSV repRNA in yeast expressing ts-srm1p was about 4-fold higher at semi-permissive temperature (29°C) and comparable level at permissive temperature (23°C) in comparison to yeast expressing wt Srm1p (Fig 5.2). This indicates that the replication of TBSV is enhanced if the nucleocytoplasmic shuttling pathway is blocked by the partial inactivation of Srm1p.

The previously identified cell-intrinsic restriction factors are possible cargoes of Xpo1. A recent global proteomic study has shown that not only nuclear proteins, but also cytosolic proteins are subjected to Xpo1-dependent nuclear export [197]. Moreover, the number of Xpo1 possible cargoes is greater than 700 in yeast *S. cerevisiae* and about 1000 in human [197], suggesting that many of the host proteins affecting TBSV replication might be involved in Xpo1-dependent nuclear export. To test if host proteins influencing TBSV replication could interact with Xpo1 in plants, I selected *Arabidopsis* nucleolin (AtNuc-L1 in plants) [55], *Arabidopsis* Arp2 and Arp3

actin nucleators [39] for the BiFC assay in *N. benthamiana* plant epidermal cells. I found that nucleolin interacted with Xpo1 in the nucleus (indicated by CFP-H2B, a nuclear marker) without virus infection, while the interaction between nucleolin and xpo1 occurred in both nucleus and the TBSV replication compartment (indicated by the RFP-SKL peroxisomal luminal marker protein) (Fig 5.3A). Interestingly, Arp2 was found only to interact with Xpo1 in the nucleus and the replication compartment in TBSV infected cells in comparison to the cells without virus infection (Fig 5.3B). I did not observe interaction between Arp3 and Xpo1 in mock-treated and TBSV-infected cells (Fig 5.3C). MBP was used as a negative control for the interaction with Xpo1 (Fig 5.3D). Altogether, it seems likely that Arabidopsis nucleolin and Arp2 are cargoes of Arabidopsis Xpo1 in plant cells.

Although nucleolin has been identified as a cell-intrinsic restriction factor that directly binds to the 3'UTR of TBSV (+)RNA and inhibits early step of the viral replication, the relocation of nucleolin from nucleolus to the TBSV replication compartment was non-detectable [24, 55]. Despite that, another study has shown that nucleolin was relocated from the nucleolus to the cytoplasm in poliovirus infected cells [219]. Since nucleolin might be a cargo of Xpo1, it is possible that nuclear-localized nucleolin was exported by Xpo1 to the cytoplasm for its restriction function. To test this possibility, the leaves of *N. benthamiana* plants transiently expressing

nucleolin or GFP control were co-infiltrated with LMB. The inhibitory effect of nucleolin expression was reduced by ~60 % by the LMB treatment in CNV-infected *N. benthamiana* plants (Fig 5.3E). This result suggests that the restriction function of nucleolin might rely on Xpo1-depedent nuclear export.

Xpo1 binds to TBSV (+) and (-)RNA. Xpo1 is known as a major RNA export receptor that is involved in the nuclear export of various RNA species including rRNAs, U snRNAs (small nuclear RNA), viral RNA (e.g. HIV RNA), microRNA and several specific mRNAs [193, 196, 220]. However, nearly all known RNA exports are associated with an adapter protein (e.g. CBC/PHAX for U snRNA export; HIV Rev for viral RNA export; TAP protein for mRNA export) or protein complex (e.g. Argonaute proteins and RNA helicase A for miRNA export) [193, 196, 220]. In order to gain insight into the interaction between Xpo1 and TBSV, I tested if XpoI binds TBSV RNA in *in vitro* gel shift assay (EMSA). Surprisingly, the recombinant Xpo1 bound to TBSV (+) and (-)repRNA without the aid of adaptor proteins (Fig 5.4A). To investigate if the binding of Xpo1 to TBSV repRNA is mediated by the NES-binding groove of Xpo1, I added LMB together with recombinant Xpo1 and TBSV (+) and (-)repRNA in the *in vitro* EMSA. I found that the binding of recombinant Xpo1 to either TBSV (+) or (-)repRNA was not blocked by the LMB treatment, suggesting

that the NES-binding groove of Xpo1 is not responsible for TBSV repRNA binding (Fig 5.4A). On the other hand, the addition of LMB in the CFE-based TBSV replicase reconstitution assay reduced the inhibitory activity of recombinant Xpo1 by ~40-50 % (Fig 5.4B; lane 2 and 3 as well as lane 5 and 6 versus lane 8 and 9). Altogether, these results suggest that the inhibitory activity of recombinant Xpo1 was attributed to the cargoes instead of the direct binding to TBSV RNA.

The cellular distribution of the antiviral RH30 DEAD-box helicase is mediated by Xpo1. It has been shown that several DEAD/H helicases are translocated in a bi-direction manner between the nucleus and the cytoplasm [206, 221-223]. To test if a previously characterized CIRF RH30 DEAD-box helicase (chapter 3) is an Xpo1-dependent shuttling protein, I detected the subcellular localization of GFP-RH30 upon LMB treatment with confocal microscopy. Interestingly, LMB treatment enriched the distribution of GFP-RH30 in the nucleus, while LMB did not influence the distribution of GFP control (Fig 5.5A). This indicates that the localization of GFP in the nucleus is due to passive diffusion [195], while the cytosolic pool of RH30 was actively exported by Xpo1 from the nucleus.

To further examine if virus infection induces the relocation of RH30 from the nucleus to the cytoplasm, I detected the amount of 6xHis-tagged RH30 in the soluble

and nuclear fractions in the *N. benthamiana* plant cells. I found that the relocation of RH30 was non-detectable in CNV infected plant cells (Fig 5.5B). The accumulation of tRNA and HSP70 was detected as cytosolic markers, while U6 snRNA was detected as nuclear markers.

5.4 Discussion

Tombusviruses as (+)RNA viruses are astonishingly efficient in replication to produce a large number of progeny viruses in a short period of time in infected cells [85, 88, 224]. Building viral replication organelles using intracellular membranes to have robust viral replication requires a complex remodeling process of the cell by viruses, such as rewiring cellular pathways and retargeting the trafficking vesicles [22, 24, 33, 88, 185, 225]. However, the process of remodeling involved in the replication of tombusviruses is incompletely understood. Previous studies of the nuclear-localized nucleolin protein have shown it to bind directly to TBSV gRNA inhibiting TBSV replication [55], suggesting that a nucleus transport pathway is likely involved in the TBSV infection. In addition, a previous yeast proteome-wide screening has shown that the overexpression of Xpo1 inhibited TBSV replication in yeast [27],

further indicating the Xpo1-mediated nuclear export plays a role in TBSV replication. Accordingly, in this work I show that the nucleocytoplasmic shuttling pathway mediated by Xpo1 is involved in TBSV replication and may transport restriction factors to the viral replication compartment.

I found that transient expression of Xpo1 inhibited CNV and CIRV accumulation in *N. benthamiana* plants (Fig 5.1A-B). The BiFC assay showed that Xpo1 interacted with TBSV p33 replication protein in the viral replication compartment in *N. benthamiana* plants (Fig 5.1C). *In vitro* reconstitution of the tombusvirus replicase in CFEs showed recombinant Xpo1 inhibited the replication of TBSV repRNA (Fig 5.1E). However, the presence of nucleocytoplasmic transport is unlikely existed in the CFEs, suggesting that recombinant Xpo1 itself might possess anti-viral activities. Yet, the chemical inhibitor LMB, which is known to selectively bind to the NES-binding groove of Xpo1 to inactivate the binding function [214, 215], could partially nullify the inhibitory effect when low amount of recombinant Xpo1 was used in *in vitro* reconstituted TBSV replicase assay (Fig 5.4B). This result led to two possibilities of how recombinant Xpo1 inhibited *in vitro* TBSV repRNA replication. Firstly, Xpo1 might bind to TBSV p33 replication in its NES-binding groove and therefore inhibit the TBSV replication. Secondly, it has been shown that Xpo1 still bound to several cargoes without the assistance of RanGTP in the *in vitro* condition [197].

Recombinant Xpo1 bringing soluble proteins with low binding affinity in the CFEs to the *in vitro* viral replication complexes (VRCs) might result in the reduction of repRNA replication. Both possibilities need further investigation for evidence. Altogether, Xpo1 shows anti-viral functions against tombusviruses.

Srm1p, also known as RCC1, is a RanGEF that facilitate to switch Ran-GDP into Ran-GTP to ensure the constant concentration gradience across the nuclear envelope. Partial depletion of the ts-srm1p at semi-permissive temperature in yeast likely shuts down the nuclear transport pathway, resulting in the increase of TBSV repRNA accumulation (Fig 5.2). This suggested that the nuclear transport pathway performs anti-viral functions in TBSV replication.

The best well-characterized function of Xpo1 is the nuclear export of cargoes containing NES [193, 195, 226]. Accordingly, the inhibitor LMB was deployed in the Xpo1 or nucleolin expressed *N. benthamiana* plants. The inhibitory effect of transient expression of Xpo1 could be nullified by treating plants with LMB, especially in the case of CIRV (Fig 5.1 A-B). Similarly, the inhibitory effect of transient expression of nucleolin could be partially nullified by treating plants with LMB (Fig 5.3E). On the other hand, BiFC for the interaction between Xpo1 and nucleolin or Arp2 (Fig 5.3A-B) as well as the sequestering RH30 DEAD-box helicase in the nucleus by the LMB treatment (Fig 5.5A) showed many CIRFs are possible cargoes of Xpo1. Altogether,

the nucleocytoplasmic shuttling by Xpo1 is required for the restriction functions of possible cargoes including nucleolin. Also, Xpo1-mediated nuclear export pathway likely transported cargoes relevant to the mitochondria membrane environment. In addition, TBSV infection strengthened the nuclear export of restriction factors such as Arp2 (Fig 5.3B), suggesting host cells likely modulated the actin dynamics through Xpo1-mediated nuclear export against TBSV infections, while TBSV recruited Cof1 to stabilize the actin filament bundle [39].

Most of RNA exports are associated with an adapter protein (e.g. CBC/PHAX for U snRNA export; HIV Rev for viral RNA export; TAP protein for mRNA export) or ribonucleoprotein complex (e.g. Argonaute proteins and RNA helicase A for miRNA export) [193, 196, 220]. Surprisingly, *in vitro* RNA gel shift assay showed that purified Xpo1 itself bound to the TBSV (+)repRNA and (-)repRNA ouside of the NES-binding groove. Previous proteome-wide screening revealed several proteins, such as Upf1 and Upf2, responsible for mRNA degradation are excellent binder to Xpo1 [197]. It is possibly Xpo1 brings Upf1 or Upf2 to TBSV RNA for degradation. Yet, this model needs to be further tested. To summarize, the data of this study supports the emerging significance of Xpo1-depedent nuclear export in viral infections.

N. O. of primers	Sequences
5910	CCGCTCGAGTCACTTGTACAGCTCGTCCATGCC
7032	GGAGTTAATACGACTCACTATAGGGAGAGAGAGAGGGGCCATGCTAATCTTCTC
7033	GGAGTTAATACGACTCACTATAGGGAGAGAGAGGAGAAGATTAGCATGGCCCCT
7034	GGAGTTAATACGACTCACTATAGGGAGAGAGAGTCGAACTCTCGACCTCAGGAT
7035	GGAGTTAATACGACTCACTATAGGGAGAGAGAGATCCTGAGGTCGAGAGTTCGA
7221	CGGGATCCATGGCGGCTGAGAAGTTAAGG
7222	ACGCGTCGACTTATGAGTCCACCATCTCGTC
7301	CGGGATCCATGGGAAAGTCTAAATCCGCCAC
7302	AACTGCAGCTCGTCACCGAAGGTAGTCTTC
7378	GCTCTAGAATGGGCAGCGTGCAGCTCGCCG
7395	GAAGATCTATGGACAACAAAAACGTCG
7396	CCGCTCGAGTTAAGCTTGGCTCATTTTATTC
7397	GAAGATCTATGGATCCGACTTCTCGAC
7398	CCGCTCGAGTCAATACATTCCCTTGAACACCGG

Table 5.1

Table 5.1 The sequence of the primers used in this study.

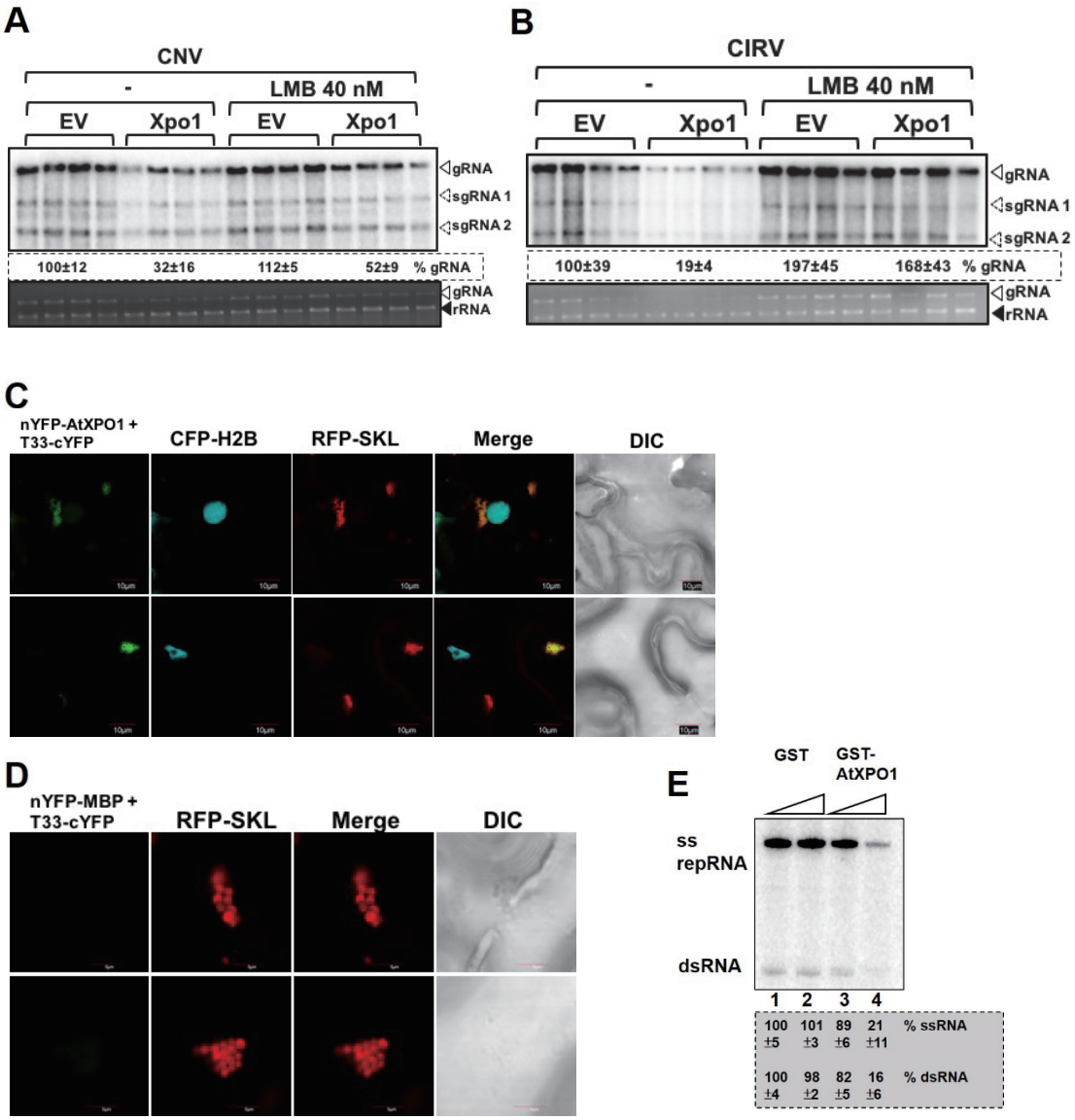
A
CNV
-
LMB 40 nM
EV
Xpo1
EV
Xpo1
gRNA
sgRNA 1
sgRNA 2
100±12
32±16
112±5
52±9
% gRNA
gRNA
rRNA
B
CIRV
-
LMB 40 nM
EV
Xpo1
EV
Xpo1
gRNA
sgRNA 1
sgRNA 2
100±39
19±4
197±45
168±43
% gRNA
gRNA
rRNA
C
nYFP-AtXPO1 +
T33-cYFP
CFP-H2B
RFP-SKL
Merge
DIC
D
nYFP-MBP +
T33-cYFP
RFP-SKL
Merge
DIC
E
GST
GST-
AtXPO1
ss
repRNA
dsRNA
1 2 3 4
100 101 89 21 % ssRNA
±5 ±3 ±6 ±11
100 98 82 16 % dsRNA
±4 ±2 ±5 ±6

Figure 5.1

Figure 5.1 The anti-viral role of Xpo1 in the replication of tombusviruses. *(A-B) Transient expression of AtXpo1 in N. benthamiana plants inhibits the accumulation of cucumber necrosis virus (CNV) and carnation Italian ringspot virus (CIRV). Top panel: Northern blot analysis of CNV or CIRV gRNA and sgRNAs was performed with CNV or CIRV 3' end specific ^{32}P-labeled probes, respectively. The 18S ribosomal RNAs were detected by ethidium bromide (EtBR) staining and were used as loading controls. The N. benthamiana leaves were infiltrated with Agrobacterium for transient expression of AtXpo1 or pGD vector (as controls). The infiltrated leaves were either infiltrated with EtOH as a control or 40 nM of Leptomycin B (LMB), a chemical inhibitor of nuclear export. (C-D) Bimolecular fluorescence complementation (BiFC) assay shows AtXpo1 interacts with TBSV p33 in TBSV-infected N. benthamiana epidermal cells. The leaves of transgenic N. benthamiana expressing CFP-H2B (a nuclear marker) were infiltrated with Agrobacterium to express nYFP-AtXpo1 or nYFP-MBP (as a control) as well as TBSV p33 (T33)-cYFP and RFP-SKL (a peroxisomal luminar marker), followed by inoculation with TBSV sap ~16 h post infiltration. (E) Recombinant GST-AtXpo1 inhibits the in vitro replication of TBSV repRNA in yeast CFE-based reconstitution of the TBSV replicase. The E. coli expressed and then purified recombinant TBSV p33 and p92 replication proteins along with the template TBSV (+)repRNA were added to launch the in vitro replication of TBSV repRNA in the reconstituted replicase. Increasing amounts (1.9 and 3.8 μM) of GST (as a control) or GST-AtXpo1 were added to the reaction. A 5% polyacrylamide PAGE containing 8 M urea shows the accumulation of ^{32}P-labeled TBSV (+)repRNAs and dsRNA replication intermediate.*

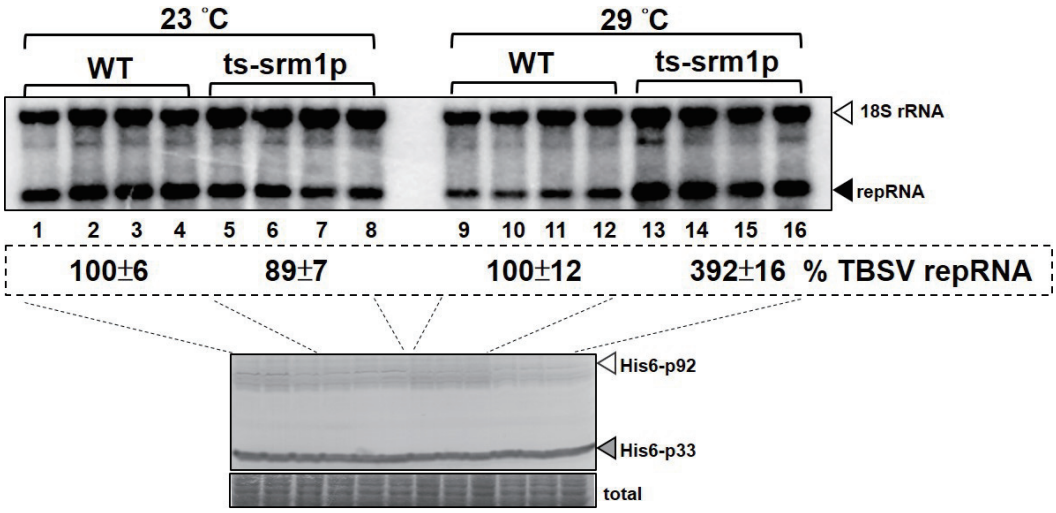
23 ˚C
29 ˚C
WT
ts-srm1p
WT
ts-srm1p
18S rRNA
repRNA
1 2 3 4 5 6 7 8 9 10 11 12 13 14 15 16
100±6
89±7
100±12
392±16 % TBSV repRNA
His6-p92
His6-p33
total

Figure 5.2

Figure 5.2 The accumulation of TBSV repRNA in srm1p^{ts} or wt yeasts at permissive temperature (23 °C) or semi-permissive temperature (29 °C). *In the yeast cells, His$_6$-p33 and His$_6$-p92 from a copper-inducible CUP1 promoter and TBSV (+)repRNA from GAL1 promoter were expressed to launch the replication of TBSV repRNA. Top panel: Northern blot analysis of TBSV repRNA accumulation was detected using a 3' end specific probe. Bottom panel: Western blot analysis of the accumulation of His$_6$-p33 and His$_6$-p92 proteins using anti-His antibody. Coomassie Brilliant Blue staining were used for the normalization of total proteins.*

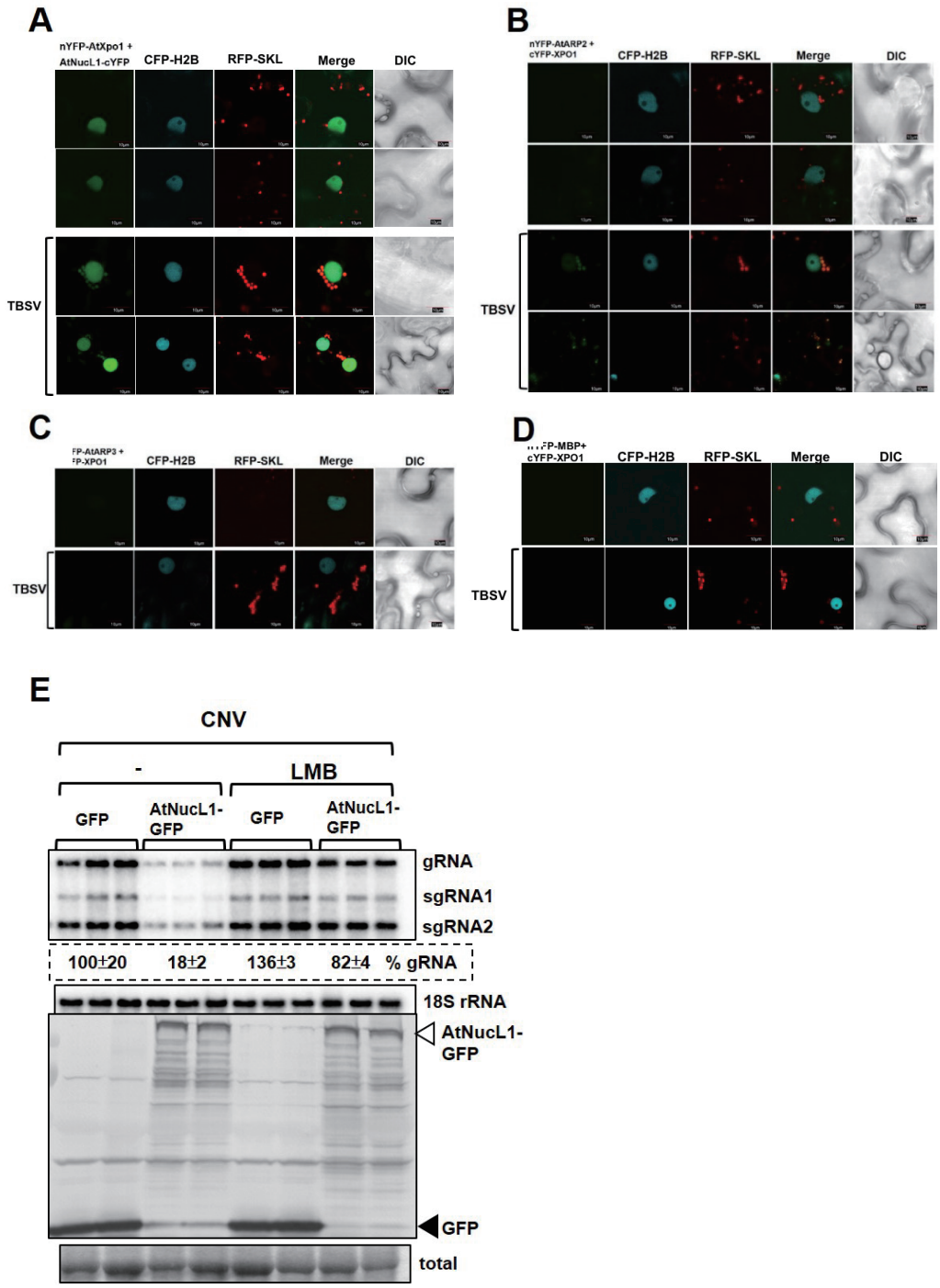
A
nYFP-AtXpo1 +
AtNucL1-cYFP
CFP-H2B
RFP-SKL
Merge
DIC
TBSV
B
nYFP-AtARP2 +
cYFP-XPO1
CFP-H2B
RFP-SKL
Merge
DIC
TBSV
C
FP-AtARP3 +
FP-XPO1
CFP-H2B
RFP-SKL
Merge
DIC
TBSV
D
,,,FP-MBP+
cYFP-XPO1
CFP-H2B
RFP-SKL
Merge
DIC
TBSV
E
CNV
-
LMB
GFP
AtNucL1-
GFP
GFP
AtNucL1-
GFP
gRNA
sgRNA1
sgRNA2
100±20
18±2
136±3
82±4
% gRNA
18S rRNA
AtNucL1-
GFP
GFP
total

Figure 5.3

Figure 5.3 AtXpo1 interacts with TBSV specific cell-intrinsic restriction factors. *(A-D) Top images: The interactions between Xpo1 and nucleolin (AtNuc-L1, panel A), Arp2 (panel B), Arp3 (panel C) or MBP (as a control, panel D) in the non-infected N. benthamiana epidermal cells were imaged using the BiFC assay. Bottom images: The same sets of the protein expression in TBSV-infected N. benthamiana epidermal cells were performed using BiFC assay. The leaves of N. benthamiana were co-infiltrated with Agrobacterium to express nYFP-AtNuc-L1, nYFP-Arp2, nYFP-Arp3 or nYFP-MBP (as a control) along with cYFP-AtXpo1 and RFP-SKL (peroxisome luminar marker). The images of interactions in the epidermal cells were taken by confocal laser microscopy. (E) LMB treatment reduces the inhibitory effect from the transient expression of AtNuc-L1 in N. benthamiana plants. Top panel: Northern blot analysis of CNV accumulation in N. benthamiana plants expressing GFP (as a control) or AtNuc-L1-GFP upon the EtOH treatment (as a control) or 400 nM LMB treatment. A ^{32}P-labeled probe specific to 3' end of CNV gRNA was used for the detection of CNV gRNA and sgRNAs. Middle panel: Northern blot with 18S ribosomal RNA specific probe was utilized as a loading control. Bottom panel: Western blot analysis of the levels of GFP and AtNuc-L1-GFP with anti-GFP antibody. Coomassie Brilliant Blue staining were used for the normalization of total proteins.*

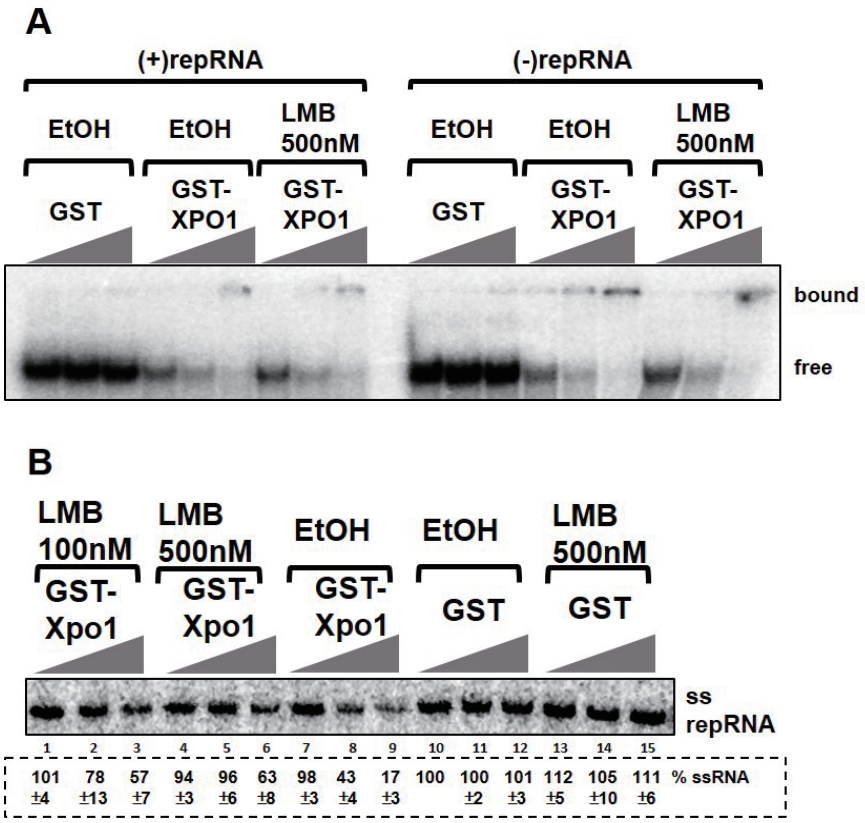
A
(+)repRNA
(-)repRNA
EtOH
EtOH
LMB 500nM
EtOH
EtOH
LMB 500nM
GST
GST-XPO1
GST-XPO1
GST
GST-XPO1
GST-XPO1
bound
free
B
LMB 100nM
LMB 500nM
EtOH
EtOH
LMB 500nM
GST-Xpo1
GST-Xpo1
GST-Xpo1
GST
GST
ss repRNA
1 2 3 4 5 6 7 8 9 10 11 12 13 14 15
101 ±4
78 ±13
57 ±7
94 ±3
96 ±6
63 ±8
98 ±3
43 ±4
17 ±3
100
100 ±2
101 ±3
112 ±5
105 ±10
111 ±6
% ssRNA

Figure 5.4

Figure 5.4 LMB reduces the anti-viral activity but not the RNA affinity of the recombinant AtXpo1. *(A) RNA gel shift assay shows that GST-Xpo1 binds to ^{32}P-labeled TBSV (+)repRNA and (-)repRNA, respectively, without being interrupted by LMB treatment in vitro. Purified GST-Xpo1 were added in increasing amounts (1.9 µM, 3.8 µM and 5.7 µM) to the reactions with either EtOH or 500 nM LMB. The purified GST with EtOH treatment was used as a control. The GST-Xpo1 - ^{32}P-labeled repRNA complex was detected on nondenaturing 5 % polyacrylamide gels. (B) The anti-viral activity of recombinant Xpo1 was inhibited by the addition of LMB in the in vitro CFE-based TBSV replicase reconstitution assay. The purified recombinant TBSV p33 and p92 replication proteins together with the template TBSV (+)repRNA were added to program the in vitro replication of TBSV repRNA in vitro. The purified GST or GST-Xpo1 were added in increasing amounts (1.9 µM, 3.8 µM and 5.7 µM) into the reactions. The reactions were suplemented with either EtOH (as a control), 100 nM of LMB or 500 nM LMB. The accumulation of ^{32}P-labeled TBSV (+)repRNAs was detected in the 5% polyacrylamide gel (PAGE) containing 8 M urea.*

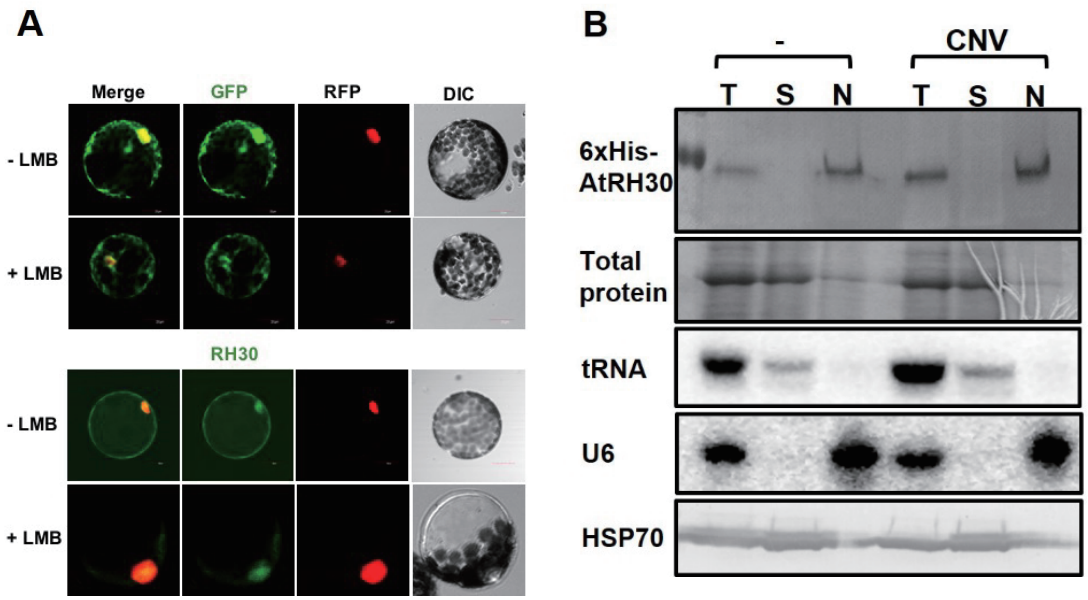
A
Merge
GFP
RFP
DIC
- LMB
+ LMB
RH30
- LMB
+ LMB
B
-
CNV
T S N T S N
6xHis-AtRH30
Total protein
tRNA
U6
HSP70

Figure 5.5

Figure 5.5 AtRH30 shuttles between nucleus and cytoplasm via Xpo1-dependent nuclear export pathway. *(A) Confocal laser microscopy images show that LMB treatment did not change the distribution of GFP in N. benthamiana protoplasts, while LMB treatment enriched the distribution of nuclear pool of RH30 in the protoplasts. GFP or GFP-RH30 was expressed by agro-infiltration in the leaves of transgenic N. benthamiana plants expressing RFP-H2B (a nuclear marker). About 2 days post infiltration, the protoplasts were isolated and imaged with the confocal laser microscopy. (B) The relocation of RH30 induced by CNV infection was not detectable in CNV-infected N. benthamiana plants. The expression of His_6-AtRH30 and CNV gRNA was launched by Agrobacterium co-infiltration. Top panel: the accumulation of His_6-AtRH30 protein in total proteins (T), soluble fractions (S) or nuclear fractions (N)was detected by anti-His antibody at 2.5 days after the inoculation of CNV. Coomassie Brilliant Blue staining were usedto show the amount of total proteins in each fraction. The accumulation of tRNA (as a cytosolic marker) or U6 snRNA (as a nuclear marker) were detected by ^{32}P-labeled probe specific to tRNA or U6 in denaturing PAGE containing 14% polyacrylamide. The accumulation of HSP70 (as a cytosolic marker) were detected by anti-HSP70 antibody.*

Chapter 6

6.1 Conclusion

Different plant DEAD-box helicases distinctly affect virus replication from their yeast and human orthologs. Tombusviruses are small (+)RNA viruses that do not encode their own helicases and might intensively recruit host RNA helicases to facilitate their replication in host cells. Indeed, retroviruses, another family that do not carry viral helicases, have been shown to interact with many cellular RNA helicases in distinct steps of viral replication [183]. Previously it has been reported that eIF4AIII-like AtRH2/AtRH5 and the DDX3-like Ded1/AtRH20 promote tombusvirus plus-strand synthesis through locally unwinding the viral dsRNA replication intermediate [78, 79]. Yet, previous yeast genome-wide screens and global proteomic approaches with TBSV have shown 11 yeast cellular RNA helicases that could be involved in TBSV replication [80, 81], suggesting that a large number of host RNA helicases might be involved in tombusvirus replication. It also indicated the complexity and diversity of cellular helicase functions in tombusvirus replication.

In chapter 2, I aimed to unravel the complex functions of host DEAD-box helicases in TBSV replication by overexpression studies in yeast and plants as well as I performed membrane yeast two-hybrid screens. By doing so, I found evidence that several DEAD-box helicases affect the accumulation of tombusviruses in plants and

yeast. Interestingly, I found that several DEAD-box helicases acted differently from their characterized orthologs in different host-virus interactions. For example, RH14 inhibited the accumulation of TBSV, while its human ortholog DDX5 promoted JEV replication [119]. In addition, RH3 inhibited the accumulation of CNV and TBSV, while its human ortholog DDX21 also inhibited influenza a virus, a negative-stranded RNA virus [118]. Another interesting group is composed of RH6, RH8 and RH12, which all showed inhibitory activities against tombusviruses. These three *Arabidopsis* helicases have the same yeast ortholog Dhh1 and human ortholog DDX6. DDX6 has been recently shown to support distinct steps of hepatitis C virus [227, 228], West Nile virus [229] and retroviruses [230]. Moreover, RH30 has been shown as a potent anti-viral factor against wide range of (+)RNA viruses (discussed in chapter 3), while its yeast ortholog Dbp2 has been characterized as pro-viral helicase during TBSV replication. Altogether, these conserved helicases from different hosts might interact with the invading viruses in different ways due to numerous years of co-evolution, likely restricting the host range of viruses.

RH30 DEAD-box helicase is an anti-viral factor that inhibits multiple steps of TBSV replication. I found several pieces of evidence showing the anti-viral functions of cellular DDX17-like RH30 DEAD-box helicase (discussed in chapter 3).

Transient expression of RH30 inhibited several (+)RNA viruses, including peroxisomal-replicating TBSV and CNV and the mitochondrial replicating CIRV and the distantly related TCV and RCNMV and the unrelated TMV in plants as well as an insect virus FHV in yeast system, showing the broad-range of the restriction function for this helicase. How does RH30 inhibit the accumulation of so many viruses? This question still needs further investigation due to the diverse strategies of replication used by different viruses. However, in this work with the well-characterized *cis*-acting elements in TBSV gRNA [96, 132, 175, 231, 232], I was able to show mechanistically how RH30 could restrict TBSV replication. I found that RH30 is able to bind to a cis-acting RNA element RII(+)SL and separate the stem-loop structure within the TBSV RII(+)SL, therefore preventing p33 replication protein from recruiting the RNA template for VRC assembly. Moreover, I showed that p33 replication proteins bound to RII(+)SL could be displaced by RH30 from RII(+)SL RNA, further demonstrating the unique features of AtRH30 involving RII(+)SL. In addition, the activation of $p92^{pol}$ is inhibited by RH30 likely through binding to the critical RII(+)SL. Another intriguing finding in this work is that RH30 lost anti-viral activities when it was sequestered inside the nucleus. We learned two things from this finding. Firstly, the nuclearcytoplasmic shuttling is critical to bring those factors including RH30 to the cytoplasm for active anti-viral functions (discussed in chapter 5). Secondly, the anti-

viral function of RH30 is not mediated by transcriptional regulation induced by the viral cytosolic PAMP [233] but is likely served as an effector-type RNA helicase by direct binding to virus RNA. The possible additional antiviral role of RH30 in signaling cannot yet excluded.

The N-terminal and C-terminal domains modulates the function of DEAD-box helicases. Through the previous comparison between helicase orthologs in plant, yeast and human hosts, I learned that the minor difference of domains might largely change the functions of helicases in host-virus interactions. Two well-characterized helicases, namely pro-viral RH20 and anti-viral RH30, share more than 87% similarity between their helicase core domains and this provided me an excellent opportunity to study the functions of amino (N)-terminal and carboxy (C)-terminal domains by the comparison between these two helicases. I found that the deletion of the N-terminal domains in both RH20 and RH30 changes the functions of the helicases in TBSV replication. The dsRNA separation assays supported that N-terminal domain is responsible for viral dsRNA binding and specificity of these RNA helicases. The single C-terminus deletion did not influence the function of either helicases. However, the deletion mutant of RH30 missing both N-terminal and C-terminal domains turned anti-viral function into pro-viral function, suggesting that N-

terminal and C-terminal domains work synergistically to modulate the helicase function of RH30. How these two domains work together still need further investigation. On the other hand, Rpn11, a critical factor in the assembly of the proteasome and the stability of the proteasome, interacts with TBSV $p92^{pol}$ and aids the recruitment of cellular factors into virus replication [40]. With the knock-down of Rpn11 expression in plants, I found that the pro-viral function of full-length RH20 became anti-viral function similar to its mutant $RH20^{\Delta N}$, while the anti-viral function of full-length RH30 turned to neutral similar to its mutant $RH30^{\Delta N}$ (data not shown), indicating Rpn11 might recruit cellular RNA helicases through the interaction with N-terminal domain. It also suggests that RNA helicases missing the N-terminal domain can be misplaced and/or missed within the tombusvirus replication complex (VRC). In addition to previous finding that the helicase core domain, two linked RecA-like domains, represented the minimal functional unit for the cellular function in nature [234], now I provide the evidence showing how the flanking regions outside of the helicase core domain modulate the function of RNA helicases in virus replication.

Xpo1 is an anti-viral factor that brings additional restriction factors into the viral replication compartment by binding to p33 replication protein. In the study of RH30 (chapter 3), I realized the importance of nucleocytoplasmic shuttling in the

replication of tombusviruses. With the assistance of a highly selective and efficient chemical inhibitor Leptomycin B (LMB), I found that Xpo1-dependent nuclear transport pathway has an inhibitory effect against the replication of tombusviruses, likely through the restriction functions of its cargoes. Furthermore, interactions between Xpo1 and CIRFs or TBSV p33 in the viral replication compartment suggest that Xpo1 might actively find the viral replication compartment through interacting with p33 replication protein. However, it could be another scenario that p33 replication protein binds to the Xpo1 and therefore inhibits the Xpo1 exporting restriction factors into the cytoplasm. Further investigation is required to get insight into the role of Xpo1 in virus-host interactions. Unlike what it was believed that only nuclear and nucleocytoplasmic shuttling proteins utilize nuclear transport pathway, Xpo1 has been reported to interact with more than 700 proteins in yeast and more than 1,000 proteins in human. Nearly half of these possible cargoes are cytoplasmic and are believed not getting into nucleus in their life time, implicating Xpo1 is possibly involved in vesicle trafficking, centrosomes, autophagy, peroxisome biogenesis, cytoskeleton, ribosome maturation, translation and mRNA degradation pathways [197]. Several of these pathways above are also critical for tombusviruses to build proper viral replication organelles, indicating the emerging significance of Xpo1 in virus replication. The connection between Xpo1-dependent nuclear export and

other host cellular pathways is intriguing and is worth further investigation.

In addition to the well-characterized function of Xpo1 that exports viral protein or viral ribonucleoprotein complex in retroviruses [203, 206, 207], respiratory syncytial virus [208], influenza a virus [209] as well as inhibits viral replication through direct interaction to the viral protein in human T cell leukemia virus type 1 [210] and adenovirus type 2 [211], the finding in this work unravels a novel function of Xpo1-dependent nuclear export in cytoplasmic-replicating tombusviruses. Therefore, my work likely opens up a new major chapter in tombusvirus replication.

6.2 Prospective

Unique domains in DEAD-box RNA helicases could determine the protein function in TBSV replication. Through the studies in Chapter 4, I learned that functions of RH20 and RH30 in tombusvirus replication can be greatly modulated by the unique N-terminal and C-terminal domains. In addition to the roles in direct binding to TBSV RNA and a host hub-like Rpn11 within replication compartments, how the unique domains affect the helicase function in TBSV replication need more investigation. Since DEAD-box helicases are ubiquitous and have numerous interacting partners in RNA metabolism processes in eukaryotic cells, N-terminal and

C-terminal domains could indirectly influence TBSV replication through other host factors involved in RNA metabolism pathways. For example, heterogeneous nuclear ribonucleoprotein (hnRNP) has been shown to work with DDX17 (RH30 in human) to process accurate splicing [235]. hnRNP has also been identified as CIRF with TBSV-based yeast temperature-sensitive library [28]. It is very likely RH30 and hnRNP work together to regulate the transcription of host genes, which might result in inhibition of TBSV replication.

In addition, the unique domains of RNA helicases could determine which steps of viral replication are targeted for their actions, resulting in different effects. For instance, it has been shown that the critical RII(+) stem-loop structure was largely separated by antiviral $RH20^{\Delta N}$, likely contributing the antiviral activity of $RH20^{\Delta N}$ in the early step of TBSV replication. In addition, RH30 lost the capability to separate RII(+)SL as long as N-terminal and C-terminal domains were deleted. By utilizing the biotinylated RNA-protein interaction assay, we could test if viral template recruitment by TBSV p33 is inhibited by either $RH20^{\Delta N}$ or $RH30^{\Delta N/\Delta C}$. Presumably, the early inhibition of the viral template recruitment could cancel out the stimulatory functions of the pro-viral host factors, including full-length RH20 that promotes viral replication in sequential steps of TBSV replication. To gain more insight into the complexity of host-virus interactions, further investigation is needed to test if

blocking early steps of TBSV replication could interrupt the stimulatory effects from pro-viral factors that are deployed in later steps of viral replication.

Unexpected role of Xpo1 in TBSV replication. There are many nuclear RNA-binding proteins that have been identified as restriction factors inhibiting the replication of RNA viruses in the previous screens [28, 236]. How can these antiviral RNA-binding proteins be retargeted into the virus replication site in cytoplasm? Xpo1 is one of the major nuclear exportins and can export more than 1,000 host components, which include many RNA-binding proteins. In my dissertation I have shown Nucleolin as one of the major nuclear restriction factors that is retargeted into the viral replication site through Xpo1. This finding opens up the possibilities that nuclear RNA-binding proteins could be exported out of the nucleus during virus infections. For example, Upf1, Upf2 and Upf3 are responsible for mRNA decay and have been shown to be associated with Xpo1 [197]. Host mRNA decay pathways can interrupt viral RNA stability. It is very important for RNA viruses to maintain the integrity of viral RNA and combat the host RNA decay pathways. For instance, poliovirus utilizes poliovirus proteinases to cleave Xrn1 exonuclease in order to enhance the viral RNA stability [237]. Therefore, RNA viruses might block Xpo1 to prevent viral RNA degradation from host mRNA decay factors.

Another question is how Xpo1 interacts with TBSV p33? If TBSV p33 binds to the NES-recognizing groove of Xpo1, it must occur when Xpo1 is not loaded with cargos. This might suggest that Xpo1 exports and releases restriction factors in the cytoplasm, followed by the binding to TBSV p33, which might lead to the inhibition of Xpo1-mediated nucleocytoplasmic shuttling pathway due to the lack of Xpo1 being recycled back to the nucleus. If Xpo1 does not bind to TBSV p33 through the NES-recognizing groove, Xpo1 might bring the restriction factors directly to the replication site by the binding to TBSV p33. I think it is possible that p33 is getting self-sacrificed to sequester the Xpo1 pool in the cytoplasm, shutting down the Xpo1-mediated nucleocytoplasmic shuttling pathway. Altogether, I propose that my discoveries with Xpo1 opens up a new, previously unexpected, and critical role for the nucleus and nuclear proteins in tombusvirus replication.

References

1. Hearne, P.Q., et al., *The complete genome structure and synthesis of infectious RNA from clones of tomato bushy stunt virus.* Virology, 1990. **177**(1): p. 141-51.
2. Newburn, L.R. and K.A. White, *Cis-acting RNA elements in positive-strand RNA plant virus genomes.* Virology, 2015. **479-480**: p. 434-43.
3. White, K.A. and P.D. Nagy, *Advances in the molecular biology of tombusviruses: gene expression, genome replication, and recombination.* Prog Nucleic Acid Res Mol Biol, 2004. **78**: p. 187-226.
4. Yamamura, Y. and H.B. Scholthof, *Tomato bushy stunt virus: a resilient model system to study virus-plant interactions.* Mol Plant Pathol, 2005. **6**(5): p. 491-502.
5. Nagy, P.D. and J. Pogany, *Yeast as a model host to dissect functions of viral and host factors in tombusvirus replication.* Virology, 2006. **344**(1): p. 211-220.
6. Oster, S.K., B. Wu, and K.A. White, *Uncoupled expression of p33 and p92 permits amplification of tomato bushy stunt virus RNAs.* J Virol, 1998. **72**(7): p. 5845-51.
7. Panavas, T. and P.D. Nagy, *Yeast as a model host to study replication and recombination of defective interfering RNA of Tomato bushy stunt virus.* Virology, 2003. **314** (1): p. 315-325.
8. Rajendran, K.S. and P.D. Nagy, *Characterization of the RNA-binding domains in the replicase proteins of tomato bushy stunt virus.* J Virol, 2003. **77**(17): p. 9244-58.
9. Navarro, B., L. Rubino, and M. Russo, *Expression of the Cymbidium ringspot virus 33-kilodalton protein in Saccharomyces cerevisiae and molecular dissection of the peroxisomal targeting signal.* J Virol, 2004. **78**(9): p. 4744-52.
10. Panavas, T., et al., *The role of the p33:p33/p92 interaction domain in RNA replication and intracellular localization of p33 and p92 proteins of Cucumber necrosis tombusvirus.* Virology, 2005. **338**(1): p. 81-95.
11. Monkewich, S., et al., *The p92 polymerase coding region contains an internal RNA element required at an early step in Tombusvirus genome replication.* J Virol, 2005. **79**(8): p. 4848-58.

12. Pogany, J., K.A. White, and P.D. Nagy, *Specific binding of tombusvirus replication protein p33 to an internal replication element in the viral RNA is essential for replication.* J Virol, 2005. **79**(8): p. 4859-69.
13. Scholthof, K.B., H.B. Scholthof, and A.O. Jackson, *The tomato bushy stunt virus replicase proteins are coordinately expressed and membrane associated.* Virology, 1995. **208**(1): p. 365-9.
14. Panavas, T., et al., *Enhancement of RNA synthesis by promoter duplication in tombusviruses.* Virology, 2003. **310**(1): p. 118-29.
15. Pogany, J. and P.D. Nagy, *Activation of Tomato Bushy Stunt Virus RNA-Dependent RNA Polymerase by Cellular Heat Shock Protein 70 Is Enhanced by Phospholipids In Vitro.* J Virol, 2015. **89**(10): p. 5714-23.
16. Paul, D. and R. Bartenschlager, *Architecture and biogenesis of plus-strand RNA virus replication factories.* World J Virol, 2013. **2**(2): p. 32-48.
17. Romero-Brey, I. and R. Bartenschlager, *Membranous replication factories induced by plus-strand RNA viruses.* Viruses, 2014. **6**(7): p. 2826-57.
18. McCartney, A.W., et al., *Localization of the tomato bushy stunt virus replication protein p33 reveals a peroxisome-to-endoplasmic reticulum sorting pathway.* Plant Cell, 2005. **17**(12): p. 3513-31.
19. Pathak, K.B., Z. Sasvari, and P.D. Nagy, *The host Pex19p plays a role in peroxisomal localization of tombusvirus replication proteins.* Virology, 2008. **379**(2): p. 294-305.
20. Diaz, A. and X. Wang, *Bromovirus-induced remodeling of host membranes during viral RNA replication.* Curr Opin Virol, 2014. **9**: p. 104-10.
21. Wang, A., *Dissecting the molecular network of virus-plant interactions: the complex roles of host factors.* Annu Rev Phytopathol, 2015. **53**: p. 45-66.
22. Nagy, P.D., J.R. Strating, and F.J. van Kuppeveld, *Building Viral Replication Organelles: Close Encounters of the Membrane Types.* PLoS Pathog, 2016. **12**(10): p. e1005912.
23. Kushner, D.B., et al., *Systematic, genome-wide identification of host genes affecting replication of a positive-strand RNA virus.* Proc Natl Acad Sci U S A, 2003. **100**(26): p. 15764-9.
24. Nagy, P.D., *Exploitation of a surrogate host, Saccharomyces cerevisiae, to identify cellular targets and develop novel antiviral approaches.* Curr Opin Virol, 2017. **26**: p. 132-140.
25. Panaviene, Z., et al., *Purification of the cucumber necrosis virus replicase from yeast cells: role of coexpressed viral RNA in stimulation of replicase activity.* J Virol, 2004. **78**(15): p. 8254-63.

26. Jiang, Y., et al., *Identification of essential host factors affecting tombusvirus RNA replication based on the yeast Tet promoters Hughes Collection.* J Virol, 2006. **80**(15): p. 7394-404.
27. Shah Nawaz-ul-Rehman, M., et al., *Proteome-wide overexpression of host proteins for identification of factors affecting tombusvirus RNA replication: an inhibitory role of protein kinase C.* J Virol, 2012. **86**(17): p. 9384-95.
28. Nawaz-ul-Rehman, M.S., et al., *Yeast screens for host factors in positive-strand RNA virus replication based on a library of temperature-sensitive mutants.* Methods, 2013. **59**(2): p. 207-16.
29. Panavas, T., et al., *Yeast genome-wide screen reveals dissimilar sets of host genes affecting replication of RNA viruses.* Proc Natl Acad Sci U S A, 2005. **102**(20): p. 7326-31.
30. Prasanth, K.R., et al., *Screening a yeast library of temperature-sensitive mutants reveals a role for actin in tombusvirus RNA recombination.* Virology, 2016. **489**: p. 233-42.
31. Pogany, J., et al., *In vitro assembly of the Tomato bushy stunt virus replicase requires the host Heat shock protein 70.* Proc Natl Acad Sci U S A, 2008. **105**(50): p. 19956-61.
32. Pogany, J. and P.D. Nagy, *Authentic replication and recombination of Tomato bushy stunt virus RNA in a cell-free extract from yeast.* J Virol, 2008. **82**(12): p. 5967-80.
33. Nagy, P.D., J. Pogany, and K. Xu, *Cell-Free and Cell-Based Approaches to Explore the Roles of Host Membranes and Lipids in the Formation of Viral Replication Compartment Induced by Tombusviruses.* Viruses, 2016. **8**(3): p. 68.
34. Chuang, C., K.R. Prasanth, and N.P. D., *The Glycolytic Pyruvate Kinase Is Recruited Directly into the Viral Replicase Complex to Generate ATP for RNA Synthesis.* Cell Host Microbe, 2018. **22**(5): p. 639-652.
35. Barajas, D., et al., *Tombusviruses upregulate phospholipid biosynthesis via interaction between p33 replication protein and yeast lipid sensor proteins during virus replication in yeast.* Virology, 2014. **0**: p. 72-80.
36. Imura, Y., et al., *Cellular Ubc2/Rad6 E2 ubiquitin-conjugating enzyme facilitates tombusvirus replication in yeast and plants.* Virology, 2015. **484**: p. 265-75.
37. Kovalev, N., et al., *Role of Viral RNA and Co-opted Cellular ESCRT-I and ESCRT-III Factors in Formation of Tombusvirus Spherules Harboring the Tombusvirus Replicase.* J Virol, 2016. **90**(7): p. 3611-26.

38. Kovalev, N., et al., *The role of co-opted ESCRT proteins and lipid factors in protection of tombusviral double-stranded RNA replication intermediate against reconstituted RNAi in yeast.* PLoS Pathog, 2017. **13**(7): p. e1006520.
39. Nawaz-ul-Rehman, M.S., et al., *Viral Replication Protein Inhibits Cellular Cofilin Actin Depolymerization Factor to Regulate the Actin Network and Promote Viral Replicase Assembly.* PLoS Pathog, 2016. **12**(2): p. e1005440.
40. Prasanth, K.R., D. Barajas, and P.D. Nagy, *The proteasomal Rpn11 metalloprotease suppresses tombusvirus RNA recombination and promotes viral replication via facilitating assembly of the viral replicase complex.* J Virol, 2015. **89**(5): p. 2750-63.
41. Prasanth, K.R., C. Chuang, and P.D. Nagy, *Co-opting ATP-generating glycolytic enzyme PGK1 phosphoglycerate kinase facilitates the assembly of viral replicase complexes.* PLoS Pathog, 2017. **13**(10): p. e1006689.
42. Xu, K. and P.D. Nagy, *Enrichment of Phosphatidylethanolamine in Viral Replication Compartments via Co-opting the Endosomal Rab5 Small GTPase by a Positive-Strand RNA Virus.* PLoS Biol, 2016. **14**(10): p. e2000128.
43. Jones, J.D. and J.L. Dangl, *The plant immune system.* Nature, 2006. **444**(7117): p. 323-9.
44. Colomer-Lluch, M., et al., *Restriction Factors: From Intrinsic Viral Restriction to Shaping Cellular Immunity Against HIV-1.* Front Immunol, 2018. **9**: p. 2876.
45. Zheng, Y.H., K.T. Jeang, and K. Tokunaga, *Host restriction factors in retroviral infection: promises in virus-host interaction.* Retrovirology, 2012. **9**: p. 112.
46. Krishnan, M.N., et al., *RNA interference screen for human genes associated with West Nile virus infection.* Nature, 2008. **455**(7210): p. 242-5.
47. Randall, G., et al., *Cellular cofactors affecting hepatitis C virus infection and replication.* Proc Natl Acad Sci U S A, 2007. **104**(31): p. 12884-9.
48. Long, J.S., et al., *Host and viral determinants of influenza A virus species specificity.* Nat Rev Microbiol, 2019. **17**(2): p. 67-81.
49. Zhou, L.Y. and L.L. Zhang, *Host restriction factors for hepatitis C virus.* World J Gastroenterol, 2016. **22**(4): p. 1477-86.
50. Villalon-Letelier, F., et al., *Host Cell Restriction Factors that Limit Influenza A Infection.* Viruses, 2017. **9**(12).

51. Sasvari, Z., P. Alatriste Gonzalez, and P.D. Nagy, *Tombusvirus-yeast interactions identify conserved cell-intrinsic viral restriction factors.* Front Plant Sci, 2014. **5**: p. 383.
52. Lin, J.Y. and P.D. Nagy, *Identification of novel host factors via conserved domain search: Cns1 cochaperone is a novel restriction factor of tombusvirus replication in yeast.* J Virol, 2013. **87**(23): p. 12600-10.
53. Lin, J.Y., et al., *The TPR domain in the host Cyp40-like cyclophilin binds to the viral replication protein and inhibits the assembly of the tombusviral replicase.* PLoS Pathog, 2012. **8**(2): p. e1002491.
54. Cheng, C.P., et al., *Expression of the Arabidopsis Xrn4p 5'-3' exoribonuclease facilitates degradation of tombusvirus RNA and promotes rapid emergence of viral variants in plants.* Virology, 2007. **368**(2): p. 238-48.
55. Jiang, Y., Z. Li, and P.D. Nagy, *Nucleolin/Nsr1p binds to the 3' noncoding region of the tombusvirus RNA and inhibits replication.* Virology, 2010. **396**(1): p. 10-20.
56. Kovalev, N. and P.D. Nagy, *Cyclophilin A binds to the viral RNA and replication proteins, resulting in inhibition of tombusviral replicase assembly.* J Virol, 2013. **87**(24): p. 13330-42.
57. Jankowsky, E., *RNA helicases at work: binding and rearranging.* Trends Biochem Sci, 2011. **36**(1): p. 19-29.
58. Cordin, O., et al., *The DEAD-box protein family of RNA helicases.* Gene, 2006. **367**: p. 17-37.
59. Jarmoskaite, I. and R. Russell, *DEAD-box proteins as RNA helicases and chaperones.* Wiley Interdiscip Rev RNA, 2011. **2**(1): p. 135-52.
60. Chen, Y., et al., *DEAD-box proteins can completely separate an RNA duplex using a single ATP.* Proc Natl Acad Sci U S A, 2008. **105**(51): p. 20203-8.
61. Liu, F., A. Putnam, and E. Jankowsky, *ATP hydrolysis is required for DEAD-box protein recycling but not for duplex unwinding.* Proc Natl Acad Sci U S A, 2008. **105**(51): p. 20209-14.
62. Aregger, R. and D. Klostermeier, *The DEAD box helicase YxiN maintains a closed conformation during ATP hydrolysis.* Biochemistry, 2009. **48**(45): p. 10679-81.
63. Yang, Q., et al., *DEAD-box proteins unwind duplexes by local strand separation.* Mol Cell, 2007. **28**(2): p. 253-63.
64. Yang, Q. and E. Jankowsky, *The DEAD-box protein Ded1 unwinds RNA duplexes by a mode distinct from translocating helicases.* Nat Struct Mol Biol, 2006. **13**(11): p. 981-6.

65. Bizebard, T., et al., *Studies on three E. coli DEAD-box helicases point to an unwinding mechanism different from that of model DNA helicases.* Biochemistry, 2004. **43**(24): p. 7857-66.
66. Jankowsky, E. and M.E. Fairman, *RNA helicases--one fold for many functions.* Curr Opin Struct Biol, 2007. **17**(3): p. 316-24.
67. Pyle, A.M., *Translocation and unwinding mechanisms of RNA and DNA helicases.* Annu Rev Biophys, 2008. **37**: p. 317-36.
68. Yoneyama, M. and T. Fujita, *Structural mechanism of RNA recognition by the RIG-I-like receptors.* Immunity, 2008. **29**(2): p. 178-81.
69. Gack, M.U., et al., *Roles of RIG-I N-terminal tandem CARD and splice variant in TRIM25-mediated antiviral signal transduction.* Proc Natl Acad Sci U S A, 2008. **105**(43): p. 16743-8.
70. Cui, S., et al., *The C-terminal regulatory domain is the RNA 5'-triphosphate sensor of RIG-I.* Mol Cell, 2008. **29**(2): p. 169-79.
71. Klostermeier, D. and M.G. Rudolph, *A novel dimerization motif in the C-terminal domain of the Thermus thermophilus DEAD box helicase Hera confers substantial flexibility.* Nucleic Acids Res, 2009. **37**(2): p. 421-30.
72. Lattmann, S., et al., *Role of the amino terminal RHAU-specific motif in the recognition and resolution of guanine quadruplex-RNA by the DEAH-box RNA helicase RHAU.* Nucleic Acids Res, 2010. **38**(18): p. 6219-33.
73. Kossen, K., F.V. Karginov, and O.C. Uhlenbeck, *The carboxy-terminal domain of the DExDH protein YxiN is sufficient to confer specificity for 23S rRNA.* J Mol Biol, 2002. **324**(4): p. 625-36.
74. Karow, A.R. and D. Klostermeier, *A structural model for the DEAD box helicase YxiN in solution: localization of the RNA binding domain.* J Mol Biol, 2010. **402**(4): p. 629-37.
75. Goh, P.Y., et al., *Cellular RNA helicase p68 relocalization and interaction with the hepatitis C virus (HCV) NS5B protein and the potential role of p68 in HCV RNA replication.* J Virol, 2004. **78**(10): p. 5288-98.
76. Lin, L., et al., *Identification of RNA helicase A as a cellular factor that interacts with influenza A virus NS1 protein and its role in the virus life cycle.* J Virol, 2012. **86**(4): p. 1942-54.
77. Huang, T.S., et al., *A host RNA helicase-like protein, AtRH8, interacts with the potyviral genome-linked protein, VPg, associates with the virus accumulation complex, and is essential for infection.* Plant Physiol, 2010. **152**(1): p. 255-66.

78. Kovalev, N., J. Pogany, and P.D. Nagy, *A Co-Opted DEAD-Box RNA Helicase Enhances Tombusvirus Plus-Strand Synthesis.* PLoS Pathog, 2012. **8**(2): p. e1002537.
79. Kovalev, N. and P.D. Nagy, *The expanding functions of cellular helicases: the tombusvirus RNA replication enhancer co-opts the plant eIF4AIII-like AtRH2 and the DDX5-like AtRH5 DEAD-box RNA helicases to promote viral asymmetric RNA replication.* PLoS Pathog, 2014. **10**(4): p. e1004051.
80. Li, Z., et al., *Translation elongation factor 1A is a component of the tombusvirus replicase complex and affects the stability of the p33 replication co-factor.* Virology, 2009. **385**(1): p. 245-60.
81. Nagy, P.D. and J. Pogany, *Global genomics and proteomics approaches to identify host factors as targets to induce resistance against Tomato bushy stunt virus.* Adv Virus Res, 2010. **76**: p. 123-77.
82. Fernandez-Garcia, M.D., et al., *Pathogenesis of flavivirus infections: using and abusing the host cell.* Cell Host Microbe, 2009. **5**(4): p. 318-28.
83. Salonen, A., T. Ahola, and L. Kaariainen, *Viral RNA replication in association with cellular membranes.* Curr Top Microbiol Immunol, 2005. **285**: p. 139-73.
84. Miller, S. and J. Krijnse-Locker, *Modification of intracellular membrane structures for virus replication.* Nat Rev Microbiol, 2008. **6**(5): p. 363-74.
85. Nagy, P.D. and J. Pogany, *The dependence of viral RNA replication on co-opted host factors.* Nat Rev Microbiol, 2011. **10**(2): p. 137-49.
86. den Boon, J.A. and P. Ahlquist, *Organelle-like membrane compartmentalization of positive-strand RNA virus replication factories.* Annu Rev Microbiol, 2010. **64**: p. 241-56.
87. den Boon, J.A., A. Diaz, and P. Ahlquist, *Cytoplasmic viral replication complexes.* Cell Host Microbe, 2010. **8**(1): p. 77-85.
88. Nagy, P.D., *Tombusvirus-Host Interactions: Co-Opted Evolutionarily Conserved Host Factors Take Center Court.* Annu Rev Virol, 2016. **3**(1): p. 491-515.
89. Nagy, P.D., et al., *Emerging picture of host chaperone and cyclophilin roles in RNA virus replication.* Virology, 2011. **411**(2): p. 374-82.
90. Li, Z. and P.D. Nagy, *Diverse roles of host RNA binding proteins in RNA virus replication.* RNA Biol, 2011. **8**(2): p. 305-15.
91. Li, Q., et al., *A genome-wide genetic screen for host factors required for hepatitis C virus propagation.* Proc Natl Acad Sci U S A, 2009. **106**(38): p. 16410-5.

92. Tai, A.W., et al., *A functional genomic screen identifies cellular cofactors of hepatitis C virus replication.* Cell Host Microbe, 2009. **5**(3): p. 298-307.
93. Sessions, O.M., et al., *Discovery of insect and human dengue virus host factors.* Nature, 2009. **458**(7241): p. 1047-50.
94. Jonczyk, M., et al., *Exploiting alternative subcellular location for replication: tombusvirus replication switches to the endoplasmic reticulum in the absence of peroxisomes.* Virology, 2007. **362**(2): p. 320-30.
95. Stork, J., et al., *RNA chaperone activity of the tombusviral p33 replication protein facilitates initiation of RNA synthesis by the viral RdRp in vitro.* Virology, 2011. **409**(2): p. 338-47.
96. Pathak, K.B., et al., *Defining the roles of cis-acting RNA elements in tombusvirus replicase assembly in vitro.* J Virol, 2012. **86**(1): p. 156-71.
97. Rajendran, K.S. and P.D. Nagy, *Interaction between the replicase proteins of Tomato bushy stunt virus in vitro and in vivo.* Virology, 2004. **326**(2): p. 250-61.
98. Li, Z., et al., *Cdc34p ubiquitin-conjugating enzyme is a component of the tombusvirus replicase complex and ubiquitinates p33 replication protein.* J Virol, 2008. **82**(14): p. 6911-26.
99. Huang, T.S. and P.D. Nagy, *Direct inhibition of tombusvirus plus-strand RNA synthesis by a dominant negative mutant of a host metabolic enzyme, glyceraldehyde-3-phosphate dehydrogenase, in yeast and plants.* J Virol, 2011. **85**(17): p. 9090-102.
100. Wang, R.Y., et al., *A temperature sensitive mutant of heat shock protein 70 reveals an essential role during the early steps of tombusvirus replication.* Virology, 2009. **394**(1): p. 28-38.
101. Li, Z., et al., *Translation elongation factor 1A facilitates the assembly of the tombusvirus replicase and stimulates minus-strand synthesis.* PLoS Pathog, 2010. **6**(11): p. e1001175.
102. Wang, R.Y., J. Stork, and P.D. Nagy, *A key role for heat shock protein 70 in the localization and insertion of tombusvirus replication proteins to intracellular membranes.* J Virol, 2009. **83**(7): p. 3276-87.
103. Chuang, C., K.R. Prasanth, and P.D. Nagy, *Coordinated function of cellular DEAD-box helicases in suppression of viral RNA recombination and maintenance of viral genome integrity.* PLoS Pathog, 2015. **11**(2): p. e1004680.

104. Kovalev, N., D. Barajas, and P.D. Nagy, *Similar roles for yeast Dbp2 and Arabidopsis RH20 DEAD-box RNA helicases to Ded1 helicase in tombusvirus plus-strand synthesis.* Virology, 2012. **432**(2): p. 470-84.
105. Ray, D. and K.A. White, *An internally located RNA hairpin enhances replication of Tomato bushy stunt virus RNAs.* J Virol, 2003. **77**(1): p. 245-57.
106. Panavas, T. and P.D. Nagy, *The RNA replication enhancer element of tombusviruses contains two interchangeable hairpins that are functional during plus-strand synthesis.* J Virol, 2003. **77**(1): p. 258-69.
107. Panavas, T. and P.D. Nagy, *Mechanism of stimulation of plus-strand synthesis by an RNA replication enhancer in a tombusvirus.* J Virol, 2005. **79**(15): p. 9777-85.
108. Kao, C.C., P. Singh, and D.J. Ecker, *De novo initiation of viral RNA-dependent RNA synthesis.* Virology, 2001. **287**(2): p. 251-60.
109. Wang, X. and P. Ahlquist, *Filling a GAP(DH) in asymmetric viral RNA synthesis.* Cell Host Microbe, 2008. **3**(3): p. 124-5.
110. Mendu, V., et al., *Cpr1 cyclophilin and Ess1 parvulin prolyl isomerases interact with the tombusvirus replication protein and inhibit viral replication in yeast model host.* Virology, 2010. **406**(2): p. 342-51.
111. Barajas, D. and P.D. Nagy, *Ubiquitination of tombusvirus p33 replication protein plays a role in virus replication and binding to the host Vps23p ESCRT protein.* Virology, 2010. **397**(2): p. 358-68.
112. Umate, P., R. Tuteja, and N. Tuteja, *Genome-wide analysis of helicase gene family from rice and Arabidopsis: a comparison with yeast and human.* Plant Mol Biol, 2010. **73**(4-5): p. 449-65.
113. Linder, P. and E. Jankowsky, *From unwinding to clamping - the DEAD box RNA helicase family.* Nat Rev Mol Cell Biol, 2011. **12**(8): p. 505-16.
114. Li, Z., et al., *Systematic exploration of essential yeast gene function with temperature-sensitive mutants.* Nat Biotechnol, 2011. **29**(4): p. 361-7.
115. Iyer, K., et al., *Utilizing the split-ubiquitin membrane yeast two-hybrid system to identify protein-protein interactions of integral membrane proteins.* Sci STKE, 2005. **2005**(275): p. pl3.
116. Kittanakom, S., et al., *Analysis of membrane protein complexes using the split-ubiquitin membrane yeast two-hybrid (MYTH) system.* Methods Mol Biol, 2009. **548**: p. 247-71.
117. Ariumi, Y., et al., *DDX3 DEAD-box RNA helicase is required for hepatitis C virus RNA replication.* J Virol, 2007. **81**(24): p. 13922-6.

118. Chen, G., et al., *Cellular DDX21 RNA helicase inhibits influenza A virus replication but is counteracted by the viral NS1 protein.* Cell Host Microbe, 2014. **15**(4): p. 484-93.
119. Li, C., et al., *The DEAD-box RNA helicase DDX5 acts as a positive regulator of Japanese encephalitis virus replication by binding to viral 3′ UTR.* Antiviral Res, 2013. **100**(2): p. 487-99.
120. Moy, R.H., et al., *Stem-loop recognition by DDX17 facilitates miRNA processing and antiviral defense.* Cell, 2014. **158**(4): p. 764-777.
121. Liu, Y. and R. Imai, *Function of Plant DExD/H-Box RNA Helicases Associated with Ribosomal RNA Biogenesis.* Front Plant Sci, 2018. **9**: p. 125.
122. Cherry, S., et al., *Genome-wide RNAi screen reveals a specific sensitivity of IRES-containing RNA viruses to host translation inhibition.* Genes Dev, 2005. **19**(4): p. 445-52.
123. Altan-Bonnet, N., *Lipid Tales of Viral Replication and Transmission.* Trends Cell Biol, 2017. **27**(3): p. 201-213.
124. Fernandez de Castro, I., R. Tenorio, and C. Risco, *Virus assembly factories in a lipid world.* Curr Opin Virol, 2016. **18**: p. 20-26.
125. Paul, D. and R. Bartenschlager, *Flaviviridae Replication Organelles: Oh, What a Tangled Web We Weave.* Annu Rev Virol, 2015. **2**(1): p. 289-310.
126. Diamond, M.S. and M. Gale, Jr., *Cell-intrinsic innate immune control of West Nile virus infection.* Trends Immunol, 2012. **33**(10): p. 522-30.
127. Aoshi, T., et al., *Innate and adaptive immune responses to viral infection and vaccination.* Curr Opin Virol, 2011. **1**(4): p. 226-32.
128. Jensen, S. and A.R. Thomsen, *Sensing of RNA viruses: a review of innate immune receptors involved in recognizing RNA virus invasion.* J Virol, 2012. **86**(6): p. 2900-10.
129. Ding, S.W., *RNA-based antiviral immunity.* Nat Rev Immunol, 2010. **10**(9): p. 632-44.
130. Nagy, P.D. and J. Pogany, *The dependence of viral RNA replication on co-opted host factors.* Nature Reviews Microbiology, 2012. **10**(2): p. 137-149.
131. Nagy, P.D., D. Barajas, and J. Pogany, *Host factors with regulatory roles in tombusvirus replication.* Curr Opin Virol, 2012. **2**(6): p. 685-92.
132. Panaviene, Z., T. Panavas, and P.D. Nagy, *Role of an internal and two 3′-terminal RNA elements in assembly of tombusvirus replicase.* J Virol, 2005. **79**(16): p. 10608-18.

133. Pogany, J. and P.D. Nagy, *p33-Independent activation of a truncated p92 RNA-dependent RNA polymerase of Tomato bushy stunt virus in yeast cell-free extract.* J Virol, 2012. **86**(22): p. 12025-38.
134. Panavas, T., et al., *The role of the p33:p33/p92 interaction domain in RNA replication and intracellular localization of p33 and p92 proteins of Cucumber necrosis tombusvirus.* Virology, 2005.
135. Linder, P. and P. Lasko, *Bent out of shape: RNA unwinding by the DEAD-box helicase Vasa.* Cell, 2006. **125**(2): p. 219-21.
136. Linder, P., *mRNA export: RNP remodeling by DEAD-box proteins.* Curr Biol, 2008. **18**(7): p. R297-9.
137. Kant, P., et al., *STRESS RESPONSE SUPPRESSOR1 and STRESS RESPONSE SUPPRESSOR2, two DEAD-box RNA helicases that attenuate Arabidopsis responses to multiple abiotic stresses.* Plant Physiol, 2007. **145**(3): p. 814-30.
138. Dalmay, T., et al., *SDE3 encodes an RNA helicase required for post-transcriptional gene silencing in Arabidopsis.* EMBO J, 2001. **20**(8): p. 2069-78.
139. Ranji, A. and K. Boris-Lawrie, *RNA helicases: emerging roles in viral replication and the host innate response.* RNA Biol, 2010. **7**(6): p. 775-87.
140. Garbelli, A., et al., *Targeting the human DEAD-box polypeptide 3 (DDX3) RNA helicase as a novel strategy to inhibit viral replication.* Curr Med Chem, 2011. **18**(20): p. 3015-27.
141. Upadya, M.H., J.J. Aweya, and Y.J. Tan, *Understanding the interaction of hepatitis C virus with host DEAD-box RNA helicases.* World J Gastroenterol, 2014. **20**(11): p. 2913-26.
142. Noueiry, A.O., J. Chen, and P. Ahlquist, *A mutant allele of essential, general translation initiation factor DED1 selectively inhibits translation of a viral mRNA.* Proc Natl Acad Sci U S A, 2000. **97**(24): p. 12985-90.
143. Bolinger, C., et al., *RNA helicase A modulates translation of HIV-1 and infectivity of progeny virions.* Nucleic Acids Res, 2010. **38**(5): p. 1686-96.
144. Li, Y., et al., *Recruitment of Arabidopsis RNA Helicase AtRH9 to the Viral Replication Complex by Viral Replicase to Promote Turnip Mosaic Virus Replication.* Sci Rep, 2016. **6**: p. 30297.
145. Ori, D., M. Murase, and T. Kawai, *Cytosolic nucleic acid sensors and innate immune regulation.* Int Rev Immunol, 2017. **36**(2): p. 74-88.
146. Barik, S., *What Really Rigs Up RIG-I?* J Innate Immun, 2016. **8**(5): p. 429-36.

147. del Toro Duany, Y., B. Wu, and S. Hur, *MDA5-filament, dynamics and disease.* Curr Opin Virol, 2015. **12**: p. 20-5.
148. Li, G., et al., *DEAD-box RNA helicase DDX3X inhibits DENV replication via regulating type one interferon pathway.* Biochem Biophys Res Commun, 2015. **456**(1): p. 327-32.
149. Zhang, Z., et al., *DDX1, DDX21, and DHX36 helicases form a complex with the adaptor molecule TRIF to sense dsRNA in dendritic cells.* Immunity, 2011. **34**(6): p. 866-78.
150. Schroder, M., *Viruses and the human DEAD-box helicase DDX3: inhibition or exploitation?* Biochem Soc Trans, 2011. **39**(2): p. 679-83.
151. Mingam, A., et al., *DEAD-box RNA helicases in Arabidopsis thaliana: establishing a link between quantitative expression, gene structure and evolution of a family of genes.* Plant Biotechnol J, 2004. **2**(5): p. 401-15.
152. Goodin, M.M., et al., *pGD vectors: versatile tools for the expression of green and red fluorescent protein fusions in agroinfiltrated plant leaves.* Plant J, 2002. **31**(3): p. 375-83.
153. Bertrand, E., et al., *Localization of ASH1 mRNA particles in living yeast.* Mol Cell, 1998. **2**(4): p. 437-45.
154. Muller, M., et al., *A ribonucleoprotein complex protects the interleukin-6 mRNA from degradation by distinct herpesviral endonucleases.* PLoS Pathog, 2015. **11**(5): p. e1004899.
155. Pogany, J., Panavas, T., Serviene, E., Nawaz-Ul-Rehman, MS., and Nagy, PD, *A high-throughput approach for studying virus replication in yeast.* Current Protocols in Microbiology, 2010. **19**: p. 16J.1.1-16J.1.15.
156. Barajas, D., et al., *Noncanonical role for the host Vps4 AAA+ ATPase ESCRT protein in the formation of Tomato bushy stunt virus replicase.* PLoS Pathog, 2014. **10**(4): p. e1004087.
157. Rajendran, K.S., J. Pogany, and P.D. Nagy, *Comparison of turnip crinkle virus RNA-dependent RNA polymerase preparations expressed in Escherichia coli or derived from infected plants.* J Virol, 2002. **76**(4): p. 1707-17.
158. Cimino, P.A., et al., *Multifaceted regulation of translational readthrough by RNA replication elements in a tombusvirus.* PLoS Pathog, 2011. **7**(12): p. e1002423.
159. Panaviene, Z., J.M. Baker, and P.D. Nagy, *The overlapping RNA-binding domains of p33 and p92 replicase proteins are essential for tombusvirus replication.* Virology, 2003. **308**(1): p. 191-205.

160. Xu, K. and P.D. Nagy, *RNA virus replication depends on enrichment of phosphatidylethanolamine at replication sites in subcellular membranes.* Proc Natl Acad Sci U S A, 2015. **112**(14): p. E1782-E1791.
161. Cheng, X., et al., *Visualizing double-stranded RNA distribution and dynamics in living cells by dsRNA binding-dependent fluorescence complementation.* Virology, 2015. **485**: p. 439-51.
162. Lindbo, J.A., *High-efficiency protein expression in plants from agroinfection-compatible Tobacco mosaic virus expression vectors.* BMC Biotechnol, 2007. **7**: p. 52.
163. Dinesh-Kumar, S.P., et al., *Virus-induced gene silencing.* Methods Mol Biol, 2003. **236**: p. 287-94.
164. Jaag, H.M. and P.D. Nagy, *Silencing of Nicotiana benthamiana Xrn4p exoribonuclease promotes tombusvirus RNA accumulation and recombination.* Virology, 2009. **386**(2): p. 344-52.
165. Banroques, J., et al., *A conserved phenylalanine of motif IV in superfamily 2 helicases is required for cooperative, ATP-dependent binding of RNA substrates in DEAD-box proteins.* Mol Cell Biol, 2008. **28**(10): p. 3359-71.
166. Sasvari, Z., et al., *Assembly-hub function of ER-localized SNARE proteins in biogenesis of tombusvirus replication compartment.* PLoS Pathog, 2018. **14**(5): p. e1007028.
167. Rochon, D., et al., *The p33 auxiliary replicase protein of Cucumber necrosis virus targets peroxisomes and infection induces de novo peroxisome formation from the endoplasmic reticulum.* Virology, 2014. **452-453**: p. 133-42.
168. Weber-Lotfi, F., et al., *Mitochondrial targeting and membrane anchoring of a viral replicase in plant and yeast cells.* J Virol, 2002. **76**(20): p. 10485-96.
169. Xu, K., T.S. Huang, and P.D. Nagy, *Authentic in vitro replication of two tombusviruses in isolated mitochondrial and endoplasmic reticulum membranes.* J Virol, 2012. **86**(23): p. 12779-94.
170. Garcia, I., M.J. Albring, and O.C. Uhlenbeck, *Duplex destabilization by four ribosomal DEAD-box proteins.* Biochemistry, 2012. **51**(50): p. 10109-18.
171. Banroques, J., et al., *Motif III in superfamily 2 "helicases" helps convert the binding energy of ATP into a high-affinity RNA binding site in the yeast DEAD-box protein Ded1.* J Mol Biol, 2010. **396**(4): p. 949-66.
172. Lloyd, R.E., *Nuclear proteins hijacked by mammalian cytoplasmic plus strand RNA viruses.* Virology, 2015. **479-480**: p. 457-74.

173. Yasuda-Inoue, M., M. Kuroki, and Y. Ariumi, *Distinct DDX DEAD-box RNA helicases cooperate to modulate the HIV-1 Rev function.* Biochem Biophys Res Commun, 2013. **434**(4): p. 803-8.
174. Ahmad, S. and S. Hur, *Helicases in Antiviral Immunity: Dual Properties as Sensors and Effectors.* Trends Biochem Sci, 2015. **40**(10): p. 576-585.
175. Pathak, K.B., J. Pogany, and P.D. Nagy, *Non-template functions of the viral RNA in plant RNA virus replication.* Curr Opin Virol, 2011. **1**(5): p. 332-8.
176. Fernandez de Castro, I., et al., *Three-dimensional imaging of the intracellular assembly of a functional viral RNA replicase complex.* J Cell Sci, 2017. **130**(1): p. 260-268.
177. Valiente-Echeverria, F., M.A. Hermoso, and R. Soto-Rifo, *RNA helicase DDX3: at the crossroad of viral replication and antiviral immunity.* Rev Med Virol, 2015. **25**(5): p. 286-99.
178. Lorgeoux, R.P., et al., *DDX17 promotes the production of infectious HIV-1 particles through modulating viral RNA packaging and translation frameshift.* Virology, 2013. **443**(2): p. 384-92.
179. Garcia-Ruiz, H., et al., *Arabidopsis RNA-dependent RNA polymerases and dicer-like proteins in antiviral defense and small interfering RNA biogenesis during Turnip Mosaic Virus infection.* Plant Cell, 2010. **22**(2): p. 481-96.
180. Andika, I.B., et al., *Different Dicer-like protein components required for intracellular and systemic antiviral silencing in Arabidopsis thaliana.* Plant Signal Behav, 2015. **10**(8): p. e1039214.
181. Aliyari, R. and S.W. Ding, *RNA-based viral immunity initiated by the Dicer family of host immune receptors.* Immunol Rev, 2009. **227**(1): p. 176-88.
182. Wu, B., et al., *Global organization of a positive-strand RNA virus genome.* PLoS Pathog, 2013. **9**(5): p. e1003363.
183. Lorgeoux, R.P., F. Guo, and C. Liang, *From promoting to inhibiting: diverse roles of helicases in HIV-1 Replication.* Retrovirology, 2012. **9**: p. 79.
184. Feng, Z., et al., *Recruitment of Vps34 PI3K and enrichment of PI3P phosphoinositide in the viral replication compartment is crucial for replication of a positive-strand RNA virus.* PLoS Pathog, 2019. **15**(1): p. e1007530.
185. Xu, K. and P.D. Nagy, *Expanding use of multi-origin subcellular membranes by positive-strand RNA viruses during replication.* Curr Opin Virol, 2014. **9**: p. 119-26.
186. Belov, G.A. and F.J. van Kuppeveld, *(+)RNA viruses rewire cellular pathways to build replication organelles.* Curr Opin Virol, 2012. **2**(6): p. 740-7.

187. Chuang, C., K.R. Prasanth, and P.D. Nagy, *The Glycolytic Pyruvate Kinase Is Recruited Directly into the Viral Replicase Complex to Generate ATP for RNA Synthesis.* Cell Host Microbe, 2017. **22**(5): p. 639-652 e7.
188. Huh, W.K., et al., *Global analysis of protein localization in budding yeast.* Nature, 2003. **425**(6959): p. 686-91.
189. Tran, E.J. and S.R. Wente, *Dynamic nuclear pore complexes: life on the edge.* Cell, 2006. **125**(6): p. 1041-53.
190. D'Angelo, M.A. and M.W. Hetzer, *Structure, dynamics and function of nuclear pore complexes.* Trends Cell Biol, 2008. **18**(10): p. 456-66.
191. Pemberton, L.F. and B.M. Paschal, *Mechanisms of receptor-mediated nuclear import and nuclear export.* Traffic, 2005. **6**(3): p. 187-98.
192. Ribbeck, K. and D. Gorlich, *Kinetic analysis of translocation through nuclear pore complexes.* EMBO J, 2001. **20**(6): p. 1320-30.
193. Hutten, S. and R.H. Kehlenbach, *CRM1-mediated nuclear export: to the pore and beyond.* Trends Cell Biol, 2007. **17**(4): p. 193-201.
194. Kimura, M. and N. Imamoto, *Biological significance of the importin-beta family-dependent nucleocytoplasmic transport pathways.* Traffic, 2014. **15**(7): p. 727-48.
195. Fischer, U., et al., *A non-canonical mechanism for Crm1-export cargo complex assembly.* Elife, 2015. **4**.
196. Merkle, T., *Nucleo-cytoplasmic transport of proteins and RNA in plants.* Plant Cell Rep, 2011. **30**(2): p. 153-76.
197. Kirli, K., et al., *A deep proteomics perspective on CRM1-mediated nuclear export and nucleocytoplasmic partitioning.* Elife, 2015. **4**.
198. Guttler, T. and D. Gorlich, *Ran-dependent nuclear export mediators: a structural perspective.* EMBO J, 2011. **30**(17): p. 3457-74.
199. la Cour, T., et al., *NESbase version 1.0: a database of nuclear export signals.* Nucleic Acids Res, 2003. **31**(1): p. 393-6.
200. Matsuyama, A., et al., *ORFeome cloning and global analysis of protein localization in the fission yeast Schizosaccharomyces pombe.* Nat Biotechnol, 2006. **24**(7): p. 841-7.
201. Dong, X., et al., *Structural basis for leucine-rich nuclear export signal recognition by CRM1.* Nature, 2009. **458**(7242): p. 1136-41.
202. Monecke, T., et al., *Crystal structure of the nuclear export receptor CRM1 in complex with Snurportin1 and RanGTP.* Science, 2009. **324**(5930): p. 1087-91.

203. Guttler, T., et al., *NES consensus redefined by structures of PKI-type and Rev-type nuclear export signals bound to CRM1.* Nat Struct Mol Biol, 2010. **17**(11): p. 1367-76.
204. Koyama, M., N. Shirai, and Y. Matsuura, *Structural insights into how Yrb2p accelerates the assembly of the Xpo1p nuclear export complex.* Cell Rep, 2014. **9**(3): p. 983-95.
205. Monecke, T., et al., *Structural basis for cooperativity of CRM1 export complex formation.* Proc Natl Acad Sci U S A, 2013. **110**(3): p. 960-5.
206. Yedavalli, V.S., et al., *Requirement of DDX3 DEAD box RNA helicase for HIV-1 Rev-RRE export function.* Cell, 2004. **119**(3): p. 381-92.
207. Fischer, U., et al., *The HIV-1 Rev activation domain is a nuclear export signal that accesses an export pathway used by specific cellular RNAs.* Cell, 1995. **82**(3): p. 475-83.
208. Ghildyal, R., et al., *The respiratory syncytial virus matrix protein possesses a Crm1-mediated nuclear export mechanism.* J Virol, 2009. **83**(11): p. 5353-62.
209. Elton, D., et al., *Interaction of the influenza virus nucleoprotein with the cellular CRM1-mediated nuclear export pathway.* J Virol, 2001. **75**(1): p. 408-19.
210. Zhang, X., et al., *CRM1, an RNA transporter, is a major species-specific restriction factor of human T cell leukemia virus type 1 (HTLV-1) in rat cells.* Microbes Infect, 2006. **8**(3): p. 851-9.
211. Strunze, S., et al., *Nuclear targeting of adenovirus type 2 requires CRM1-mediated nuclear export.* Mol Biol Cell, 2005. **16**(6): p. 2999-3009.
212. Kojima, H., et al., *Sugar-inducible expression of the nucleolin-1 gene of Arabidopsis thaliana and its role in ribosome synthesis, growth and development.* Plant J, 2007. **49**(6): p. 1053-63.
213. Wang, W., et al., *An importin beta protein negatively regulates MicroRNA activity in Arabidopsis.* Plant Cell, 2011. **23**(10): p. 3565-76.
214. Kudo, N., et al., *Leptomycin B inactivates CRM1/exportin 1 by covalent modification at a cysteine residue in the central conserved region.* Proc Natl Acad Sci U S A, 1999. **96**(16): p. 9112-7.
215. Sun, Q., et al., *Nuclear export inhibition through covalent conjugation and hydrolysis of Leptomycin B by CRM1.* Proc Natl Acad Sci U S A, 2013. **110**(4): p. 1303-8.
216. Fried, H. and U. Kutay, *Nucleocytoplasmic transport: taking an inventory.* Cell Mol Life Sci, 2003. **60**(8): p. 1659-88.

217. Nakielny, S. and G. Dreyfuss, *Transport of proteins and RNAs in and out of the nucleus.* Cell, 1999. **99**(7): p. 677-90.
218. Izaurralde, E., et al., *The asymmetric distribution of the constituents of the Ran system is essential for transport into and out of the nucleus.* EMBO J, 1997. **16**(21): p. 6535-47.
219. Waggoner, S. and P. Sarnow, *Viral ribonucleoprotein complex formation and nucleolar-cytoplasmic relocalization of nucleolin in poliovirus-infected cells.* J Virol, 1998. **72**(8): p. 6699-709.
220. Castanotto, D., et al., *CRM1 mediates nuclear-cytoplasmic shuttling of mature microRNAs.* Proc Natl Acad Sci U S A, 2009. **106**(51): p. 21655-9.
221. Tang, H., et al., *A cellular cofactor for the constitutive transport element of type D retrovirus.* Science, 1997. **276**(5317): p. 1412-5.
222. Askjaer, P., et al., *RanGTP-regulated interactions of CRM1 with nucleoporins and a shuttling DEAD-box helicase.* Mol Cell Biol, 1999. **19**(9): p. 6276-85.
223. Senissar, M., et al., *The DEAD-box helicase Ded1 from yeast is an mRNP cap-associated protein that shuttles between the cytoplasm and nucleus.* Nucleic Acids Res, 2014. **42**(15): p. 10005-22.
224. Nagy, P.D., *Yeast as a model host to explore plant virus-host interactions.* Annu Rev Phytopathol, 2008. **46**: p. 217-42.
225. Nagy, P.D., *Viral sensing of the subcellular environment regulates the assembly of new viral replicase complexes during the course of infection.* J Virol, 2015. **89**(10): p. 5196-9.
226. Fung, H.Y., S.C. Fu, and Y.M. Chook, *Nuclear export receptor CRM1 recognizes diverse conformations in nuclear export signals.* Elife, 2017. **6**.
227. Biegel, J.M., et al., *Cellular DEAD-box RNA helicase DDX6 modulates interaction of miR-122 with the 5' untranslated region of hepatitis C virus RNA.* Virology, 2017. **507**: p. 231-241.
228. Jangra, R.K., M. Yi, and S.M. Lemon, *DDX6 (Rck/p54) is required for efficient hepatitis C virus replication but not for internal ribosome entry site-directed translation.* J Virol, 2010. **84**(13): p. 6810-24.
229. Chahar, H.S., S. Chen, and N. Manjunath, *P-body components LSM1, GW182, DDX3, DDX6 and XRN1 are recruited to WNV replication sites and positively regulate viral replication.* Virology, 2013. **436**(1): p. 1-7.
230. Yu, S.F., et al., *The DEAD-box RNA helicase DDX6 is required for efficient encapsidation of a retroviral genome.* PLoS Pathog, 2011. **7**(10): p. e1002303.

231. Chkuaseli, T. and K.A. White, *Intragenomic Long-Distance RNA-RNA Interactions in Plus-Strand RNA Plant Viruses.* Front Microbiol, 2018. **9**: p. 529.
232. Kovalev, N., J. Pogany, and P.D. Nagy, *Template role of double-stranded RNA in tombusvirus replication.* J Virol, 2014. **88**(10): p. 5638-51.
233. Fairman-Williams, M.E., U.P. Guenther, and E. Jankowsky, *SF1 and SF2 helicases: family matters.* Curr Opin Struct Biol, 2010. **20**(3): p. 313-24.
234. Banroques, J., et al., *Analyses of the functional regions of DEAD-box RNA "helicases" with deletion and chimera constructs tested in vivo and in vitro.* J Mol Biol, 2011. **413**(2): p. 451-72.
235. Dardenne, E., et al., *RNA helicases DDX5 and DDX17 dynamically orchestrate transcription, miRNA, and splicing programs in cell differentiation.* Cell Rep, 2014. **7**(6): p. 1900-13.
236. Panda, D. and S. Cherry, *Cell-based genomic screening: elucidating virus-host interactions.* Curr Opin Virol, 2012. **2**(6): p. 784-92.
237. Dougherty, J.D., J.P. White, and R.E. Lloyd, *Poliovirus-mediated disruption of cytoplasmic processing bodies.* J Virol, 2011. **85**(1): p. 64-75.

VITA

Cheng-Yu Wu

EDUCATION

MS	2011	Plant Pathology, National Chung Hsing University, Taichung, Taiwan.
B.S.	2008	National Chung Hsing University, Taichung, Taiwan. Major, Plant Pathology.

PUBLICATIONS

- **Wu, C. Y.** and Nagy, P. D. 2019. Blocking tombusvirus replication through the antiviral functions of DDX17-like RH30 DEAD-box helicase. PLoS Pathog. (Accepted, in press)
- Barajas, D., Xu, K., Sharma, M., **Wu, C. Y.**, Nagy, P. D. 2014. Tombusviruses upregulate phospholipid biosynthesis via interaction between p33 replication protein and yeast lipid sensor proteins during virus replication in yeast. Virology 471-473:72-80
- **Wu, C. Y.** and Nagy, P. D. Changing functional identity: dissecting features affecting pro-viral versus antiviral functions of cellular DEAD-box helicases in tombusvirus replication. (Manuscript in preparation)
- **Wu, C. Y.** and Nagy, P. D. The XPO1-dependent nucleocytoplasmic shuttling inhibits the replication of tombusviruses. (Manuscript in preparation)

NATIONAL CONFERENCES AND MEETINGS

- **Wu, C. Y.** and Nagy, P. D. 2017. A DDX5-like RNA helicase inhibits tombusviral replication as a novel anti-viral factor. Annual meeting of American Society for Virology, Madison, WI, USA.
- **Wu, C. Y.** and Nagy, P. D. 2015. Identification of plant RNA helicases inhibiting tombusvirus replication in yeast and plants. Annual meeting of American Society for Virology, London, ON, Canada.

HONORS AND AWARDS

- The 3rd-place winner of 3 Minute Thesis Competition. Department of Plant and Soil Science and Department Plant Pathology, University of Kentucky. 2018
- Travel Award from Graduate School at University of Kentucky, 2017
- Travel Award from American Society for Virology, 2015
- Travel Award from Graduate School at University of Kentucky, 2015
- The ninth-place student winner of the thesis competition in the annual meeting of Taiwan Phytopathological Society, 2011